SYSTEMATIC STUDY OF SELECTED SORBENTS AVAILABLE IN SOUTH AFRICA FOR DESULPHURISATION OF FLUE GAS DURING IN-BED FLUIDISED BED COMBUSTION OF COAL

By Koogendran Govender[1]

Submitted in fulfilment of the requirements for the degree of Masters in the School of Chemical Engineering in the Faculty of Engineering at the University of Kwa-Zulu Natal

Supervisor: M. Carsky[1]

Joint Supervisor: J. N. Dunlevey[2]

Date submitted: 21 April 2006

[1] University of KwaZulu-Natal, Westville Campus; School of Chemical Engineering, Private Bag X54001, Durban, 4000, South Africa;
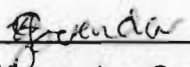[2] University of KwaZulu-Natal, Westville Campus; School of Geology, Private Bag X54001, Durban, 4000, South Africa;

Declaration

I, Koogendran Govender, declare that this thesis, unless specific indication to the contrary is made in the text, is my own original work. It is being submitted for the degree of Master of Science in Engineering to the University of KwaZulu-Natal and has not been submitted for any degree at any other university.

Koogendran

Koogendran Govender

On the 21st day of April 2006

Acknowledgements

Abstract

Sulphur dioxide (SO_2) is an atmospheric pollutant that has the ability to negatively impact on local vegetation, farming activities and human health. South Africa's coal fired power stations release this pollutant into the atmosphere during the combustion of coal. Current coal fired power stations operating in South Africa are not required to install any form of SO_2 removal equipment however, the new Air Quality Act to be implemented in South Africa could change this situation. The use of Fluidised Bed Technology with the addition of limestone or dolomite (sorbent) has the ability to absorb and convert SO_2 from a gaseous phase into a solid phase for easy disposal. The objective of this study was to evaluate potential commercial sorbent sources in South Africa that could potentially be used for the reduction of SO_2 released into the atmosphere during fluidised bed combustion of coal.

Eight commercially mined sorbents within a two hundred kilometre radius of large economically mineable coalfields were selected. The study was divided into two parts in order to identify any possible links between the physical and chemical composition of the sorbents and their performance under fluidised bed combustion conditions.

In Part 1, the chemical composition of the sorbents was determined by X-Ray Fluorescence (XRF) and X-Ray Diffraction (XRD) analysis. The sorbents hardness property was determined by Hardgrove Grindability Index (HGI) testing. The physical structure of the sorbent was analysed by both Petrographical and Scanning Electron Microscope (SEM) analysis of the original/parent sorbents.

In Part 2, SO_2 absorption capability by the sorbents was determined through batch tests conducted in a 1.6m high stainless steel, 10kW electrically heated Atmospheric Fluidised Bed Reactor (AFBR). Three different bed temperatures (800, 850 and 900°C) and three different particle size ranges (425-500, 600-710 and 850-1000μm) were tested for each of the eight sorbents.

The highest Maximum Sulphur Retention for all of the sorbents was found to occur at a temperature of 850°C and at the smallest particle size tested, 425-500μm. The best desulphurisation sorbent of the eight sorbents tested was found to be Sorb1 with a SO_2 Maximum Sulphur Retention of 92.30% and a Removal Efficiency of 84.54%. Additional tests were also performed on the sorbents to get a better understanding of their desulphurisation ability.

For the area calculation on the performance test graphs, it was found that the sorbent that produced the best SO_2 removal efficiency was not necessarily the sorbent that had the highest maximum sulphur retention.

For varying quantities of sorbent added to the AFBR, it was found that each sorbent had an optimum quantity that produced the best removal efficiency. However, for desulphurisation beyond certain limits any further increase in the amount of sorbent added to the AFBR resulted only in a marginal increase in the sorbent's SO_2 removal.

The calcium and magnesium composition of the sorbents was found to have no noticeable influence on the sorbents ability to reduce SO_2. The silica and inherent moisture content of the sorbent showed signs whereby an increase in their compositions produced an increase in desulphurisation.

The Hardgrove Grindability Index of the sorbents indicated that the softer the sorbent, the better the SO_2 reduction. The petrographical analysis performed on the eight sorbents showed no obvious reason for the difference between the sorbents ability to remove SO_2.

Contents

Chapter 7

7. Conclusions and Recommendations

Appendices

List of Figures

List of Tables

List of Symbols

C   -Concentration
Re   -Reynolds number
Ar   -Archimedes number

Greek

μ -Micron
ρ -Density, $kg.m^{-3}$

Subscripts

o   -Initial
p   -Particle
f   -Fluid

Superscripts

o   -Degrees
mf   -Minimum fluidising

Definitions

Abrasion	: A wearing, grinding or rubbing away by friction, usually (but not always) involving the action of particles against or between surfaces.
Atmospheric	: Derived from the noun atmosphere. A unit of pressure equal to the mean pressure at sea level, 101 325 pascals.
Attrition	: The process in which solids are worn down or ground down by friction, often between particles of the same material.
Beneficiation	: The preparation and treatment of ore for recovery of mineral commodities. Beneficiation includes, but is not linked, to crushing, sizing, drying and leaching.
Calcination	: A process by which a material is heated to a high temperature without fusing, so that hydrates, carbonates, or other compounds are decomposed and the volatile material is released.
Combustion	: Burning accompanied by release of energy and light. Refers to controlled burning of waste, in which heat chemically alters organic compounds, converting into stable inorganics such as carbon dioxide and water. Many important pollutants, such as sulphur dioxide, nitrogen oxides, and particulates are combustion products, often products of the burning of fuels such as coal, oil, gas or wood.
Crystalline	: Material consisting of minerals in a crystalline state, in contrast to very fine-grained amorphous material.
Decrepitation	: The cracking or breaking up of certain crystals when they are heated.

Desulphurisation	: Process of removing sulphur from fossil fuel combustion flue gas thus preventing the formation of acid rain.
Detrital	: Descriptive of a particle, generally of a resistant mineral, that has been derived from an existing rock by erosion and weathering.
Dolomite	: A mineral composed of calcium-magnesium carbonate, or a rock composed of this mineral. Many dolomitic rocks are limestone that are 'dolomitised' by the action of ground-water solutions rich in magnesium.
Earthy	: Composed of a loosely bonded aggregate of fine-grained material.
Elutriation	: Decanting or racking off finer particles from heavier.
Flotation	: Process used to separate particulate solids by causing one group of particles to float; utilises differences in surface chemical properties of the particles, some of which are entirely wetted by water, others are not.
Flue Gas	: The air coming out of a chimney after combustion in the burner it is venting. It can include nitrogen oxides, carbon oxides, water vapour, sulphur oxides, particles and many chemical pollutants.
Fly ash	: The finely divided particles of ash suspended in gases resulting from the combustion of fuel.
Limestone	: A sedimentary rock consisting mainly of calcium carbonate that was deposited by the remains of marine animals.
Lithology	: The description of rock or soil in outcrop or hand sample on the basis of such characteristics as colour, mineralogical composition and grain size.
Marble	: Limestone or dolomite when subject to high temperature and/or pressure changes into marble by totally recrystallising. In geological terms the only true marbles are metamorphosed limestones and dolomites.
Oolitic	: Composed of small (0.25 – 2mm diameter) spherical to ellipsoid particles which may or may not have a nucleus, normally composed of calcium carbonate but may be silica or iron oxides.
Reactor	: A vessel, tank or tower in which a specific chemical reaction takes place.

Recrystalline	: A material having undergone a process that involved crystallisation from a previous but not necessarily primary amorphous or crystalline material.
Sintering	: The mechanism by which solid particles coalesce when heated to temperatures below their melting point.
Sorbent	: Limestone, dolomite or any other material which has a relatively high calcium carbonate content that can be used to reduce the SO_2 emissions.
SO_2	: Chemical symbol for the gas sulphur dioxide
Stratigraphy	: The branch of geology concerned with the formation, composition, ordering in time, and arrangement in space of sedimentary rocks.
Stoichiometry Ratio	: Description of the quantitative relationships among elements and compounds as they undergo chemical changes.
Thermal Shock	: A test to determine the ability of a material to withstand heat and cold by subjecting it to rapid and wide changes in temperature.
X-Ray Diffraction (XRD)	: A technique for establishing the structures of crystalline solids by directing X rays of a single wavelength at a crystal and obtaining a diffraction pattern from which interatomic spaces are determined.
X-Ray Fluorescence (XRF)	: An analytic instrument for non-destructive testing to determine composition.

Chapter One

Introduction

1.1. General

The coal used in power stations to produce electricity consists of various elements such as carbon, nitrogen, sulphur, etc. The coal is burnt in a coal-fired power station to generate the heat required to convert water into steam. The steam produced is then used to drive a steam turbine coupled to a generator, which converts the energy in the steam into electrical energy. A consequence of burning the coal is the release of combustion gases, namely CO_2, CO, NO, SO_2 etc. These combustion gases are released into the atmosphere via tall flue gas stacks. At present, the typical sulphur dioxide (SO_2) emissions levels in the flue gas released from South African power stations is on average 8.22 g/kW.h (2003 Eskom Annual Report). This is high when compared to the SO_2 emissions of a country like Poland that is part of the European Union whose emissions range between 3.56 to 5.54 g/kW.h (REC: Reduction of SO_2 and Particulate Emissions: Legal Framework (4.5) (2006)).

Studies by the United States Environmental Protection Agency have shown that SO_2 emissions by their electricity utility companies seriously endanger both vegetation and animal life around their power stations (EPA's Clean Air Market Programs – Effects of Acid Rain (2002)). In the late 70's, an ecological disaster was experienced in Central Europe when large areas of forest and other vegetation were destroyed by acid rain and ash fallout in the areas of close proximity to European power stations. Spilkova and Carsky (2002) reported on the destruction that occurred and the changes implemented in order to reduce emissions of the main pollutants. With no methodology currently in place to reduce SO_2 emission at South African power stations, the same environmental problems will inevitably arise in the areas around our power stations as was experienced by USA and Central Europe.

1

International fossil fuel boiler manufacturing companies and other organisations have developed many methods to reduce SO_2 emissions from coal-fired power stations. The three common methodologies currently being utilised are: (1) the coal beneficiation processes, (2) back end Flue Gas Desulphurisation (FGD) process (wet or dry), and (3) the Fluidised Bed Combustion (FBC) process with in furnace SO_2 reduction.

For the construction of future coal fired power stations in South Africa there may be a requirement to install equipment such as those developed by international boiler manufacturing companies that can reduce air pollution. Desulphurisation during FBC is able to achieve this while also being able to effectively utilise low-grade coal.

The effective operation of either the FGD or FBC processes are achieved through the use of some type of calcium based mineral (sorbent) to trap the sulphur in a solid form (desulphurisation), which limits the release of SO_2 into the atmosphere. Lime, limestone and dolomite, which have a substantial amount of calcium, are used in these processes.

An observation was made by an independent source at one of South Africa's power station that if all the current and new power stations were to be retrofitted with FGD and FBC units respectively, large quantities (1563 ktons) of limestone would be required. This was calculated based on Eskom's 2004 coal consumption of 109508 ktons, an average sulphur content of 0.87% and an assumption of a 1.05 Calcium/Sulphur molar ratio to obtain a 50% sulphur removal. Looking at these large amounts, there would therefore be a need to optimise these materials by determining the best desulphurisation sorbent that is closest to our minable coal.

This study was initiated to investigate sorbent's desulphurisation capability under FBC conditions, which is one of the possible generating technologies capable of providing future electricity capacity in South Africa. The aim of this study was to evaluate potential commercial sorbent sources in South Africa that could potentially be used for the reduction of SO_2 released into the atmosphere during fluidised bed combustion of coal.

In this study four sources of limestone and four sources of dolomite were investigated for their desulphurisation capability in an Atmospheric Fluidised Bed Reactor (AFBR). These sorbents were tested at three temperature ranges, with three particle size fractions tested at each temperature range. The chemical composition, physical properties and structure of the sorbents tested were also determined, using X-Ray Diffraction (XRD), X-Ray Fluorescence (XRF), Hardgrove Grindability Index (HGI), Scanning Electron Microscope (SEM) and Petrographical

analysis. This allowed for the effect of these properties on the sulphur removal capability of the sorbents tested to be investigated.

1.2. Implications of Sulphur Dioxide as a Pollutant

SO_2 emissions released during the coal combustion process at smelters and power stations travel thousands of kilometers into the atmosphere where they combine with water vapour to form a dilute solution of sulphurous acid (H_2SO_3). Rain, snow, hail, fog and other precipitation wash this solution down to earth as 'acid rain'.

A survey that was conducted by the United States Geological Survey (USGS) (Acid rain data and reports (2003)) found that stone sculptures, buildings, forests, vegetation, bricks, inland waterways and lakes in close proximity to electricity generation power stations were being damaged or destroyed. These destructions were found to be strongly related to the formation of acid rain from these power stations. This has prompted the USA government into implementing stricter emission standards to power stations and other industrial companies (15th Anniversary of the Clean Air Act – U.S. Environmental Protection Agency (2006)).

In South Africa's smelters and power stations, tall stacks are presently being utilised in order to ensure proper dispersion of flue gases away from these industries. This does exacerbate the problem of acid rain formation as the gases are dispersed further away from the power stations thus polluting larger areas, however with lower concentrations of acidity. With cognisance of this there is a need to reduce the SO_2 emissions levels from the flue gases of the power stations so that there is a preservation of the environment and animal life.

1.3. Limestone and Dolomite Definitions

Limestones and dolomites are formed in similar geological environments and therefore tend to have the same chemical and physical properties. This is the reasoning behind why both these materials are being considered as a desulphurisation agent.

Bates and Jackson (1980) found that there were two uses for the word dolomite. One is a sedimentary rock and the other is a mineral. The following are Bates and Jackson's definitions of limestones and dolomites:

3

Dolomite [mineral]: A common rock-forming mineral of the composition $CaMg(CO_3)_2$. Part of the magnesium may be replaced by ferrous iron and less frequently by manganese. Mineral dolomite is white, colourless, or tinged yellow, brown, pink, or grey. It is found in extensive beds as dolomite rock. It is a common vein mineral and is found in serpentinite and other magnesian rocks.

Dolomite [sedimentary]: A carbonate sedimentary rock of which more than 50% by weight or by area percentages under the microscope consists of the mineral dolomite, or a variety of limestone or marble rich in magnesium carbonate. A sedimentary dolomite is a carbonate rock containing more than 90% dolomite and less than 10% calcite or one having a Ca/Mg ratio in the range of 1.5-1.7. It can also be one having an approximate MgO equivalent of 19.5-21.6% or magnesium-carbonate equivalent of 41.0-45.4%. Dolomite is often interbedded with limestone and usually represents a postdepositional replacement of limestone.

For limestone, Bates and Jackson (1980) defined it as a sedimentary rock consisting chiefly of calcium carbonate, primarily in the form of the mineral calcite, and with or without magnesium carbonate. The carbonate sedimentary rock contains more than 95% calcite and less than 5% dolomite. Limestone contain common minor constituents include silica, feldspar, clays, pyrite and siderite. Limestones are formed by either organic or inorganic processes and may be structurally described as detrital, chemical, oolitic, earthy, crystalline, or recrystallised. Many are highly fossiliferous and clearly represent ancient shell banks or coral reefs.

1.4. Limestone/Dolomite as a Desulphurisation agent

During Fluidised Bed Combustion (FBC) via limestone and dolomite injection, the reaction that occurs between SO_2 and these sorbents involves two steps (Anthony and Granatstein (1999)). The first is the calcination of carbonate whilst the second step is the sulphation of the carbonate in an atmosphere with excess air.

These steps will be discussed in the subsections that follow.

1.4.1 Calcination Process of Limestone and Dolomite

Calcination is the initial chemical reaction that converts calcium carbonate ($CaCO_3$) to calcium oxide (CaO) and magnesium carbonate ($MgCO_3$) to magnesium oxide (MgO) (equations 1-3). From these equations it can be seen that the gas carbon dioxide (CO_2) is released from both

limestone and dolomite. The effect of releasing CO_2 is the increase in the sorbents porosity due to the reduction in the sorbents molar volume thus creating an ideal material to absorb SO_2 emissions. The product formed is similar to a porous sponge that has the ability to absorb water.

Calcination

Limestone: $CaCO_3$ (s) → CaO (s) + CO_2 (g)   T> 1030K   [1]

Dolomite: $CaCO_3.MgCO_3$ (s) → $MgO.CaCO_3$ (s) + CO_2 (g)   T> 890K   [2]

$MgO.CaCO_3$ (s) → CaO (s) + MgO (s) + CO_2 (g)   T > 1030K   [3]
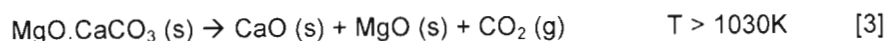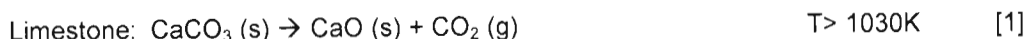
The greater surface area created by the sorbents porosity increases its efficiency in capturing SO_2 thus making it an ideal material. It has been found by Anthony and Granatstein (1999) that the porosity of the sorbent can increase from anything between 5 to 50 times during the calcination process.

1.4.2 Sulphation Process of Limestone and Dolomite

Sulphation is the reaction that follows calcination, which converts calcium oxide (CaO) to calcium sulphate ($CaSO_4$) (equation 4).

Sulphation CaO (s) + SO_2 (g) + ½ O_2 → $CaSO_4$ (s)   T < 1500K   [4]
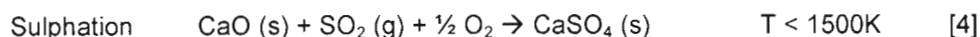
$CaSO_4$ initially forms on the surface of the sorbent, creating an impregnable shell that blocks the pores within the sorbent. The formation of the shell is due to the volume increase during the conversion from CaO to $CaSO_4$. This leaves a significant amount of unreacted CaO in the core, which makes complete conversion of the sorbent unachievable (Adanez et al. (1994)).

At the temperature range at which the fluidised bed reactor operates (>800°C), magnesium has little to no participation in the sulphation process. This is due to $MgSO_4$ being unstable above a temperature of 760°C. Therefore only the calcium present in the sorbents is of significance during the sulphation process (Pisupati et al. (1996)).

1.5. South Africa's Situation regarding Emissions Control

South Africa's regulations with respect to the emissions of gases into the atmosphere are relaxed. The method currently being used for emissions control is based on a site-by-site inspection of the area around industrial companies, including power stations.

The South African government has just passed legislation that should see the implementing of stricter emissions limits of gaseous pollutants released into the atmosphere from power stations and other industries. This may result in current and future power stations being required to implement new methodologies or techniques that can clean the gaseous emissions before they are released from their flue gas stacks.

In South Africa, most of the mined coals are upgraded to improve the quality of the coal prior to sale or utilisation. This upgrade in coal quality is achievable through the beneficiation process. Flotation is an example of a beneficiation process whereby most of the ash and inorganic sulphur that exists in the coal is removed. From the beneficiation process, three types of coal products are produced with different qualities viz. Tops, Middlings and Discard (slurry & sink). The tops has the highest quality and is exported in the Atlantic and Pacific markets while the middlings are sold to smelter and power station plants in South Africa. The third type, discard coal, is disposed of in discard dumps around current and abandoned mines.

These discard coals in the discard dumps are exposed to the sun, which has the ability to gradually combust. In some areas of South Africa, this has already occurred, releasing large quantities of CO_2 and SO_2 into the atmosphere.

The currently produced discard coal is not compatible as a source of fuel in the pulverised fuel combustors currently in operation in South African power stations due to its high sulphur and ash content. However, these coals could be used in FBC plants. This is an advantage that FBC has over other coal combustion technologies. Given the continuing decline in locally available coal qualities FBC could become the coal combustion technology of preference (World Coal Institute – The Role of Coal as an Energy Source (2006)).

1.6. Scope of Thesis

This thesis consists of seven chapters. The literature study reviews and discusses literature concerning flue gas desulphurisation during Fluidised Bed Combustion. Chapter Three discusses the geological stratigraphy of the sorbents deposits whilst Chapter Four deals with the methods of screening and preparation of the sorbents used during testing. The experimental equipment used for testing the sorbents utilisation is discussed in Chapter Five. Experimental results from batch laboratory fluidised bed reactor tests are presented in Chapter Six. Chapter Seven presents the conclusions derived from the experimental work performed and recommendations for further studies to be implemented in the near future.

Chapter Two

Literature Survey

2.1. Introduction

Due to the increasing awareness of governments, communities and companies on the impacts of emissions from industrial processes, a concerted effort is being made by most stakeholders to reduce the negative impacts of these processes on communities and the environment. The South African government is addressing these concerns and has recently introduced a new air quality legislation, which lays down the mechanisms for reducing the current gas emissions from industrial processes. One of the emission gases that will be eventually targeted in South Africa is sulphur dioxide (SO_2).

During the past forty years there has been extensive experimental investigation into the use of fluidised bed combustion as a process to reduce SO_2 emissions in the flue gases of coal combustion plants (Pisupati et al. (1996), Adanez et al. (1994), Lyngfelt and Leckner (1999), etc.). It was found that this could be achieved in the fluidised bed boiler through the introduction of a calcium-based material together with the coal into the fluidised bed combustion chamber, which would result in "in-bed" sulphur retention thus lowering SO_2 emissions. The calcium bearing materials that were found to be best suited in achieving this were limestone and dolomite and were subsequently referred to as sorbents.

Sorbents have been found by Pisupati et al. (1996) to vary in their geological depositional history. This affects their chemical composition and physical properties, which influences their ability to react with SO_2. The sorbent properties can deviate such that sorbents obtained from different locations within the same quarry can exhibit different SO_2 absorption properties, despite having similar chemical compositions. Therefore the sorbents physical and chemical properties

7

have to be characterised in order to determine the SO_2 removal potential during the desulphurisation process.

For the sorbents used in the desulphurisation process of fluidised bed reactors, there is a clear lack of sufficient empirical understanding to determine the reactivity of sorbents or the optimal temperature, particle size, stoichiometry ratio etc. at which plants should operate for maximum sorbent efficiency. Hence there is a need to conduct individual tests on sorbents available in South Africa to determine their suitability and effectiveness for the fluidised bed desulphurisation process. Another reason for the determination of the best available sorbents is to reduce compliance cost (transport, sorbent quantity, etc.) as was found by Anthony et al. (1999).

This literature review was conducted to establish the current progress and direction of research in the field of fluidised bed sorbent characterisation. The literature review has been divided into two sections viz.:

- Characterisation of Sorbent properties that affect Sulphur Absorption
- Experimental Equipment for Testing Sorbents.

A limitation was experienced with regards to the comparison of the results produced during this study to published data from South Africa. It was found that there was no locally available data to make a comparison. Thus comparisons were made with literature data from European and American countries.

2.2. Characterisation of Sorbent Properties that affect Sulphur Absorption

Adanez et al. (1994b) found that the chemical and physical properties individually do not give a true indication of the sorbent performance. He explains further that both these properties work hand in hand and are equally important for an effective desulphurisation process to occur. This was consistent with the findings of Haji-Sulaiman et al. (1991). In general, they found that the interrelationship of the chemical and physical properties made it extremely difficult to determine their individual influence on desulphurisation.

The following are some of the many sorbent physical, chemical and plant operational properties that were found to have importance for sulphur capture during fluidised bed combustion:

- Temperature
- Calcium to sulphur (Ca/S) molar ratio
- Particle size distribution
- Chemical composition

> ➢ Sorbent impurities
> ➢ Sorbent particle residence time
> ➢ Combustor design
> ➢ Sorbent particle porosity

The above sorbent sulphur capture properties can be categorised into two groups namely, process variables and physical and chemical properties. Each aspect deals with a different characteristic regarding improvement to sorbent utilisation during the flue gas desulphurisation processes. This section of the review will discuss these observations amongst others, under the following subheadings:

2.2.1. Influence of Process Variables

2.2.2. Influence of Physical and Chemical Properties

2.2.1. Influence of Process Variables

This section discusses the influence of the process variables that affect the desulphurisation process. The following variables were concentrated on during the literature review as these variables were to be tested during the research program:

1) Temperature
2) Calcium to sulphur (Ca/S) molar ratio
3) Particle size.

Temperature

Studies by Pisupati et al. (1996) on fluidised bed combustion have shown that for different sorbents there is an optimum temperature at which the fluidised bed reactor should operate to ensure the best sulphur retention. Figure 2-1 shows the temperature sensitivity of sorbents over the temperature range tested by Pisupati et al. (1996). They found that for the three limestone sorbents tested, the optimum temperatures were in the same temperature ranges of between 1650-1700°F (899-927°C). This temperature dependant behaviour confirms that there is an optimum temperature range for sulphation of sorbents.
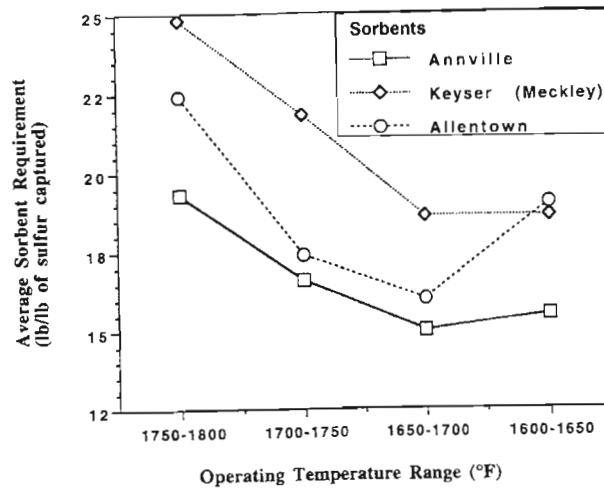
Figure 2-1 Average Sorbent Requirement as a Function of Operating Temperature, Pisupati et al. (1996)

A study by Adanez et al. (1994a) found that for all sorbents tested, the optimum sulphation temperature was around 850°C. The effect of sulphation temperature can be clearly observed from Figure 2-2, which shows the temperature sensitivity of the sorbents. Figure 2-2 together with Figure 2-1 clearly indicates that there is an optimum temperature at which the sorbents would experience the highest sulphur retention.
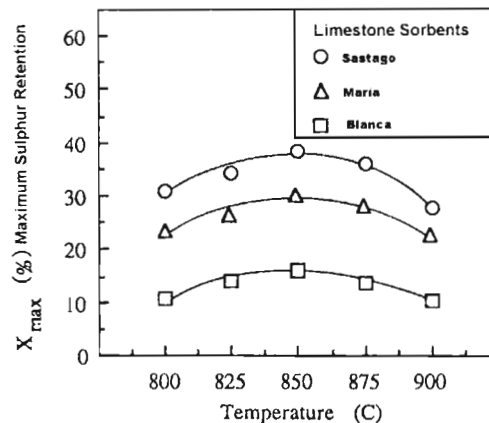
Figure 2-2 Maximum sulphation conversions, x_{max} vs. Temperature (°C), Adanez et al. (1994a)

Haji-Sulaiman et al. (1990) also confirmed the findings by Adanez et al. (1994a) that the optimum sulphation temperature for a sorbent was a function of operating conditions and ranged between 800 and 900°C. They state that the parameters that have an influence on the optimum sulphation temperature are the physical structure of the sorbent (pore size and surface area), the operating temperature and sorbent residence time.

Hartman et al. (1976) suggests that when both sulphation and calcination occur simultaneously, an optimum temperature can be expected to result from these two opposing tendencies. This was also found to occur by Haji-Sulaiman et al. (1990). Hartman et al. (1976) goes on to say that there are different optimum temperatures for different types of sorbents and that for each sorbent these have to be evaluated experimentally.

Pisupati et al. (1996) states that at temperatures higher than the optimum temperature, the sorbent requirement for desulphurisation will increase rapidly due to the blockage of pores on the surface of the particle. This was due to the formation of $CaSO_4$ and the sintering of the free CaO particles, which reduces the reactive surface area. This finding was consistent with Haji-Sulaiman et al. (1990) who reported that with the accumulation of the $CaSO_4$ product layer, there was an increase in sulphur reaction rate with an increase in temperature. This prevented the access to the porous interior, which reduces the reactive surface area.

Conversely, Haji-Sulaiman et al. (1990) found that when the fluidised bed reactor operating temperature dropped 50-100°C below the optimum temperature, there was a reduction in the conversion of sorbents. They state that the reduction is due to the competition between recarbonation of CaO with CO_2 and sulphation of the sorbents. This was in contradiction to Chi et al. (1994) who reported that the reduction in conversion was due to the formation of small pores of the calcined particles and that their entrances tend to plug up rapidly during sulphation.

Haji-Sulaiman et al. (1990) reported that at the optimum operating temperatures, SO_2 penetrates deeper into the particle interior, since the rate of surface reaction is much slower. This created a delay in pore mouth closure, which gave a more uniform conversion throughout the particle and generally a higher overall calcium utilisation. They noted that with smaller particles, the optimum temperature for sulphur retention was much higher than it was for the same sorbent with a larger particle size.

From Figure 2-3, Haji-Sulaiman et al. (1990) found that the particle residence time for high calcium limestones was also an important variable in the determination of the optimum sulphation temperature. Figure 2-3 shows that the curves obtained at different temperatures continue to increase throughout the duration of the investigation. The test performed at 650°C exhibited the highest sulphur uptake at the longest residence time which demonstrates the known trend of an increase in desulphurisation with an increase in time.

11
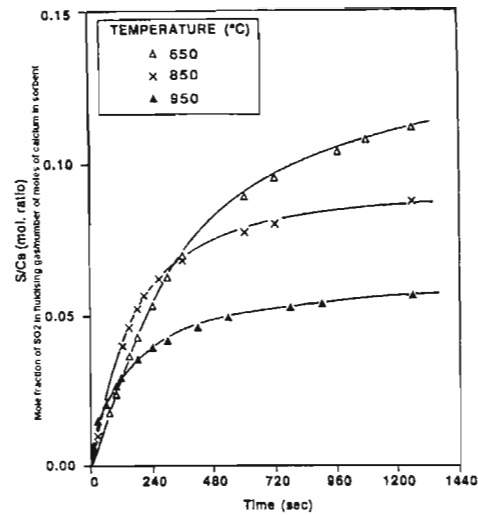
Figure 2-3 Effect of temperature on the kinetics of sulphur uptake of high calcium limestones, Haji-Sulaiman et al. (1990)

Calcium to Sulphur molar (Ca/S) Ratio

Ca/S molar ratio is the ratio of the number of moles of calcium present in the limestone or dolomite feed to the number of moles of sulphur that is present in the coal feed. The molar ratio can range from between one and ten depending on the sulphur reduction that is required and the reactivity of the sorbent. It should be noted that with an increase in the molar ratio there is an increase in the quantity of sorbent that is required for desulphurisation.

In the study conducted by Svoboda et al. (1988), it was reported that there was an increase in SO_2 removal with an increase in molar ratio. This can clearly be seen in Figure 2-4 and Figure 2-5. Four types of sorbents – limestone, CaO, magnesite and MgO were used in their investigation. With each type of sorbent in Figure 2-4 and Figure 2-5 there was a distinct increase in SO_2 removal as the molar ratio increased. In Figure 2-4 it can be seen that CaO (calcined limestone) was a much better sorbent when compared to the original limestone. Figure 2-5 shows that magnesite was a better sorbent than MgO (calcined magnesite). From Figure 2-4 and Figure 2-5 it can be seen that the efficiency of the magnesite in Figure 2-5 is almost equivalent to the efficiency of the limestone in Figure 2-4. This is quite interesting as it indicates the similarity in the performance of sorbents with different compositions at a bed temperature of between 750 and 850°C.

12
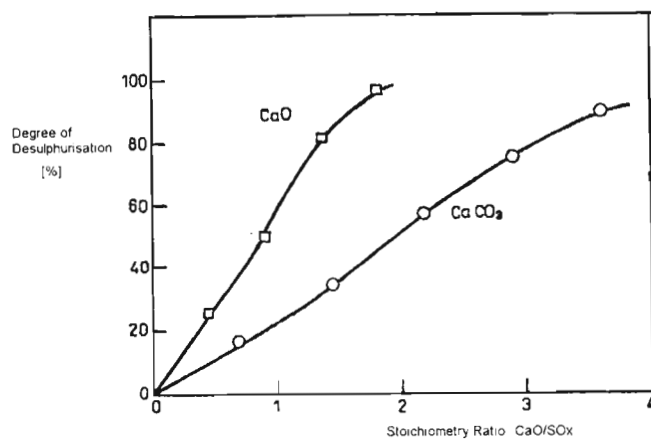
Figure 2-4 Relationship of Degree of Desulphurisation vs. Ca/S molar ratio, Svoboda et al.
(1988)
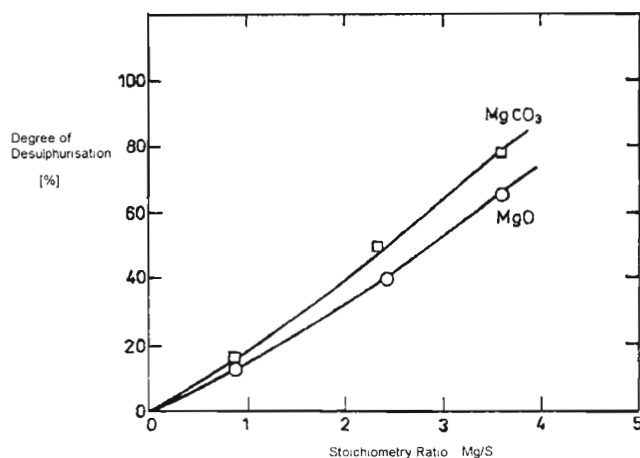
Figure 2-5 Relationship of Degree of Desulphurisation vs. Mg/S molar ratio, Svoboda et al.
(1988)

Svoboda et al (1988) stated that with the increase in molar ratio and the increase in the quantity of sorbent, there was a period when this increase was not economically feasible. They explain that this was as a result of a decreasing rate of reaction of SO_2 with the sorbent at the low concentrations of SO_2.

Particle Size

Sorbents particle size is an important property that has a significant influence on the sorbents ability to remove SO_2. For the sorbents particle size, a situation arises as to the importance of either a higher flue gas SO_2 removal or a higher sorbent calcium carbonate conversion.

Many reports (Lyngfelt and Leckner (1999), Ozer et al. (2002), Chu et al. (2000)) have concluded that for a high SO_2 removal efficiency, large quantities of sorbents are required which have a low calcium conversion. For higher calcium conversion, the opposite is true whereby less sorbent is required with a lower SO_2 removal efficiency.

For the desulphurisation process, many researchers have found different reaction resistances for sorbents that were dependant on both temperature and particle size. According to Adanez et al. (1994a,b) at high temperatures when the sorbent particle size increases, the principal resistance to the reaction changes from pore diffusion and surface reaction to diffusion through the $CaSO_4$ layer. Hartman et al. (1976) found that at low temperatures (590 to 680°C) the overall reaction rate was controlled by the chemical reaction taking place on the surface of the sorbent.

Figure 2-6 shows the molar calcium to sulphur ratio of the sulphated sorbents as determined in the laboratory reactors for various size fractions tested by Pisupati et al. (1996). From this figure it can be seen that there was an increase in the sorbent quantity requirement with increasing the particle size from 150-500 μm to 500-1000 μm. Those sorbents that were above 150 μm were tested in a Bench-Scale Fluidised Bed Reactor (BSFBR) and those that were less than 150 μm were tested in an Entrained Flow Reactor (EFR). This was consistent with Chu et al. (2000) and Chi et al. (1994). Figure 2-6 indicates a better performance by the finer material which is in agreement with the concept that gas-solid contact efficiency improves as the particle size decreases although it is not directly proportional to the increase in the surface area.
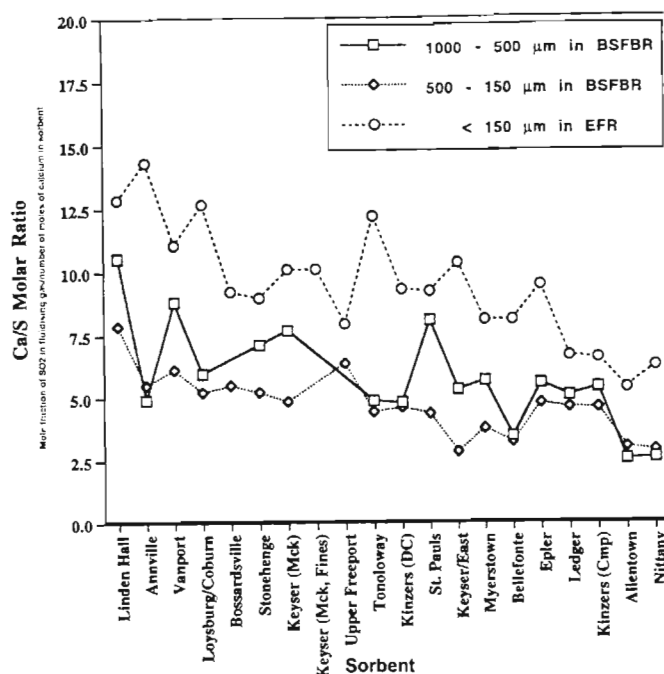
Figure 2-6 Calcium to Sulphur Molar Ratio of Various Size Fractions of Sulphated Sorbents, Pisupati et al. (1996)

Chi et al. (1994) reported that with an increase in the particle size there were larger unsulphated sorbent cores, which reduced conversion and limited the extent of sulphation. They found that for fluidised bed reactors there was an optimum particle size for sorbents that is dependant on the grade efficiency of the dust collection equipment (cyclone, etc.) and the sorbents reactivity dependency on size. They go on to say that the optimum size may be crucial to the optimum operation of the plant.

According to Pisupati et al. (1996), sorbent particles that were below the optimum particle size had insufficient contact time to react with SO_2. If the particles were fluidised above their terminal velocity, it was found that they were elutriated from the fluidised bed reactor before they had time to be fully sulphated. This often led to the premature removal of unreacted sorbent from the system, which is consistent with the findings of Chi et al. (1994). They found that sorbents below optimum size were more reactive, with a higher susceptibility to entrainment, which decreased the overall sulphur capture efficiency.

Chu et al. (2000) reported that with an increase in the particle size there was an increase in sorbent conversion in the cyclone due to attrition and a decrease in the instantaneous SO_2 reduction in the fluidised bed combustion chamber. The decrease was due to the decreasing particle surface area during the sulphation reaction and the plugging of the surface pores by the

15

formation of a calcium sulphate product layer that creates a SO_2 diffusion limitation. However, it is known that larger particles (>1000μm) have the tendency to remain in the bed longer and therefore are more susceptible to attrition and abrasion thus permitting further sulphation to the core of the sorbent particles.

In the FBC process, the particle size of the limestone and dolomite has a significant effect on both residence time and reactivity of the sorbent. From the time the sorbent enters the reactor until it leaves, there is a significant reduction in the particle size of the sorbent (Lyngfelt and Leckner (1999)). There is a rapid reduction in size during the calcination process due to the sorbents becoming softer and porous thus fragmenting. Thereafter during the sulphation process the reduction in size is slow. This is due to abrasion and attrition of the sorbent with the bed material, other sorbents and the reactor walls.

Lyngfelt and Leckner (1999) reported that the residence time of sorbents were largely dependent on boiler design, cyclone efficiency, riser height, etc. This was also found to be the case by Pisupati et al. (1996). Lyngfelt and Leckner (1999) found that the residence time of sorbent particles increases with an increase in sorbent particle size. This can result from anything between a few seconds for the particles smaller than the cut-size of the cyclone, up to a point where the particles are so large that they are not able to leave the system as fly ash. The particle size remaining in the reactor is normally the optimum size for sulphur capture as it spends the most amount of time in the reactor thus ensuring larger sulphur capture (Lyngfelt and Leckner, (1999)).

2.2.2. Influence of Physical and Chemical Properties

This section discusses the physical and chemical properties of the sorbents that affects the desulphurisation process. The analysis used to determine these properties are:
1) The chemical analysis
2) Petrographical analysis, and
3) Hardgrove Grindability Index.

Chemical Analysis

The composition of limestones is predominantly calcium carbonate whereas dolomites are a calcium magnesium carbonate combination. Dolomites are classified according to the amount of magnesium carbonate compared to calcium carbonate that is present in the rock.

16

Haji-Sulaiman et al. (1990) and Adanez et al. (1994a) found that the optimum temperature range that fluidised bed reactors should operate at was 800 to 900°C. Magnesium sulphate has been found to be unstable above a temperature of 760°C and therefore at the temperature range that fluidised bed reactors operate at, little to no magnesium sulphate is produced.

For the past forty years that fluidised beds have been investigated there has been a misconception that only pure limestone ($CaCO_3 > 95\%$) could be used to reduce SO_2 emission levels, (Adanez et al. (1994)). According to Pisupati et al. (1996) the use of the content of calcium carbonate present in the sorbent is not a significant predictor of sorbent reactivity. Figure 2-7 is a graph of the average sorbent requirement as a function of calcium carbonate, and it clearly shows that the calcium carbonate content was not a good indicator of sorbent requirement for a given level of sulphur capture.
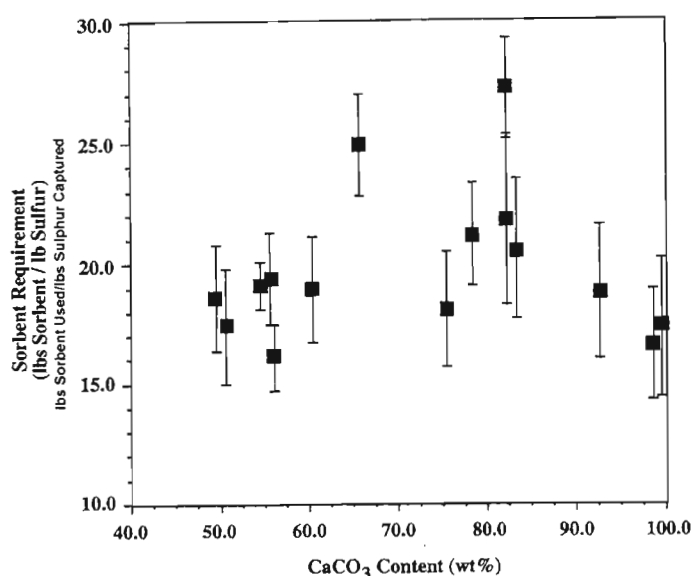
Figure 2-7 Effect of Calcium Carbonate content, Pisupati et al. (1996)

Haji-Sulaiman et al. (1991) reports that naturally occurring limestone and dolomites generally contain impurities, varying from less than 1% to as high as 20%. Most of these impurities are in the form of quartz and clay minerals, with the presence of others such as manganese oxide, copper oxide and iron oxide as trace elements. This variation with respect to chemical composition and the number of species present were found to be largely dependant on the location from which the stone was quarried. They found that during sulphation the presence of impurities delayed pore closure during the formation of $CaSO_4$, and hence higher calcium utilisation was achieved from the lower purity materials. He concluded that these impurities act as structural modifiers during calcination to produce CaO with different physical properties that exhibited different reactivity on sulphation. These results indicated the catalytic effect of

17

impurities. This was consistent with work conducted by Alvarez and Gonzalez (1999) and Ozer et al. (2002).

Haji-Sulaiman et al. (1991) explained that the reason for the higher sulphation with the presence of impurities was due to the delay in the blockage of the pores. They suggest that an improved sorbent utilisation can be achieved by the combination of physical properties together with the amount of impurities present in the sorbent.

The sulphation performances of one precalcined dolomite (DM1) and two precalcined limestones (LS2, LS3) that were investigated by Haji-Sulaiman et al. (1991) are compared in Figure 2-8. In this experiment the performance of the dolomite calcine was superior to that of the two calcium limestones. At the highest residence time investigated (90 minutes) the calcium utilisation achieved by the dolomite was 65% as compared to 20% and 10% obtained for LS2 and LS3 respectively. Therefore the calcium utilisation increased as the impurity level of the sorbent increased.
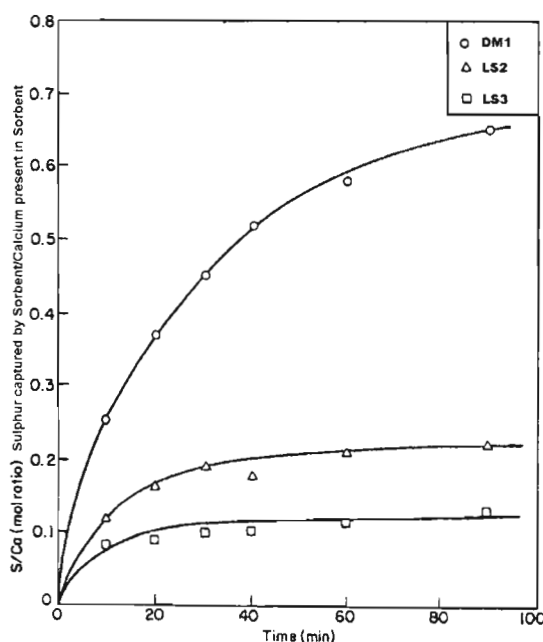
Figure 2-8 Effect of impurity content on the sulphation behaviour of precalcined sorbents, Haji-Sulaiman et al. (1991)

Alvarez and Gonzalez (1999) found that dolomites where much more reactive than the limestones due to the dolomites having a more open porous structure thus ensuring that the calcium utilisation was more effective.

18

Petrographical Analysis

Petrography is the branch of geology that deals with the systematic description of rocks in hand specimen thin sections. It is defined as the 'science of the description or classification of rocks' (Coal Utilisation Center Research Activities (2002)). This description or classification is based on texture, structure and composition, which is a reflection of its geological history. The overall objective of petrographical analysis is to identify the behaviour of various petrographical constituents during calcination and sulphation.

Pisupati et al. (1996) used a scanning electron microscope to determine the sulphur distribution maps of sorbents and to determine the sorbents structure in closer detail. He found that the majority of the sulphur captured was concentrated along well defined reaction rims along the boundaries of grains and particles. He concluded that with $CaSO_4$ having a higher molar volume, the pores tend to block, which does not allow the diffusion of SO_2 molecules to the interior of the particle thus limiting calcium utilisation. This finding is consistent, as many researchers Morrison et al. (1990) and Hartman et al. (1976) have made the same conclusion. Hartman et al. (1976) concluded from their research that the carbonate rocks and their calcines with large pore volumes and small grain sizes would be better suited for the SO_2 sorption reaction than dense, coarse grained limestones.

Pisupati et al. (1996) also found on the sulphur distribution maps, Thermally Induced Fractures (TIF) on the surface of the sorbent particles. They concluded that the TIF generated during calcination aided in sulphur capture.

Petrographic variability influences the crushing of the sorbents by allowing the sorbent to break along 'planes of weakness'. The pertrographic variability of the sorbent influences sorbent performance by promoting the formation of TIF.

Hardgrove Grindability Index (HGI)

HGI is an indication of the softness or hardness of rocks. This value helps in the determination of how easily the sorbents can be crushed into their optimum particle size range for their use in a fluidised bed reactor.

Schmitz (1996) found that the HGI of the sorbents provided no relationships to distinguish between a good sorbent and a bad sorbent. However he did find that the HGI was an important indication for the milling performance and milling cost of the sorbents.

19

As the HGI value increases, the material becomes softer. A good sorbent is a rock that is neither too soft nor too hard. If the sorbent is too soft, it can easily undergo rapid attrition in the fluidised bed reactor and is therefore vulnerable to high rates of elutriation out of the reactor. Conversely, if the sorbents were too hard, then they become difficult to crush and would thus increase maintenance and production cost.

2.3. Experimental Equipment for Testing Sorbents

There have been numerous studies that have investigated the properties of sorbents that affect the desulphurisation process. However, most of this research has used different types of equipment. Adanez et al. (1994b) and O'Neill et al. (1979) found that the equipment used in sorbent evaluation plays a vital role in the determination of their SO_2 reduction.

There are many different techniques and equipment that have been developed for the evaluation of sorbent SO_2 absorption capability. These are as follows:
- Laboratory fluidised bed reactors (bubbling, circulating and pressurised)
- Pilot fluidised bed reactors (bubbling, circulating and pressurised), and
- Thermogravimetric analysers (TGA).

From literature (Chi et al. (1994), Pisupati et al. (1996), Adanez et al. (1994a)), the most popular technique used to determine sorbent reactivity is the laboratory bubbling fluidised bed reactors and TGA.

Adanez et al. (1994a) reports that to obtain good sorbent characterisation, the method used must reproduce as efficiently as possible the behaviour of the sorbent in a fluidised bed combustion chamber, where the phenomena of calcination and sulphation take place simultaneously. They found that characterisation in a batch fluidised bed was able to reproduce both the physical and chemical phenomena that takes place in a fluidised bed combustor. Thus a conclusion was made that the processes such as thermal shock, decrepitation, attrition and calcination-sulphation, occurs both in the characterisation testing and in the full-scale combustion chamber. For the parameters that are to be investigated in this study, Adanez et al. (1994a,b) have shown that bubbling fluidised bed reactors is a better option as compared to TGA analysis.

According to Adanez et al. (1994b), sorbent requirements predicted by a fluidised bed sulphur retention model produced inaccurate results and was dependant on the method and working conditions used to determine characterisation parameters of the sorbent. The comparisons that

they made showed the need for characterisation of sorbents by batch fluidised bed reactors. This was consistent with Romans et al. (1993).

Chi et al. (1994) made a comparison of the different measurement techniques for limestone reactivity using the measured values of the final conversion. This can be seen in Table 2-1 below. The sorbent size was 500 to 1000 μm and the sulphation temperature was 850°C. He noticed that the data from the Quartz Wool Matrix (QWM), Bubbling Fluidised Bed Reactor (BFBR) and Turbulent Fluidised Bed Reactor (TFBR) were close but the data from the TGA were substantially lower than those of the other three methods. They suggested that this was due to the fact that during TGA testing the sorbent particles are in a packed state hence the gas-solid contact was not good. He also states that the minor differences between the data from the QWM, BFBR and TFBR were attributed to the difference between the gas-solid contact and sorbent attrition in the reactor.

Table 2-1 Final conversion (%) at 850°C using different measurement techniques, Chi et al. (1994)

QWM	BFBR	TFBR	TGA
45.06	46.83	47.50	37.34

A disadvantage found by Adanez et al. (1994b) when using a fluidised bed reactor for characterisation testing was the inability to extrapolate results to other conditions. This meant that the results from one type of fluidised bed reactor could not be directly compared to another, which is not of the same type, size and shape.

The major advantages found by Adanez et al. (1994b) in using a fluidised bed:
1. The tumbling action of the coal with the sorbents allows for the capture of the sulphur whilst it is being released from the coal
2. The 'cooler' burning of the coal reduces the formation of NO_x, and
3. The attrition rate of the sorbents with other sorbents, walls of the reactor and coal removes the product layer during the sulphation process and thus increases the utilisation of the calcium sorbent.

The TGA is a simple and effective method for sorbent evaluation, but it overlooks the physical mixing process involved in fluidised bed combustors. Another disadvantage of using TGA sorbent measurement analysis is that it can only be used for small sample quantities. This results in a selective process and is not a true representation of the entire sorbent.

New equipment is continuously being designed and developed for the determination of the most effective way to evaluate available sorbents for the desulphurisation process. However, due to the many methods used for the characterisation of sorbents, Anthony and Granatstein (1999), O'Neill et al. (1979), Chu et al. (2000) found that a comparison of results was difficult.

2.4. Summary

The following are important points that were obtained from this literature review:

- Many researchers have found that there is an optimum temperature at which fluidised bed desulphurisation occurs. This was found to occur between the temperature range, 800 to 900°C. The present study aims to establish the optimum temperature for the sorbents tested.

- Researchers have shown that for an increase in the Ca/S molar ratio, there is a requirement of either an increase in the quantity of sorbent or the use of sorbents with higher calcium content. This study will determine whether this phenomena is present for South African sorbents and establish the optimum Ca/S molar ratio for each sorbent.

- Several reports and publications have shown that for each sorbent there is an optimum particle size for desulphurisation. The optimum size of the sorbents will be determined in this study.

- Conflicting reports were obtained with regards to the importance of the chemical analysis in predicting sorbents desulphurisation capability. This study aims to determine the relevance of chemical analysis in predicting desulphurisation performance of sorbents.

- Some researchers investigated the contribution of petrographical analysis towards desulphurisation. This will be investigated further in this study.

- The influence of Hardgrove Grindability Index on desulphurisation performance is not known. This will be considered during this study.

- An increase in fluidisation velocity has an adverse effect on the desulphurisation process. There is a higher rate of attrition between sorbents, bed material and the reactor walls; however the high fluidisation velocity elutriates the finer sorbent particles thus reducing desulphurisation efficiency.

- For this study, the Bubbling Atmospheric Fluidised Bed Reactor (BAFBR) was chosen over TGA analysis as the method for sorbent evaluation. The BAFBR was able to simulate hydrodynamic conditions similar to that present in a Fluidised Bed Combustor.

Chapter Three

Stratigraphy of South African Limestone and Dolomite Deposits

3.1. Introduction

"It is essential for any modern industrial community to have a good supply of limestone and dolomite, conveniently situated and of a suitable quality and quantity." This statement by Martini from Coetzee, (1976) places great emphasis and significance on the quantity, location and quality of the limestone and dolomite deposits that would be used by industrial countries. The use of limestone and dolomite for the Flue Gas Desulphurisation (FGD) and the Fluidised Bed Combustion (FBC) processes is no exception.

Chapter two described in detail the literature survey of flue gas desulphurisation with respect to the limestone and dolomite process variables, physical and chemical properties and operational properties of fluidised bed test equipment. This chapter was included to add more clarity into the geology of sorbents and their possible impacts on the desulphurisation process by discussing the resources and stratigraphy of sorbent deposits in South Africa.

3.2. Limestone and Dolomite Resources

A map of the distribution of the commercially mined limestone and dolomite deposits in South Africa has been compiled by Coetzee (1976), which is shown in Figure 3-1. On this map it can be seen that limestone and dolomite deposits are scattered throughout South Africa's nine provinces. Coetzee (1976) mentioned in the statement from section 3-1 above that sorbents should be located near the place at which it is utilised. The current location of sorbent deposits throughout South Africa creates an economical problem with respect to their use at South Africa's power stations.

23
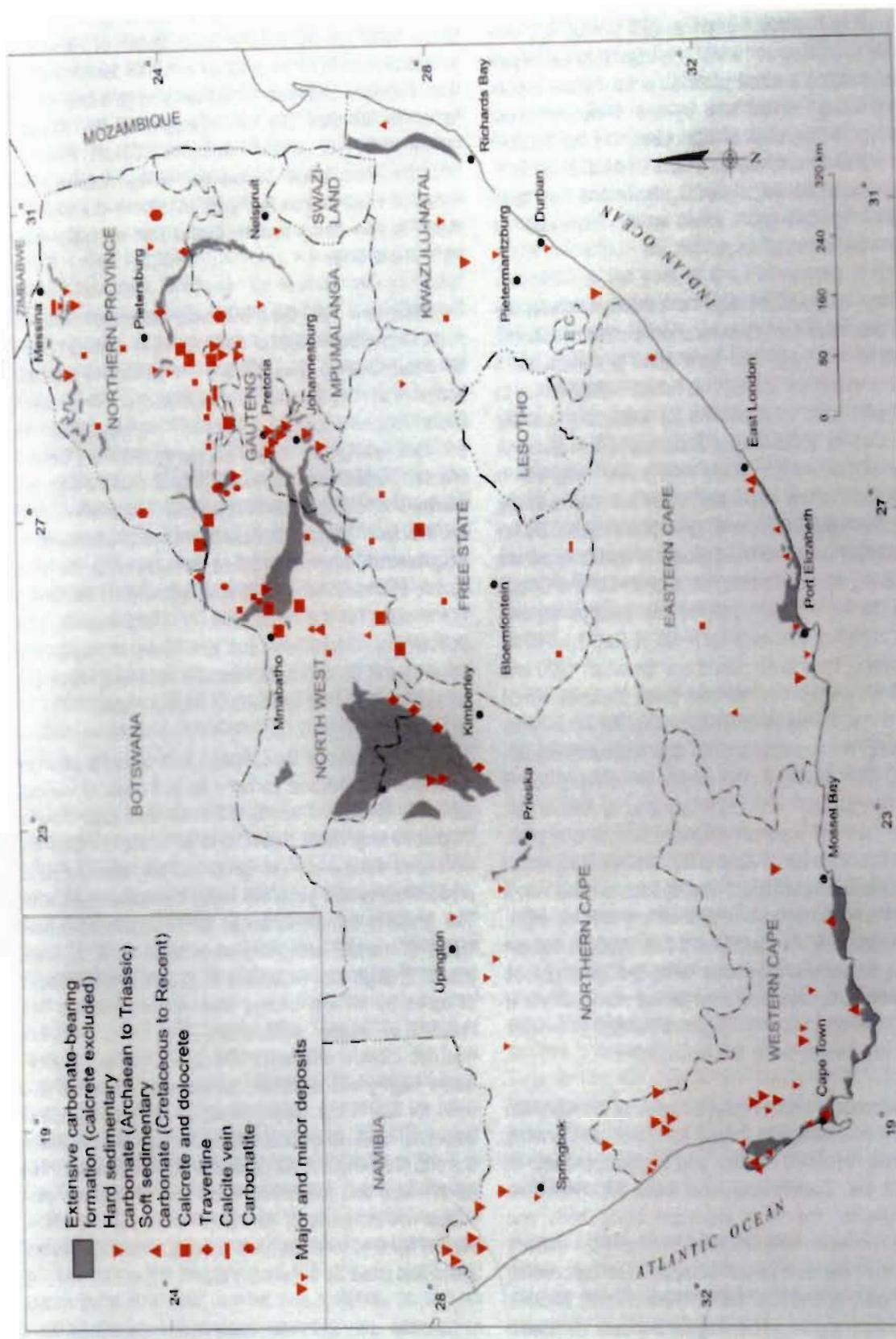
Figure 3-1 Map of commercially mined Limestone and Dolomite in RSA, Coetzee (1976)

24

A map of the power stations in South Africa is shown in Figure 3-2. This map shows that the coal baseline power stations are located in three provinces in South Africa, viz. Mpumalanga, Free State and Limpopo (Northern Province). This is due to large coal resources being situated in these regions. Since desulphurisation of flue gases would be implemented at current and potentially new power stations located close to the coal resources, our study was focussed on limestone and dolomite deposits in these provinces. This was employed with the intention of reducing transportation costs of sorbents from the mines to the power stations.
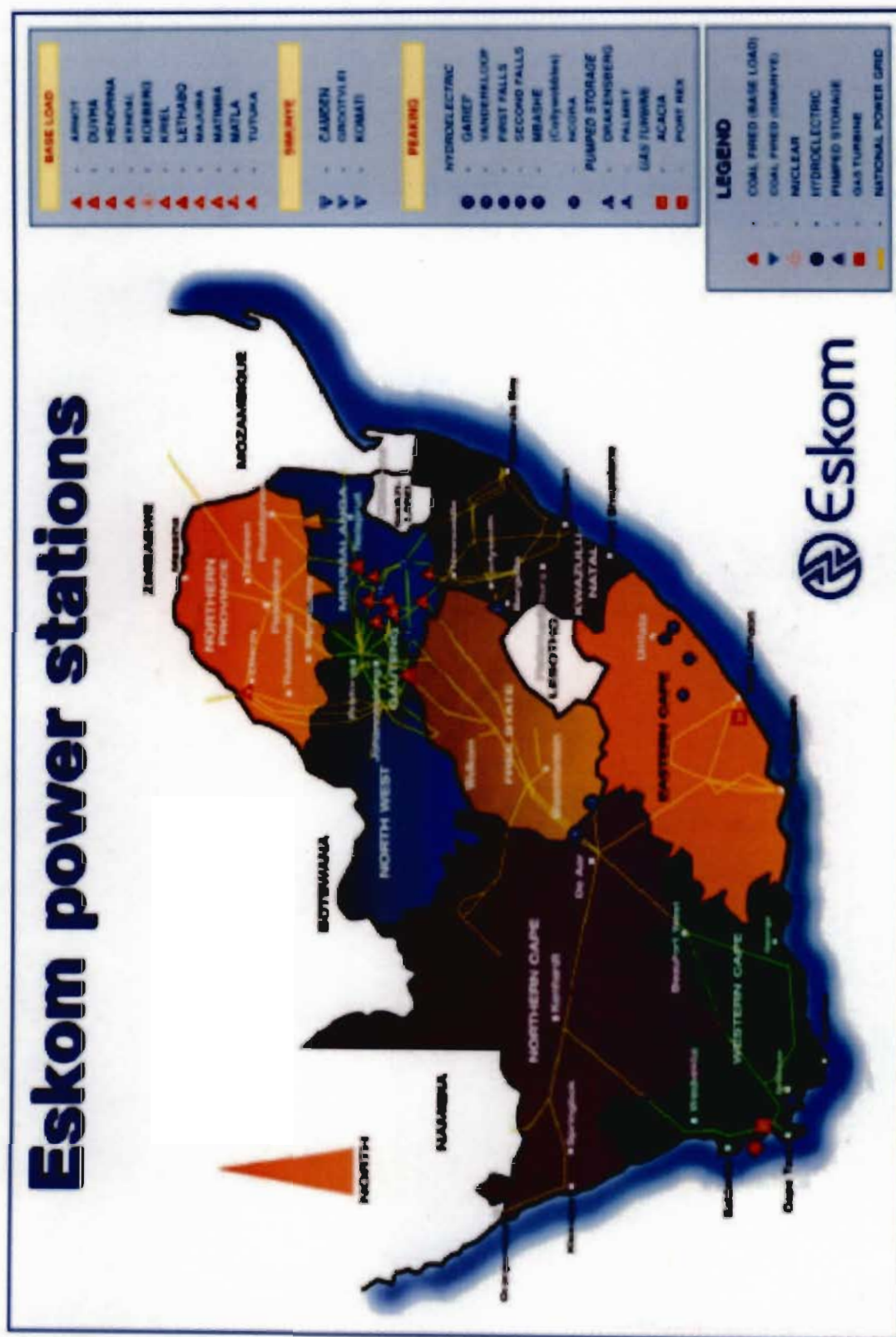
Figure 3-2 Map of Electricity Power Stations in RSA, Eskom – Power Stations (2006)

There are various types of limestone and dolomite deposits in South Africa, Coetzee (1976). These deposits can be classified by the following five categories:

- Sedimentary carbonates
- Calcrete and dolocrete
- Travertine
- Cave limestones and vein deposits, and
- Carbonatites.

Sedimentary carbonate is of a highly variable grade which constituents South Africa's major resource of limestone and dolomite whilst the other categories are small but still significant.

The following are explanations for the formation of calcrete (Coetzee (1976)):

- The precipitation of calcium carbonate owing to the decomposition of the unstable soluble bicarbonate upon evaporation or some other factor, which disturbs the equilibrium after the bicarbonate solution has found its way to the surface either by capillary attraction or along subsurface drainage.
- Accumulation of calcium carbonate in the soil, which forms when carbonate-rich ground water is drawn to the surface during long dry periods in semi-arid climates and evaporates there, precipitating its salts and minerals. It may contain variable amounts of magnesia and when dolomite is dominant it is termed *dolocrete*.
- The leaching of basic lavas and intrusions. This results in the formation of calcretes with higher magnesia and silicate contents than those formed from other sources.

Travertine has been found by Coetzee (1976) to develop on the slopes of the escarpments through precipitation from surface water whilst he found that carbonates resulted from the intrusion or extrusion of carbonate-rich magmas associated with alkaline complexes.

The quantity of limestone and dolomite varies throughout South Africa, Coetzee (1976). In the Slurry region of the Northern West Province an estimated resource of one hundred million tons of calcrete was developed over a 200 km^2 plain. Twenty kilometres northwest of Northam in the Limpopo Province, a resource of limestone in excess of fifty three million tons was uncovered. Near Chuniespoort in the Northern West Province fifty million tons of dolocrete occurs which is generally magnesia-rich. In the Lichtenberg region of the Northern West Province, the resources of good quality limestone and dolomite are in the range of about five hundred million tons.

In 1994, some 16.419 million tons of limestone was produced of which 87% was sold (Coetzee (1976)). The majority of that sold was used in the cement industry. In the same year, 3.129 million tons of dolomite was produced of which only 69% was sold. The major sale of dolomite was to the agriculture industry. The limestone and dolomite that was not sold was lost during product extraction, product preparation and product sale.

In 2003, 16.6 million tons of limestone was sold to the cement, metallurgy and agriculture industries (Coetzee (1976)). In the same year 2.869 million tons of dolomite was sold to metallurgy, construction and agriculture industries. As can be seen from the difference between 1994 and 2003 there was an increase in limestone and dolomite sale to industries. With the implementation of the desulphurisation process, there would be an even greater increase in production of limestone and dolomite.

3.3. Stratigraphy of Limestone and Dolomite deposits

In the provinces of Mpumalanga, Gauteng and Northern Province, the stratigraphic distribution of limestone and dolomite is in the Transvaal Supergroup, Kent (1980). The age of this supergroup ranges from between 2200 and 2400 millions years. The Transvaal Supergroup is divided into four groups viz. Wolkberg, Chuniespoort/Malmani, Pretoria and Rooiberg. Table 3-1 gives a detailed description of each group, showing information with respect to their distribution of age, formation, lithology and thickness of formations in the subgroups.

Table 3-1 Lithostratigraphic subdivision of the Transvaal Supergroup, Kent (1980)

AGE	GROUP		FORMATION	LITHOLOGY	Thickness (m)
	Rooiberg		Smelterskop Quartzite	Alternating andesitic lava and quartzite	
			Leeuwpoort	Blaauwbank Shale	400
				Boschoffsberg Quartzite	
	PRETORIA		Rayton	Beynestpoort Quartzite	1200
				Silty shale, andesitic lava	
				Feldspatic quartzite	
				Shale	
				Quartzite	
				Subgraywacke and shale	
				Baviaanspoort Quartzite	
				Shale and quartzite	
			Magaliesberg Quartzite	Orthoquartzite	0 - 300
				Quartzite	
			Silverton Shale	Silty and graphitic shale with thin interbedded limestone	300 - 600
				Hornfels	
			Daspoort Quartzite	Orthoquartzite	80 - 190
				Shale and siltstone	
			Strubenkop Shale	Iron-rich shale and siltstone	105 - 130
				Iron-rich quartzite	
				Conglomerate	
2224 +/- 21 million years			Hekpoort Andesite	Andesitic lava, agglomerate and tuff	280 - 550
				Conglomerate, tuffaceous quartzite and shale	
				Amygdaloidal	
			Timeball Hill	Shale	270 - 660
				Diamictite	
				Klapperkop Quartzite wacke and ferruginous quartzite	
				Graphitic and silty shale	
			Rooihoogte	Quartzite	10 - 150
				Shale	
				Bevets Conglomerate Member	
				Breccia	
	CHUNIESPOORT		Penge	Iron Formation	320
		Malmani Subgroup	Frisco	Chert – free dolomite	30
			Eccles	Chert – rich dolomite with large and small stromatolites	380 - 490
			Lyttelton	Dark chert – free dolomite with large elongated stromatolitic mounds	150 - 290
			Monte Cristo	Light coloured recrystallised dolomite with abundant chert, stromatolitic, basal part oolitic	700 - 740
			Oaktree	Dolomite, becoming darker upwards, chocolate coloured	200 - 330
2318 +/- 17 million years	WOLKBERG		Black Reef Quartzite	Feldspathic quartzite and shale	0 - 500
				Arkosic grit	
				Conglomerate	
			Sadowa Shale	Quartzite	0 - 150
				Shale, mudstone	
			Mabin Quartzite	Feldspathic quartzite, some subgraywacke	0 - 100
			Selati Shale	Shale	0 - 1000
				Argillaceous quartzite, subgraywacke and carbonate	
			Schelem	Sericitic quartzite, subgraywacke	0 - 140
				Shale	
				Arkose	
				Conglomerate	
			Abel Erasmus Basalt	Basalt, pyroclastics	0 - 500
				Sericitic quartzite, arkose, subgraywacke	
				Basalt	
				Dolomitic shale	
			Sekororo	Arkose	0 - 240
				Shale	
				Sericitic quartzite, subgraywacke	
				Conglomerate	

From Table 3-1 it can be seen that the Wolkberg Subgroup consists mainly of quartzite with lenses of grit and shale, which is overlying with dolomite. The Chuniespoort/Malmani Group includes dolomite, limestone, chert, and iron formation whilst the Pretoria and Rooiberg Group consists predominantly of quartzite and shale. A detailed description of the subgroup formations found in this supergroup is given on a map in Figure 3-3.
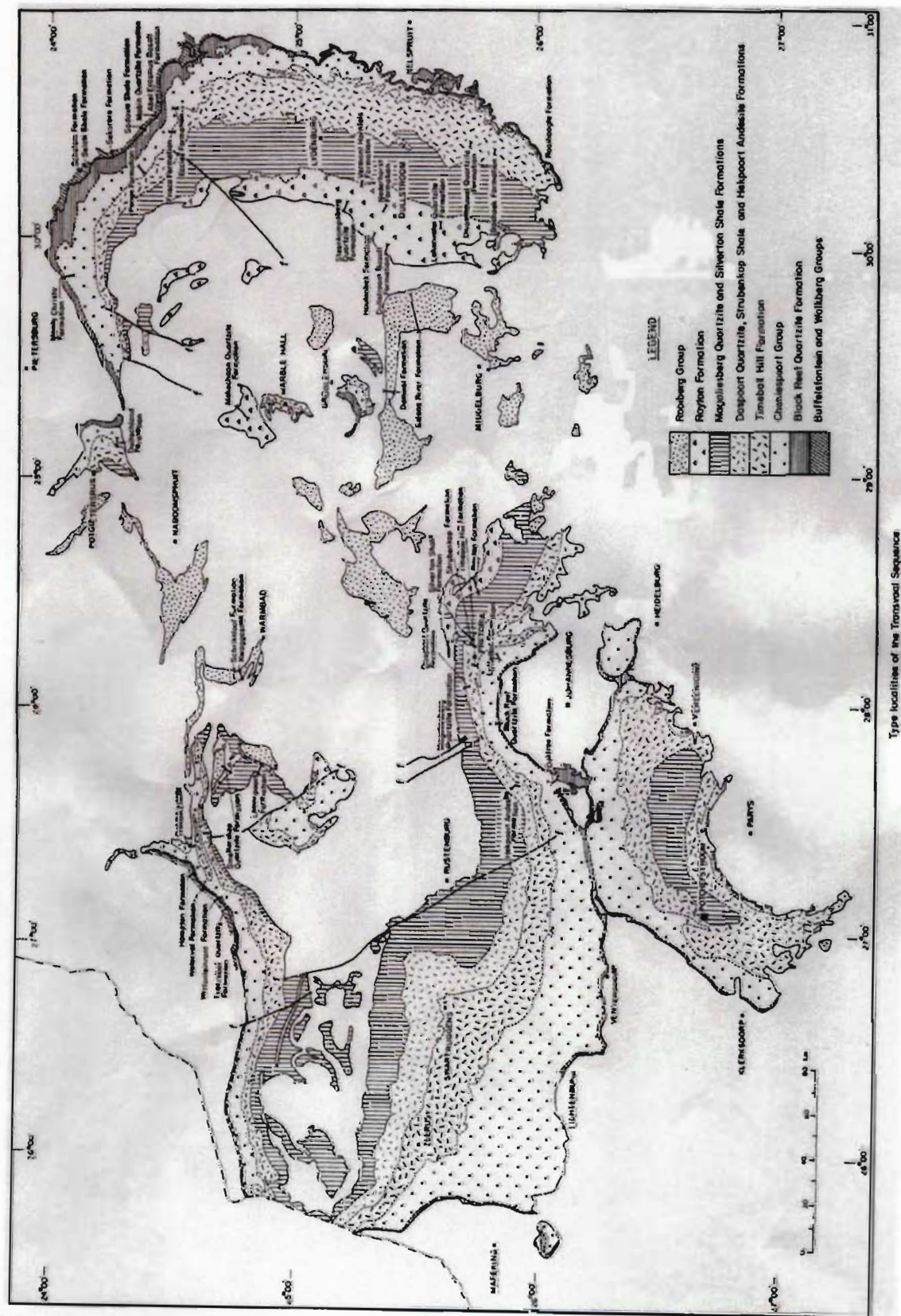
Figure 3-3 Type localities of the Transvaal Supergroup, Kent (1980)

Most limestone and dolomite in the Transvaal Supergroup originated by the precipitation of calcium carbonate from fresh or seawater aided directly or indirectly by organisms, or by the accumulation of calcareous organic remains (Kent (1980)).

Coetzee (1976) reported that the limestone and dolomite that forms part of the Chuniespoort/Malmani subgroup was severely metamorphosed by the Bushveld Igneous Complex.

Anthony et al. (1999) found that sorbents obtained from different locations within the same quarry can exhibit different SO_2 absorption properties. This creates a high degree of variability among sorbents. The variability can be attributed to the differences in depositional and post depositional histories of the sorbents.

South Africa's limestone and dolomite are approximately 2200 to 2400 millions years old as compared to limestone and dolomite from the European and American countries which are 100 to 300 million years old. During this additional period of time, the South African deposits have undergone several tectonic events and recrystallisation, which altered many of their original features. After each recrystallisation process, the sorbents were converted from a porous sorbent into much more compact varieties.

The European and American limestone and dolomite deposits were also found to have undergone digenesis (shallow burial) and were not subjected to temperatures above 300°C. Being much older, the South African carbonate rocks have undergone in addition to digenesis, metamorphism and tectonism involving much deeper burial and temperatures up to 800°C. This extended time and temperature regime has recrystallised the carbonate component of the rocks and converted most of the silicate minerals into higher temperature forms as well as dehydrating primary clay minerals.

In Chapter 2 section 2.2.1, it was found that one of the requirements for effective desulphurisation to take place is for the sorbents to be highly porous. With old limestone and dolomite, recrystallisation decreases their porosity, thus making them less suitable for desulphurisation. Therefore it would be necessary to determine the most suitable sorbent in South Africa that would be able to perform the desulphurisation process.

3.4. Observations of Chapter Three

- Limestone and dolomite resources have been found to be scattered throughout South Africa with little to no sorbent resources located near South African coal resources. To reduce transportation costs of sorbents from the mines to current and potentially new power stations, focus will be placed on sorbents that are commercially mined close to these coal resources.
- There are various categories of limestone and dolomite with high degrees of variability with respect to their chemical composition and physical properties. Due to their difference in performance, it was found that the best method in determining the sorbents desulphurisation ability was by experimental methods, which will be discussed in the chapter that follows.

Chapter Four

Sorbent Sample Preparation and Evaluation

4.1. Introduction

The following are the current applications of limestones in South African industries:
- In the manufacture of cement
- In water treatment and purification, etc.
- Manufacture of paper, rubber, paint, etc.
- Purification of juices in the sugar industry, Coetzee (1976).

Whereas the applications for dolomites in South African industries are as follows:
- In agriculture where it is used as a fertiliser and to neutralise acid soils
- A form of flux in the production of pig iron and non-ferrous metals
- Together with soda ash and silica sand in the manufacture of glass, Coetzee (1976).

The mining of limestone and dolomite is controlled by local demand and the availability of the resources. The use of limestone and dolomite for the desulphurisation of flue gas during electricity generation at power stations would result in an increase in limestone and dolomite production.

Chapter three described the stratigraphy and resources of the limestone and dolomite formation in South Africa. This chapter discusses how the sorbent samples were obtained, their preparation for the different chemical and physical tests and the results of these tests.

4.2. Sourcing Limestones and Dolomites for the Study

The Department of Minerals and Energy (DME) publishes a directory (Department of Minerals and Energy, 2002) which lists the producers of industrial minerals commodities in South Africa. The directory contains all the mining companies in South Africa that commercially mine minerals, including limestones and dolomites. The directory states the type of operation that is used for limestone and dolomite mining, the use of the limestone and dolomite and the chemical analysis together with the specifications of the limestone and dolomite that is produced. The directory was used as the starting point to identify possible limestone and dolomite mining companies that would be of relevance to our study.

At this point of the thesis, a review of the aim of this study is necessary. The aim of this study was to evaluate potential commercial sorbent sources in South Africa that could potentially be used for the reduction of SO_2 released into the atmosphere during fluidised bed combustion of coal. In South Africa there is one large national electricity utility company, Eskom, which produces more than ninety percent of the electricity used in South Africa (2004 Eskom Annual Report) and is a net exporter of power to neighbouring African countries. Our research concentrated on areas in close proximity to mineable coal resources and locations of substantial coal mine dumps.

Schmitz (1996) and O'Neill et al. (1979) found that transportation of sorbents from the mines to the power stations had a substantial effect on the overall running cost of the power stations. It was therefore necessary to find sorbent mines of adequate quantity and quality in close proximity to Eskom current and future power stations to minimise the costs for the desulphurisation process. The location of coal resources together with sorbent mines in South Africa can be seen in Figure 4-1. From this map it can be seen that most of the coal resources are in the northern regions of South Africa, which lies in the Limpopo, Mpumalanga and Free State provinces. The Highveld, Southrand, Sasolburg-Vereeninging and Ellisras Coalfields have several limestone producers on and around their coalfields. However, these coalfields are currently not considered economically feasible to mine.
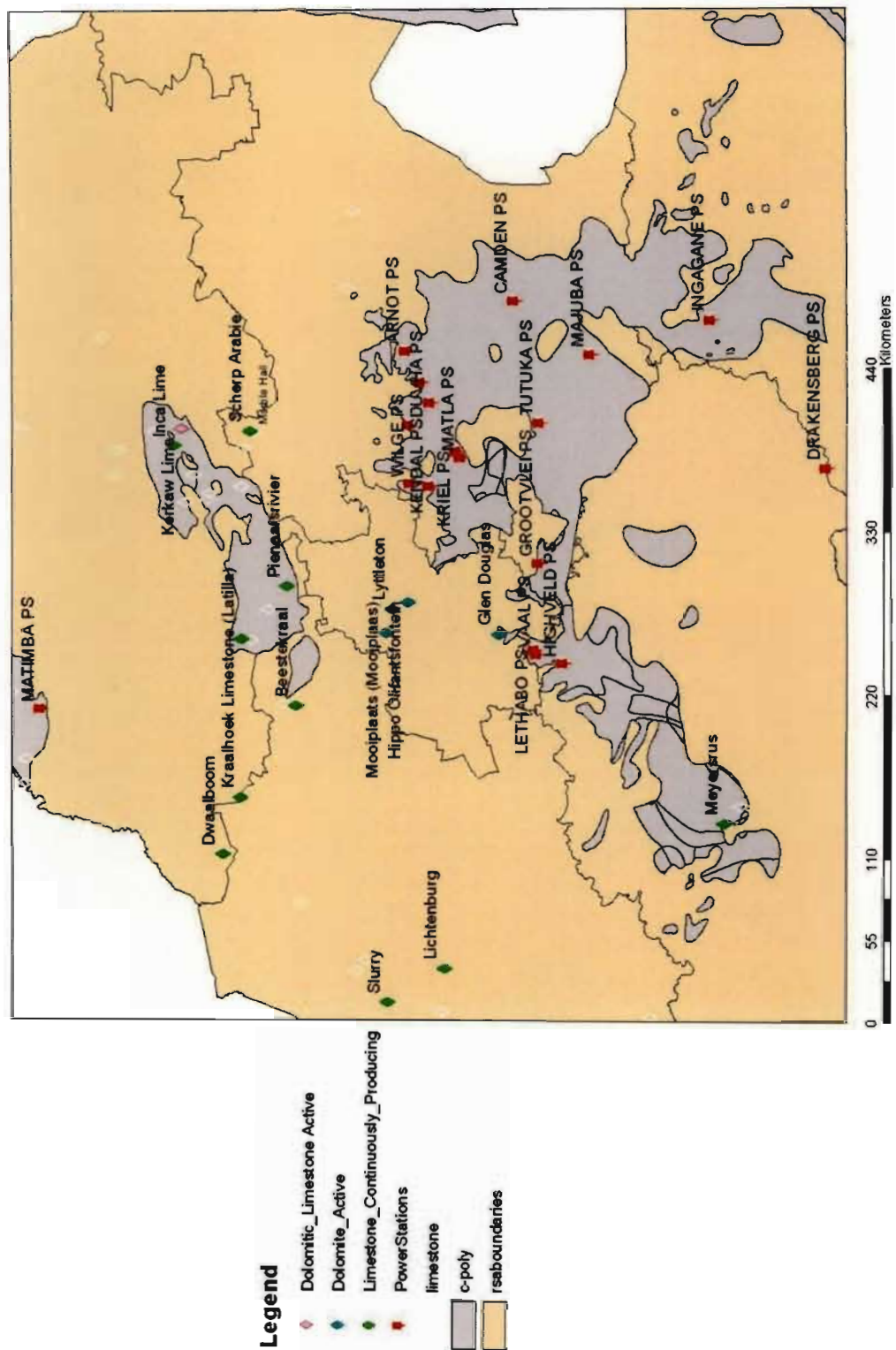
Figure 4-1 Map of Coalfields, Power Stations and commercial Limestone and Dolomite producing mines

The limestone and dolomite sample search was concentrated in a two hundred kilometre radius of all Eskom power stations, which lie on or in the vicinity of the minable coal resources in South Africa. This eliminated many limestone and dolomite mines, as they are located in the southwestern regions of South Africa, namely Western, Eastern and Northern Cape Provinces. This reduced the number of limestone and dolomite mines from forty-three in the DME directory to sixteen. The mines were contacted for a supply of fifty kilograms of either limestone or dolomite sample with a particle size greater than five millimeters for research purposes. Of these sixteen companies, seven supplied material. The list of companies that supplied material can be seen in Table 4-1.

Table 4-1 List of Limestone and Dolomite Companies that supplied samples

Names of Companies	Limestone	Dolomite
Glen Douglas Dolomite	No	Yes
Grasland Ondernemings	Yes	Yes
Latilla Mineral Marketing	Yes	No
Leo Dolomite	No	Yes
Lyttelton Dolomite	No	Yes
Marble Hall Mine	Yes	No
PPC - Slurry	Yes	Yes

From the table it can be seen that of the seven sorbent mining companies, two were able to supply both limestone and dolomite samples. Therefore an overall of nine sorbents were obtained for the study. The nine sorbent samples consisted of four limestone samples and five dolomite samples.

For the confidentiality of the mining companies, the sorbent samples were named as Sorb1 to Sorb4 for the four limestone samples and Sorb5 to Sorb9 for the five dolomite samples.

4.3. Sample Preparation for Physical, Chemical and AFBC Testing

Of the nine sorbent samples obtained, eight consisted of a particle size of five millimetres. The ninth dolomite sorbent was of a very fine particle size (<425μm), which was composed mostly of quartz sand and organic material. In view of the physical composition and particle size of this ninth sorbent, it was not deemed feasible as a desulphurisation material and therefore no further testing was performed on it.

37

From the remaining eight samples, sub samples were taken from each of the fifty kilograms samples for quantitative petrographical mineralogy analysis. The results of these tests are presented in Chapter 6.

The remaining fifty kilograms samples were crushed to a particle size of less than one millimetre using an AEG rotating crusher. From the crushed material, fifty grams of each of the eight sorbent samples were randomly collected for X-Ray Diffraction analysis. The preparation and reasoning for these tests are explained in subsection 4.5.2 that follows.

The remaining crushed sorbent samples were dry sieved into the three different particle size ranges of 425-500μm, 600-710μm and 850-1000μm using an Endecotts vibrating sieve machine.

From the three size ranges of interest in this research, fifty grams were randomly selected to perform Hardgrove Grindability Index analysis and a further forty grams was taken for X-Ray Fluorescence analysis. These two tests were used to determine the sorbents hardness and their chemical composition respectively. The remaining sieved material was thereafter used for the Atmospheric Fluidised Bed Reactor batch testing.

4.4. Physical Characterisation of the Limestone and Dolomite Samples

The following subsections explain the preparation of the samples and test results from Petrographical analysis, Scanning Electron Microscope analysis and Hardgrove Grindability Index analysis.

4.4.1. Petrographical Analysis of the Sorbent Samples

Petrographical sections were prepared using the standard technique described by Hutchison (1974) and examined using a polarising microscope.

The petrographical slides where prepared by the School of Geological at the University of KwaZulu-Natal, Westville Campus. The sorbent samples were analysed for their mineralogy grain size, grain structure and diagenetic features.

The analysis of the results of the petrographical slides can be seen in Table 4-2.

Table 4-2: Description of the Petrographical Slides under a polarising microscope

Sorb1	Fine grains, massive interlocking carbonate grains with traces of primary sedimentary structures preserved, patches of recrystalline calcite filling primary voids and these are often associated with secondary iron staining, no pholiation, traces of banding still preserved, banding is due to the variation in the carbonate grain size and staining, mixture of coarser and finer grain particles, low porosity
Sorb2	Grains composed of mass interlocking calcite grains and courser grains carbonate, some oolites present, quartz grains are small and not common, same banding, no pholiation, mixture of grain size present, some fragment have medium grains, both fine grains and very fine grains, extensive iron staining in some fragments which are usually the coarser grain ones, low porosity
Sorb3	Massive interlocking, quite coarse calcite grains, iron staining is well developed in some fragments particularly coarser grain ones, evidence of primary testures destroyed by recrystallisation, low porosity, irregular patches of coarse grain carbonate in finer grain carbonate and irregular patches of finer grain carbonate in coarser grain carbonate
Sorb4	Granules of coarse calcite in a fine grain calcite matrix, probably representing oolitic texture, patches of coarse grain material, reminisant of bioclasts, low porosity, slight iron staining, no pholiation, least metamorphism, low grade metamorphic grade
Sorb5	Composed of a mass of interlocking calcite and dolomite crystals, all primary sedimentary features have been destroyed by metamorphism and porosity reduced to a minimal by recrystallisation of the original carbonate, occasionally well rounded, quartz grains are present, no apparent pholiation, banding visible in the enhance sample is due to variation in the carbonate grain size, occasional quartz grain, few and far between, occasional bands of fine heamotite, randomly orientated calcite veins in the coarser grain material, laths of green chlorite and magnetite grains visible
Sorb6	Massive fine interlocking carbonate grains with irregular coarser grain particles, same iron staining along grain boundaries and tiny magnetite grains, a few fine rounded small quartz grains, low porosity
Sorb7	Fine grain dolomite with small quartz grains dispersed throughout the grains, massive interlocking calcite and dolomite grains with quartz grains standing out, no signs of iron or chlorite, low porosity, calcite filled veins, coarse grain calcite with traces of heamotite along the vein boundaries, shows a slight pholiation which is not parallel to the veins
Sorb8	Massive interlocking calcite and chromite fine grain crystals, rare and scattered quartz grains, faint banding is due to the variation in the grain size, low porosity, magnetite grains scattered in the sample, no pholiation

4.4.2. Scanning Electron Microscope (SEM) Analysis of the Sorbent Samples

Scanning electron microscope analysis of the eight sorbent samples prior to the Atmospheric Fluidised Bed Combustion desulphurisation testing was performed using the Jeol JSM 6100 Scanning Microscope at the University of KwaZulu-Natal, Westville Campus. The standard technique described by Tucker (1991) was used as the method for the analysis of these samples.

Fractured surface of the sorbent particles were carbon coated and examined at magnitudes between 200 and 1000X with an accelerating voltage of 25kV. SEM analysis was performed on all three particle size ranges of each of the eight sorbent samples. Pictures of these sorbent samples are shown in Figures B-1 to B-42 in Appendix B.

From the area representation photographs of the sorbent samples in Appendix B, it was noted that the samples were round to cylindrical in shape with specs of dust on the sorbent particle surface. Spot analysis was performed throughout the different parts of the sorbent samples by means of the Energy Dispersive Spectroscopy (EDS) analysis of the SEM. The samples were found to contain many elements such as calcium, magnesium, silica, iron, sodium, manganese, chlorine and potassium. It was found that quartz/silica grains were the most visible mineral on the samples. These grains were spread throughout the sample and were not concentrated at any particular point of the particle.

It was noted from the SEM photographs in Appendix B that the shape and chemical composition of the sorbent samples found in the smaller particle size range of 425–500μm was also observed for the particle size ranges of 600-710μm and 850-1000μm. Thus a conclusion can be made that the particle size of the sorbent had no effect on the surface structure and composition.

For the limestone particles in Figures B-1 to B-25, it was observed that the particles were covered by specs of quartz on the calcite particle. From these photographs it was noted that there were no significant porosity visible but there were definitely grain boundaries within the particle.

There was a significant difference between the SEM photographs for the limestone and dolomite particles. For the dolomite particles in Figures B-26 to B-42, it was noted that on the particles surface there were tiny individual mineral grains. There were no noticeable mineral grains on the limestone particle surface. The EDS analysis of the dolomite particles found that these particles were composed of calcium and magnesium with trace elements of other elements (iron,

manganese, aluminium). This was verified by the chemical analysis via X-Ray Fluorescence (XRF) and mineralogy variability shown by X-Ray Diffraction (XRD). XRD and XRF would be explained in subsections 4.6.1 and 4.6.2 respectively.

4.4.3. Hardgrove Grindability Index (HGI) Analysis of the Sorbent Samples

Hardgrove Grindability Index (HGI) tests of the eight sorbent samples were undertaken at Eskom's Research & Innovation Centre (ERIC) in Rosherville, Johannesburg. These tests were performed on each of the eight samples three different particle size ranges. This assisted in differentiating each sorbent's hardness with respect to their particle size. The results from these tests can be seen in Table C-1 in Appendix C. The ASTM and British Standard method of D409-71 and BS1016 Part 20 1981, respectively, was used as the method for the analysis of these samples.

During HGI testing at CR&D, the limestone sample Sorb4 with a particle size of 425µm was mislaid. The limestone sample, Sorb3 arrived late and therefore could not be prepared into their different particle size ranges for the HGI tests. Thus an overall sample size of less than one millimetre was made available to CR&D for Sorb3 HGI testing.

The hardness of the sorbent depends on the physical conditions the original mineral has undergone during its geological history. As the severity of the metamorphic recrystallisation of the sorbent increases, there is an increase in the sorbents hardness.

4.5. Chemical and Mineral Analysis of Sorbents

In the early 90's, the requirement for effective desulphurisation by Fluidised Bed Combustion manufacturers in USA was to have a calcium carbonate content greater than ninety percent. The assumption by these manufacturers was that the higher the calcium carbonate content, the better the sorbents desulphurisation ability. When this concept was used as the method of selecting sorbents, dolomites were disregarded, as their calcium carbonate content was much lower than that of limestones.

The chemical analysis was performed to determine the amount of calcium and other chemical components present in the sorbent samples as it assisted in the understanding of how the sorbents chemical composition affected the sorbents ability to reduce SO_2.

Two types of analyses were performed in determining the sorbents mineral and chemical composition. These were the X-Ray Diffraction analysis and X-Ray Fluorescence analysis, respectively. The method and results of these tests would be discussed in the subsequent sections.

4.5.1. X-Ray Diffraction (XRD) Analysis of the Sorbent Samples

The XRD chemical composition analysis of the eight sorbents was determined at The University of KwaZulu-Natal, Westville Campus. The standard technique described by Hutchison (1974) was used as the method for the analysis of these samples. A Philips based PW1830 system was used with a cobalt X-Ray tube (Kα = 1.7889A), graphite monochromator and Philips ADP software. Scans were undertaken between 5 and 60°, 2θ with a step size of 0.025 and a counting time of 1 second. The sorbents mineral composition can be seen in Table D-1 to D-8 together with their respective XRD graphs in Figure D-1 to D-8 in Appendix D.

The limestone samples were found to be composed of basically calcite and quartz. For the dolomite samples, it was composed of dolomite and quartz. These compositions in both the limestones and dolomites were expected to be discovered in their respected samples.

4.5.2. X-Ray Fluorescence (XRF) Analysis of the Sorbent Samples

The XRF analysis was conducted with the Philips PW1600 at The University of KwaZulu-Natal, Howard Campus. The standard technique described by Hutchison (1974) was used as the method for the analysis of these samples. Many textbooks give details of the XRF technique; see, e.g. Norris & Chappell (1977), Jenkins & de Vries (1970), Bertin (1975), Johnson & Maxwell (1981), Tertian & Claisse (1982) and Potts (1987). The results from these tests can be seen in Table E-1 in Appendix E.

XRF is ideally used for the determination of the major and minor elements such as aluminium, magnesium, calcium, iron, potassium, sodium, titanium, sulphur and phosphorous that are present in the sorbent samples.

The XRF analysis was conducted to obtain a comprehensive chemical composition of the sorbents with respect to the quantities of each chemical present in the sorbent. It was necessary to obtain this information as there was a need in determining the effect that the different amounts of each chemical constituent has on the sorbents ability to reduce SO_2 emissions.

4.6. Observations of Chapter Four

From the XRF, XRD, SEM and petrographical analysis tests that were performed on the sorbent samples, it was found that many test methods can be used in the determination of the sorbents desulphurisation ability. The applicability of these tests with respect to predicting a sorbents ability to remove sulphur dioxide would be investigated further through Atmospheric Fluidised Bed Combustion testing, the results of these tests are presented in subsequent chapters.

Chapter Five

Laboratory Fluidised Bed Reactor Testing Equipment

5.1. Scope

The aims of this study were to:

1. Determine the best operating conditions for different test parameters,
2. Determine the best sorbent by comparing their maximum sulphur retention, removal efficiency, physical properties and chemical composition, and
3. Find relationships between the physical and chemical properties of South African sorbents to their performance during the desulphurisation process.

To achieve these aims, batch sorbent feed testing on a laboratory scale Atmospheric Fluidised Bed Reactor (AFBR) was conducted.

The requirements to perform these tests were:

- A suitable inert bed material,
- A reactor that could heat the bed under fluidising conditions to the desired temperatures,
- Exit gas cleanup e.g. cyclone, water trap etc., and
- A gas analyser that could measure SO_2 gas concentrations.

Using the concept by Svoboda et al. (1988) that certain gases such as CO_2, NO_x and water vapour present in the flue gas behave similar to inerts at temperatures above 800°C, it was therefore accepted to ignore these gases and simulate the flue gas for sorbent desulphurisation using only a mixture of air and SO_2.

During batch testing, three parameters were varied to determine their impact on sorbent capture viz.:

1. Sorbents (Four Limestones and Four Dolomites),
2. Baseline bed temperatures (800°C, 850°C and 900°C), and
3. Sorbent particle sizes (425-500μm, 600-710μm and 850-1000μm).

A table listing the batch test runs performed in the AFBR is given in Table 5-1 below.

Table 5-1 Summary of Batch tests performed in the Atmospheric Fluidised Bed Reactor (AFBR)

Sorbents	Temperature	Particle Size
Sorb1	A	i, ii, iii
	B	i, ii, iii
	C	i, ii, iii
Sorb2	A	i, ii, iii
	B	i, ii, iii
	C	i, ii, iii
Sorb3	A	i, ii, iii
	B	i, ii, iii
	C	i, ii, iii
Sorb4	A	i, ii, iii
	B	i, ii, iii
	C	i, ii, iii
Sorb5	A	i, ii, iii
	B	i, ii, iii
	C	i, ii, iii
Sorb6	A	i, ii, iii
	B	i, ii, iii
	C	i, ii, iii
Sorb7	A	i, ii, iii
	B	i, ii, iii
	C	i, ii, iii
Sorb8	A	i, ii, iii
	B	i, ii, iii
	C	i, ii, iii

A – 800°C, B – 850°C, C – 900°C, i – 425-500μm, ii – 600-710μm, iii – 850-1000μm

Over and above those tests mentioned in Table 5-1, additional tests were performed to obtain a better understanding of the sorbents desulphurisation ability. These were:

- Varying quantities of sorbent, and
- Fixed Ca/S molar ratio tests.

5.2 Experimental Equipment

The experiment equipment used in this study consisted of a laboratory scale Atmospheric Fluidised Bed Reactor (AFBR) capable of reaching temperatures of 975°C. A schematic diagram of the equipment layout is shown in Figure 5-1.

Figure 5-1 Schematic diagram of experimental equipment

(1) Air Compressor (2) SO_2 Cylinder (3) Air Rotameter (4) Needle Valve (5) Buffer Tank (6) Sparger (7) Distributor Plate (8) Stainless Steel Reactor (9) Electric Heater (10) Cyclone (11) Gas Chiller (12) SO_2 Bacharach Analyser (13) Disposal Water Tank
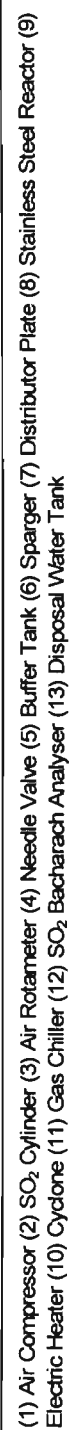
Compressed air, sourced from an Atlas Copco GA22 air compressor in the School of Chemical Engineering laboratory at the Westville campus of the University of KwaZulu-Natal, was filtered by an autodrain filter/pressure regulator to remove entrained moisture. The pressure of the air was regulated at 200 kPa (g) prior to entering the calibrated float rotameter.

Compressed sulphur dioxide from a gas cylinder was transferred to a forty-five litre buffer tank in small dosages via a gas bottle regulator and needle valve. A photograph of the buffer tank can be seen in Figure F-1 in Appendix F. The buffer tank was used to ensure there was a constant flow of SO_2 gas entering the AFBR. The SO_2 gas capacity in the buffer tank was maintained such that a 60 kPa (g) pressure was observed prior to the beginning of every test run. This capacity was sufficient to last throughout a test run.

The regulated air and sulphur dioxide gas converged at a T-Piece were they were mixed prior to entering the AFBR. SO_2 gas concentration of 1100 parts per million (ppm) volume basis which is typical of SO_2 emissions from average world coals was used as the initial SO_2 gas concentration. Figure 5-2 is a photograph of the experimental equipment.
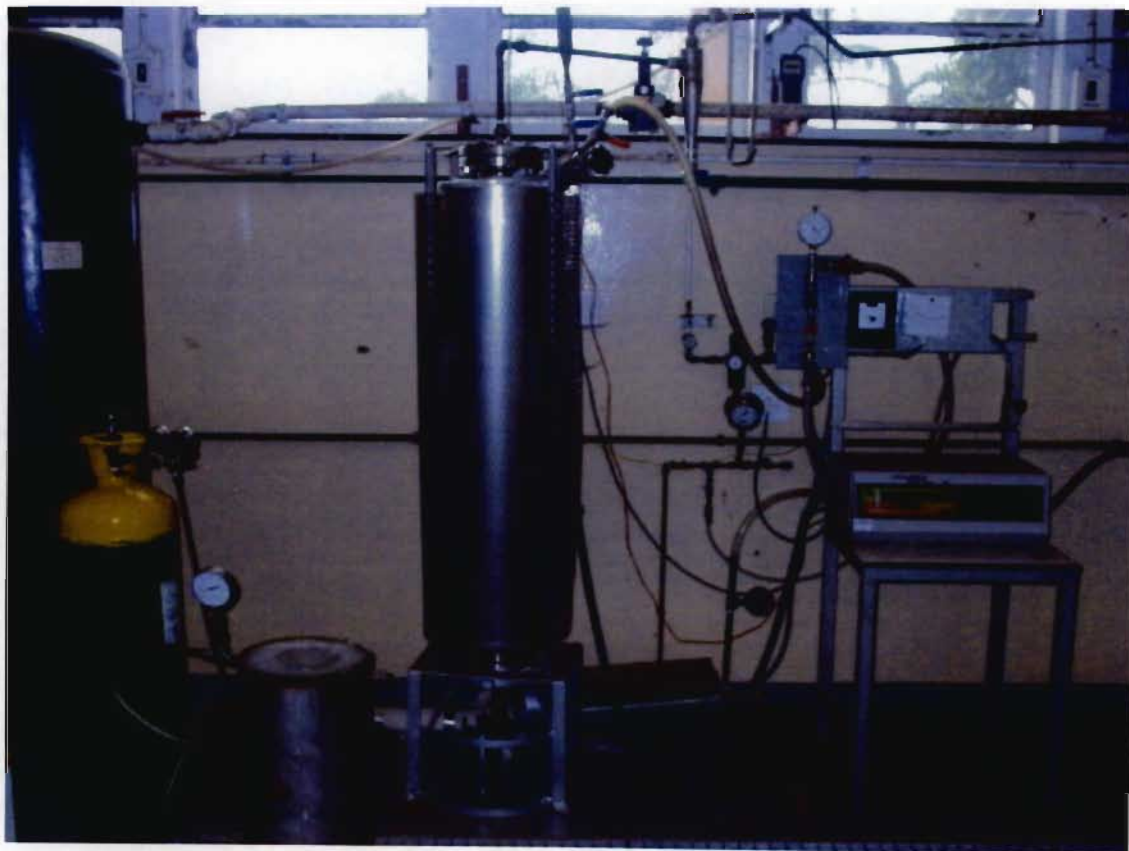

Figure 5-2 Photograph of the experimental setup

Figures F-2 to F-12 in Appendix F contains additional pictures relating to the experimental set-up. The discussion of the construction of the major experimental equipment and set-up of apparatus for testing will be discussed in the relevant subsections that follow.

5.2.1 Atmospheric Fluidised Bed Reactor (AFBR)

The fluidised bed reactor was constructed of 310 stainless steel with an internal diameter and height of 0.102m and 1.6m, respectively. A photograph of the stainless steel reactor can be seen in Figure F-13 in Appendix F. The fluidised bed reactor is divided into two sections viz. the 0.35m windbox located below the distributor and the 1.25m freeboard section that contained the fluidised bed located above the distributor.

The distributor was constructed of 316 stainless steel perforated plate with a 316 stainless steel 250 micron mesh on top of the perforated plate. The perforated plate was 2mm thick with 5mm holes at a pitch of 5mm. The perforated plate was used to hold the mesh and bed material in position thus preventing the mesh and bed material from falling into the windbox.

The windbox was composed of a cross-shaped sparger with 3mm holes that were 5mm apart on the top of the cross, facing the distributor. The sparger was used to ensure there was an even distribution of inlet gases throughout the bed. A photograph of the windbox, sparger, perforated plate and mesh can be seen in Figure F-14 in Appendix F.

On the side of the stainless reactor was a 0.05m diameter 316 stainless steel pipe, 0.5m in length and approximately 0.12m above the distributor. This stainless steel pipe protruded out of the casing enclosing the AFBR and was used to remove the bed material together with the spent sorbent by means of a vacuum cleaner.

A ceramic glass cloth was used to cover the stainless steel reactor onto which the heating element was placed. Figure F-16 in Appendix F displays a photograph of the ceramic glass cloth used on the reactor. The ceramic glass cloth was used to hold the heating elements in position hence preventing them from sliding due to gravity during testing.

Two 5kW heating elements were thereafter wrapped onto the cloth. Figure F-17 shows a photograph of the installation of the heating elements on the ceramic glass cloth. A greater number of heating element turns were positioned towards the area where the bed material was

situated in the stainless steel reactor. This reduced the overall time required to heat the bed material to the desired test temperatures.

Over the heating elements, three layers of refractory insulation lining were placed. Photographs of the installation of the refractory insulation can be seen in Figure F-18 and F-19 in Appendix F. The insulation was used to reduce the heat loss from the surface of the reactor thus maintaining the bed temperature. A 2mm stainless steel sheet was used to form a shell around the refractory lining followed by a steel mesh, which acted as a precaution against any accidents. Figure 5-3 displays the set-up of the lining around the stainless steel reactor.
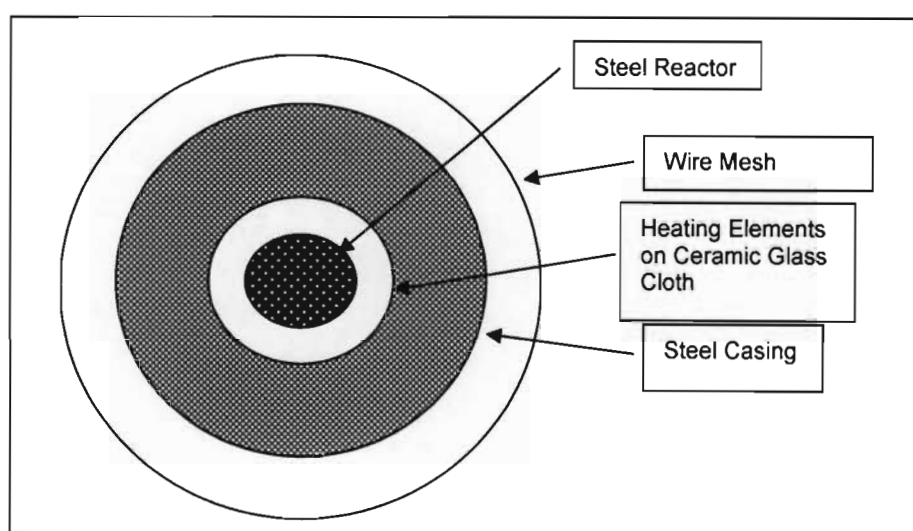

Figure 5-3 Set-up of the lining around the stainless steel Atmospheric Fluidised Bed Reactor

The reactor bed temperature was measured using a K-type thermocouple placed in the centre of the bed material and controlled using a Carbolite PID temperature controller. The variation between the set and actual bed temperatures was found to be plus minus two degrees Celsius.

5.2.2 AFBR Sorbent Feeder

Batch testing was accomplished by the feeding of sorbent through a side port on the AFBR. A photograph of the sorbent feeder can be seen in Figure F-20 in Appendix F.

It was essential to find a method that could feed sorbent into the reactor whilst preventing the release of SO_2 gas from the reactor into the laboratory. This was achieved by the use of two half-inch ball valves with a half-inch nipple in-between the two valves. A schematic diagram of the sorbent feeder designed for the AFBR can be seen in Figure 5-4.
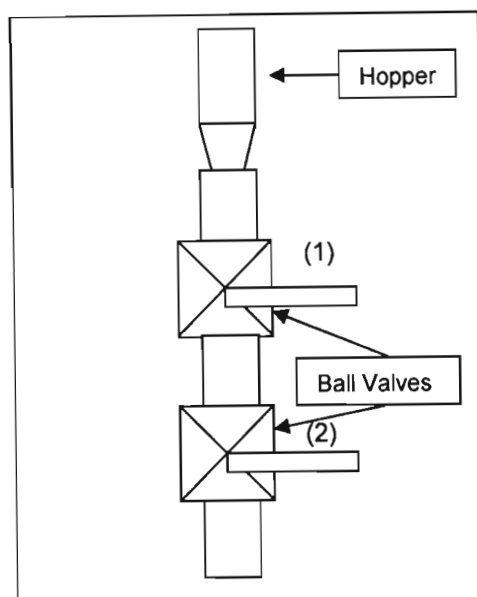
Figure 5-4 Schematic drawing of the Sorbent Feeder

The feeder operated using an alternating valve mode operation. Initially, both valves were closed. The valve closest to the hopper (1) was opened to allow the sorbent from the hopper to fall into the space between the two valves. Valve (1) was closed and valve (2) below valve (1) was opened, allowing the sorbent from between the two valves to fall into the reactor. Thereafter, valve (2) was closed and valve (1) was opened. The above procedure was repeated until all the material within the hopper was transferred into the AFBR.

Figure F-21 in Appendix F illustrates a photograph of the sorbent feeder being utilised to add sorbent into the AFBR.

5.2.3 Exhaust Gas from AFBR

The exhaust gas from the AFBR passed through to a 0.064m diameter cyclone to remove the fine particles that were entrained during fluidisation. The sluice of the cyclone collected solid particles that were larger than the cut off point for the cyclone (>50μm). The use of a cyclone was a precaution to prevent the solid particles from entering the gas analyser.

Due to the toxic nature of the SO_2 gas, precautions were taken for the safe disposal of the exhaust gas. This was accomplished by bubbling the exit gas from the cyclone and SO_2 analyser into a water tank outside the laboratory. SO_2 gas is soluble in water and was therefore used to

capture virtually all of the SO_2 from the exhaust gas. A photograph of the water tank used for the disposal of the SO_2 gas in the exhaust gas line can be seen in Figure F-22 in Appendix F.

5.2.4 Analysis of Sampled Gas

A gas stream from the main exhaust gas line was tapped off after the cyclone for SO_2 gas analysis. A schematic drawing of the gas sample analysis set-up is shown in Figure 5-5.
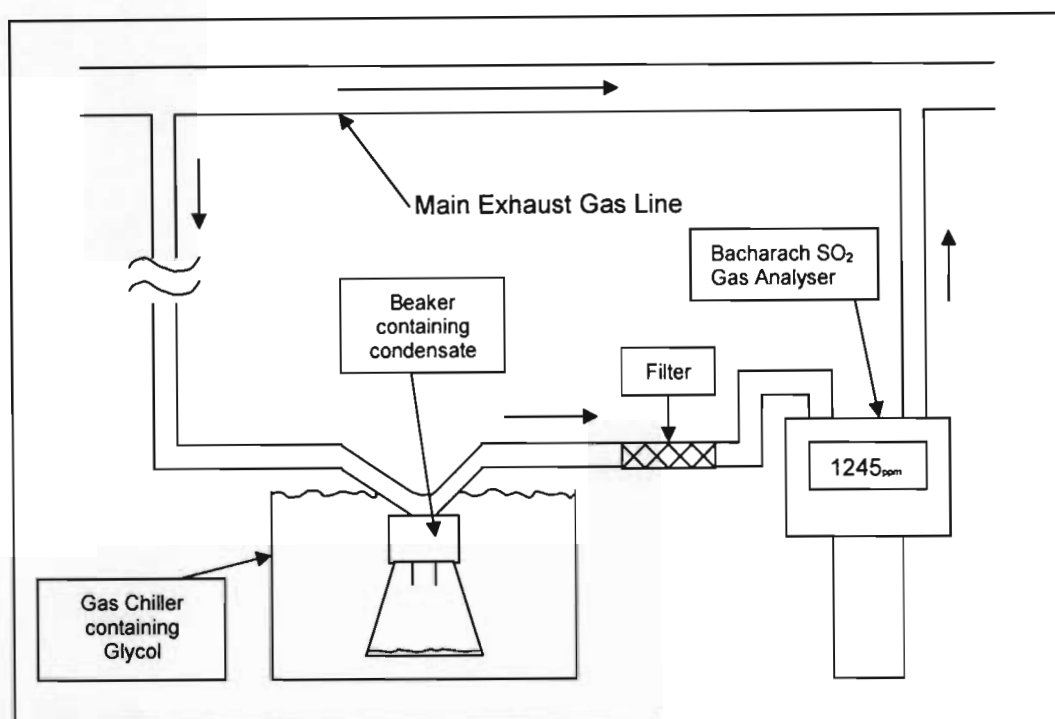
Figure 5-5 Schematic drawing of the gas analysis set-up

The gas stream passed through a gas chiller to condense the water vapour present in the exhaust gas line. The condensed water vapour was removed from the exhaust gas by passing the exhaust gas through a beaker submerged in glycol at a temperature of $-10°C$ as can be seen in Figure 5-5. A photograph of the gas chiller can be seen in Figure F-23 and F-24 in Appendix F. The water vapour free gas was thereafter passed through a filter, which was another precautionary measure to remove any remaining water and solid particles not captured in the gas chiller and cyclone, respectively. The gas was now ready to be analysed using the Bacharach Dioxor II electrochemical SO_2 analyser. Figure F-25 and F-26 in Appendix F illustrates photographs of the Bacharach Dioxor II electrochemical SO_2 analyser.

The distance from the AFBR to the gas line was calculated to be equivalent to a volume of 0.5 litres. This small delay in analysis was found to have no significance on the overall results from the AFBR.

5.3 Choice of Bed Material

Pool filter sand (SiO_2 = 99%, density = 2650 kg/m^3) was chosen as the bed material due to it being the cheapest and the most readily available material with a high quartz content.

During testing, it was found to be difficult and time consuming to change the bed material after every test conducted on a sorbent. A methodology was devised whereby after every test, the sorbent was exhausted using excess SO_2 gas thus making the sorbent inert. The validation for the use of the same bed material to do different tests can be seen in Chapter 6.

5.4. Choice of Operating Variables

As in all studies on sorbents desulphurisation ability, there are several variables that form a meaningful comparison of results. The following subsections discuss these variables on the sorbents ability to reduce SO_2.

5.4.1 Temperature

As noted in Chapter 2, the bed temperature in fluidised beds has shown to promote sorbents desulphurisation abilities in the temperature range between 800°C and 900°C. From Table 5-1 it can be seen that there were significant testing to be performed on the AFBR with the three different sorbent test parameters. Three baseline temperature tests were chosen to be performed on the sorbents between 800°C and 900°C i.e. 800°C, 850°C and 900°C. Three additional tests were performed on the 850-1000µm particle size range sorbents to determine temperature influence on either side of the baseline temperature range.

5.4.2 Particle Size

The small quantities of sorbent and the density difference between the silica sand bed material (2650 kg/m^3) and sorbent (Limestone – 2700kg/m^3, Dolomite – 2800kg/m^3) was found to have no overall effect on fluidisation in the AFBR. Thus the particle size of the sorbent to be tested in the AFBR was used to determine the particle size of the silica sand bed material, which ensured that good mixing occurred throughout the bed.

Figures F-27 to F-29 in Appendix F illustrates photographs of the sorbents used in the AFBR that where tested.

5.4.3 Fixed Parameters

Cold minimum fluidisation velocity (U_{mf}) tests were performed on the pool silica sand bed material in a perspex column of similar dimensions to the stainless steel AFBR. The standard technique explained by Geldart (1986) was used for the cold U_{mf} tests. Figure 5-6 represents a graph used for the U_{mf} determination of the silica sand bed material for the particle size range of 850-1000µm. These results were compared to the literature correlation by Broadhurst and Becker's (1975) shown in equation 5 below. Table 5-2 lists the results for the experimental tests and literature calculations performed on the different particle size ranges and at the temperature of 25°C.
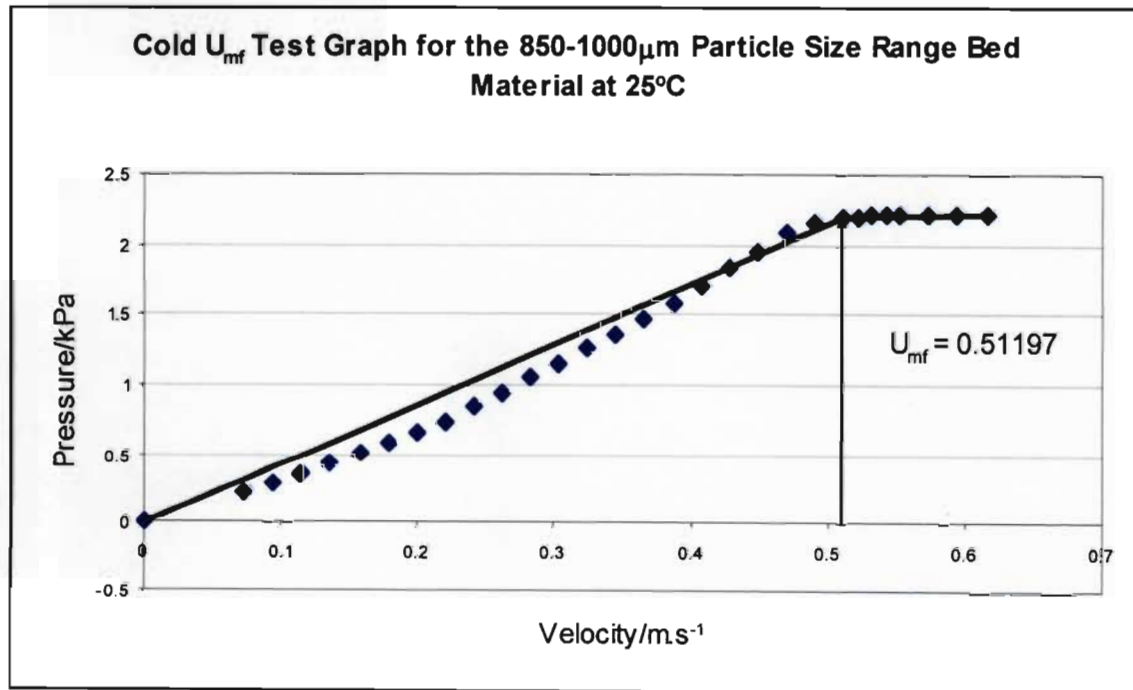
Figure 5-6 Cold U_{mf} Test Graph for the Silica Sand Bed Material

$$\text{Re}_{mf}^2 = \frac{Ar^{1.85}}{37.7 Ar^{0.85} + 242000\left(\frac{\rho_p}{\rho_f}\right)^{0.13}} \qquad (5)$$

Table 5-2: Cold Minimum Fluidisation Velocity test results

Particle Size Range/μm	Experimental U_{mf}/m.s^{-1}	Literature U_{mf}/m.s^{-1}
425-500	0.189	0.190
600-710	0.332	0.325
850-1000	0.512	0.514

From the small difference between the experimental and literature values in Table 5-2, it was assumed that the correlation by Broadhurst and Becker's (1975) could be used on the hot experimental tests conducted on the eight sorbents in the AFBR.

A fluidisation velocity of between 1.5 and 2 times U_{mf} was visually found by opening the flange at the top of the reactor to achieve the best mixing. Thus a fluidisation velocity of 1.5 times U_{mf} was used during AFBR testing. The calculated minimum fluidisation velocity and velocities utilised in the AFBR can be seen in Table 5-3 below.

Table 5-3 Calculated U_{mf} values and Applied Velocities in the AFBR

Temperature/$^{\circ}$C	Particle Size/μm	U_{mf}/m.s^{-1}	1.5 * U_{mf}/m.s^{-1}
800	425-500	0.099	0.149
800	600-710	0.183	0.274
800	850-1000	0.332	0.498
850	425-500	0.097	0.145
850	600-710	0.178	0.267
850	850-1000	0.324	0.487
900	425-500	0.094	0.142
900	600-710	0.174	0.261
900	850-1000	0.317	0.476

An initial bed height of 1.7 times the diameter of the AFBR was used during start-up. This was calculated to be 1.4 litres of silica sand. With the addition of the small quantities of test sorbent (20 grams or less) into the AFBR, it was found that there was no significant difference in the bed height in the AFBR.

5.5 Sample Preparation

Samples of the sorbents were prepared as was mentioned in Chapter 4 section 3. Twenty grams of the sample to be tested was weighed in a 50ml beaker and added to the sorbent feeder

hopper. The addition of the small quantities of sorbent into the AFBR was to ensure that the test was considered as batch operation due to the method of feeding.

5.6 Methods of Determining Efficiency of the Sorbent

5.6.1 Maximum Sulphur Retention (MSR)

The maximum (instantaneous) sulphur retention was calculated using the equation (6) by Chu et al. (2000) below,

$$\text{Maximum Sulphur Retention } (MSR) = \frac{C_o - C}{C_o} * 100 \qquad (6)$$

C_o – Initial SO_2 Concentration, C – Final SO_2 Concentration

The initial SO_2 concentration prior to testing was read from the SO_2 analyser and was recorded as C_o. The lowest SO_2 concentration measured by the analyser that was achieved by the sorbent was recorded as C. From these tests it was possible to obtain the sorbents maximum achievable sulphur retention during batch testing.

5.6.2 Removal Efficiency (RE)

Graphical integration calculations were performed on the area between the inlet and measured SO_2 gas concentration curves from the performance graphs in Appendix G. The results of these area calculations are displayed in Appendix G, Table G-1. The area in these performance graphs represents the total amount of SO_2 absorbed by the sorbents throughout the test run. An increase in the area of the performance graphs resulted in the better overall performance of the sorbents.

In some of the performance graphs it should be noted that the tests were conducted for a period longer than fifteen minutes. However a baseline of fifteen minutes was used for the area calculations on all performance graphs.

Chapter Six

Discussion of Test Results from the Atmospheric Fluidised Bed Reactor (AFBR)

6.1 Introduction

Chapter five has described in detail the equipment used for the necessary experiments required for the accomplishment of the aims of this study. Also discussed in chapter five was the operating variables chosen to be used during testing on a laboratory scale Atmospheric Fluidised Bed Reactor (AFBR). This chapter is dedicated to the analysis of the results and a discussion of the findings from the laboratory scale AFBR.

6.2. Interpretation of Results obtained from the AFBR

Graphs for each of the desulphurisation tests performed on the AFBR were drawn. These desulphurisation test graphs can be seen in Figures G1 to G112 in Appendix G. Figure 6-1 displays a sample of a desulphurisation test graph for sorbent Sorb6 at a bed temperature of 800°C and a particle size range of 850-1000µm. The graph displays data of the inlet and outlet SO_2 gas concentration versus time experienced in the AFBR.
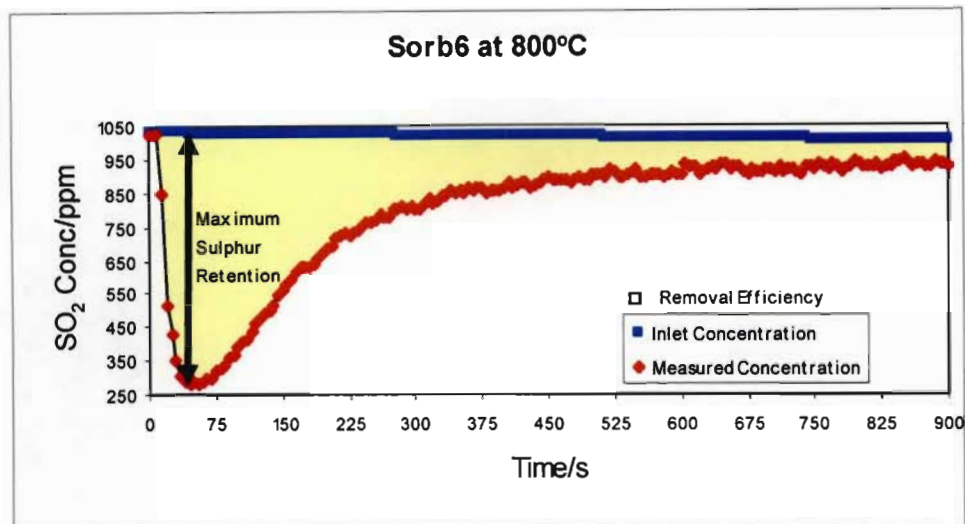
Figure 6-1 Performance graph of sorbent Sorb6 at a particle size range of 850-1000μm and a bed temperature of 800°C

At time t = 0, a dosage of sorbent was introduced into the AFBR. The inlet SO_2 gas concentration remained constant whilst the outlet SO_2 gas concentration responded to the sorbent addition. After an initial ten second delay between the AFBR and the gas analyser, the outlet SO_2 gas concentration decreased steeply indicating an initial fast rate of desulphurisation. After reaching the minimum outlet SO_2 gas concentration, the concentration advanced back towards the inlet SO_2 gas concentration indicating a gradual saturation of the sorbent.

From the graph in Figure 6-1, two calculations were made. The first was the maximum instantaneous sulphur retention of the sorbent, which was calculated using equation 5 in Chapter 5.6 by Chu et al. (2000) whilst the second calculation was for the sorbents removal efficiencies by the area calculation methodology described in Chapter 5.7. Table 6-1, 6-3, 6-4, 6-6, 6-7, 6-8 and 6-9 lists the results of the maximum sulphur retention whilst Table 6-2, 6-3, 6-5, 6-6, 6-7, 6-8 and 6-10 lists the results of the removal efficiency obtained from the tests performed on the AFBR.

On examining the different concentration data lines in Figure 6-1, there were two significant observations. The first was the decrease in the inlet SO_2 gas concentration with time, which was due to the loss of SO_2 gas from the buffer tank during the test. The other observation was that the measured and inlet SO_2 gas concentration lines do not meet towards the end of the test run (time = 900s). However, it is known that theoretically after a fairly lengthy period of time these two lines would eventually converge. With respect to this, tests on the operating variables for the sorbents were conducted for a fixed time period of fifteen minutes, which was sufficient to notice the initial behaviour of the sorbents. This time period was also short enough for additional

58

experiments to be performed on the AFBR thus facilitating a better understanding of the sorbents desulphurisation behaviour.

6.3. Effect of Bed Temperature on Sorbents Desulphurisation Ability

One of the three parameters that were investigated for the sorbents desulphurisation ability was bed temperature. Tests were conducted on the eight different sorbents with three different particle sizes and three baseline bed temperatures of 800, 850 and 900°C. Tests at bed temperatures of 600, 700 and 950°C were also performed on the 850-1000μm particle size material such that a better understanding of the bed temperature dependence of the sorbents could be obtained. The maximum sulphur retention and removal efficiency results obtained from the tests conducted on the AFBR are listed in Table 6-1 and 6-2, respectively.

Table 6-1 Results of Maximum Sulphur Retention tests performed in the Atmospheric Fluidised Bed Reactor at the three operating variables of Bed Temperature, Particle Size and Sorbents

425-500µm			
Sorbent	**800°C**	**850°C**	**900°C**
Sorb1	89.93	92.30	90.40
Sorb2	86.94	87.83	86.25
Sorb3	85.43	89.85	87.02
Sorb4	90.83	91.62	87.62
Sorb5	84.25	89.98	86.85
Sorb6	83.66	87.10	84.58
Sorb7	86.84	88.56	86.74
Sorb8	85.20	88.80	84.16

600-710µm			
Sorbent	**800°C**	**850°C**	**900°C**
Sorb1	89.13	91.26	89.16
Sorb2	84.33	86.03	83.61
Sorb3	70.90	85.78	82.75
Sorb4	89.66	90.33	87.65
Sorb5	84.37	89.07	86.78
Sorb6	82.85	86.00	81.25
Sorb7	82.74	83.94	83.06
Sorb8	81.20	85.42	83.65

850-1000µm					
Sorbent	**600°C**	**700°C**	**800°C**	**850°C**	**900°C**	**950°C**
Sorb1	7.92	36.09	82.09	87.02	84.23	73.04
Sorb2	16.21	30.90	77.56	84.10	82.15	74.86
Sorb3	14.82	28.51	64.78	71.61	68.76	63.88
Sorb4	18.45	29.01	79.35	87.07	84.62	73.36
Sorb5	20.79	29.28	76.62	87.51	84.25	65.92
Sorb6	11.96	20.59	72.69	74.37	69.45	62.52
Sorb7	8.31	21.78	71.57	73.67	68.26	64.45
Sorb8	9.76	21.62	69.16	75.24	70.37	65.31

Table 6-2 Results of Removal Efficiency tests performed in the Atmospheric Fluidised Bed Reactor at the three operating variables of Bed Temperature, Particle Size and Sorbents

425-500μm			
Sorbent	800°C	850°C	900°C
Sorb1	71.83	84.54	76.92
Sorb2	55.81	62.53	43.46
Sorb3	50.22	56.30	38.46
Sorb4	79.24	74.23	62.36
Sorb5	17.53	34.52	35.59
Sorb6	40.64	35.48	30.21
Sorb7	47.60	41.68	45.97
Sorb8	48.20	56.48	25.32

600-710μm			
Sorbent	800°C	850°C	900°C
Sorb1	75.09	68.76	69.32
Sorb2	68.30	52.05	45.45
Sorb3	42.42	37.19	35.10
Sorb4	69.78	67.69	32.29
Sorb5	21.60	22.54	29.75
Sorb6	31.79	30.98	27.66
Sorb7	30.53	20.75	25.66
Sorb8	32.03	33.78	31.15

850-1000μm						
Sorbent	600°C	700°C	800°C	850°C	900°C	950°C
Sorb1	5.81	15.24	45.27	52.25	57.45	39.00
Sorb2	3.34	10.15	42.05	43.06	31.53	29.81
Sorb3	2.95	13.98	22.99	23.78	20.34	19.13
Sorb4	3.28	9.33	44.40	44.95	47.82	31.65
Sorb5	6.15	11.59	20.84	22.55	20.75	14.10
Sorb6	2.51	8.99	21.81	22.48	19.91	17.39
Sorb7	2.65	9.43	17.26	18.01	18.64	16.26
Sorb8	3.28	9.33	44.40	44.95	47.82	31.65

The results for the particle size range of 850-1000μm in Table 6-1 and 6-2 have been plotted in Figure 6-2 and 6-3, respectively. These graphs assist in the visualisation of the influence of bed temperature on the sorbents ability to remove SO_2.
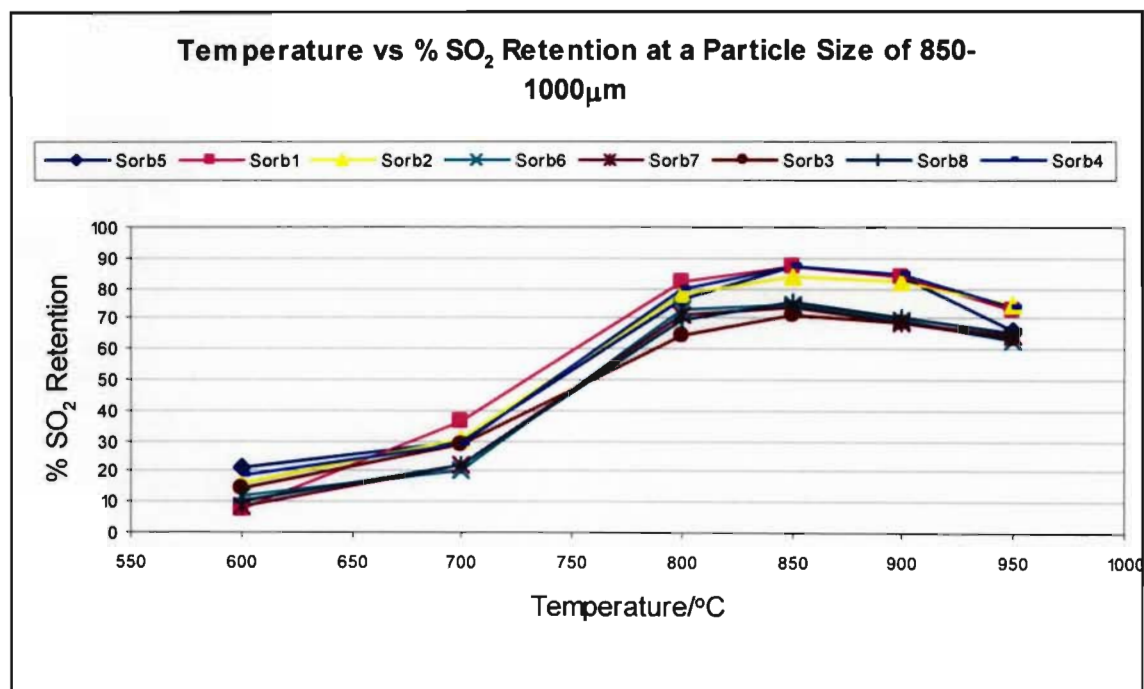
Figure 6-2 The Effect of Bed Temperature on Maximum Sulphur Retention at a particle size of 850-1000μm

Temperature vs % Removal Efficiency at a Particle Size of 850-1000µm
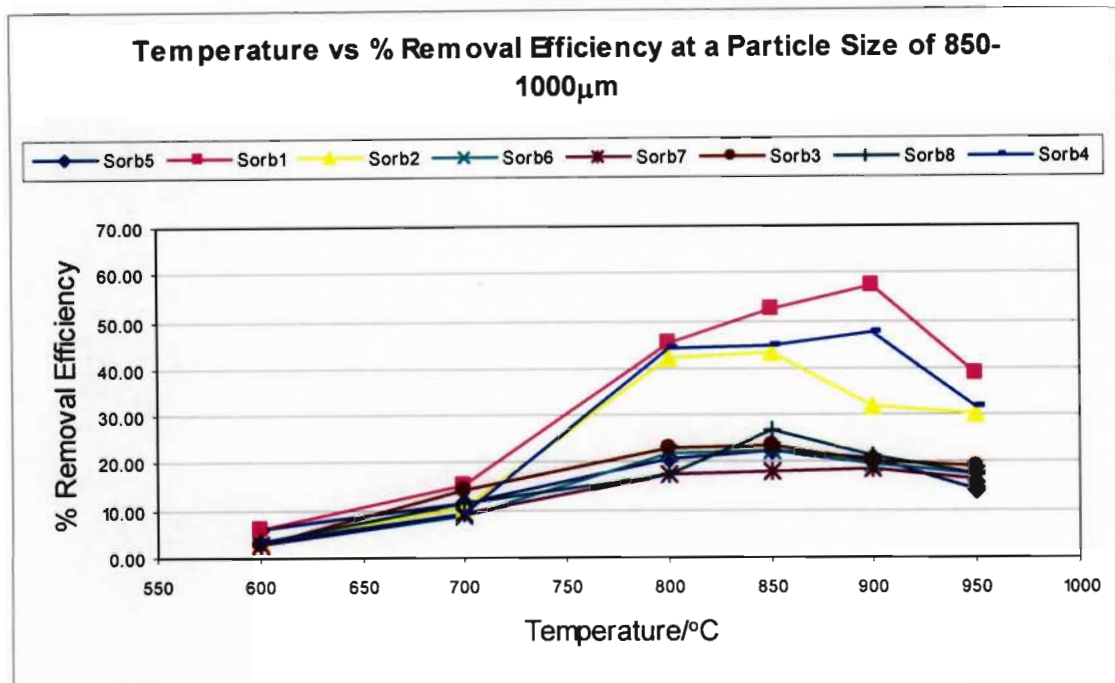
Figure 6-3 The Effect of Bed Temperature on Removal Efficiency at a particle size of 850-1000µm

Bed temperature was found to play a significant role in the desulphurisation behaviour of the sorbents as was discussed in chapter two. The variation in desulphurisation of the sorbents as bed temperature changed in Figure 6-2 and 6-3 displays the sensitivity of the sorbents on bed temperature. The phenomenon experienced above was also observed by Pisupati et al. (1996) and Adanez et al. (1994a).

In Figure 6-2, it was observed that all eight sorbents experienced their highest maximum sulphur retention at a bed temperature of 850°C for the particle size range of 850-1000µm. The highest SO_2 retention for the limestones was Sorb4 at 87.07% whilst the highest SO_2 retention for the dolomites was Sorb5 at 87.51%. This small difference in desulphurisation between the limestone and dolomite sorbents displays their closeness in performance.

To confirm the conclusions that no significant desulphurisation occurs at temperatures below 800°C and above 900°C made by many researchers (Pisupati et al. (1996), Adanez et al. (1994a), Haji-Sulaiman et al. (1990)) further tests were performed on the 850-1000µm particle size range sorbents to determine their desulphurisation behaviour below and above the baseline bed temperature range of 800 to 900°C.

63

It was found that at a bed temperature of 600°C, the MSR ranged between 7.92 and 18.45% for the limestones and between 8.31 and 20.79% for the dolomites. At a higher bed temperature of 700°C, there was no significant difference in the sorbents ability to reduce SO_2 as compared to the reductions obtained at 600°C. It was found that at this bed temperature of 700 °C the limestones MSR ranged between 28.51 and 36.09% whilst the dolomites ranged between 20.59 and 29.26%.

During the bed temperature change from 700 to 800°C, there was a rapid increase in the desulphurisation ability of the sorbents. The highest and lowest MSR change was found to occur to Sorb6 and Sorb3, respectively. It was found that Sorb6 had a change of 52.1% whilst Sorb3 had a change of 36.27%.

For the bed temperature of 950°C, it was noted that there was a reduction in the desulphurisation ability of the sorbents as compared to the desulphurisation observed at 900°C. The highest and lowest change in SO_2 retention from the bed temperature of 950 to that of 900°C occurred to sorbents Sorb5 and Sorb7, respectively. This was calculated to be 21.76% for Sorb5 and 5.58% for Sorb7.

In Figure 6-3, for the baseline bed temperature test range, it was observed that the highest removal efficiencies for the eight sorbents occurred at either 850 or 900°C. With this variation, it was not possible to find an optimum bed temperature at which the highest removal efficiency of the sorbent would be obtained but rather a range of between 800 and 900°C. This indicates a need for experimental determination for sorbents desulphurisation ability during fluidised bed combustion of coal containing sulphur.

For bed temperatures below and above the baseline bed temperature range of 800 to 900°C, it was also observed that there were no significant SO_2 reductions for the sorbents removal efficiencies as can be seen in Figure 6-3.

This verifies the assumption made by many researchers (Pisupati et al. (1996), Adanez et al. (1994a), Haji-Sulaiman et al. (1990)) that no significant SO_2 reduction occurs at bed temperatures below and above the bed temperature range of 800 to 900°C. As a result of this trend occurring for the particle size range of 850-1000μm, it was safe to stipulate that similar results would occur for the other two test particle size ranges of 425-500μm and 600-710μm. Thus no further tests were performed on bed temperatures lower than 800°C and bed temperatures higher than 900°C.

For the particle size range of 600-710µm and 425-500µm, it was noted from Table 6-1 that all eight sorbents experienced their highest maximum sulphur retention at a bed temperature of 850°C. For the particle size range of 600-710µm, the highest MSR for the limestones was Sorb1 at 91.26% and for the dolomites was Sorb5 at 89.07%. For the particle size range of 425-500µm, the highest limestone MSR was Sorb1 at 92.30% and the dolomites was Sorb5 at 89.98%.

For the removal efficiencies of the eight sorbents at the particle size ranges of 600-710µm and 425-500µm in Table 6-2, it was observed that the optimum desulphurisation bed temperature ranged between 800 and 900°C. Similarly to that experienced for the removal efficiencies of the 850-1000µm particle size range sorbents. The highest removal efficiencies for the particle size range 600-710µm was found to occur to the limestone, Sorb1, at 75.09% and to the dolomite, Sorb8, at 33.78%. For the particle size range of 425-500µm, the limestone Sorb1 and dolomite Sorb8 was found to obtain the best removal efficiencies of 84.54% and 56.48%, respectively.

Overall, all the sorbents at the three particle size ranges experienced an optimum bed temperature for their maximum sulphur retention of 850°C which is consistent with the findings of Adanez et al. (1994a).

6.4. Effect of Sorbent Particle Size on Desulphurisation

Another parameter investigated for the sorbents desulphurisation ability was particle size. Tests were conducted on the eight different sorbents with three different bed temperatures discussed in section 6.3 at the three test particle sizes ranges of 425-500, 600-710 and 850-1000µm. Table 6-1 and 6-2 lists the results obtained from the tests conducted on the AFBR for the maximum sulphur retention and removal efficiency, respectively.

The influence of particle size on the sorbents desulphurisation ability using the results from Table 6-1 was plotted in Figure 6-4 to 6-6 whilst the results from Table 6-2 were plotted in Figure 6-7 to 6-9.
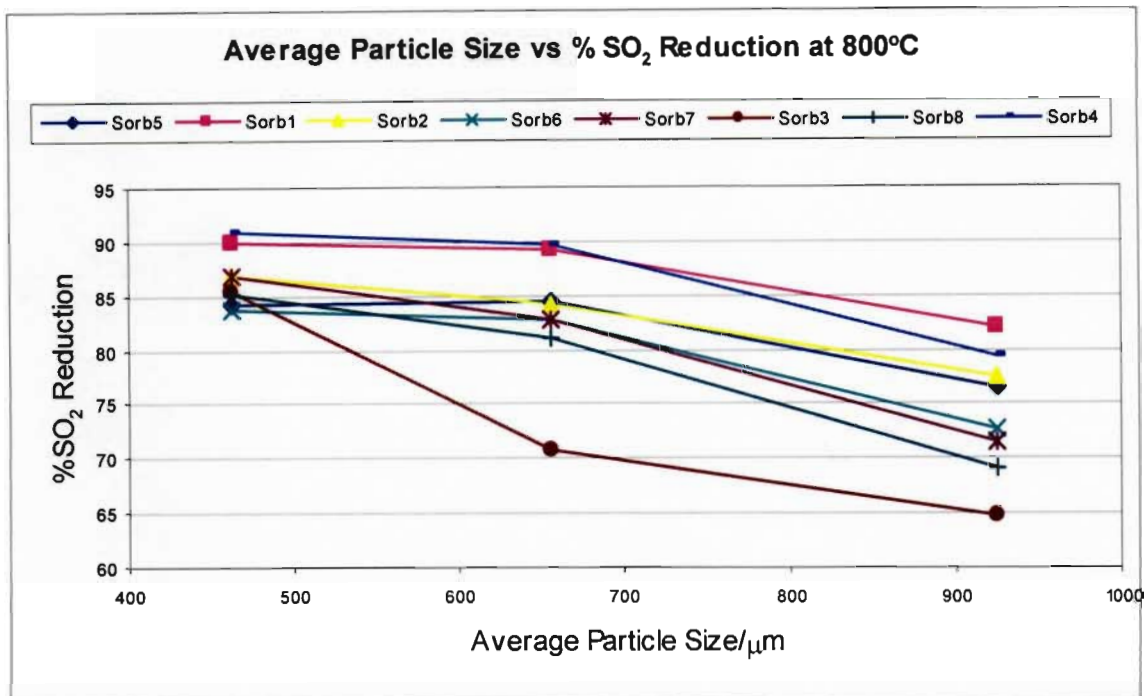
Figure 6-4 Effect of Particle Size on Maximum Sulphur Retention at a Bed Temperature of 800°C
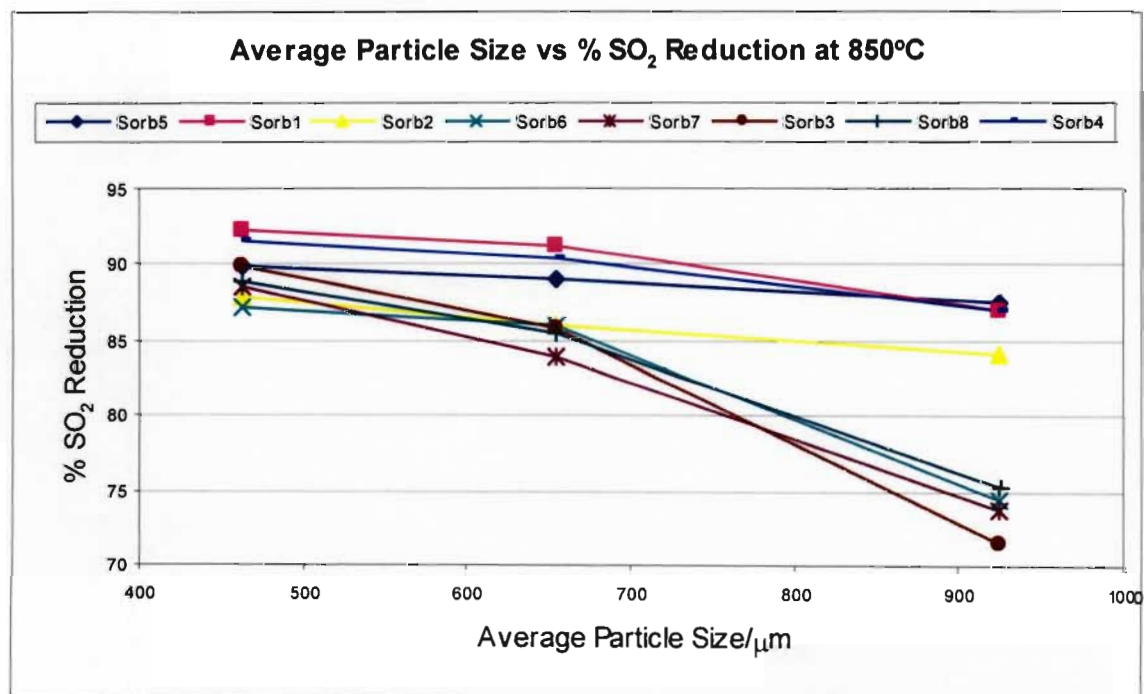
Figure 6-5 Effect of Particle Size on Maximum Sulphur Retention at a Bed Temperature of 850°C
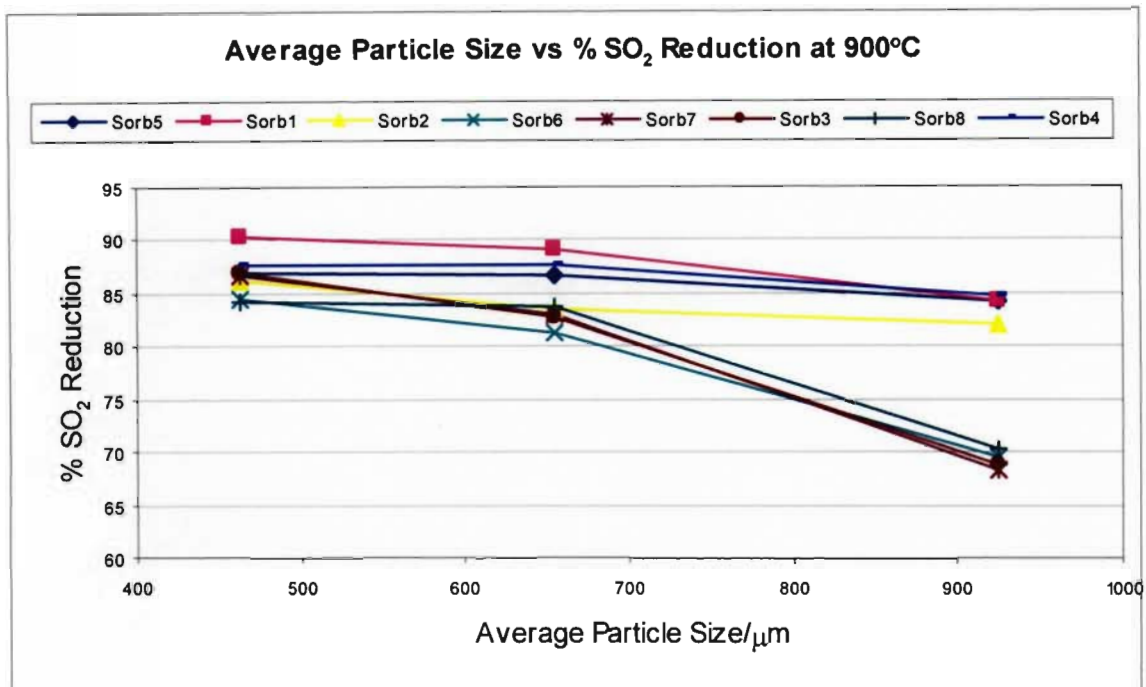
Figure 6-6 Effect of Particle Size on Maximum Sulphur Retention at a Bed Temperature of 900°C
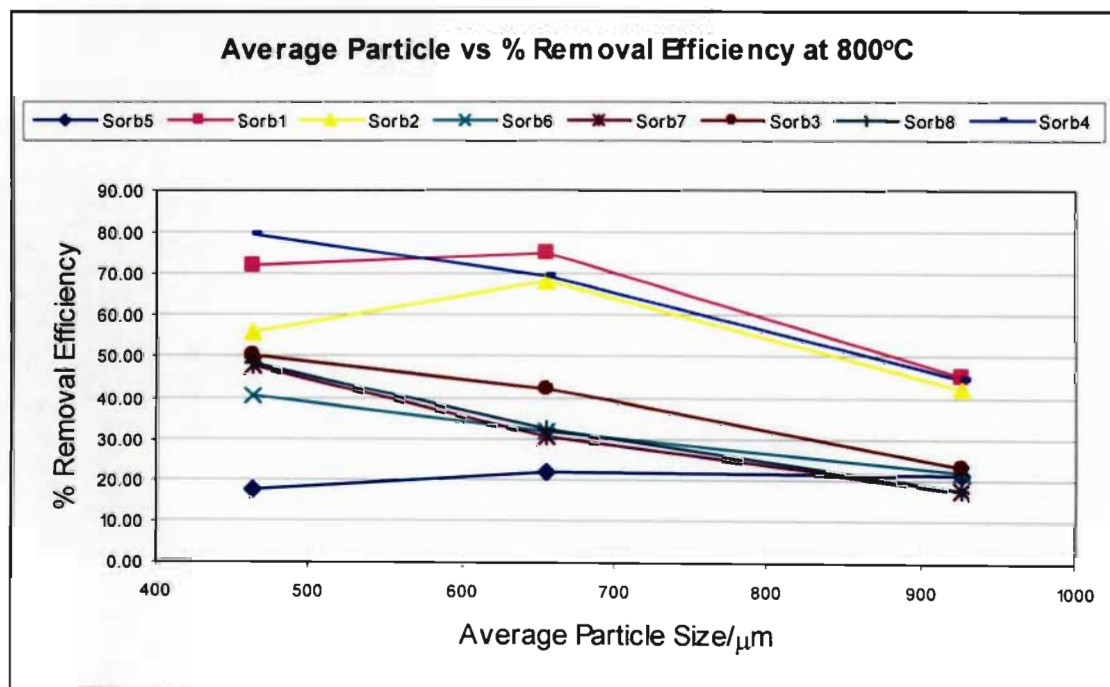
Figure 6-7 Effect of Particle Size on Removal Efficiencies of Sorbents at a Bed Temperature of 800°C
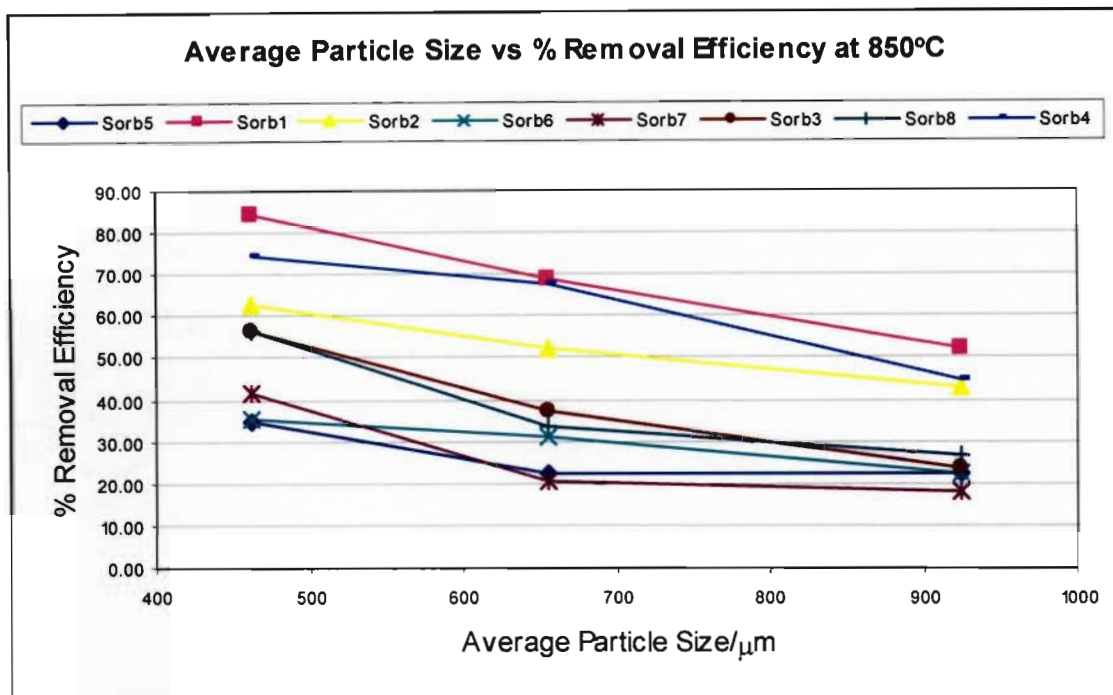
Figure 6-8 Effect of Particle Size on Removal Efficiencies of Sorbents at a Bed Temperature of 850°C
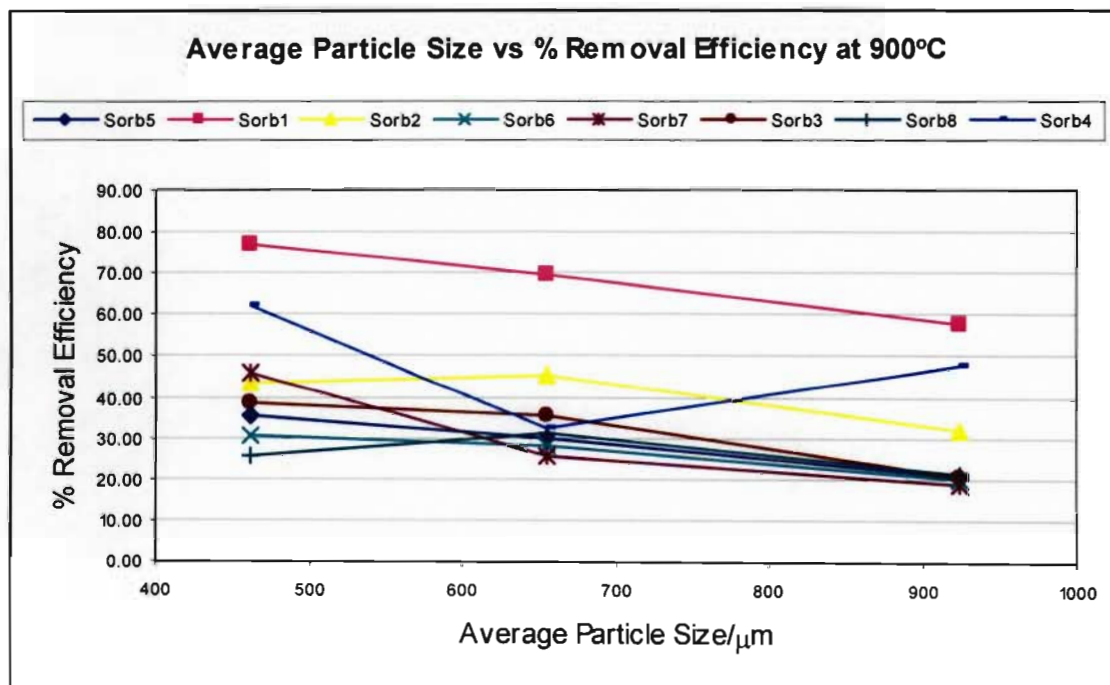
Figure 6-9 Effect of Particle Size on Removal Efficiencies of Sorbents at a Bed Temperature of 900°C

In Figure 6-4 to 6-9, the average particle size was used as the representation of the three particle size ranges tested in the AFBR. These were calculated to be 462.5μm for the 425-500μm particle size range, 655μm for the 600-710μm particle size range and 925μm for the 850-1000μm particle size range.

In Figure 6-4, at a bed temperature of 800°C, it was noted that the highest MSR occurred at the average particle size of 462.5μm. With an increase in the average particle size from 462.5μm to 655μm to 925μm, it was observed that there was a decrease in the desulphurisation ability of the sorbents.

From Figure 6-5 and 6-6, the trend observed in Figure 6-4 at the bed temperature of 800°C was also observed at the bed temperatures of 850 and 900°C, respectively. This trend of an increase in average particle size resulting in a decrease in the desulphurisation ability of the sorbents. This resulted in the average particle size of 462.5μm in Figure 6-5 and 6-6 obtaining the highest MSR.

This tendency of an optimum particle size range for the maximum sulphur retention for all sorbents was consistent with the findings of Pisupati et al. (1996), Chu et al. (2000) and Chi et al. (1994).

It should be noted that although the smallest particle size range sorbents of 425-500μm obtained the highest maximum sulphur retention in the AFBR; it was incorrect to stipulate that this is the optimum particle size range. This was the lowest particle size range tested in the AFBR with higher desulphurisation being possible with lower particle size ranges but this would be limited to factors of the fluidisation process in the AFBR such as entrainment, minimum fluidisation, etc.

For the sorbents removal efficiencies at the three average particle size ranges, it was found that there was a similarity in the trend experienced by the maximum sulphur retention at the three test temperatures. The deviations seen in Figures 6-7 to 6-9 can be attributed to experimental errors due to the high sensitivity of the removal efficiency. Thus it can be concluded that the highest removal efficiency would have been experienced at an average particle size range of 462.5μm for the three test temperatures.

In Figure 6-5, it was observed that the sorbents showed signs of separation into groups of good sorbents (Sorb1, Sorb2, Sorb4 and Sorb5) and bad sorbents (Sorb3, Sorb6, Sorb7 and Sorb8) as the average particle size increased with respect to their maximum sulphur retention. In Figure 6-6, this separation was much more visible. At the average particle size of 462.5μm the

maximum sulphur retention of the sorbents were clustered together and as the average particle size increased to 655μm, separation into groups became more visible. At 925μm, the group separation was the most visible.

From the separation of sorbents in Figure 6-5 and 6-6, it was noted that there was not much change in the maximum sulphur retention of the good sorbents as the average particle size increased as compared to the bad sorbents whose maximum sulphur retention dropped significantly. With this in mind a quick investigation into the desulphurisation ability of the sorbents can be made by tests performed on the larger particle size range with good sorbents obtaining better maximum sulphur retentions as compared to the bad sorbents.

6.5. Effect of Desulphurisation on Various Sorbents

The third parameter investigated for the sorbents desulphurisation ability in the AFBR was various sorbents. Tests were conducted on four different limestone sorbents and four different dolomite sorbents. Table 4-1 lists the names of the sorbent companies with Table 6-1 and 6-2 listing the results obtained from tests conducted on the AFBR for the maximum sulphur retention and removal efficiency, respectively. Table 6-3 lists the results and parameters for the best desulphurisation obtained for each of the eight sorbents.

Table 6-3 Desulphurisation Rankings of the Eight Sorbents

Sorbent	Maximum Sulphur Retention	Particle Size/μm	Temperature/°C	Ranking	Removal Efficiency	Particle Size/μm	Temperature/°C	Ranking
Sorb1	92.30	425-500	850	1	84.54	425-500	850	1
Sorb2	87.83	425-500	850	7	68.30	600-710	800	3
Sorb3	89.85	425-500	850	4	56.30	425-500	850	5
Sorb4	91.62	425-500	850	2	79.24	425-500	800	2
Sorb5	89.98	425-500	850	3	35.59	425-500	900	8
Sorb6	87.10	425-500	850	8	40.64	425-500	800	7
Sorb7	88.56	425-500	850	6	47.60	425-500	800	6
Sorb8	88.80	425-500	850	5	56.48	425-500	850	4

The highest maximum sulphur retention for the eight sorbents occurred at a bed temperature of 850°C and at the particle size range of 425-500μm. The highest removal efficiencies for the eight sorbents occurred at all of the three different baseline test bed temperatures and at the two lower particle size ranges of 425-500 and 600-710μm. However, this could be attributed to experimental error. As such, it would have been expected that the highest removal efficiencies

for the sorbents would have occurred at a bed temperature of 850°C and at the particle size range of 425-500μm, similar to that of the maximum sulphur retention.

From Table 6-3 it can be observed that the highest maximum sulphur retention occurred to the limestone Sorb1 with a value of 92.30%. This was followed by the limestone Sorb4 and then the dolomite Sorb5 with values of 91.62% and 89.98%, respectively. For the highest removal efficiencies, it was observed to occur to the limestone Sorb1 with a value of 84.54%, followed by the limestones Sorb4 and Sorb3 with values of 79.24% and 68.30%, respectively.

In Table 6-3, it was noted that the sorbents that performed well in their maximum sulphur retention did not necessarily perform well in their removal efficiencies. The most noticeable sorbent which showed this tendency was the dolomite, Sorb5, which had the third highest maximum sulphur retention but the lowest removal efficiency. It can therefore be concluded that the sorbents that perform well with their maximum sulphur retention would not necessarily perform well at their removal efficiency and vice versa. Thus the performance of all sorbents would have to be determined experimentally.

A good desulphurisation sorbent is a sorbent that has both high maximum sulphur retention and high removal efficiency. Thus from the results in Table 6-3 it was observed that Sorb1 followed by Sorb4 is the overall best suited material for desulphurisation.

6.6. Effect of New and Used Bed Material and Repeatability Desulphurisation Tests

One of the tasks in the operational procedure for the test work conducted on the sorbents in the AFBR was to remove the bed material after every test and replace it with a fresh silica sand bed. However this was not practically possible due to the time delay required to open the AFBR and replace the bed material after every run. To simplify and speed up the testing on the sorbents in the AFBR, the sorbents were saturated with excess SO_2 after every test run. This assumed that the saturated sorbents were inert and thus did not take part in the reaction during other test runs. This assumption was verified by the results for the maximum sulphur retention and removal efficiency tests conducted on inert sorbents within the silica sand bed material that can be seen in Table 6-4 and 6-5, respectively.

Table 6-4 New and Used Silica Sand Bed Material Maximum Sulphur Retention results on the desulphurisation of the sorbents

Particle Size/μm	Name of Sorbent	Temperature/ °C	Test1	Test2	Test3	% Error
425-500	Sorb8	850	89.26	88.80	89.52	0.804
600-710	Sorb4	900	87.65	86.13	88.67	2.865
600-710	Sorb7	800	82.74	82.30	83.89	1.895
850-1000	Sorb1	900	84.23	83.94	85.16	1.433

Table 6-5 New and Used Silica Sand Bed Material Removal Efficiency results on the desulphurisation of the sorbents

Particle Size/μm	Name of Sorbent	Temperature/ °C	Test1	Test2	Test3	% Error
425-500	Sorb8	850	84.48	84.54	85.18	0.822
600-710	Sorb4	900	32.29	31.68	33.12	4.348
600-710	Sorb7	800	30.53	29.97	30.35	1.834
850-1000	Sorb1	900	57.45	57.10	58.13	1.772

Fresh silica sand was used as the initial start-up bed material for the desulphurisation tests in the AFBR. After the completion of the first test on the fresh silica sand bed material, the bed material was identified as spent as it contained the saturated inert sorbents.

The values of Test1 in Table 6-4 and 6-5 were the results from the use of new clean bed material whilst the values for Test2 and Test3 were the results from the use of used or spent sorbent bed material. These tests were performed on different sorbents, at different bed temperatures and different particle size ranges as can be seen in these tables. The difference in operating conditions was used to ensure that a good representation for the use of new and used bed material was obtained.

The percentage error calculated for the use of new and used bed material can be seen in the last column of Table 6-4 and 6-5 for the sorbents maximum sulphur retention and removal efficiency, respectively. The percentage error was found to be below 2% for both the maximum sulphur retention and removal efficiencies with the exception of Sorb4 at the bed temperature of $900°C$ and a particle size range of 600-710μm. The rationale for the larger error for Sorb4 could be attributed to experimental error. It can therefore be concluded that the use of new and used

bed material in the AFBR had no effect on the overall desulphurisation ability of the sorbents, which proved to be a correct assumption.

The results from the tests conducted on new and used bed material were also used to substantiate the repeatability of the results for the desulphurisation ability of the sorbents. With the percentage error less than two percent it can be concluded that the repeatability of the results obtained for the sorbents desulphurisation ability were acceptable.

6.7. Tests on varying Quantities of Sorbents during Desulphurisation

Tests were conducted on the effect of increasing quantities (mass) of sorbent, on the sorbents ability to reduce sulphur dioxide. Tests were performed on one of the best performing sorbents, Sorb4, at its optimum maximum sulphur retention operating conditions of a particle size range of 425-500μm and a bed temperature of 850°C. The results of these tests can be seen in Table 6-6.

Table 6-6 Results of tests performed on varying quantities of the sorbent Sorb4

Weight/grams	Maximum Sulphur Retention	Removal Efficiency
10	79.65	51.28
15	87.37	66.75
20	91.23	79.00
25	92.28	81.31

The results from Table 6-6 were plotted on a graph, which can be seen in Figure 6-10.
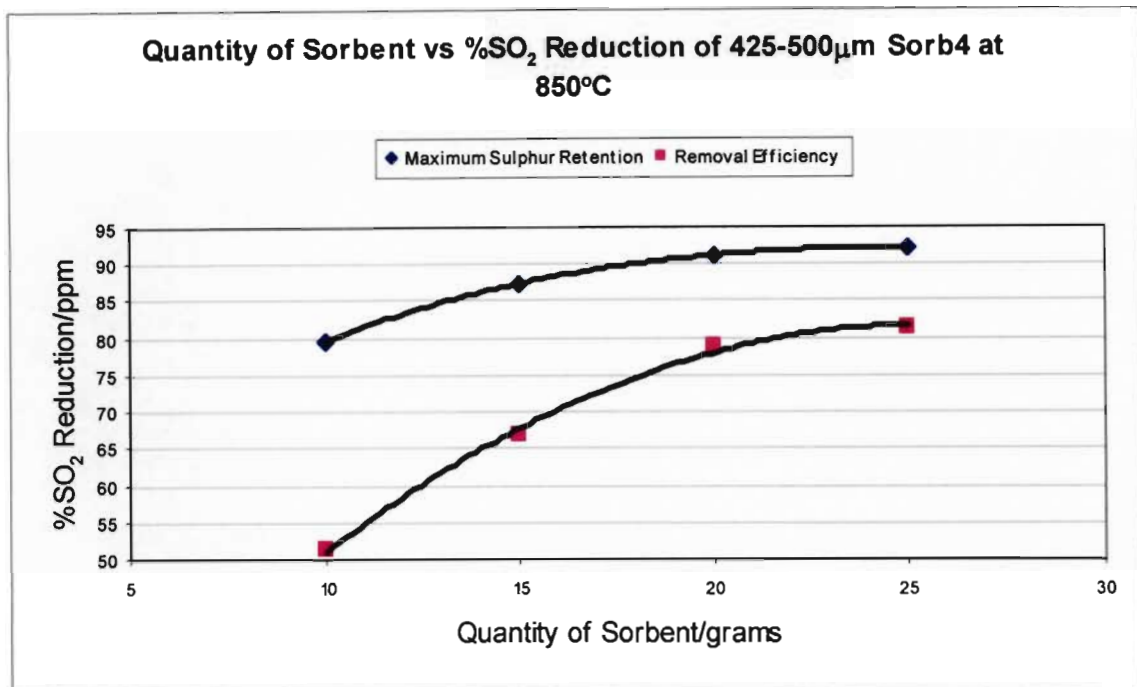
Figure 6-10 Effect of Quantity of Sorbents on Desulphurisation

The asymptotic curved lines in Figure 6-10 indicate that as the quantity of sorbents increased, the sorbents maximum sulphur retention and removal efficiency also increased.

Towards the end of the asymptotic curves in Figure 6-10, it was noted that a stage with regard to the quantity of sorbent was reached whereby any further increase in the quantity of sorbent added to the AFBR produced little desulphurisation. Although there was no optimum quantity with respect to obtaining the highest desulphurisation, there was a range where it was economically feasible to run the AFBR. Any further increase in the quantity of sorbents would not be feasible due to the marginal increase in desulphurisation.

For each sorbent, their optimum quantity range would have to be determined experimentally, similarly to the test performed above.

6.8. Effect of Ca/S Molar Ratios on Sorbents Desulphurisation Ability

Tests of fixed Ca/S molar ratios and fixed sorbent quantities were performed on two limestones and one dolomite at their optimum maximum sulphur retention operating conditions of a particle size range of 425-500µm and a bed temperature of 850°C.

For batch sorbent feed operation, a fixed Ca/S molar ratio for the entire period of the test cannot be achieved due to the fixed amount of calcium present in the quantity of sorbent added to the AFBR at the start of the test run. With the continuous feed of SO_2 at a constant rate into the AFBR during the test, there was a continuous decrease in the calcium content with time during the test, which produced a continuous decrease in the Ca/S molar ratio. However, it was possible to integrally determine the Ca/S molar ratios for a fixed time period, which had to be calculated for each sorbent due to their difference in calcium content.

For these tests, the quantity of sorbent required for a Ca/S molar ratio of 2 for a period of fifteen minutes in the AFBR was used. The Ca/S molar ratio of 2 was chosen as it was found to be the frequently used ratio for fluidised bed reactor designs. The results of the fixed Ca/S molar ratio tests are given in Table 6-7.

Table 6-7 Results of the tests performed at a fixed Ca/S molar ratio of 2

Name of Sorbent	Quantity of Sorbent/grams	Maximum Sulphur Retention/Fixed Ca/S Molar Ratio	Removal Efficiency/Fixed Ca/S Molar Ratio
Sorb3	11.42	47.14	14.69
Sorb4	8.73	52.76	22.38
Sorb5	17.55	70.00	20.53

Table 6-8 tabulates the results for a fixed quantity of sorbent added to the AFBR.

Table 6-8 Results of the tests performed at a fixed quantity of 20 grams of sorbent

Name of Sorbent	Ca/S Ratios	Maximum Sulphur Retention/Fixed Ca/S Molar Ratio	Removal Efficiency/Fixed Ca/S Molar Ratio
Sorb3	3.52	89.85	56.30
Sorb4	4.60	91.62	74.23
Sorb5	2.29	89.98	34.52

The results in Table 6-7 and 6-8 are represented in Figure 6-11 and 6-12, respectively.
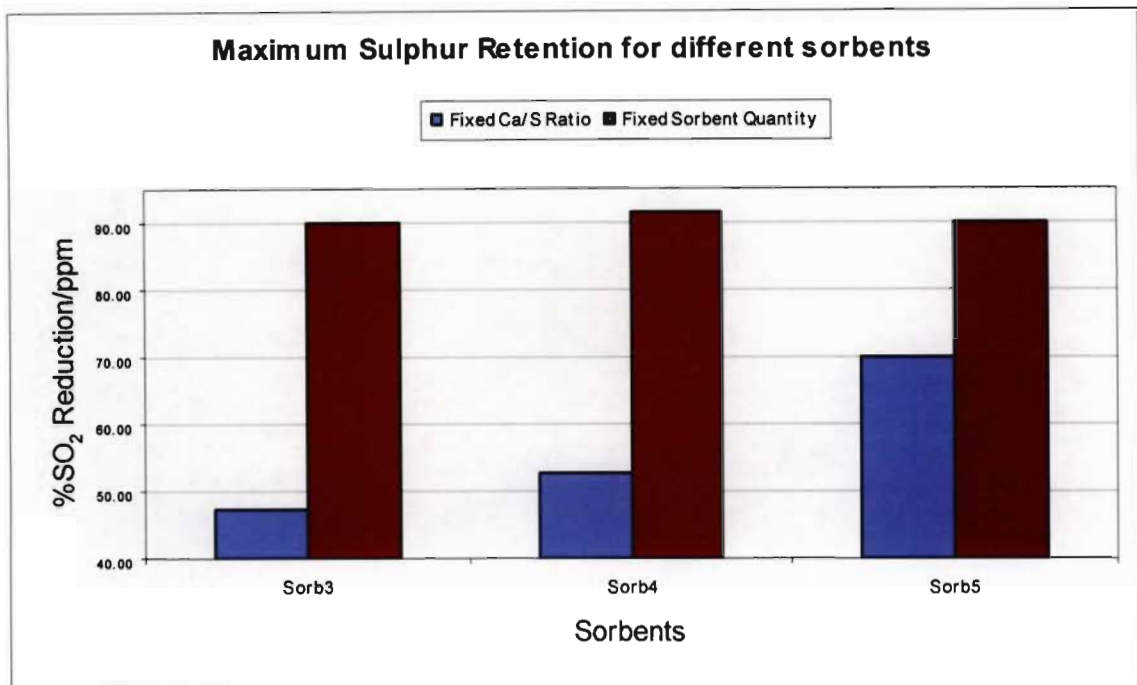
Figure 6-11 Effect of a fixed Ca/S Molar Ratio on the sorbents Maximum Sulphur Retention
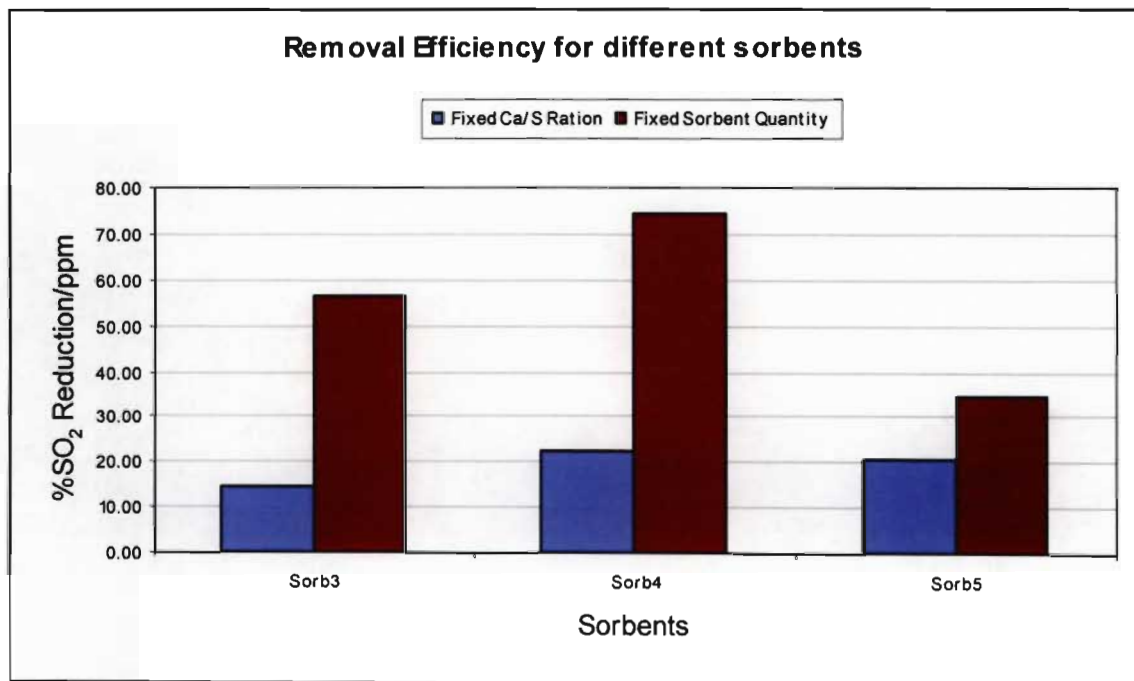
Figure 6-12 Effect of a fixed Ca/S Molar Ratio on the sorbents Removal Efficiency

For Sorb5, it was noted that with an increase of 2.45 grams of the sorbent, there was an increase of 42.71% in its maximum sulphur retention and an increase of 13.99% in its removal efficiency. For Sorb4 with an increase of 11.27 grams of sorbent there was an increase of 38.86% and 51.85% for its maximum sulphur retention and removal efficiency, respectively.

Both these sorbents look feasible proposals for their increase in sorbent quantity added to the AFBR but for different reasons. For Sorb5, with a small increase in quantity there was a significant change in maximum sulphur retention. For Sorb4 with more than double the quantity of sorbent, there was a significant change in both its maximum sulphur retention and removal efficiency. However, no matter how feasible these proposals may look, their cost implication in their application in a commercial FBC plant would be responsible for the final decision.

6.9. Effect of Chemical composition on Sorbents Desulphurisation Ability

The influence of the chemical composition on the desulphurisation ability of the sorbents was compared in this section. Table 6-9 displays some of the chemical compositions for the sorbents together with their maximum sulphur retention at their best operating conditions of a particle size range of 425-500µm and a bed temperature of 850°C.

Table 6-9 Sorbents XRF Results and best Maximum Sulphur Retention

Sorbent	CaO	MgO	SiO_2	Inherent H_2O	Maximum Sulphur Retention
Sorb1	22.36	0.66	9.45	1.42	92.30
Sorb2	33.96	0.81	2.92	0.49	87.83
Sorb3	39.15	9.97	5.23	0.39	89.85
Sorb4	51.21	0.64	3.94	0.63	91.62
Sorb5	25.48	13.89	2.42	0.12	89.98
Sorb6	25.39	16.48	0.91	0.13	87.10
Sorb7	29.76	19.86	2.24	0.23	88.56
Sorb8	25.49	13.13	2.82	0.17	88.80

These results in Table 6-9 are represented in Figure 6-13 to 6-16.
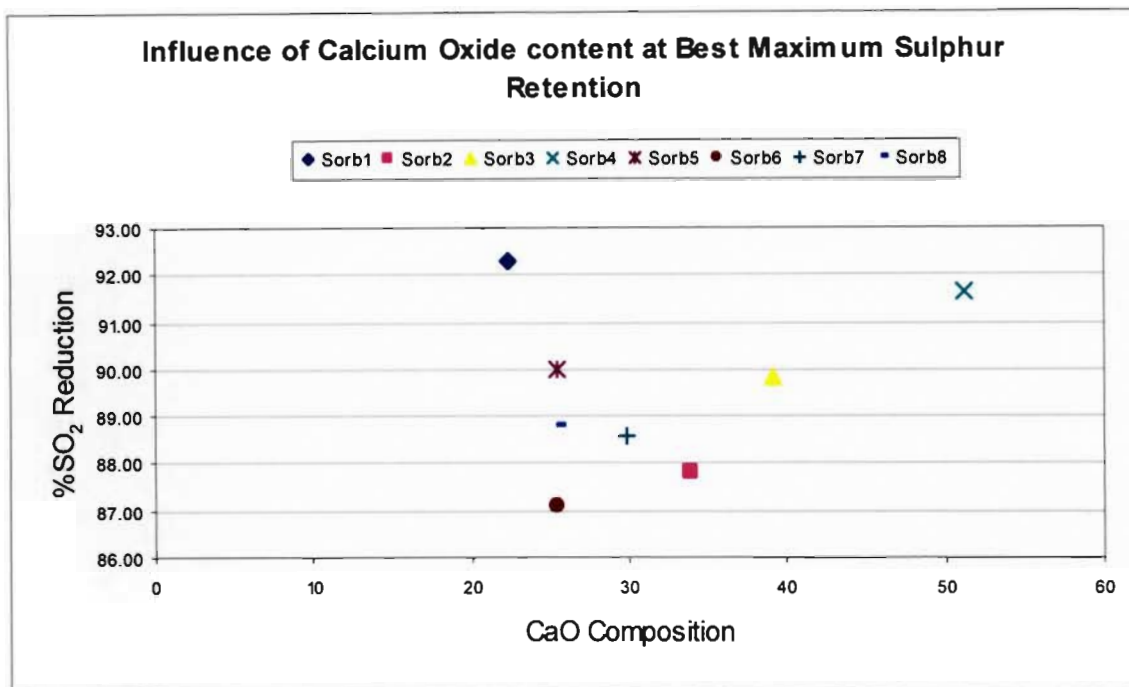
Figure 6-13 Effect of Calcium Oxide on the sorbents desulphurisation ability
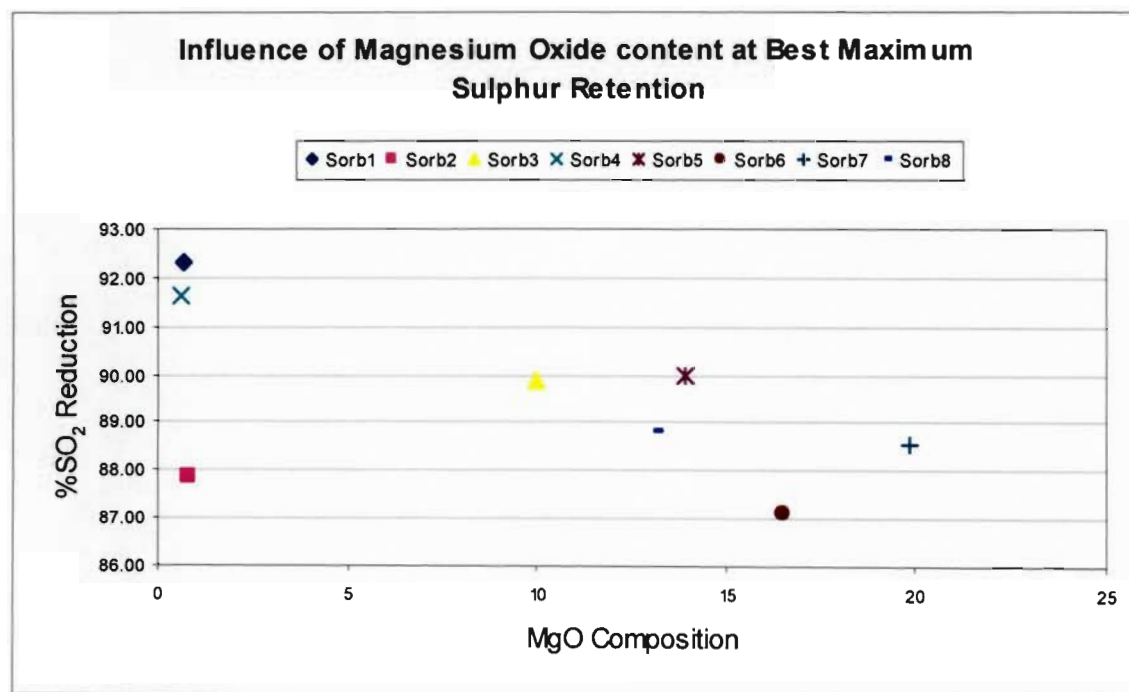
Figure 6-14 Effect of Magnesium Oxide on the sorbents desulphurisation ability
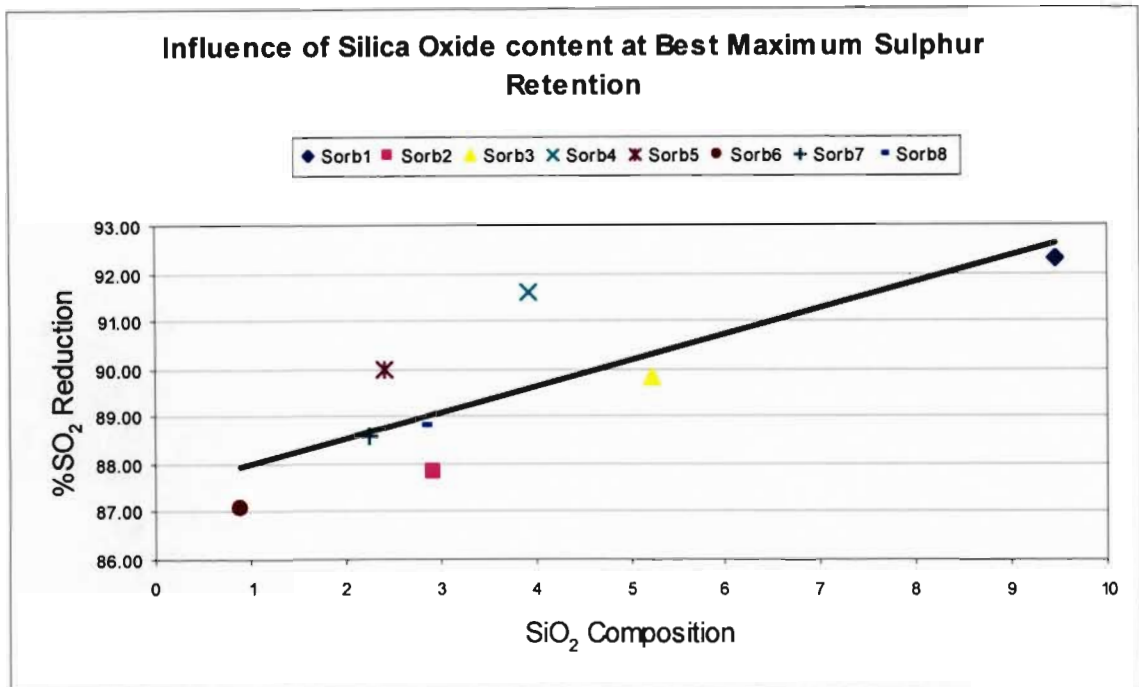
Figure 6-15 Effect of Silica Oxide on the sorbents desulphurisation ability
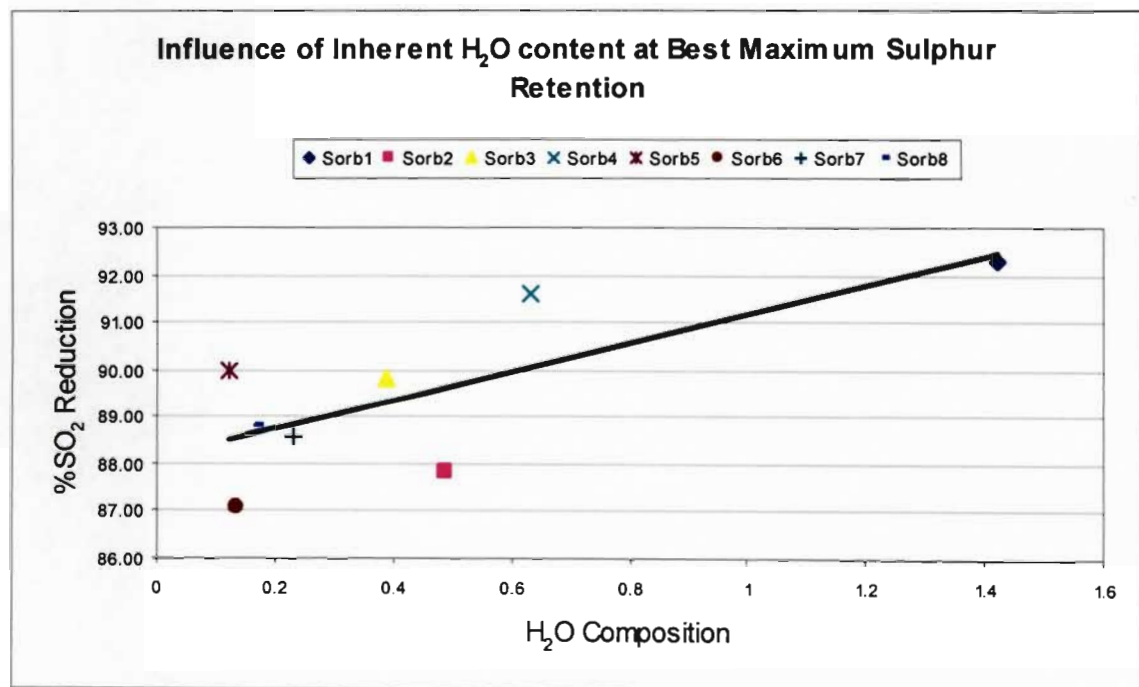
Figure 6-16 Effect of Inherent Water on the sorbents desulphurisation ability

From Table 6-9, it can be seen that for the limestone samples (Sorb1 to Sorb4), CaO composition varied between 21.83 and 51.74 as compared to the dolomite samples (Sorb5 to Sorb8) whose CaO composition varied between 24.33 and 30.24. It was also noticed that the MgO composition for the limestone varied between 0.64 and 10.23 and that for the dolomites varied from 11.33 to 20.64.

From the best maximum sulphur retention sorbent (Sorb1) it can be seen that the CaO content was the lowest of all the eight sorbent material and therefore the conception that the highest CaO performs the best is untrue. This concept of the chemical composition of the sorbent not influencing the desulphurisation ability of the sorbent is consistent with the findings of Pisupati et al. (1996) and Haji-Sulaiman et al. (1991). Further verification of this can be seen in Figure 6-13, which displays the variation in CaO contents not being consistent with the desulphurisation ability of the sorbents.

For the MgO content it was shown in Figure 6-14 that this composition had no significant influence on the desulphurisation ability of the sorbent. The only noticeable chemical composition that can be seen in Table 6-9 to have any significance to the sorbent desulphurisation was the silica and inherent water content of the sorbent, which can be seen in Figure 6-15 and 6-16, respectively. From these figures it can be seen with reasonable doubt that as the quantity of silica and inherent water increased the desulphurisation ability of the sorbents also increased.

6.10. Effect of Hardgrove Grindability Index on Sorbents Desulphurisation Ability

Hardgrove Grindability Index (HGI) tests were performed on the sorbents to determine their texture i.e. softness or hardness. These results were found to be directly related to the ease at which the sorbents could be crushed which has an overall effect on production cost. The results of the tests conducted on the eight sorbents can be seen in Table C-1 in Appendix C. From these results it was noted that as the HGI values increased, the material became softer and vice versa.

The average HGI values in Table C-1 can be seen in Table 6-10 together with the removal efficiencies at the particle size range of 425-500μm and a bed temperature of 850°C.

Table 6-10 Results of Average HGI and Removal Efficiency at the best operating conditions

Sorbent	HGI	Removal Efficiency
Sorb1	99	84.54
Sorb2	83	62.53
Sorb3	58	56.30
Sorb4	84	74.23
Sorb5	46	34.52
Sorb6	63	35.48
Sorb7	55	41.68
Sorb8	57	56.48

From Table 6-10, it can be seen that the limestones (Sorb1 – Sorb4) are a much softer material as compared to the dolomites (Sorb5 – Sorb8). The limestones HGI values ranged between 58 and 99 whilst the dolomites HGI values ranged between 46 and 63. Fluidised beds are known to have high attritions of sorbent particles with other sorbents, bed material and to reactor walls, which results in the removal of the product layer of sulphate thus increasing the utilisation of the calcium sorbent. Softer sulphating product layers are produced with softer sorbents and therefore with limestones being the softer material it was expected that the limestones would be a much better desulphurisation material than the dolomite.

From Figure 6-1 it was noted that the maximum sulphur retention took place at the beginning of the test run when the sorbent was added to the AFBR. At this period of time there was no influence of the HGI on the sorbents as the initial sulphation takes place on the surface of the sorbent. With time during the test, the sorbents are exposed to the abrasion and attrition processes that expose the interior of the sorbent which influences the removal efficiency results of the sorbents.

The results in Table 6-10 are represented in Figure 6-17.

Comparison of Removal Efficiency to HGI
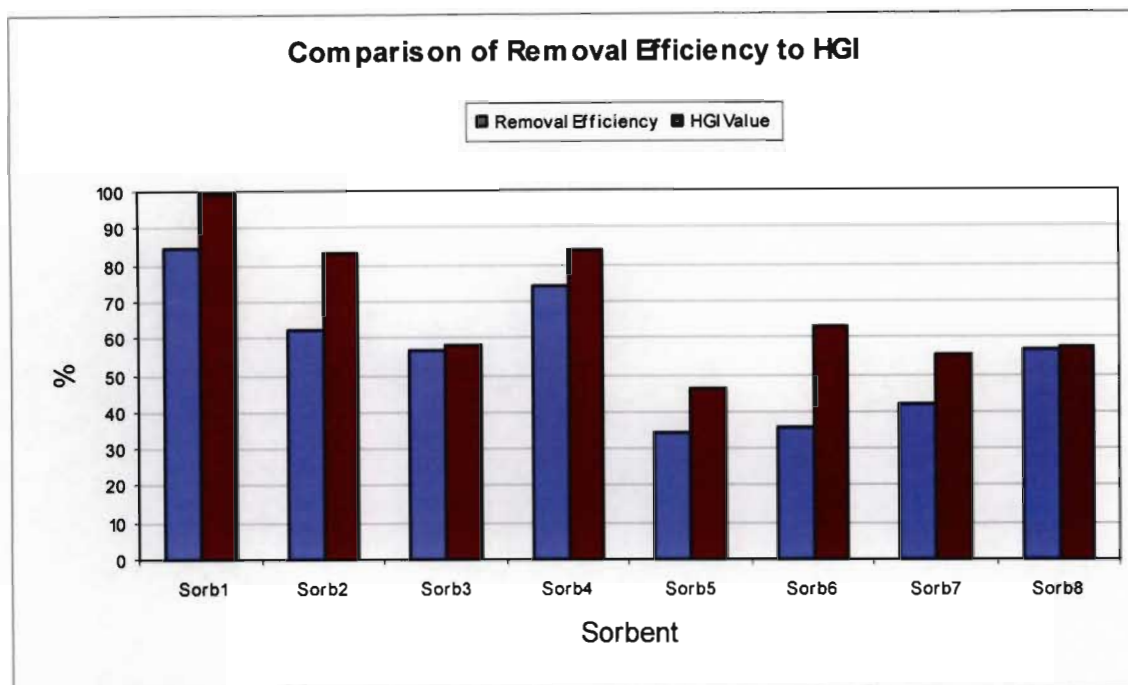
Figure 6-17 Comparison of Average HGI and Removal Efficiency tests conducted on sorbents

In Figure 6-17, the removal efficiency tests for the limestones (Sorb1 – Sorb4) and dolomites (Sorb5 – Sorb8) were found to have a relation to the average HGI results. In this figure, it can be seen that the overall desulphurisation ability increased with the increase in the softness of the limestones and dolomite with the exception of Sorb6. It can therefore be stated that the softer the material, the higher their overall SO_2 reduction.

6.11 Effect of Petrographical analysis on Sorbents Desulphurisation Ability

The petrographical analysis description of the eight sorbent samples with respect to their thin sections can be seen in Table 4-2 in Chapter 4. Pictures of these petrographical slides can be seen in Figure A1 – A8 in Appendix A. This table in Chapter 4 explains the sorbents structure, porosity, compositions etc.

The sorbent particles have shown significant differences in carbonate crystallise size with some samples containing both small and large crystallite. Iron and iron staining was found to be well developed in some samples but not in others. All the sorbents showed signs of low porosity. From the descriptions given for the eight sorbents in Table 4-2, there was no obvious reason found for the difference between the sorbents ability to remove SO_2.

Chapter Seven

Conclusions and Recommendations

7.1. Conclusions

This study was initiated to evaluate the effects of three primary operating variables viz. bed temperature, particle size of the sorbents and various sorbents commercially available in South Africa, ability to reduce SO_2 during atmospheric fluidised bed combustion. The findings were as follows:

1. For an overall good sorbent, it was concluded that the sorbent would have to have both high maximum sulphur retention and high removal efficiency.

2. Increasing the bed temperature to 850°C resulted in an increase in the maximum sulphur retention of the sorbents. Any further increase in the bed temperature resulted in the decrease of the maximum sulphur retention of the sorbents. This indicated the existence of an optimum bed temperature for the highest maximum sulphur retention, which was 850°C for all the sorbents tested in this study. The highest removal efficiencies for the eight sorbents varied between the baseline test temperatures of 800 and 900°C. It can therefore be concluded that there is no optimum temperature for the removal efficiencies of the eight sorbents and their performance would have to be determined experimentally.

3. As the particle size range decreased from 850-1000µm to 425-500µm, there was an increase in the maximum sulphur retention of the sorbents. For this study it was found that the optimum range was our smallest particle size range of 425-500µm. However, it is possible that smaller particle size ranges could obtain higher desulphurisation but this would be limited to the fluidisation characteristic of the AFBR. The removal efficiencies for the sorbent particle size ranges tested showed no particular trend and can thus be attributed to experimental error due to the high sensitivity of the removal efficiency

calculation. However, it can be noted that the trend experienced for MSR would have occurred for the removal efficiencies of best efficiency at lower particle size ranges.

4. For the four limestone and four dolomite sorbents tested at the baseline bed test temperature ranges of between 800 and 900°C, it was found that the limestones Sorb1 and Sorb4 obtained the best desulphurisation. This suggests that the limestone sorbents tested are a better overall performing desulphurisation material as compared to the dolomites.

Additional tests were performed on the sorbents to get a better understanding of their desulphurisation ability. The findings were as follows:

1. Increasing the quantity of sorbent added to the AFBR resulted in an increase in desulphurisation ability of the sorbent. Nevertheless for desulphurisation beyond certain limits any further increase in the quantity of sorbent added to the AFBR resulted in a marginal increase in desulphurisation.

2. The calcium and magnesium composition of the sorbents were found not to have an influence on their desulphurisation ability. This confirms that the calcium content of sorbents is not a good indicator in determining the desulphurisation ability of sorbents and therefore cannot be used to choose sorbents as was done in the past. However, the silica and inherent water content of the sorbents showed signs of a direct proportionality correlation with SO_2 reduction.

3. The Hardgrove Grindability Index of the sorbents was found to have an influence on the sorbents removal efficiency with the softer material producing a better removal efficiency.

4. From the petrographical analysis performed on the eight sorbents, it was found that there was no obvious reason for the difference between the sorbents ability to remove SO_2.

7.2. Recommendations

As a result of this research, the following may prove useful possibilities for future research. They are:

1. To investigate the influence of sorbents on greenhouse gases such as N_2O and CO_2.

2. To investigate the influence of other operating parameters on the desulphurisation of the sorbents, besides those that were investigated in this thesis. Researchers such as Alvarez and Gonzalez (1999), Chu et al. (2000), etc. have found parameters such as SO_2 concentration, relative humidity, gas velocity, pore volume, CO_2 concentration, surface area, O_2 concentration etc. to have a significant influence on desulphurisation.

3. To change the method of operation of the AFBR from batch sorbent feed that was investigated in this study to continuous sorbent feed. This would assist in the addition of another parameter to be investigated, constant Ca/S molar ratio. All commercial scale and pilot scale FBC plants operate on a continuous feed system so it would be a feasible change.

4. To further investigate the influence sorbents geological properties has on desulphurisation. This has only been touched lightly in this thesis with much greater research possible. This could prove crucial in determining the best sorbents available in South Africa.

5. To investigate the performance of sorbents during the combustion of coal in a laboratory scale Fluidised Bed Combustion reactor.

References

1. 15th Anniversary of the Clean Air Act – U.S. Environmental Protection Agency. Available from http://epa.gov/air/cleanairact/ [Assessed 03 March 2006].

2. 2003 Eskom Annual Report

3. 2004 Eskom Annual Report

4. Abanades, J.C. et al., *The Sulphation Reaction of Limestone Particles over a Time Scale of Weeks.*

5. Acid rain data and reports. Available from http://www.bqs.usgs.gov/acidrain.html [Accessed 18 June 2003]

6. Adanez, J. et al., 1994a. Fuel. *Methods for characterization of sorbents used in fluidized bed boilers*, 73(3), 355-362.

7. Adanez, J. et al., 1994b. Fuel Processing Technology. *Sulfur retention in AFBC. Modelling and sorbent characterization*, 36, 73-79.

8. Alvfors, P. and Svedberg, G., 1992. Chemical Engineering Science. *Modelling of the Simultaneous Calcination, Sintering and Sulphation of Limestone and Dolomite*, 47(8), 1903-1912.

9. Alvarez, E. and Gonzalez, J.F., 1999. Fuel. *High pressure thermogravimetric analysis of the direct sulphation of Spanish calcium-based sorbents*, 78, 341-348.

10. Anthony, E.J. and Granatstein, D.L., 1999. *Sulphation phenomena in high temperature systems.*

11. Bates, R.L. and Jackson, J.A., 1980. *Glossary of Geology.* 2nd ed. United States of America: McGraw-Hill.

12. Broadhurst, T.E. and Becker, H.A., 1975. AIChE. *Onset of fluidisation and slagging in beds of uniform particles,* 21, 238-247.

13. Chang, E.Y. and Thodos, G., 1984. AIChE Journal. *Complex Nature of the Sulfation Reaction of Limestones and Dolomites,* 30(3), 450-457.

14. Chi, Y. et al., 1994. Fuel. *A simplified technique for measurement of sorbent reactivity for use in circulating fluidized bed combustors,* 73(1), 117-122.

15. Chu, C.Y. et al, 2000. Journal of Hazardous Materials. *Sulphation and attrition of calcium sorbent in a bubbling fluidised bed,* B80, 119-133.

16. Chu, C.Y. and Hwang, S.J., 2002. Powder Technology. *Attrition and Sulfation of Calcium Sorbent and Solids Circulation Rate in an Internally Circulating Fluidized Bed,* 127, 185-195.

17. Coal Utilization Center Research Activities. Available from: http://www.personal.psu.edu/faculty/s/f/sfm1/activitiestext.html [Accessed 28 August 2002].

18. Coates, N.H. and Rice, R.L., 1976. AIChE Symposium Series. *Sulfur Dioxide Reduction by Combustion of Coals in Fluidized Beds of Limestone,* 70(141), 124-129.

19. Coetzee, C.B., 1976. *Mineral Resources of the Republic of South Africa – Limestone and Dolomite.* Geological Survey of South Africa. Handbook 7.

20. Dennis, J.S. and Hayhurst, A.N., 1990. Chemical Engineering Science. *Mechanism of the Sulphation of Calcined Limestone Particles in Combustion Gases,* 45(5), 1175-1187.

21. Department of Minerals and Energy, Republic of South Africa, 2002. *Producers of Industrial Minerals Commodities in South Africa.* D11/2002

22. Department of Minerals and Energy, Republic of South Africa, 2003. *A Review of the Dolomite and Limestone Industry in South Africa.* R43/2003

23. DOE – Fossil Energy: Education Page – Introduction to Coal. Available from http://www.fossil.energy.gov/education/intro_coal.html [Accessed 25 October 2002].

24. EPA's Clean Air Market Programs – Effects of Acid Rain. Available from: http://www.epa.gov/airmarkets/acidrain.html [Accessed 29 August 2002]

25. Eskom – Power Stations. Available from http://www.eskom.co.za/live/content.php?Category_ID=82 [Accessed 03 March 2006]

26. Fee, D.C. et al., 1983. Chemical Engineering Science. *Fluidized-Bed Coal Combustion: In-Bed Sorbent Sulfation Model*, 38(11), 1917-1925.

27. Fuertes, A.B. et al., 1993. Fuel Processing Technology. *Sulphur Retention by Limestone Particles under PFBC Conditions*, 36, 35-71.

28. Garcia-Labiano, F. and Adanez, J., 1992. The Canadian Journal of Chemical Engineering. *Characterization of the Reactivity of Limestones with SO_2 in a Fluidized Bed Reactor*, 70, 734-741.

29. Geldart, D., 1986. *Gas Fluidization Technology*. London: John Wiley and Sons

30. Haji-Sulaiman, M.Z. et al., 1990. Fuel Processing Technology. *Optimum Sulfation Temperature for Sorbents Used in Fluidised Bed Combustion*, 25, 227-240.

31. Haji-Sulaiman, M.Z. and Scaroni, A.W., 1991. Fuel. *The calcination and sulphation behaviour of sorbents in fluidized bed combustion*, 70, 169-175.

32. Hartman, M. and Coughlin, R.W., 1976. AIChE Journal. *Reaction of Sulfur Dioxide with Limestone and the Grain Model*, 22(3), 490-498.

33. Hartman, M. et al., 2000. Chemical Engineering Science. *Fluidization Characteristics of Dolomite and Calcined Dolomite Particles*, 55, 6269-6274.

34. Hutchison, C.S., 1974. *Laboratory Handbook of Petrographic Techniques*. London: John Wiley and Sons.

35. Jenkins, R. and Snyder, R.L., 1996. *Introduction to X-Ray Powder Diffraction*. Vol 138 in Chemical Analysis Monographs on Analytical Chemistry. London: John Wiley and Sons.

36. Kearey, P., 2001. *The new Penguin Dictionary of Geology*. 2nd Edition. London: Penguin Books.

37. Kent, L.E., 1980. *Part1: Lithostratigraphy of the Republic of South Africa, South West Africa/Namibia and the Republics of Bophuthatswana, Transkei and Venda.* The South African Committee for Stratigraphy (SACS). Handbook 8.

38. Khan, W.Z. and Gibbs, B.M., 2000. The Canadian Journal of Chemical Engineering. *High Temperature Desulphurization by Fine Limestone During Staged Fluidized-Bed Combustion,* 78, 1102-1110.

39. Kocaefe, D. et al., 1985. The Canadian Journal of Chemical Engineering. *Comparison of the Sulfation Rates of Calcium, Magnesium and Zinc Oxides with SO_2 and SO_3,* 63, 971-977.

40. Laursen, K. et al., 2000. Fuel. *Sulfation and Reactivation Characteristics of Nine Limestones,* 79(200), 153-163.

41. Lee, D.C. and Georgakis, C., 1981. AIChE Journal. *A Single, Particle-Size Model for Sulfur Retention in Fluidized Bed Coal Combustors,* 27(3), 472-481.

42. Lu, A. et al., 2003. Mineralogical Magazine. *Application of Vermiculite and Limestone to Desulphurization and to the Removal of Dust During Briquette Combustion,* 67(6), 1243-1251.

43. Lyngfelt, A. and Leckner, B., 1998. Journal of the Institute of Energy. *Sulphur capture in Circulating Fluidised-Bed Boilers: Decomposition of $CaSO_4$ under local Reducing conditions,* 71, 27-32.

44. Lyngfelt, A. and Leckner, B., 1999. Chemical Engineering Science. *Sulphur capture in circulating fluidised-bed boilers: Can the efficiency be predicted?,* 54, 5573-5584.

45. Mann, M.D. et al., *Characterization of Alkali and Sulfur Sorbents for Pressurized Fluidized-Bed Combustion.*

46. Mattisson, T. and Lyngfelt, A., 1998. The Canadian Journal of Chemical Engineering. *A Method of Evaluating Limestone Reactivity with SO_2 under Fluidized Bed Combustion Conditions,* 76, 762-770.

47. Minerals and Energy. Available from: http://www.gov.za/yearbook/2001/minerals.html [Accessed 25 October 2002].

48. Morrison, J.L. et al., *Evaluation of Sorbent Performance for Atmospheric Circulating Fluidized-Bed Combustor Applications.*

49. O'Neill, E.P. and Keairns, D.L., 1979. AIChE Symposium Series. *Selection of Calcium-Based Sorbents for High-Temperature Fossil Fuel Desulfurization*, 73(161), 100-107.

50. Ozer, A.K., et al., 2002. Fuel. *Flue gas desulphurisation with phosphate rock in a fluidised bed*, 81, 41-49.

51. Petrie, J.G., 1988. *Sulphur Sorbent Particle Effects in Fluidised Combustion.* Thesis (PhD). University of Cape Town.

52. Pisupati, S.V. et al., 1993. Fluidized Bed Combustion. *Importance of Calcium Carbonate Content on the Sulphur Capture Performance of Naturally-Occurring Sorbents in a 30 MW (e) Circulating Fluidized-Bed Plant*, 2, 1069-1078.

53. Pisupati, S.V. et al., 1995. *Evaluation of Sorbents in a Pilot-Scale, Circulating Fluidized Bed Combustor.*

54. Pisupati, S.V. et al., 1996. Fuel. *Sorbent behaviour in circulating fluidized bed combustors*, 75(6), 759-768.

55. Pisupati, S.V. and Scaroni, A.W., *Sorbent Characterisation for FBC Application.*

56. Potts, P.J., 1987. *Handbook of Silicate Rock Analysis.* Glasgow: Blackie.

57. Pressurized Fluidized Bed Combustion. Available from: http://www.siu.edu/~coalctr/presfbc.htm [Accessed 28 August 2002].

58. REC: Reduction of SO_2 and Particulate Emissions: Legal Framework (4.5). Available from: http://www.rec.org/REC/Publications/SO2/chapter45.html [Accessed 16 March 2006].

59. Romans, D.E. et al., 1993. The effect of Experimental Technique in Determining Sorbent Performance for FBC Applications. *In:* K.H. Michaelian, ed. *International Conference on Coal Science*, 12-17 September 1993 Canada. 550-553.

60. Rozelle, P.L. et al., *Prediction of Sorbent Performance in a CFB Boiler Based on Sorbent Petrographic Properties.*

61. Saxena, S.C. and Vogel, G.J., 1976. The Canadian Journal of Chemical Engineering. *The Properties of a Dolomite Bed of a Range of Particle Sizes and Shapes at Minimum Fluidization*, 54, 453-455.

62. Schmitz, W., 1996. Technology Group Research Report. *Limestone Enquiry for Komati FBC Re-Powering*, Confidential.

63. Spilkova, T. and Carsky, M., 2002. Chemical Technology. *Environmental Protection in Central Europe during the last decade*, 24-27.

64. Svoboda, K. et al., 1988. Ochrana Ovzdusi. *The Effect of Amount and Quality of a Sorbent and Flue Gas Composition on Desulphurization in a Fluidised Bed*, 2, 40-44.

65. Svoboda, K. et al., 2001. Acta Montana IRSM AS CR. *Desulfurization under Conditions of Substoichiometric Pressurized Fluidized Bed Combustion of Coal – Comparison with TG – Tests and Equilibrium Limits*, 11(120), 39-53.

66. Trikkel, A. et al., *Estonian Calcareous Rocks as SO_2 Sorbents in AFBC and PFBC Conditions.*

67. Trikkel, A., Zevenhoven, R. and Kuusik, R., *Estonian calcareous rocks as SO_2, sorbents in AFBC and PFBC conditions.*

68. Tucker, M., 1991. *Techniques in Sedimentology.* London: Blackwell Science Publications.

69. World Coal Institute – The Role of Coal as an Energy Source. Available from http://www.worldcoal.org/pages/content/index.asp?PageID=35 [Accessed 31 March 2006].

70. Wu, Y.H. et al., *Experimental and Mechanism Studies on a Pilot-Scale Circulating Fluidized Bed for Flue Gas Desulfurization.*

Appendix A

Petrographical Slide Analysis of the Sorbents
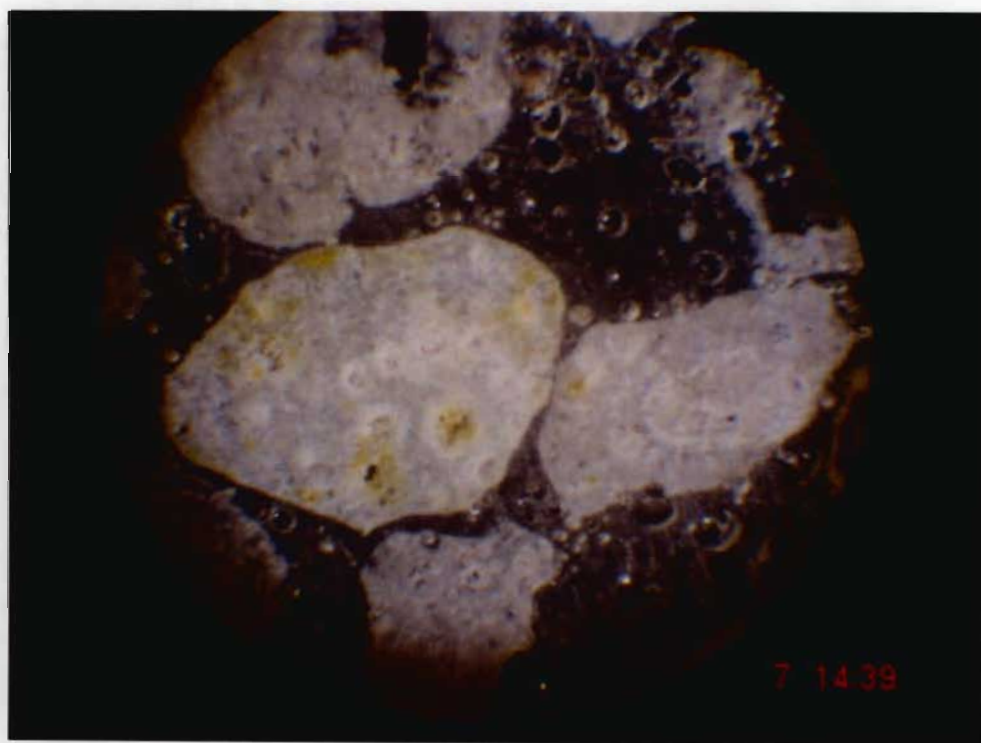
Figure A-1: Petrographical slide of Sorbent Sorb1
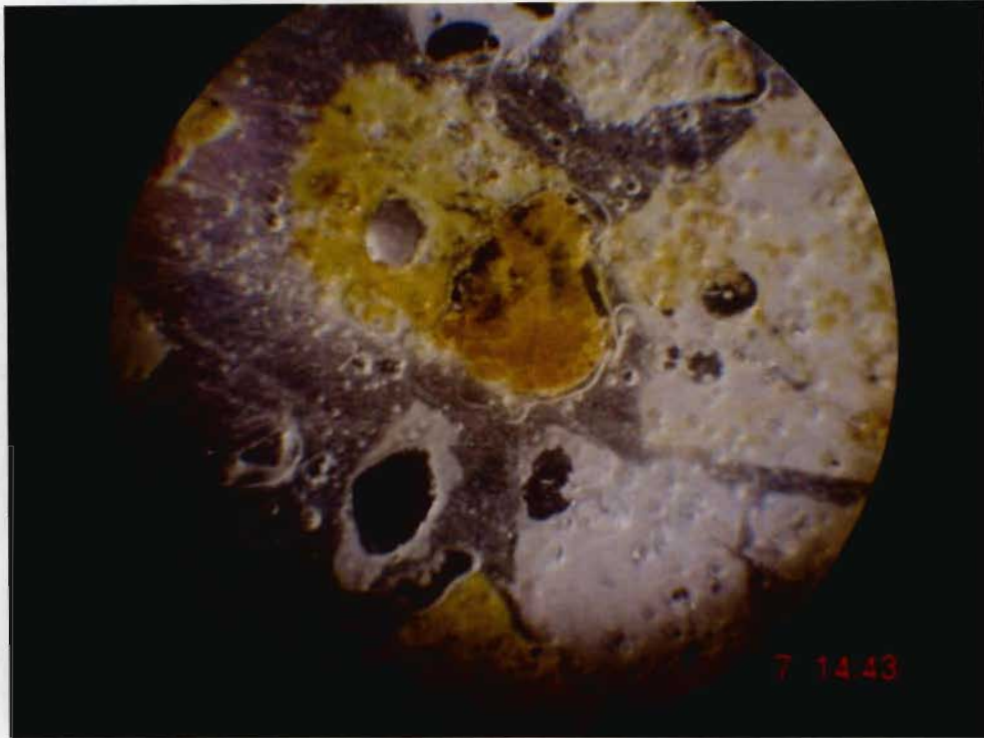
Figure A-2: Petrographical slide of Sorbent Sorb2
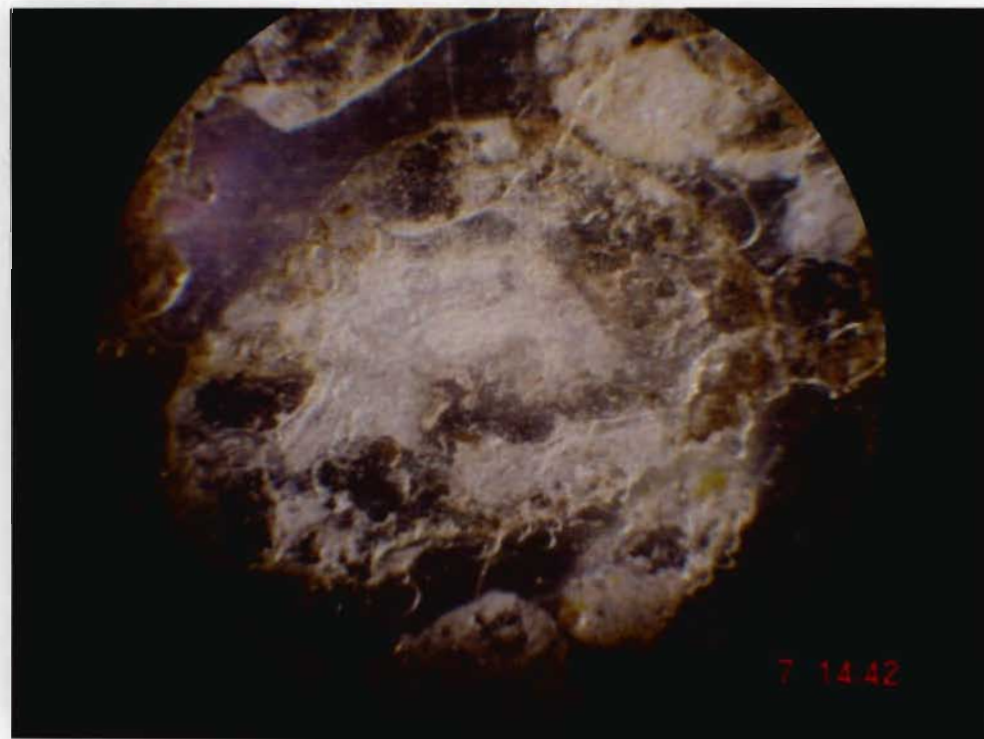
Figure A-3: Petrographical slide of Sorbent Sorb3
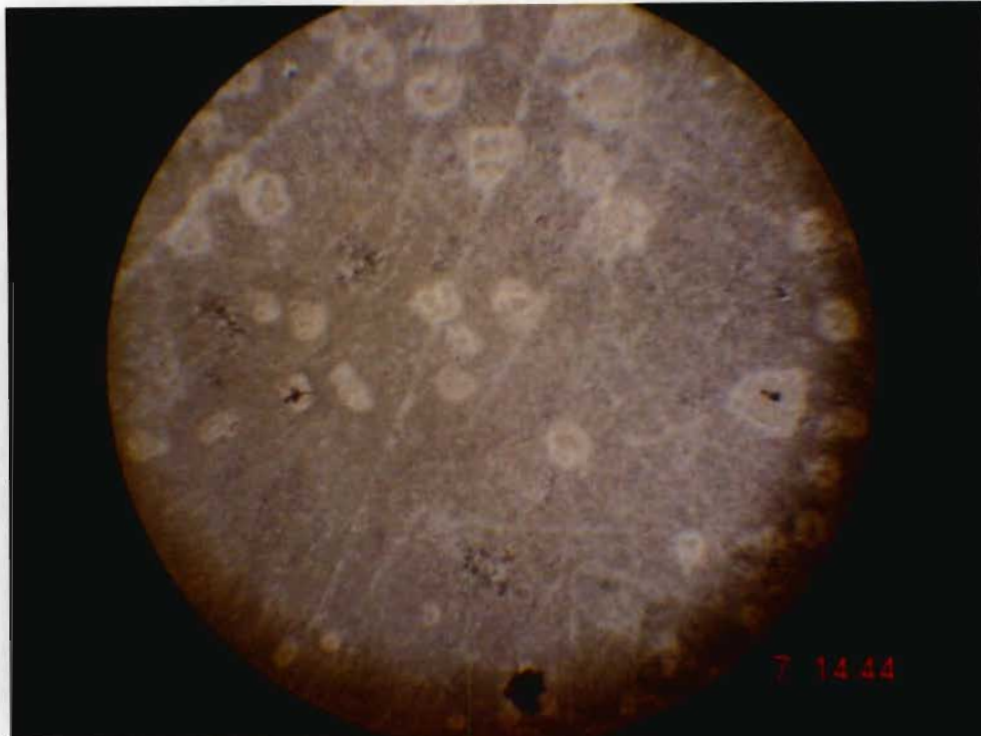
Figure A-4: Petrographical slide of Sorbent Sorb4
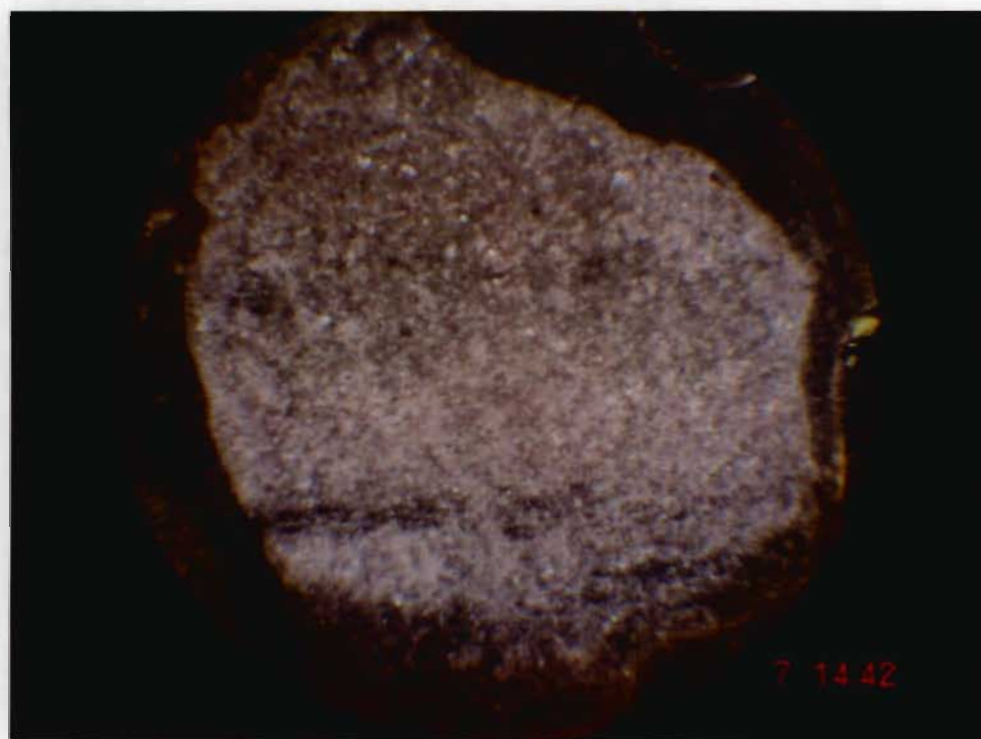
Figure A-5: Petrographical slide of Sorbent Sorb5

Figure A-6: Petrographical slide of Sorbent Sorb6
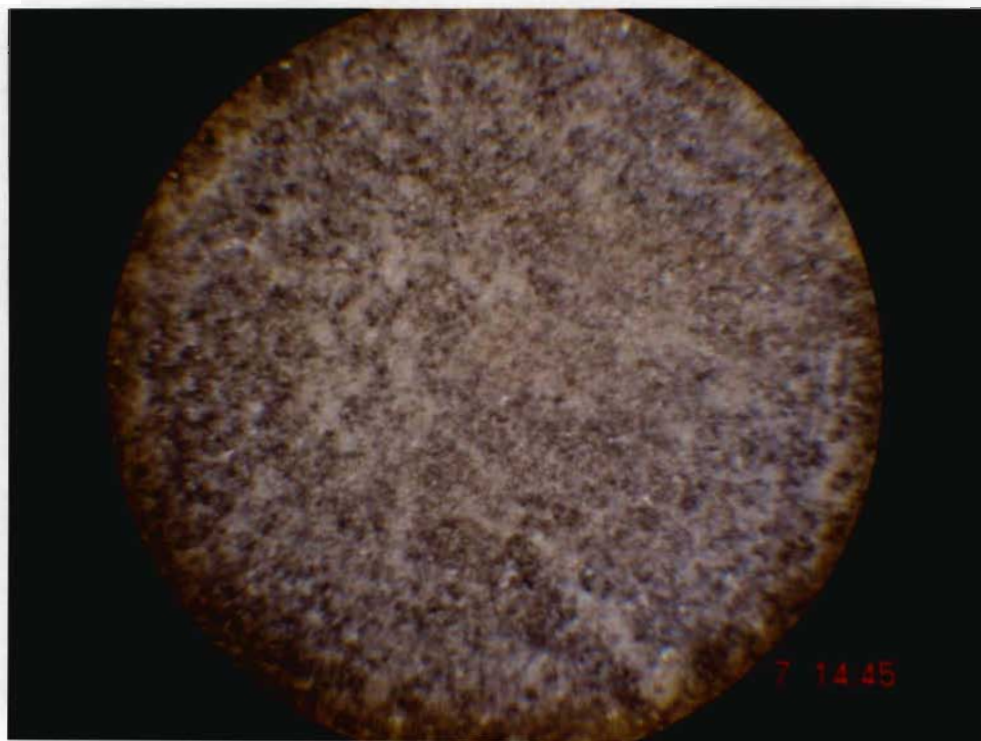
Figure A-7: Petrographical slide of Sorbent Sorb7

Figure A-8: Petrographical slide of Sorbent Sorb8

Appendix B

Scanning Electron Microscope Imaging of Sorbents

Sorb1
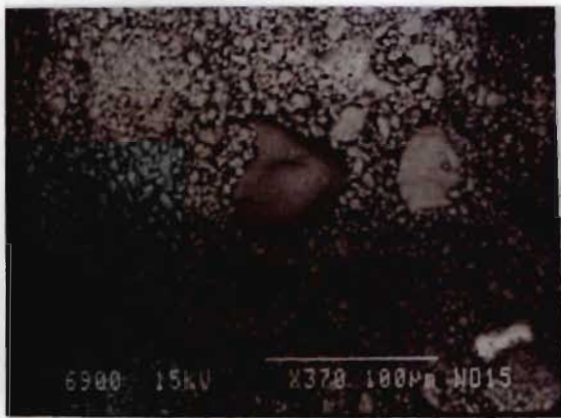
Figure B-1: Spot analysis of a Quartz grain on Sorb1 at a particle size of 425 – 500 μm
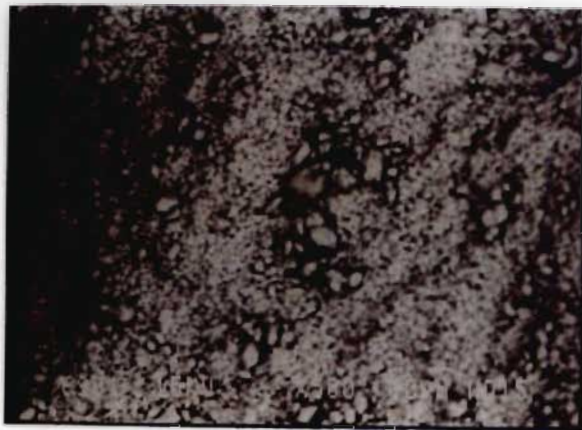
Figure B-2: Spot analysis of a Quartz grain on Sorb1 at a particle size of 425 – 500 μm
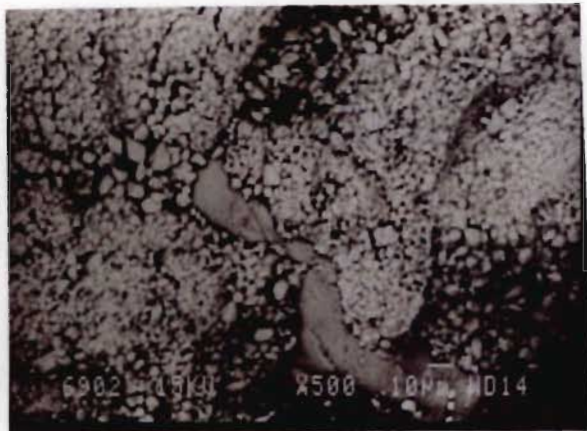
Figure B-3: Spot analysis of a Quartz grain on Sorb1 at a particle size of 425 – 500 μm
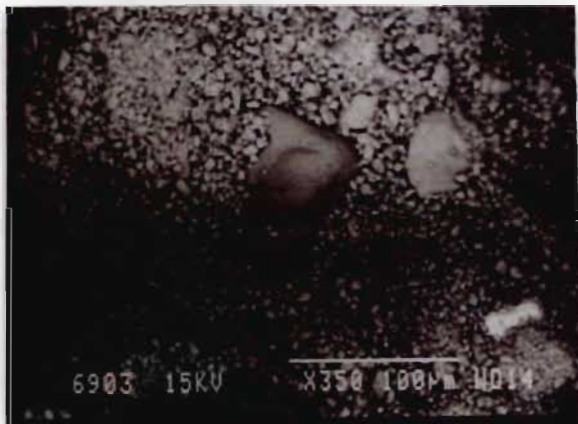
Figure B-4: Spot analysis of a Quartz grain on Sorb1 at a particle size of 425 – 500 μm

Figure B-5: Area representation of Sorb1 at a particle size of 425 – 500 μm

Figure B-6: Area representation of Sorb1 at a particle size of 425 – 500 μm
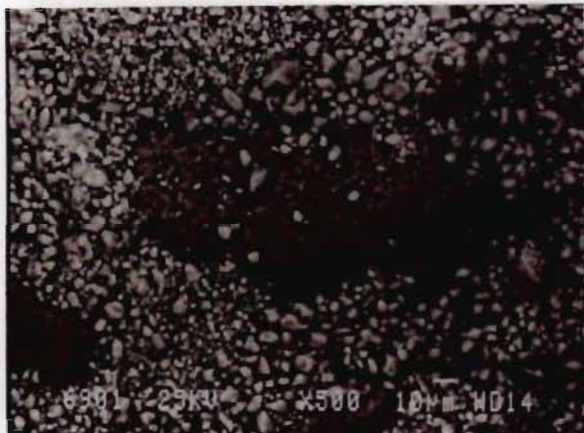
Figure B-7: Spot analysis of a Quartz grain on Sorb1 at a particle size of 600 – 710 μm
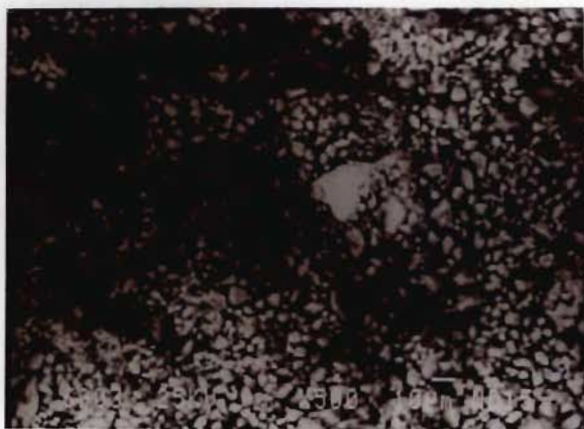
Figure B-8: Spot analysis of both Quartz and Iron grains on Sorb1 at a particle size of 850 – 1000 μm
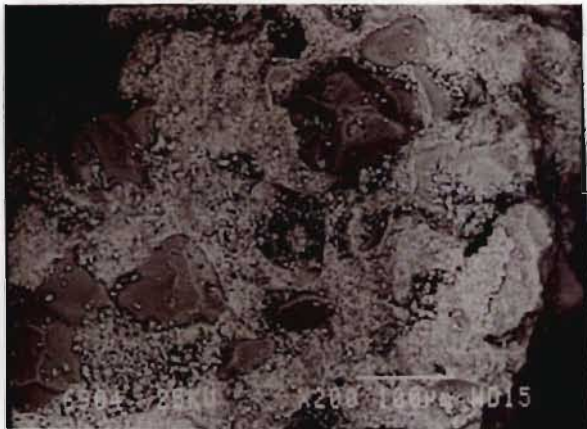
Figure B-9: Area representation of Sorb1 at a particle size of 850 – 1000 μm

Sorb2

Figure B-10: Spot analysis of a Quartz grain on Sorb2 at a particle size of 425 – 500 μm

Figure B-11: Area representation of Sorb2 at a particle size of 425 – 500 μm
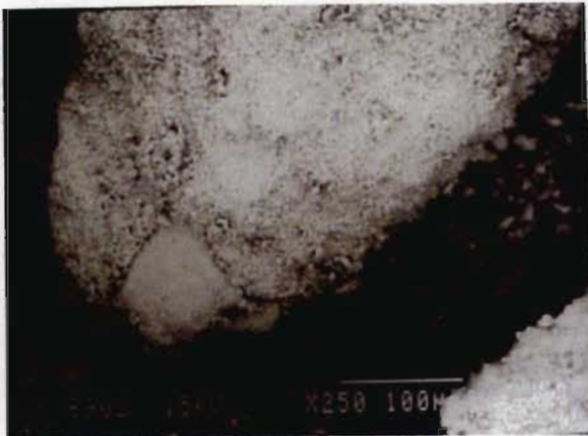
Figure B-12: Area representation of Sorb2 at a particle size of 425 – 500 μm
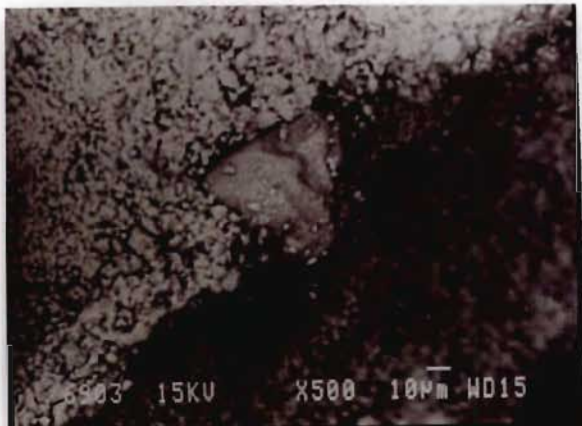
Figure B-13: Spot analysis of a Quartz grain on Sorb2 at a particle size of 425 – 500 μm

Figure B-14: Spot analysis of a Quartz grain on Sorb2 at a particle size of 425 – 500 μm
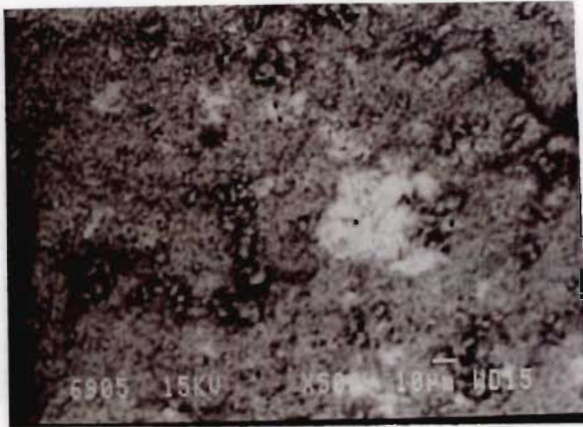
Figure B-15: Area representation of Sorb2 at a particle size of 425 – 500 μm
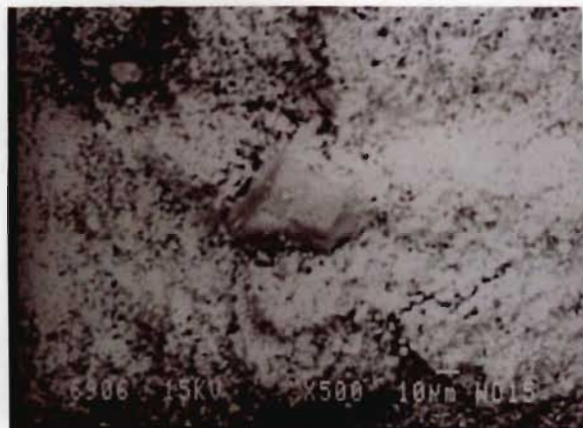
Figure B-16: Spot analysis of a Quartz Grain on Sorb2 at a particle size of 600 – 710 μm

Sorb3
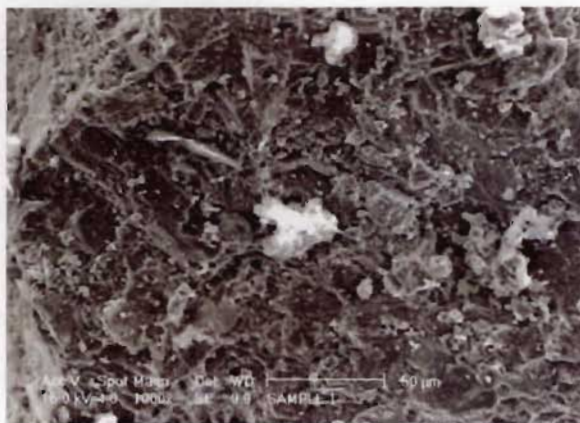
Figure B-17: Area representation of Sorb3 at a particle size of 425 – 500 μm
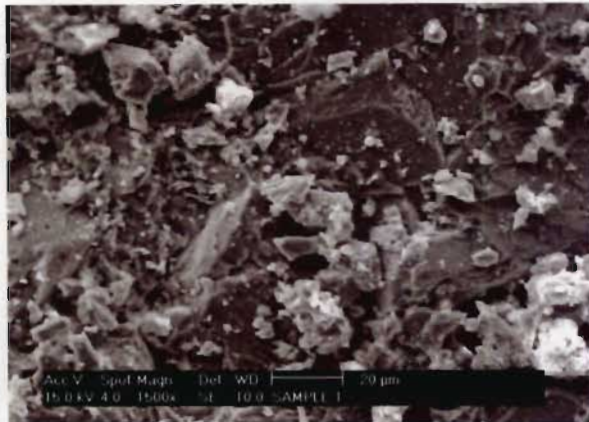
Figure B-18: Spot analysis of a Silica grain on Sorb3 at a particle size of 425 – 500 μm
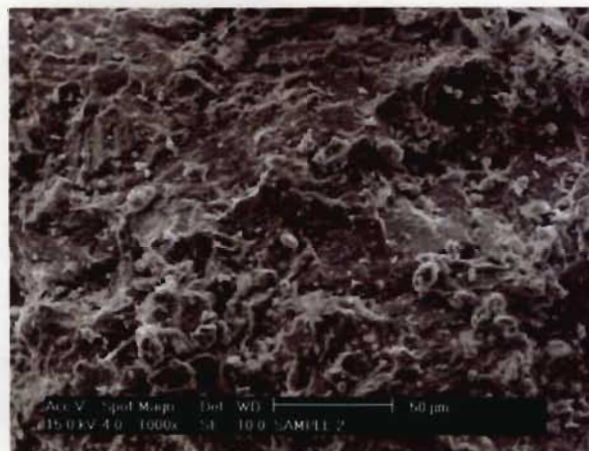
Figure B-19: Area representation of Sorb3 at a particle size of 600 – 710 μm
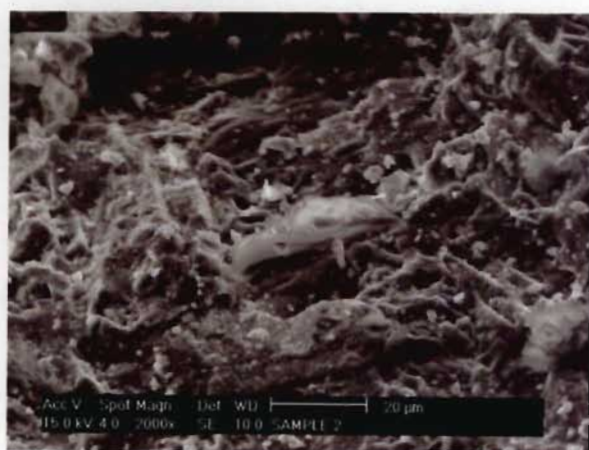
Figure B-20: Spot analysis of a Silica grain on Sorb3 at a particle size of 600 – 710 μm

B7
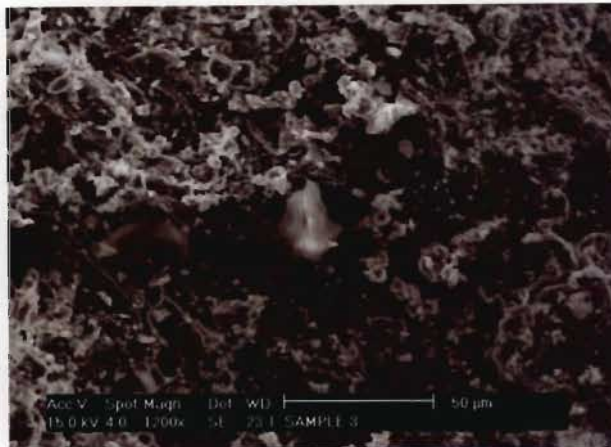
Figure B-21: Area representation of Sorb3 at a particle size of 850 – 1000 μm

Sorb4
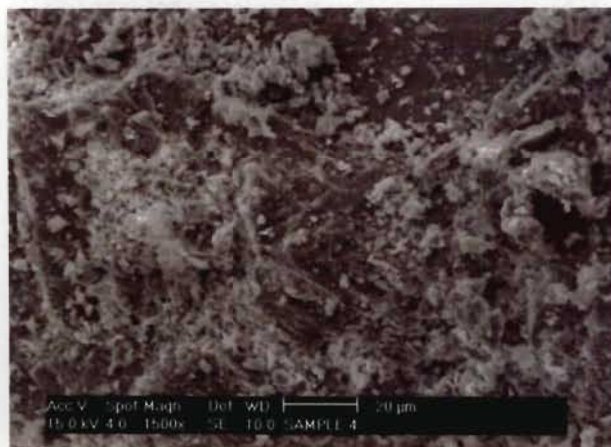
Figure B-22: Area representation of Sorb4 at a particle size of 425 – 500 μm
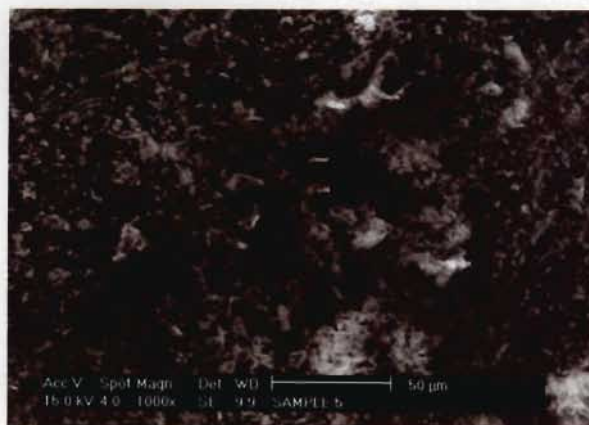
Figure B-23: Area representation of Sorb4 at a particle size of 600 – 710 μm
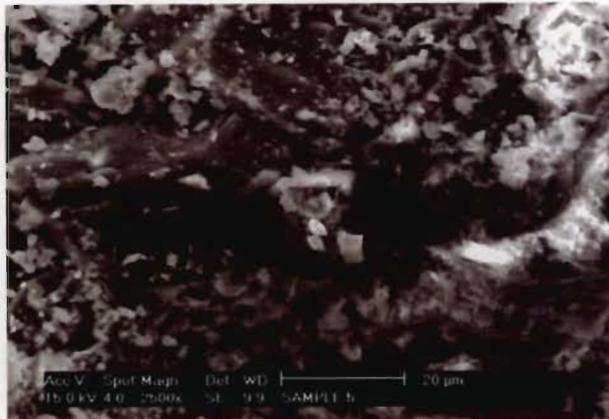
Figure B-24: Spot analysis of a Silica grain on Sorb4 at a particle size of 600 – 710 μm
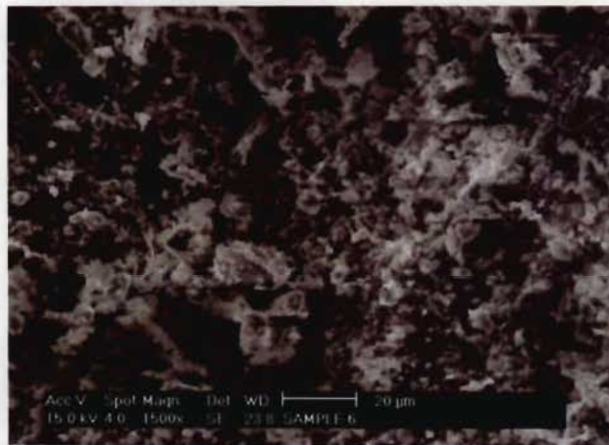
Figure B-25: Area representation of Sorb4 at a particle size of 850 – 1000 μm

Sorb5
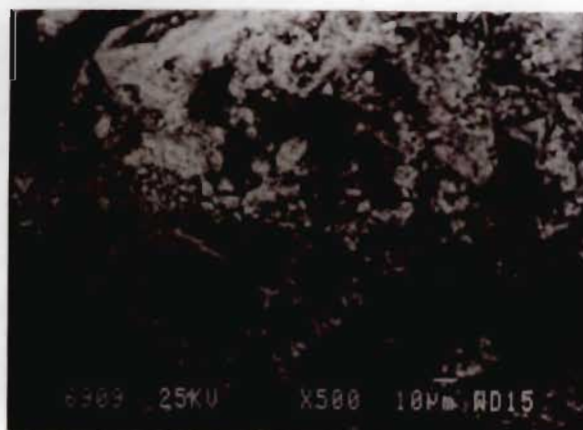
Figure B-26: Spot analysis of Iron and Aluminium grains on Sorb5 at a particle size of 425 – 500 μm
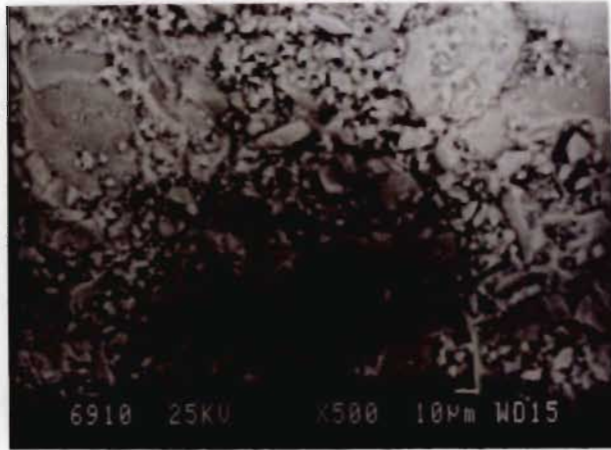
Figure B-27: Area representation of the Grain Structure in Sorb5 at a particle size of 425 – 500 µm

Figure B-28: Spot analysis of a Quartz grain on Sorb5 at a particle size of 425 – 500 µm

Figure B-29: Area representation of the Grain Structure on Sorb5 at a particle size of 600 – 710 μm
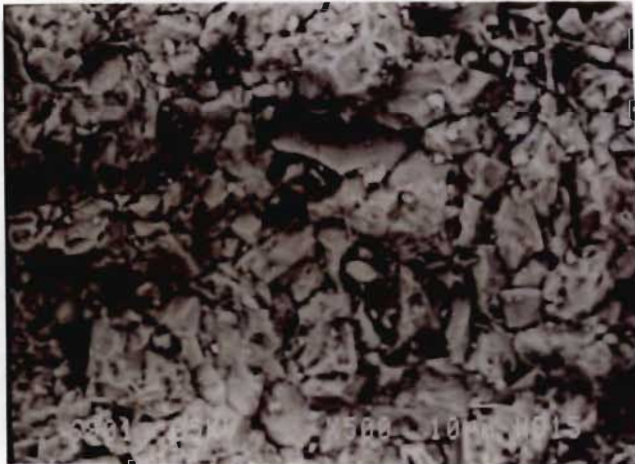
Sorb6

Figure B-30: Area representation of the Grain Structure on Sorb6 at a particle size of 425 – 500 μm

Figure B-31: Area representation of the Grain Structure on Sorb6 at a particle size of 425 – 500 µm
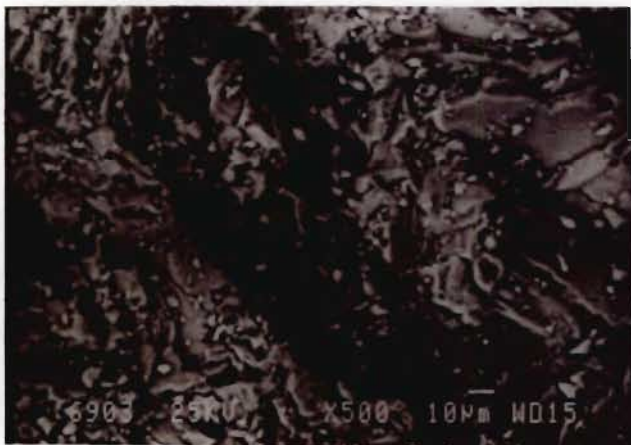
Figure B-32: Area representation of the Grain Structure on Sorb6 at a particle size of 600 – 710 µm
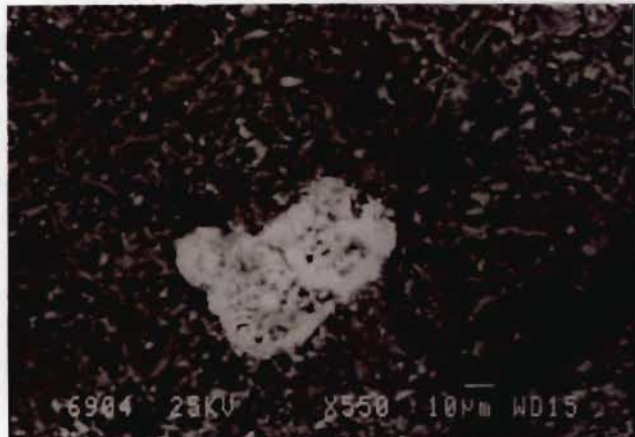
Figure B-33: Spot analysis of an Iron grain on Sorb6 at a particle size of 850 – 1000 μm
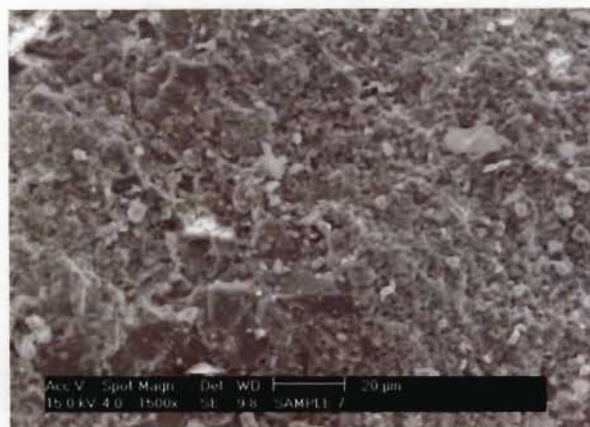
Sorb7

Figure B-34: Area representation of Sorb7 at a particle size of 425 – 500 μm
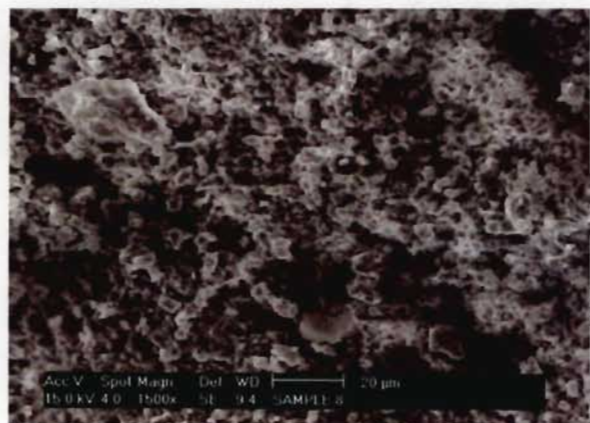
Figure B-35: Area representation of Sorb7 at a particle size of 600 – 710 μm
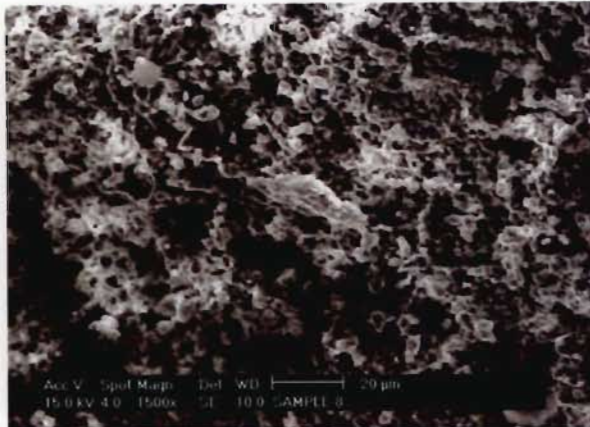
Figure B-36: Spot analysis of a Silica grain on Sorb7 at a particle size of 600 – 710 μm
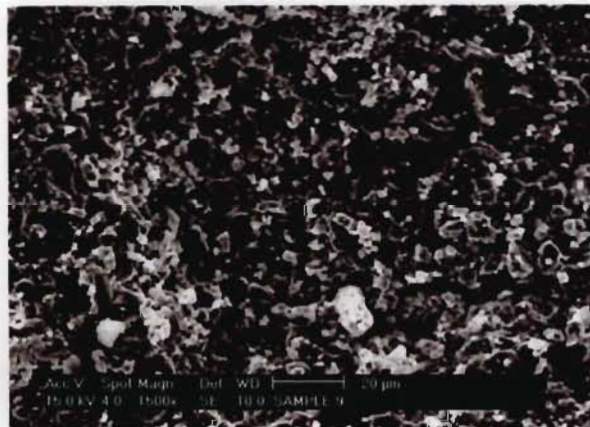
Figure B-37: Area representation of Sorb7 at a particle size of 850 – 1000 μm
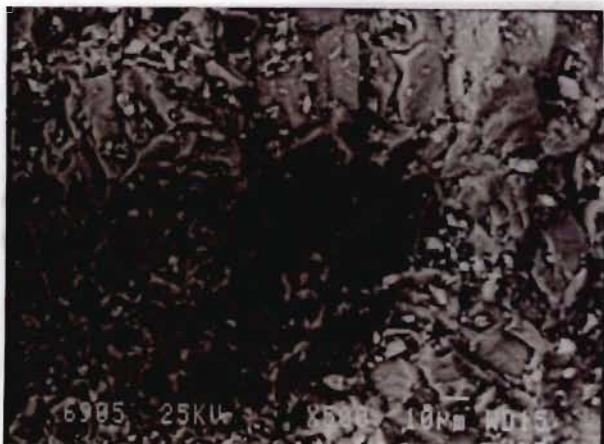
Sorb8

Figure B-38: Spot analysis of a Magnesium grain on Sorb8 at a particle size of 425 – 500 μm

Figure B-39: Spot analysis of a Quartz grain on Sorb8 at a particle size of 425 – 500 μm

Figure B-40: Spot analysis of a Quartz grain on Sorb8 at a particle size of 425 – 500 μm

Figure B-41: Area representation of the Grain Structure of Sorb8 at a particle size of 425 – 500 μm

Figure B-42: Area representation of the Grain Structure of Sorb8 at a particle size of 600 – 710 μm

Figure B-43: Spot analysis of a Quartz grain of Sorb8 at a particle size of 600 – 710 μm

Appendix C

Hardgrove Grindability Index Results

Table C-1: HGI results

Sample ID	Relative HGI Using an Upper scale of 100	Average
Sorb1		
425µm	106	
600µm	99	
850µm	91	99
Sorb2		
425µm	91	
600µm	82	
850µm	76	83
Sorb3		
Random Particle Size	58	58
Sorb4		
600µm	90	
850µm	78	84
Sorb5		
425µm	51	
600µm	44	
850µm	42	46
Sorb6		
425µm	71	
600µm	62	
850µm	57	63
Sorb7		
425µm	63	
600µm	55	
850µm	46	55
Sorb8		
425µm	68	
600µm	54	
850µm	48	57

Appendix D

X-Ray Diffraction Analysis Results

Sorb1

Table D-1: XRD test for Sorb1

Sorb1				
Angle[°2θ]	α[A]	Counts	I_{rel}	Name
9.780	10.4933	5	1.091703	
24.275	4.2542	71	15.50218	Quartz
26.870	3.8499	59	12.8821	
31.045	3.3424	100	21.83406	Quartz
34.320	3.0317	458	100	Calcite
36.690	2.8420	6	1.310044	Calcite
42.070	2.4920	59	12.8821	
46.145	2.2825	76	16.59389	
50.610	2.0927	62	13.53712	
52.400	2.0260	14	3.056769	Aluminium
53.790	1.9774	1	0.218341	
55.335	1.9264	27	5.895197	
55.815	1.9111	74	16.15721	
57.020	1.8740	62	13.53712	
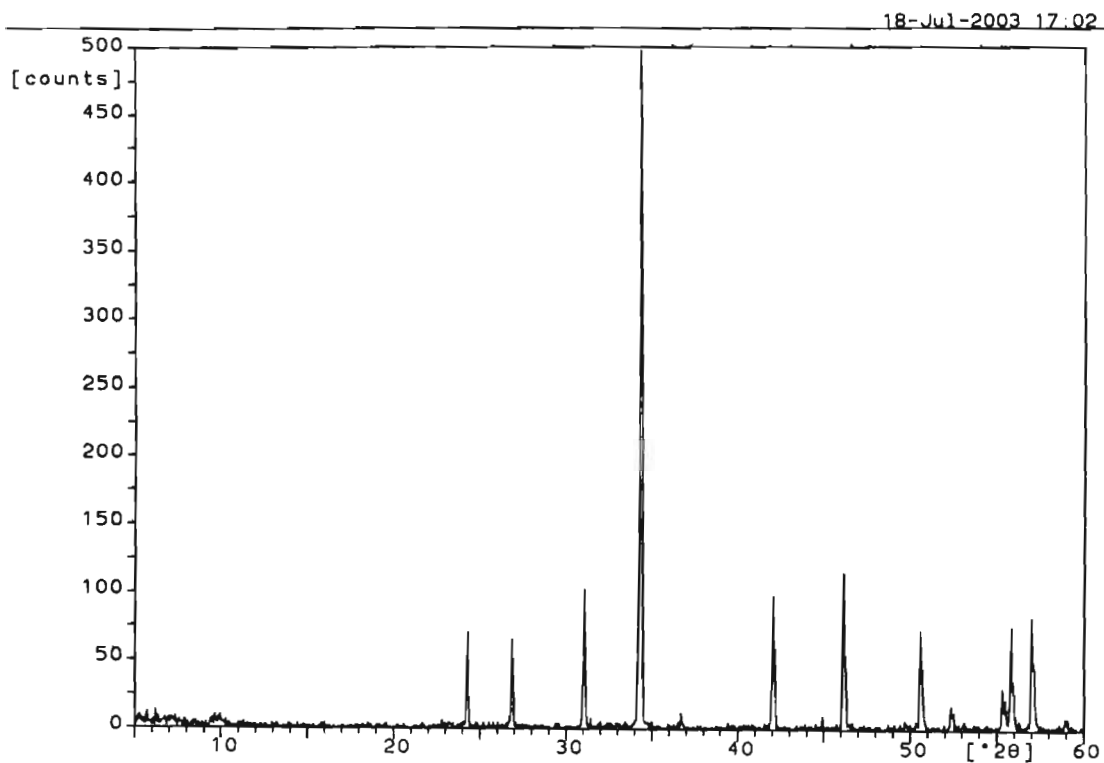
Figure D-1: Graph of the XRD results for Sorb1

Sorb2

Table D-2: XRD test for Sorb2

Sorb2				
Angle[°2θ]	d-value α	Counts	I_rel	Name
21.705	4.7508	1	0.769231	
23.575	4.3787	1	0.769231	
24.435	4.2268	17	13.07692	Quartz
27.025	3.8282	12	9.230769	
31.160	3.3304	130	100	Quartz
34.475	3.0185	130	100	Calcite
35.985	2.8958	1	0.769231	
42.200	2.4847	26	20	
46.305	2.2750	34	26.15385	Calcite
48.000	2.1992	1	0.769231	
49.890	2.1209	8	6.153846	
50.760	2.0869	28	21.53846	Calcite
55.550	1.9195	9	6.923077	Calcite
56.035	1.9042	18	13.84615	
57.240	1.8674	25	19.23077	
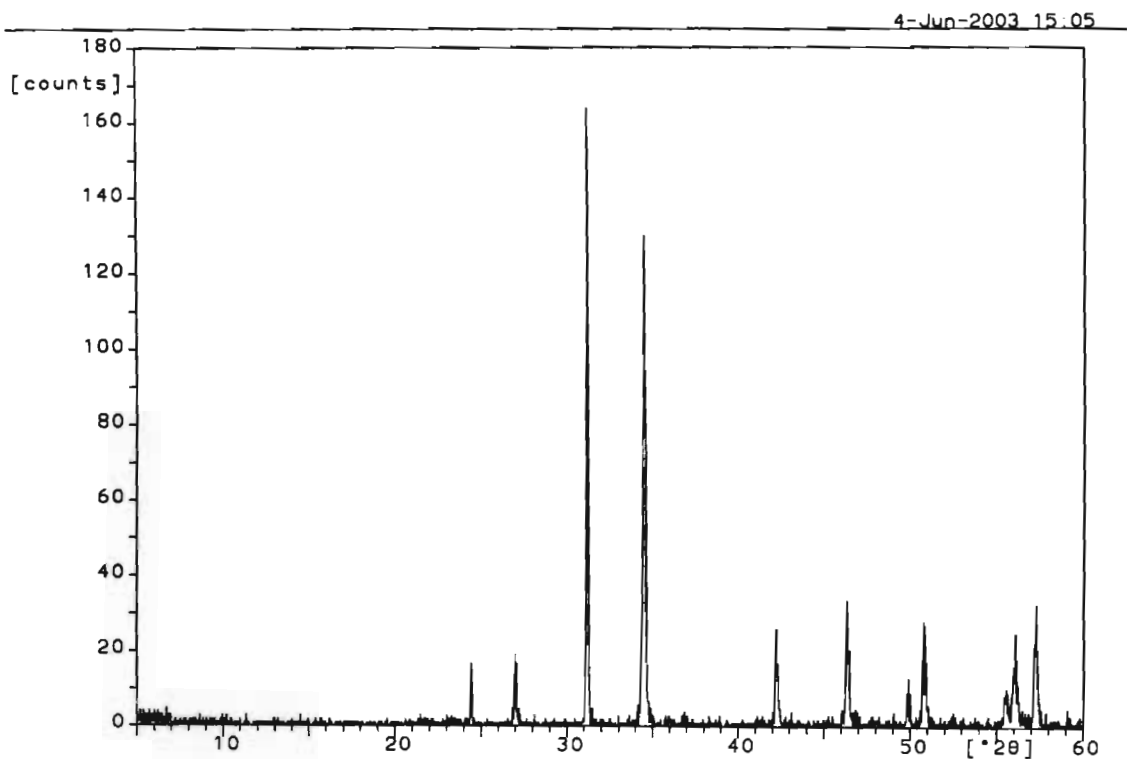
Figure D-2: Graph of the XRD results for Sorb2

Sorb3

Table D-3: XRD test for Sorb3

Sorb3				
Angle[°2θ]	α[A]	Counts	I_{rel}	Name
5.730	17.8958	3	0.680272	
7.330	13.9932	7	1.587302	
14.510	7.0830	8	1.814059	
21.740	4.7432	3	0.680272	
23.605	4.3732	2	0.453515	
26.975	3.8351	11	2.494331	Calcite
28.095	3.6851	11	2.494331	
29.285	3.5385	4	0.907029	
31.140	3.3325	3	0.680272	Quartz
34.415	3.0236	441	100	Calcite
36.185	2.8803	130	29.47846	
36.855	2.8297	6	1.360544	Calcite
39.260	2.6626	4	0.907029	
42.170	2.4864	18	4.081633	Calcite
46.295	2.2755	19	4.30839	Calcite
48.225	2.1895	6	1.360544	
50.755	2.0871	14	3.174603	Calcite
55.980	1.9059	26	5.895692	Calcite
57.135	1.8705	26	5.895692	Calcite

D3
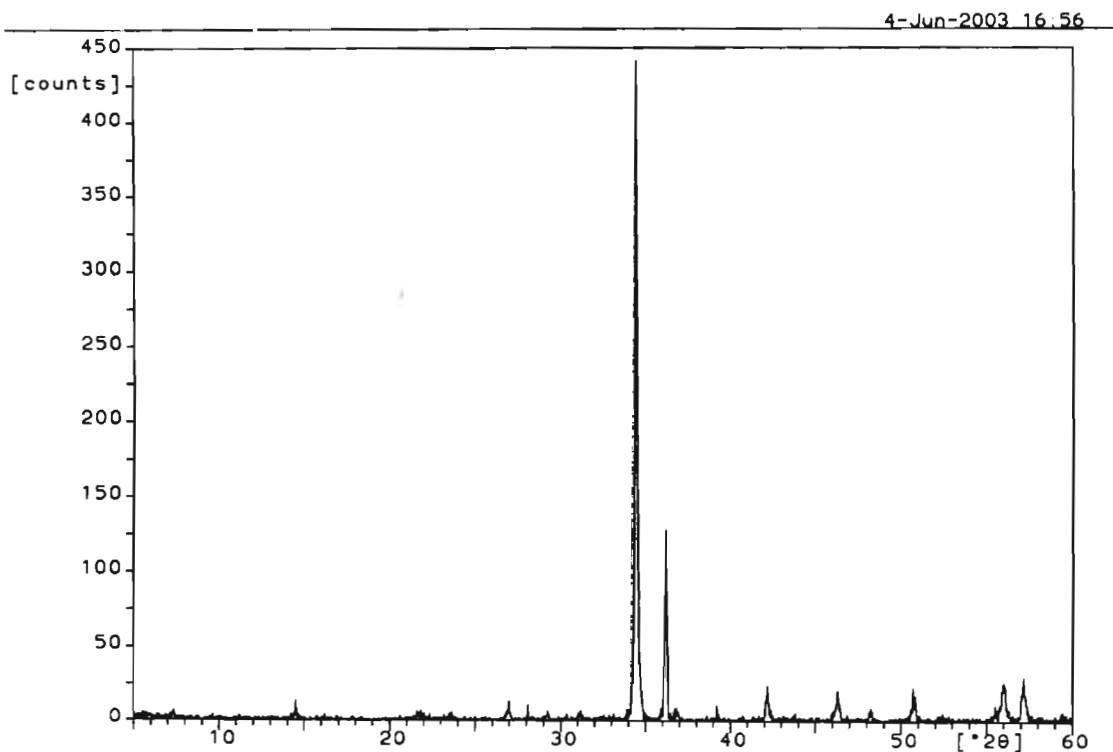
Figure D-3: Graph of the XRD results for Sorb3

Sorb4

Table D-4: XRD test for Sorb4

Sorb4				
Angle[°2θ]	α[A]	Counts	I_rel	Name
26.920	3.8428	79	9.461078	Calcite
31.105	3.3361	17	2.035928	
34.375	3.0270	835	100	Calcite
36.080	2.8884	36	4.311377	
36.780	2.8353	49	5.868263	
42.125	2.4889	90	10.77844	
45.055	2.3347	12	1.437126	Aluminium
46.215	2.2792	128	15.32934	Calcite
50.680	2.0900	92	11.01796	Calcite
52.495	2.0226	8	0.958084	Aluminium
55.425	1.9235	40	4.790419	Calcite
55.920	1.9078	76	9.101796	
57.115	1.8711	94	11.25749	Calcite
59.065	1.8147	4	0.479042	
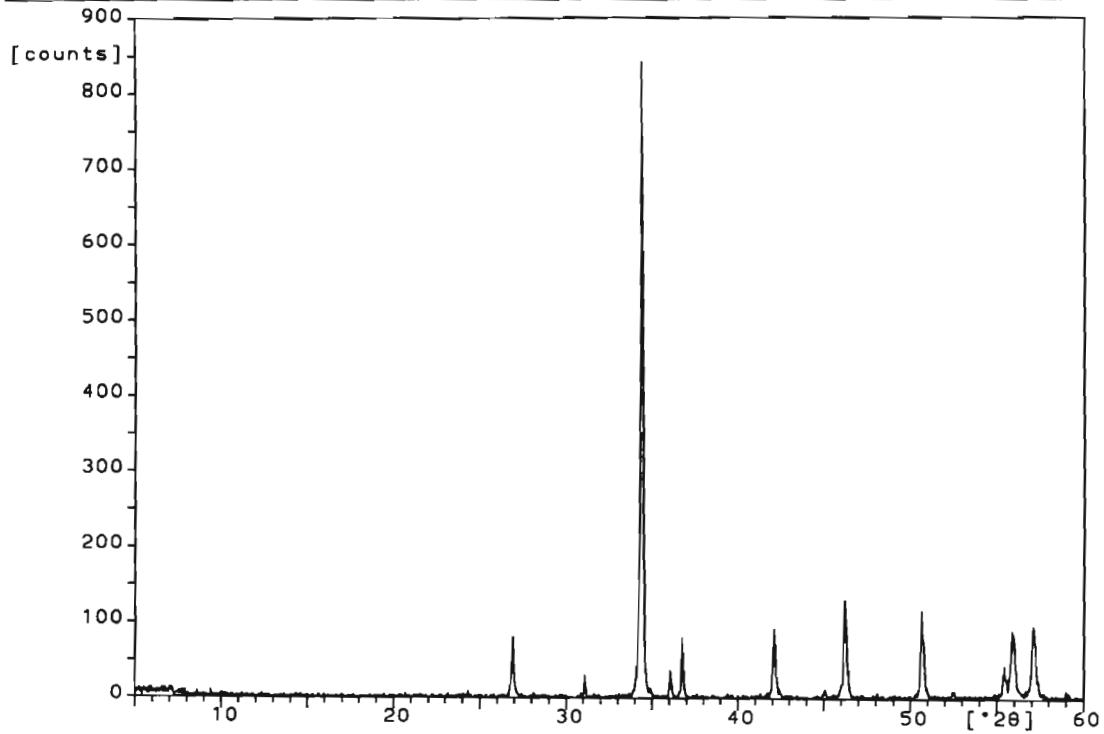
Figure D-4: Graph of the XRD results for Sorb4

Sorb5

Table D-5: XRD test for Sorb5

Sorb5				
Angle[°2θ]	α[A]	Counts	I_{rel}	Name
11.850	8.6652	1	0.041649	
24.290	4.2516	12	0.499792	Quartz
25.655	4.0289	21	0.874636	Dolomite
28.030	3.6935	53	2.207414	Dolomite
31.055	3.3414	36	1.499375	Quartz
36.135	2.8842	2401	100	Dolomite
39.170	2.6685	55	2.290712	Dolomite
41.300	2.5364	52	2.165764	Dolomite
43.720	2.4023	46	1.915868	Dolomite
48.180	2.1914	193	8.038317	Dolomite
49.150	2.1508	4	0.166597	
51.365	2.0639	22	0.916285	Dolomite
52.410	2.0256	28	1.166181	Aluminium
52.725	2.0144	119	4.956268	Dolomite
57.940	1.8468	18	0.749688	Dolomite
59.450	1.8040	128	5.331112	Dolomite

D5
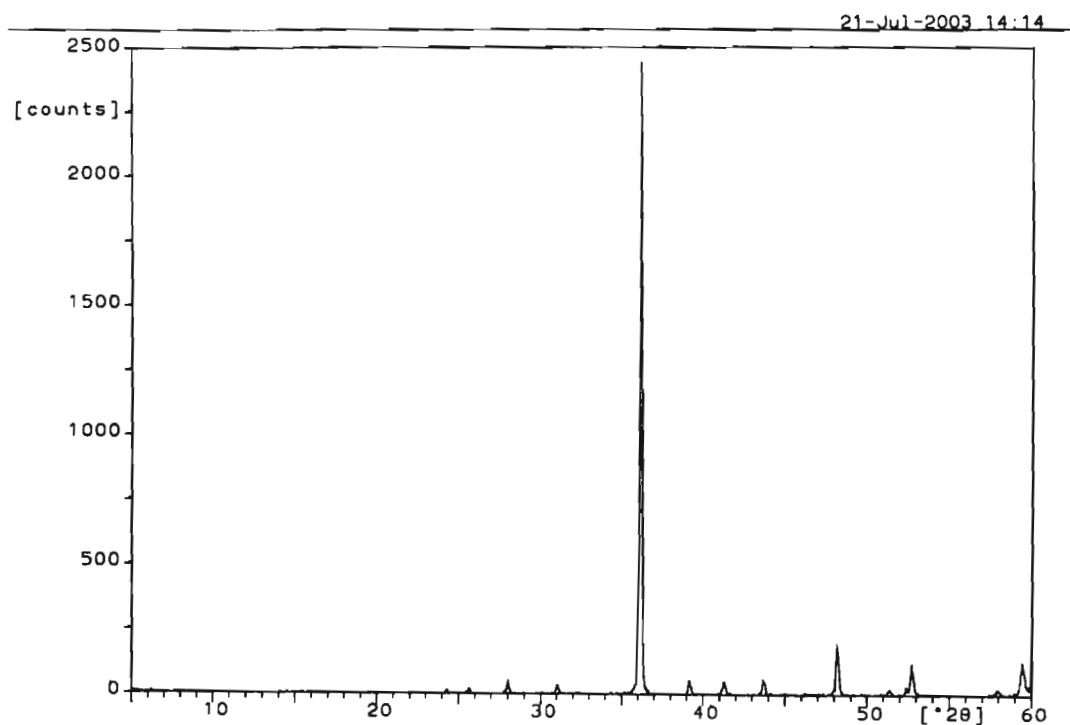
Figure D-5: Graph of the XRD results for Sorb5

Sorb6

Table D-6: XRD test for Sorb6

Sorb6				
Angle[°2θ]	α[A]	Counts	I_rel	Name
13.465	7.6299	1	0.049826	
24.310	4.2482	7	0.348779	Quartz
25.650	4.0297	20	0.996512	
28.025	3.6942	46	2.291978	Dolomite
31.060	3.3408	42	2.092676	Quartz
34.320	3.0317	7	0.348779	Calcite
36.140	2.8838	2007	100	Dolomite
39.175	2.6681	61	3.039362	
41.290	2.5370	58	2.889885	Dolomite
43.690	2.4039	61	3.039362	Dolomite
48.170	2.1919	246	12.2571	Dolomite
51.380	2.0634	23	1.145989	Dolomite
52.710	2.0149	108	5.381166	Dolomite
57.935	1.8469	27	1.345291	Dolomite
59.470	1.8034	146	7.274539	Dolomite

D6
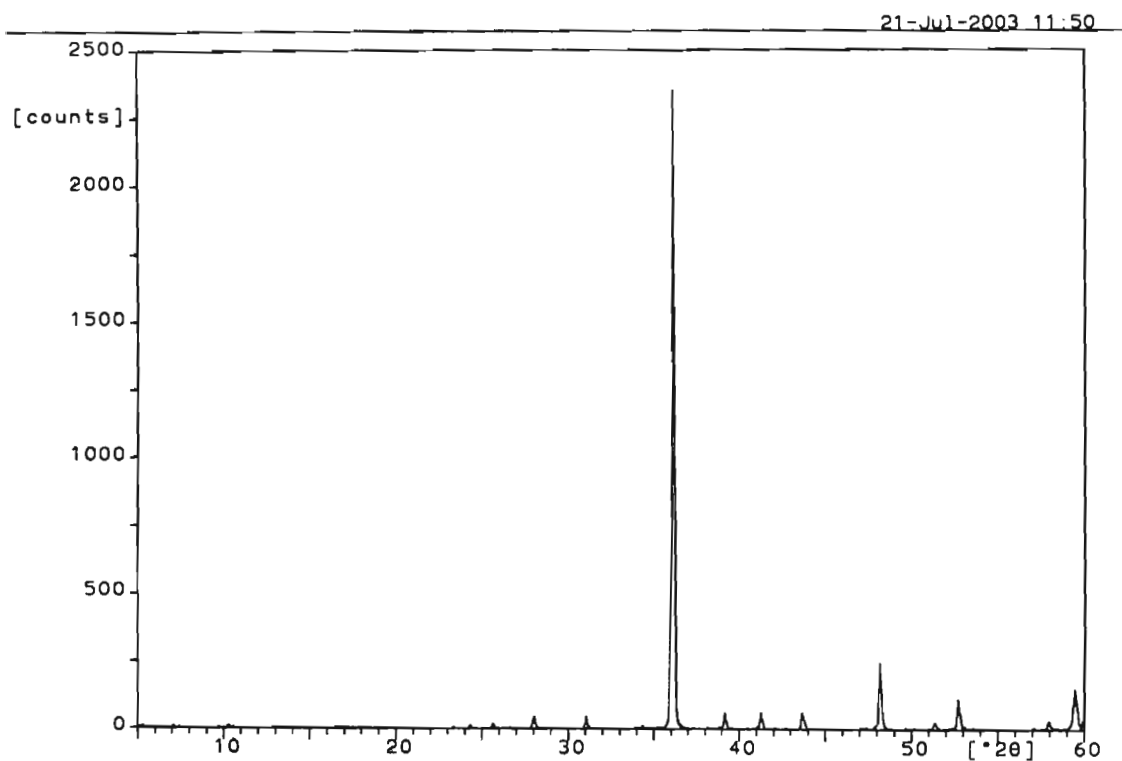
Figure D-6: Graph of the XRD results for Sorb6

Sorb7

Table D-7: XRD test for Sorb7

Sorb7				
Angle[°2θ]	α[A]	Counts	I_{rel}	Name
24.215	4.2646	10	0.70373	Quartz
25.650	4.0297	12	0.844476	Dolomite
28.010	3.6961	26	1.829697	Dolomite
31.070	3.3398	52	3.659395	Quartz
36.125	2.8849	1421	100	Dolomite
39.155	2.6694	42	2.955665	Dolomite
41.250	2.5393	19	1.337087	Dolomite
43.705	2.4031	29	2.040816	Dolomite
48.165	2.1921	125	8.796622	Dolomite
49.755	2.1263	3	0.211119	
51.375	2.0636	13	0.914849	Dolomite
52.700	2.0153	49	3.448276	Dolomite
57.920	1.8473	11	0.774103	Dolomite
59.445	1.8041	106	7.459536	Dolomite
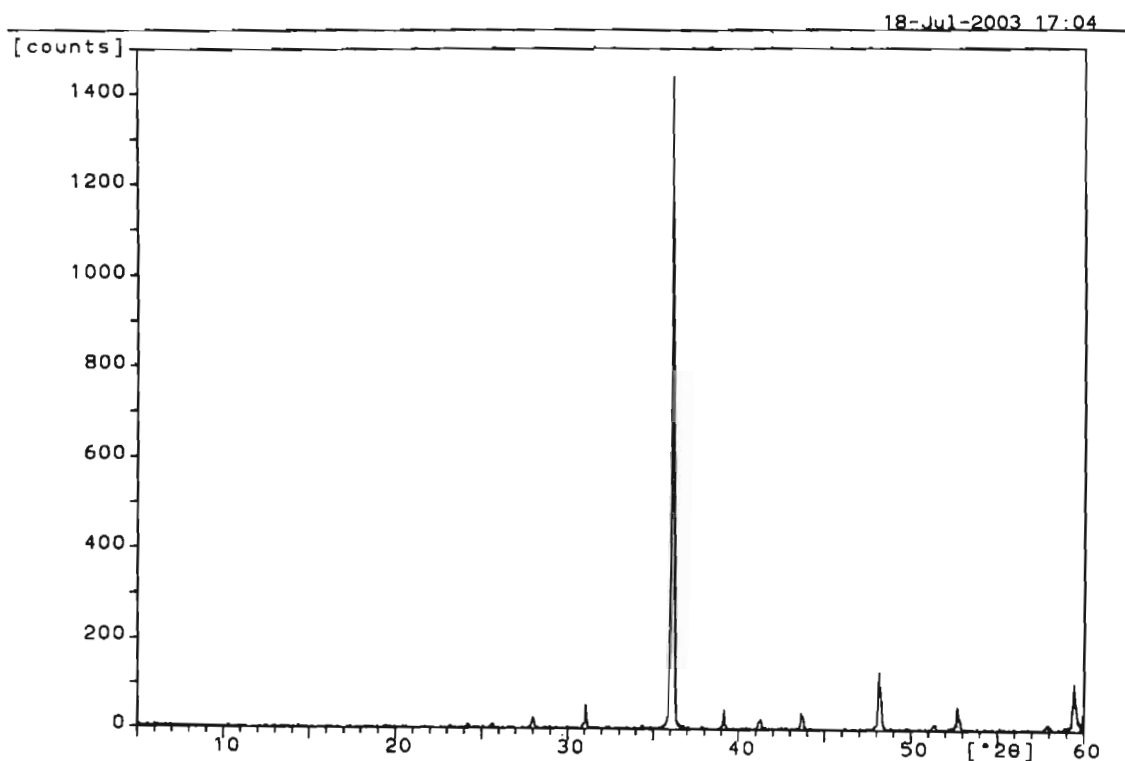
Figure D-7: Graph of the XRD results for Sorb7

Sorb8

Table D-8: XRD test for Sorb8

Sorb8				
Angle[°2θ]	α[A]	Counts	I_{rel}	Name
24.310	4.2482	4	0.215285	Quartz
25.615	4.0351	10	0.538213	Dolomite
25.965	3.9816	3	0.161464	
28.030	3.6935	46	2.47578	Dolomite
31.050	3.3419	12	0.645856	Quartz
34.350	3.0292	28	1.506997	Calcite
36.110	2.8861	1858	100	Dolomite
39.160	2.6691	86	4.628633	Dolomite
41.270	2.5382	46	2.47578	Dolomite
43.665	2.4052	64	3.444564	Dolomite
46.175	2.2810	7	0.376749	Calcite
48.150	2.1927	185	9.956943	Dolomite
51.335	2.0651	24	1.291712	Dolomite
52.695	2.0154	94	5.059203	Dolomite
55.680	1.9154	3	0.161464	
57.170	1.8695	5	0.269107	
57.920	1.8473	28	1.506997	Dolomite
59.425	1.8047	128	6.889128	Dolomite
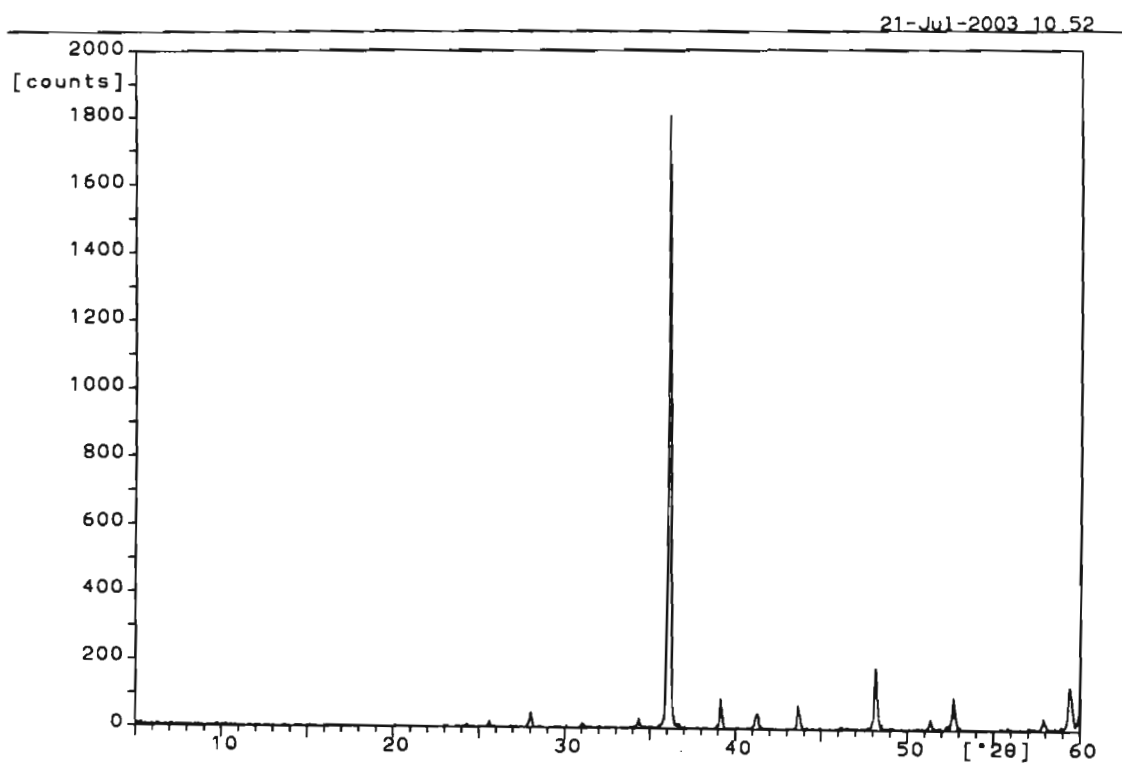
Figure D-8: Graph of the XRD results for Sorb8

Appendix E

X-Ray Fluorescence Table on Sorbent Composition

Table E-1: XRF Sorbent Composition

		SiO_2	TiO_2	Al_2O_3	Fe_2O_3	MnO	MgO	CaO	Na_2O	K_2O	P_2O_5	H_2O	LOI	Sum
	KG07	9.68	0.05	0.80	0.54	0.02	0.66	22.45	0.01	0.02	0.00	1.23	64.71	100.17
Sorb1	KG08	9.47	0.05	0.86	0.58	0.02	0.68	21.82	0.02	0.02	0.00	1.57	65.08	100.17
	KG09	9.20	0.05	0.81	0.50	0.02	0.64	22.81	0.02	0.02	0.00	1.47	64.56	100.10
	KG01	2.70	0.03	0.58	0.71	0.07	0.79	34.33	0.03	0.01	0.00	0.45	59.69	99.39
Sorb2	KG02	3.40	0.04	0.62	0.70	0.06	0.82	33.17	0.02	0.02	0.00	0.55	60.01	99.41
	KG03	2.66	0.03	0.52	0.67	0.07	0.81	34.39	0.00	0.01	0.00	0.46	59.85	99.47
	KG20	5.62	0.09	0.76	2.49	0.39	9.71	38.97	0.08	0.04	0.02	0.35	40.69	99.21
Sorb3	KG21	5.49	0.09	0.73	2.59	0.45	9.97	39.14	0	0.04	0.01	0.41	40.79	99.71
	KG22	4.57	0.09	0.68	2.51	0.43	10.23	39.33	0	0.03	0.01	0.41	41.42	99.71
	KG23	3.44	0.07	0.51	0.58	0.1	0.65	51.74	0	0.03	0.01	0.54	42.06	99.73
Sorb4	KG24	3.96	0.09	0.63	0.57	0.08	0.57	51.45	0	0.03	0.01	0.65	41.84	99.88
	KG25	4.42	0.09	0.74	0.58	0.09	0.69	50.43	0	0.03	0.01	0.71	41.46	99.25
Sorb5	KG13	5.62	0.02	0.65	3.78	0.83	5.98	13.21	0.03	0.07	0.01	0.60	68.23	99.03
	KG14	2.36	0.01	0.30	0.83	0.60	14.05	25.52	0.11	0.04	0.00	0.10	55.19	99.11
Sorb6	KG15	2.37	0.01	0.32	0.87	0.61	13.86	25.49	0.13	0.04	0.00	0.12	55.25	99.07
	KG16	2.53	0.01	0.35	0.84	0.60	13.77	25.42	0.03	0.04	0.00	0.15	55.38	99.12
	KG04	1.13	0.01	0.24	1.75	0.80	17.22	24.33	0.00	0.04	0.01	0.20	54.98	100.71
Sorb7	KG05	0.71	0.01	0.28	0.95	0.83	14.59	26.76	0.01	0.03	0.01	0.12	54.52	98.82
	KG06	0.88	0.00	0.20	0.85	0.82	17.63	25.08	0.01	0.03	0.00	0.08	54.64	100.22
	KG17	1.72	0.04	0.27	1.44	0.80	20.64	29.64	0.05	0.03	0.01	0.22	45.38	100.24
Sorb8	KG18	1.76	0.03	0.25	1.18	0.79	20.25	29.41	0.03	0.04	0.01	0.14	45.49	99.38
	KG19	3.24	0.03	0.35	1.33	0.74	18.68	30.24	0.03	0.04	0.01	0.33	44.62	99.64
	KG10	1.66	0.01	0.30	0.75	1.30	15.43	24.99	0.08	0.06	0.00	0.16	55.36	100.10
Sorb9	KG11	1.51	0.02	0.48	0.75	1.31	12.64	26.73	0.12	0.10	0.00	0.16	55.57	99.39
	KG12	5.29	0.02	0.49	0.70	1.19	11.33	24.74	0.05	0.11	0.00	0.18	55.77	99.87

Appendix F

Pictures of Experimental Equipment

Figure F-1 Photograph of the Buffer Tank

Figure F-2 Photograph on the Initial Experimental Set-up of the Equipment

Figure F-3 Photograph on the Initial Experimental Set-up of the Equipment

Figure F-4 Photograph on the Initial Experimental Set-up of the Equipment

Figure F-5 Photograph on the Initial Experimental Set-up of the Equipment
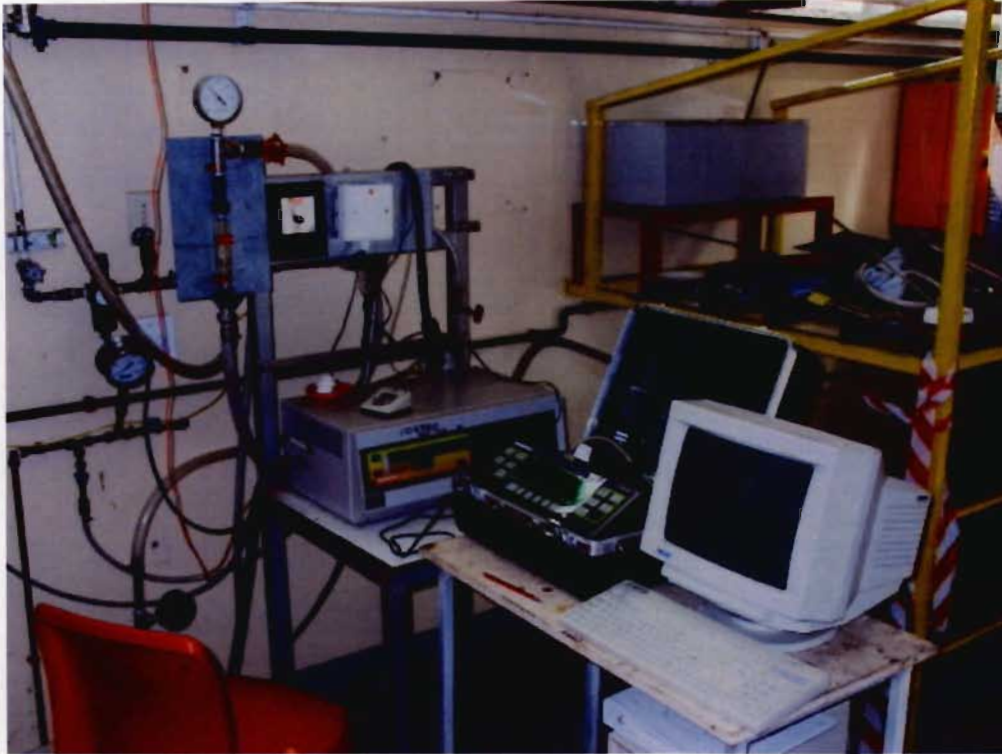
Figure F-6 Photograph on the Initial Experimental Set-up of the Equipment
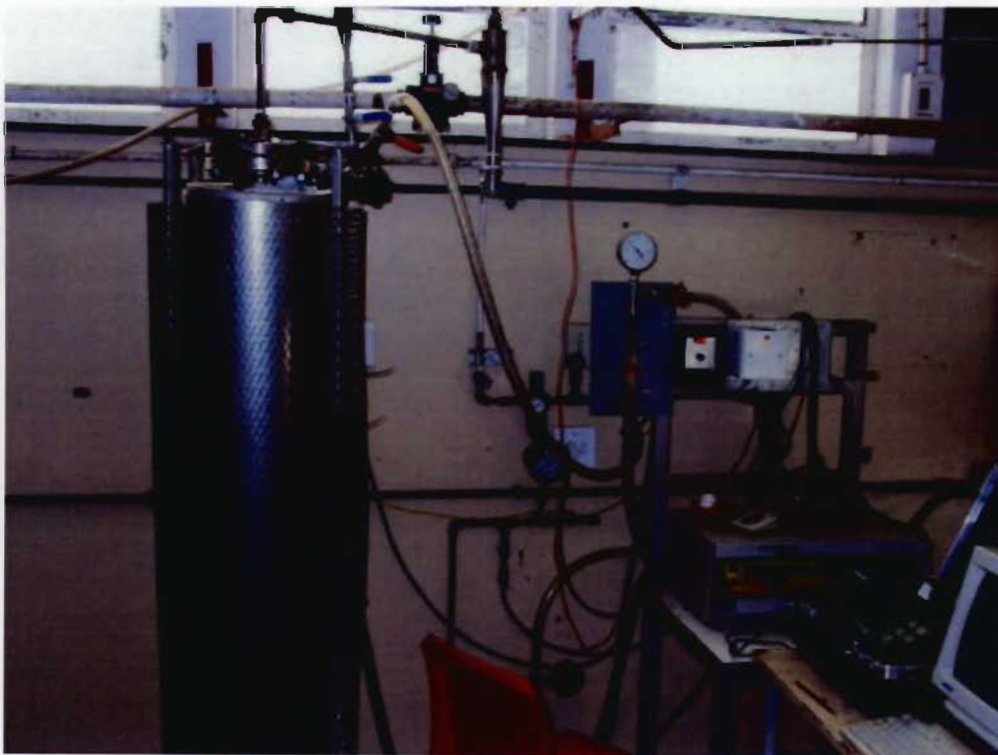
Figure F-7 Photograph on the Initial Experimental Set-up of the Equipment
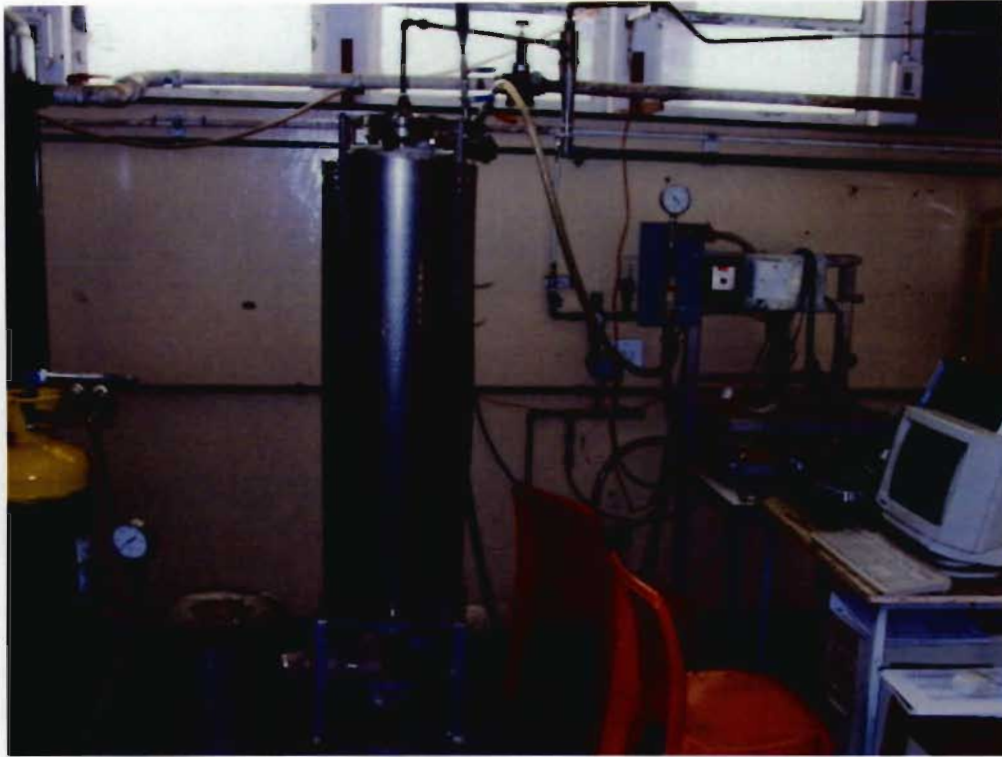
Figure F-8 Photograph on the Initial Experimental Set-up of the Equipment
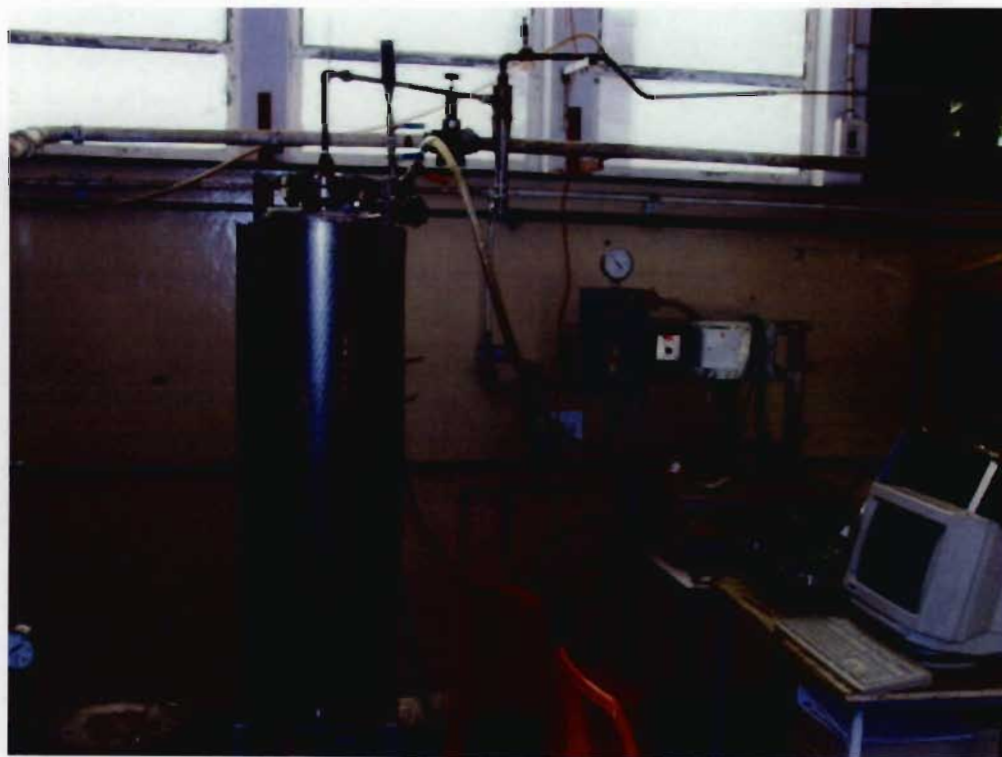
Figure F-9 Photograph on the Experimental Set-up of the Equipment

Figure F-10 Photograph on the Experimental Set-up of the Equipment

Figure F-11 Photograph on the Experimental Set-up of the Equipment
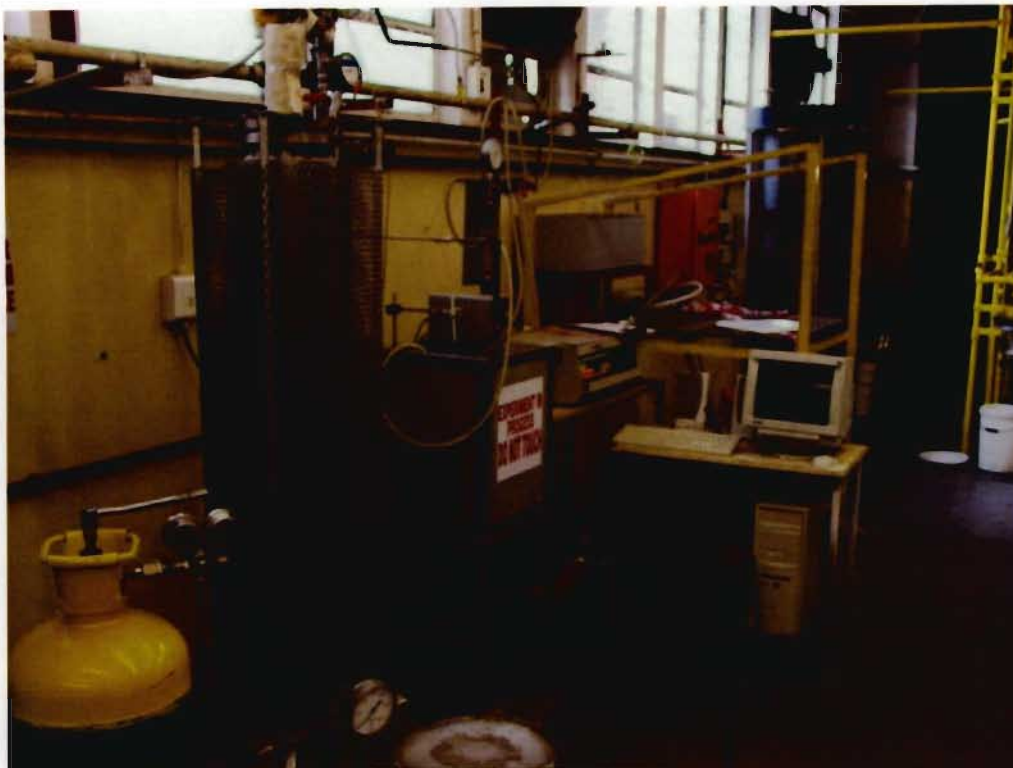
Figure F-12 Photograph on the Current Experimental Set-up of the Equipment

Figure F-13 Photograph of the Laboratory Fluidised Bed Reactor

Figure F-14 Photograph of the Laboratory Fluidised Bed Reactor

Figure F-15 Photograph of the Gas Exit configuration of the AFBR

Figure F-16 Photograph of the material used to hold the Heating Elements in place

Figure F-17 Photograph of the installation of the Heating Elements

F9

Figure F-18 Photograph of the installation of the Heating Insulation

Figure F-19 Photograph of the installation of the Heating Insulation
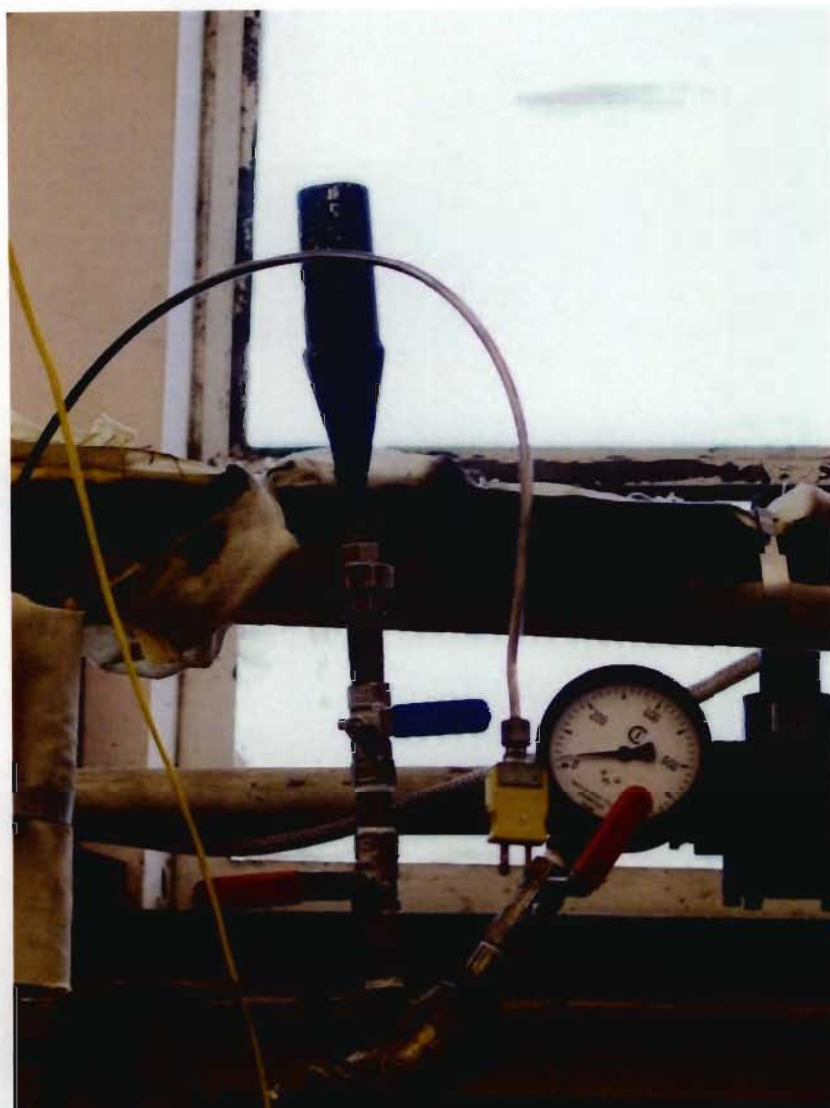
Figure F-20 Photograph of Sorbent Feeder on the Laboratory Atmospheric Fluidised Bed Reactor
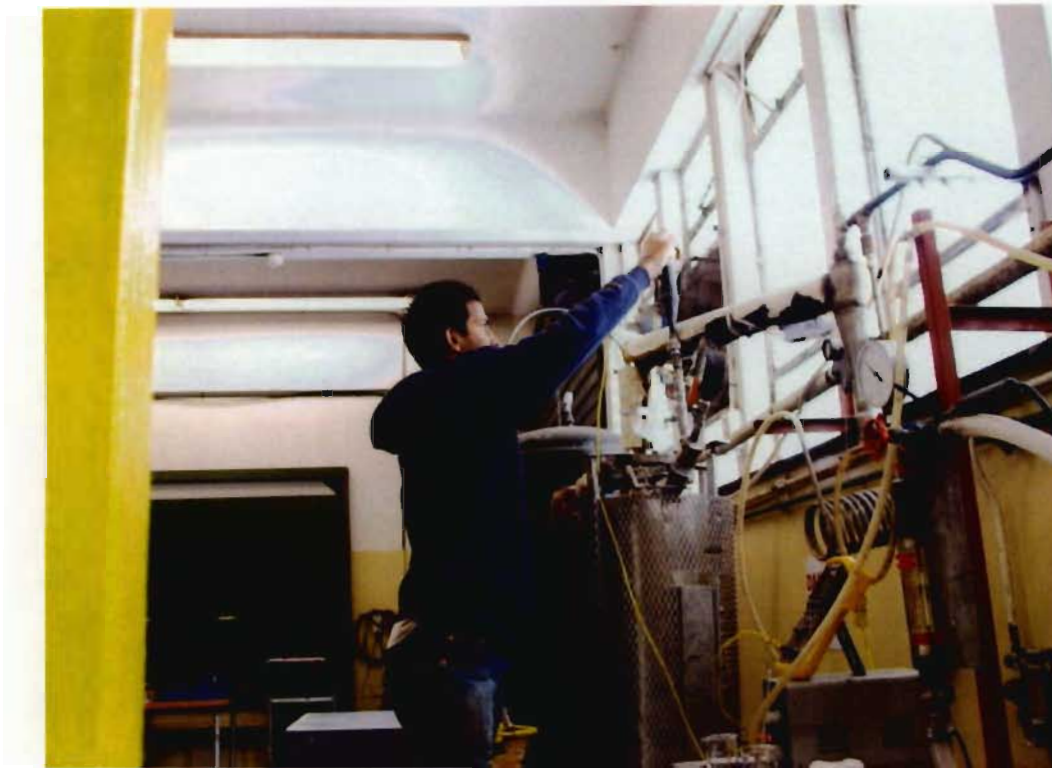
Figure F-21 Photograph of the method used to feed Sorbents into the AFBR

Figure F-22 Photograph of the Environmental Security used
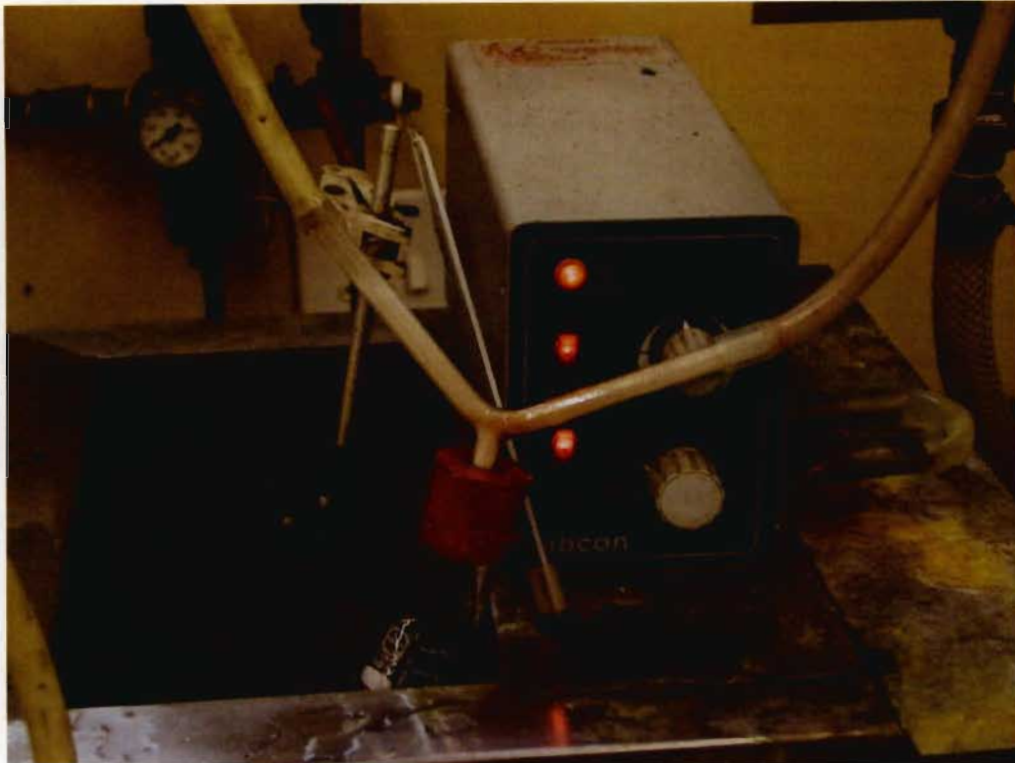
Figure F-23 Photograph of the Gas Chiller prior to entering the SO_2 Analyser

Figure F-24 Photograph of the Gas Chiller prior to entering the SO_2 Analyser

F14
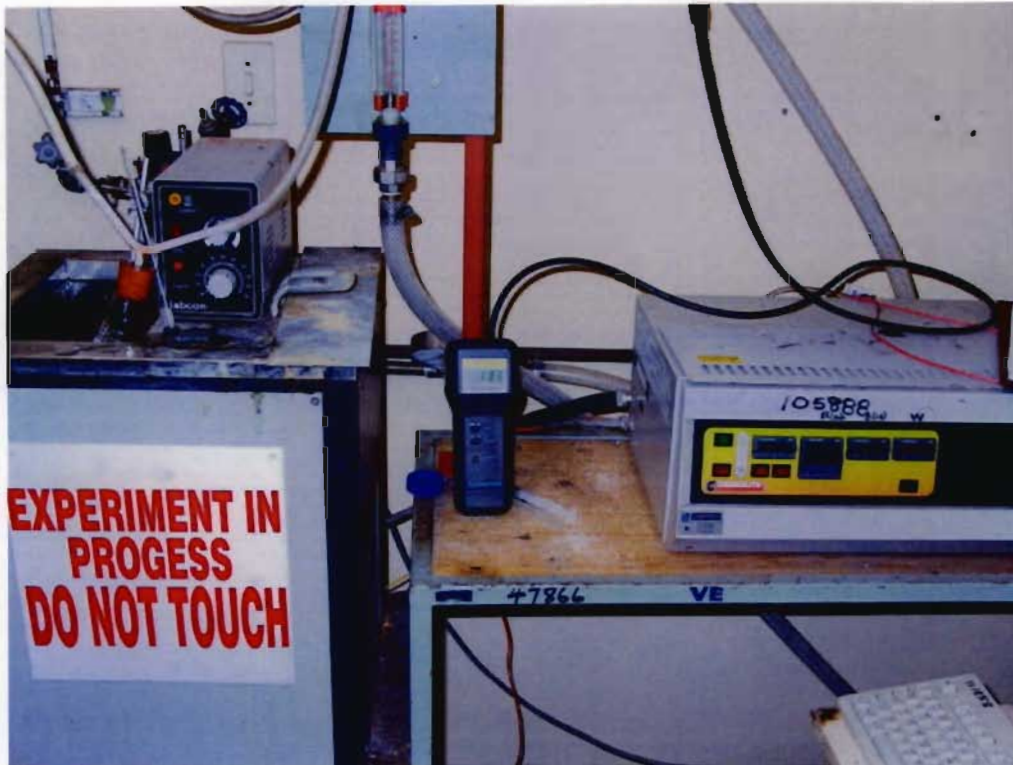
Figure F-25 Photograph of the Bacharach SO₂ Electrochemical Analyser

Figure F-26 Photograph of the Bacharach SO₂ ElectroChemical Analyser

Figure F-27 Photograph of the 425-500μm Sorbents used in the Study

Figure F-28 Photograph of the 600-710μm Sorbents used in the Study
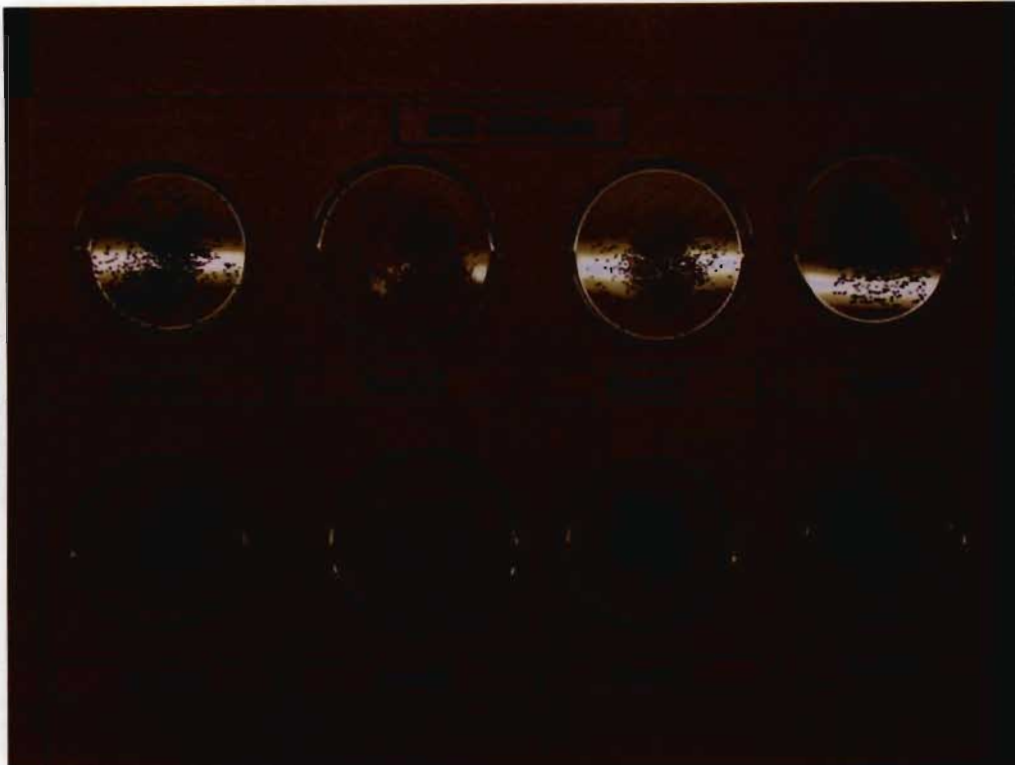
Figure F-29 Photograph of the 850-1000µm Sorbents used in the Study
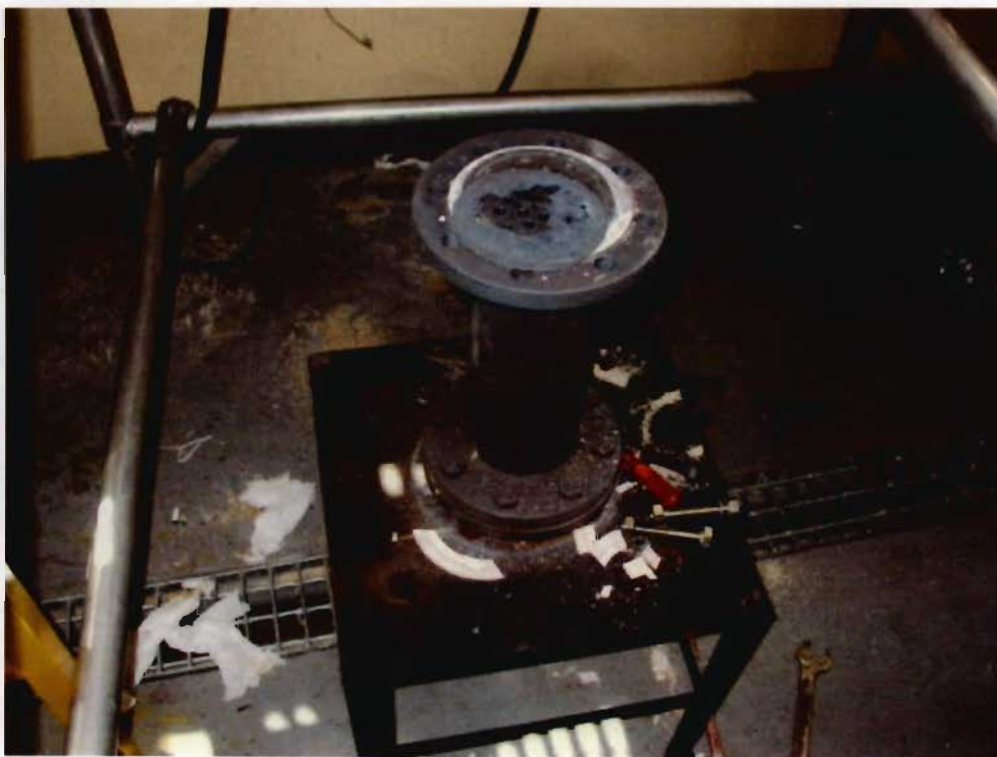
Figure F-30 Photograph of the Problem Experienced with the Equipment
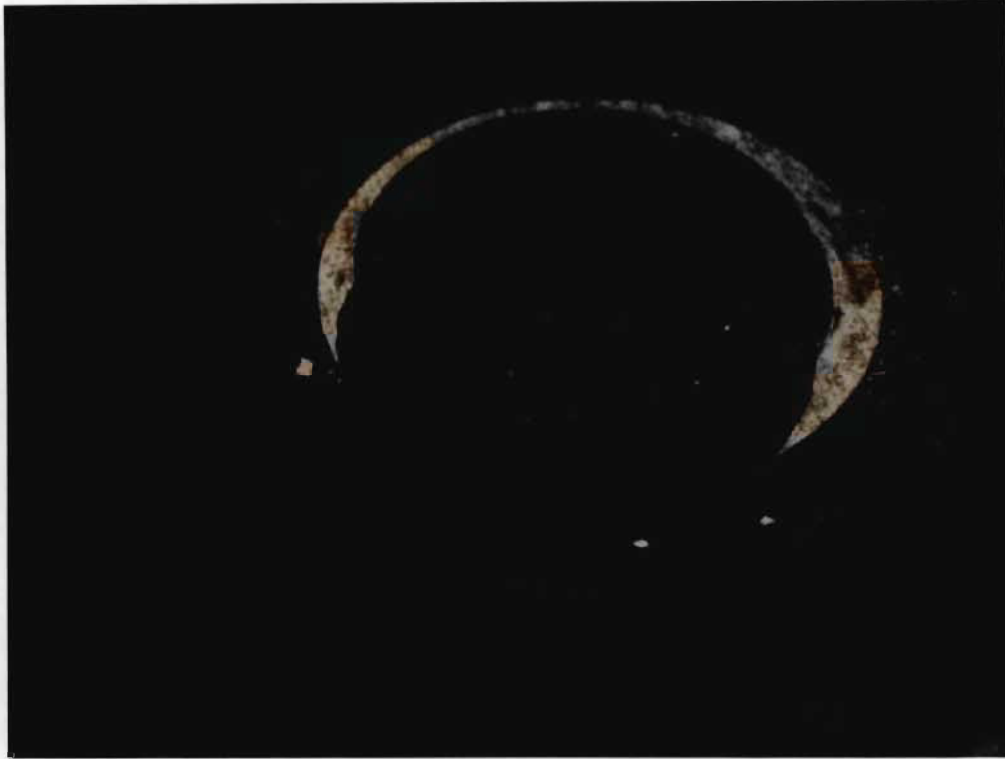
Figure F-31 Photograph of the Problem Experienced with the Equipment
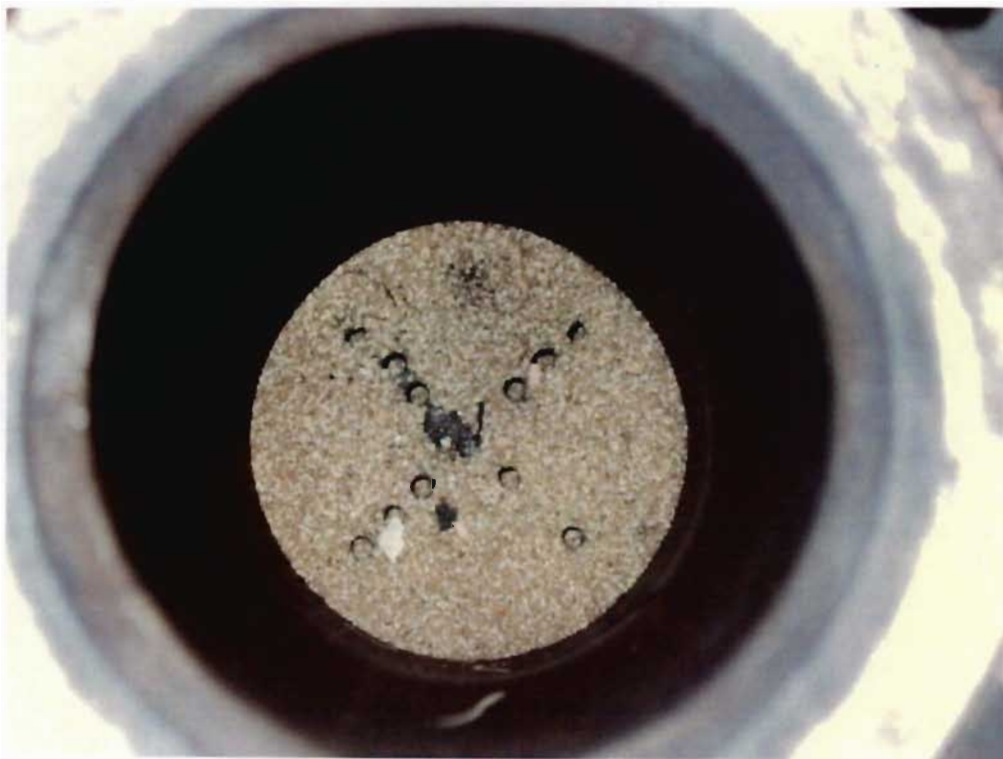
Figure F-32 Photograph of the Problem Experienced with the Equipment

Appendix G

Fluidised Bed Reactor Results

Particle Size: 850-1000μm

Temperature: 600°C
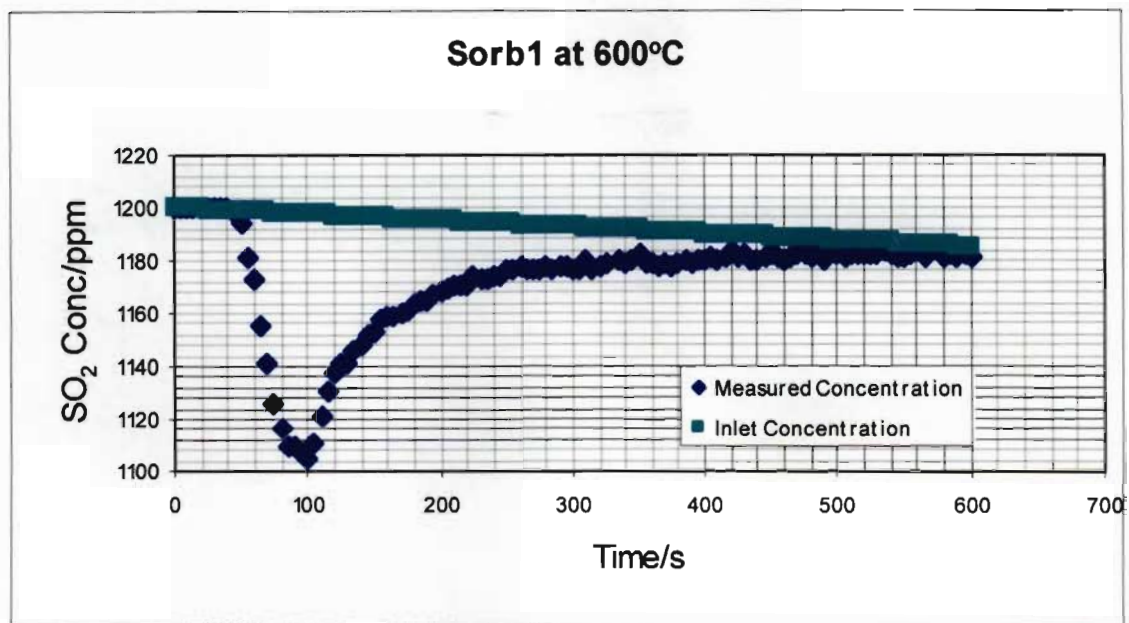
Figure G-1 Performance graph of sorbent Sorb1 of particle size 850-1000μm at 600°C
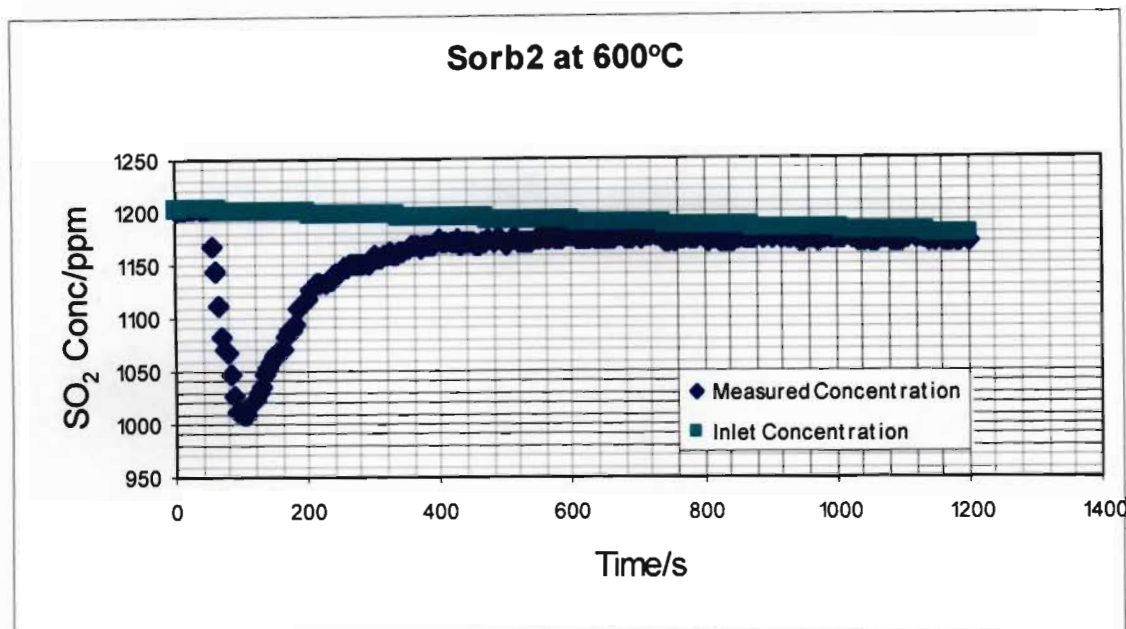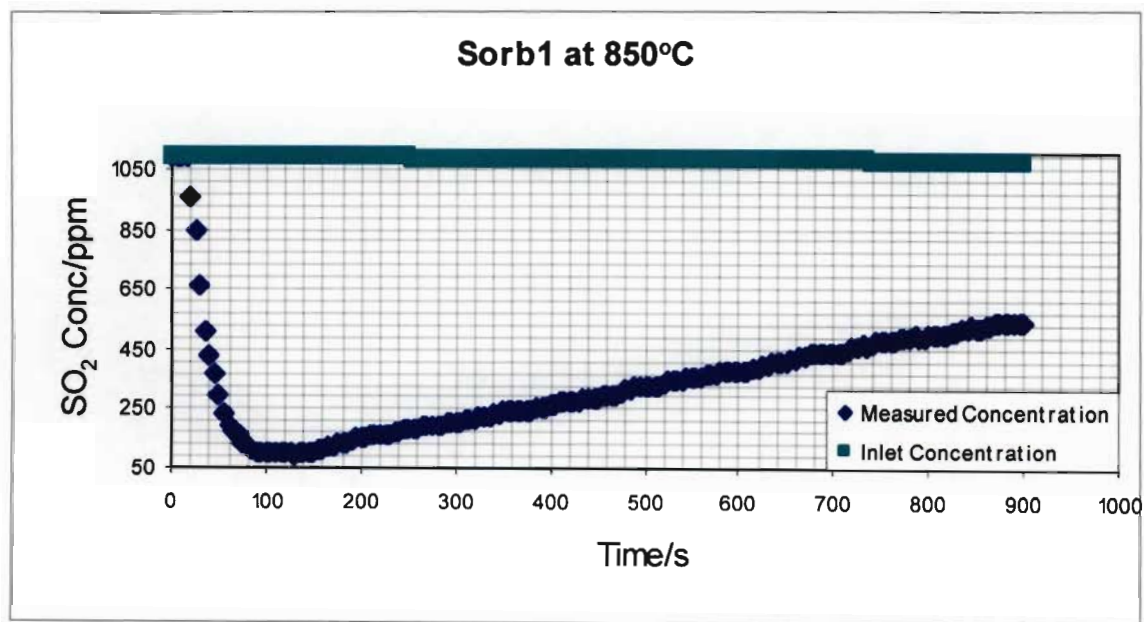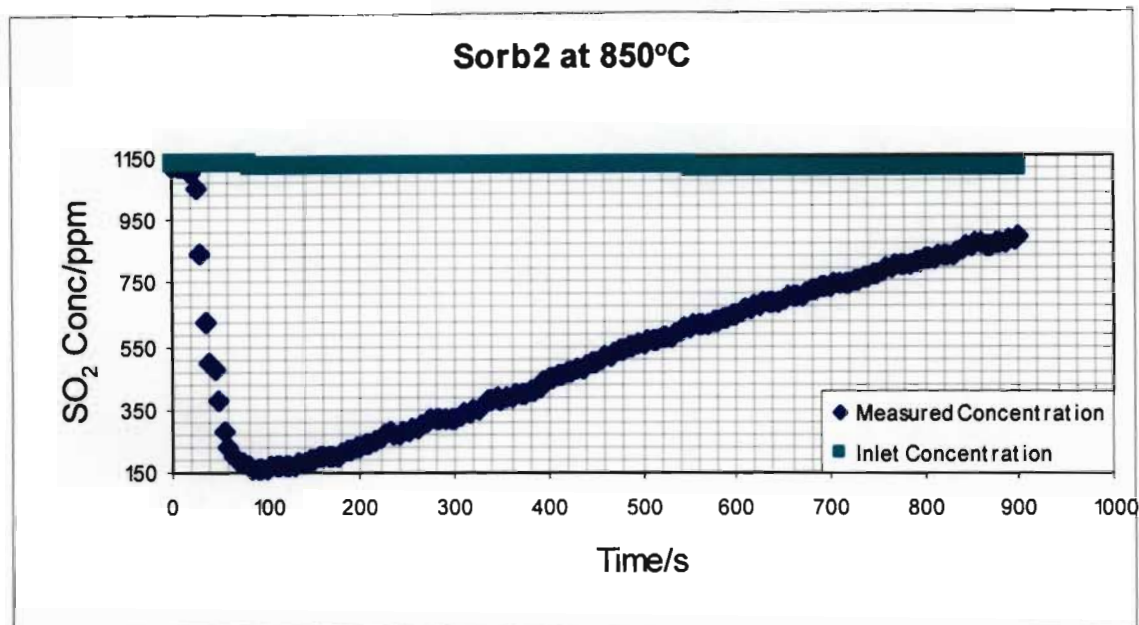
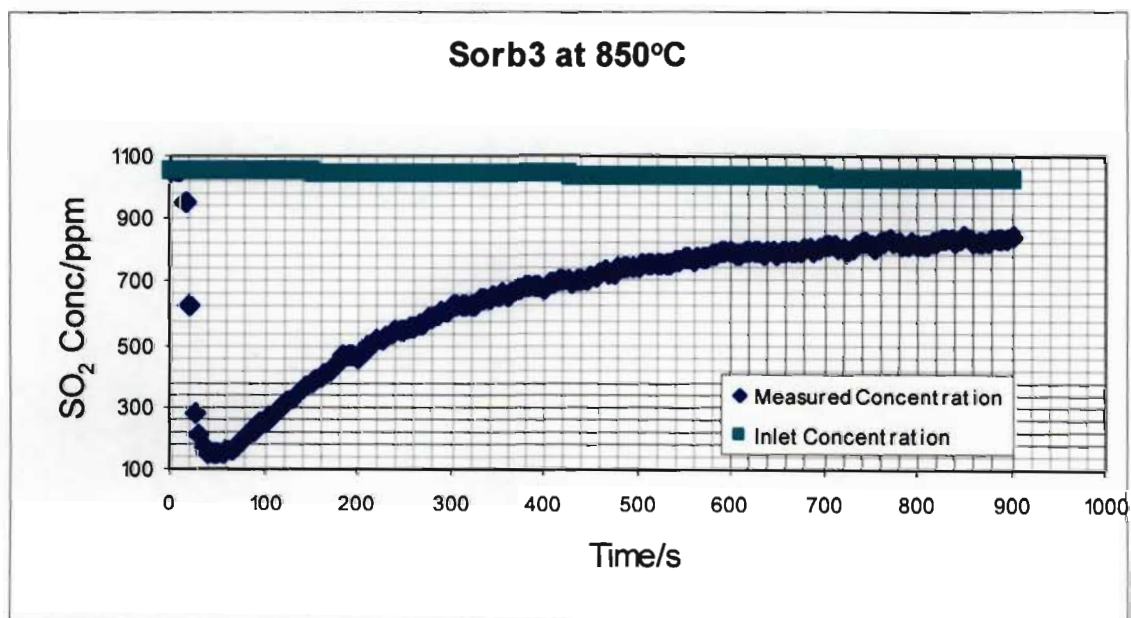Figure G-2 Performance graph of sorbent Sorb2 of particle size 850-1000μm at 600°C
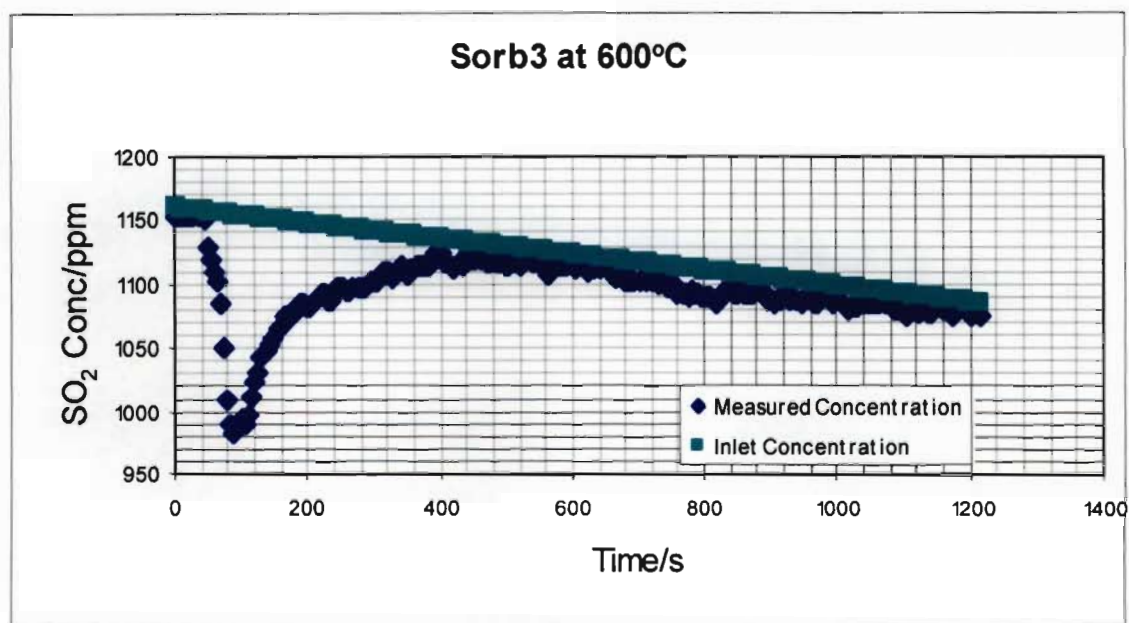
Figure G-3 Performance graph of sorbent Sorb3 of particle size 850-1000μm at 600°C
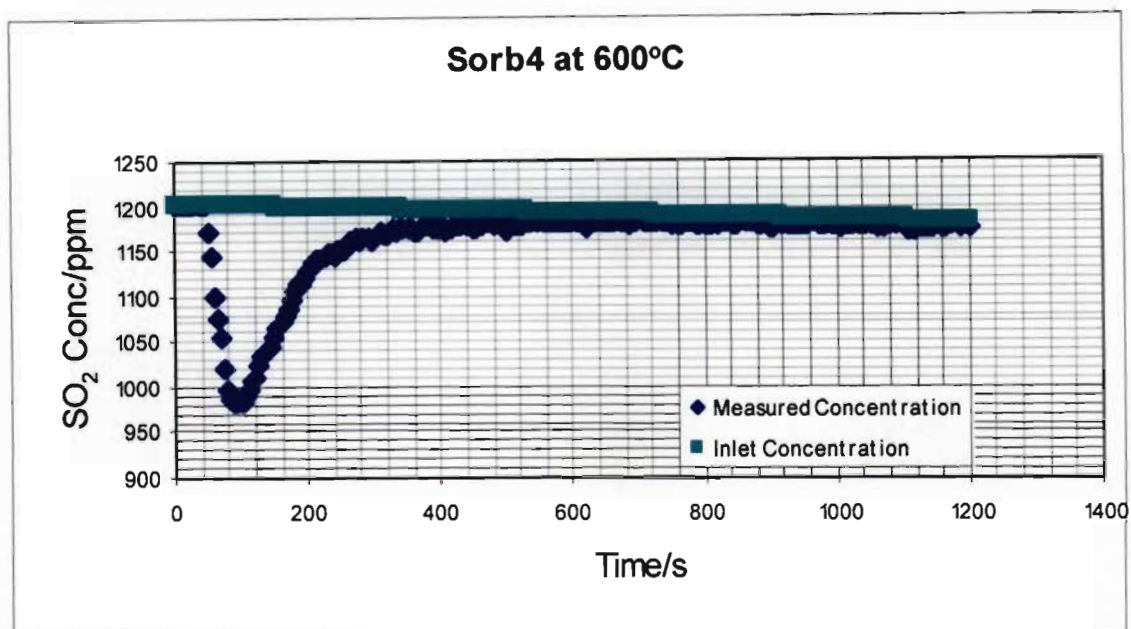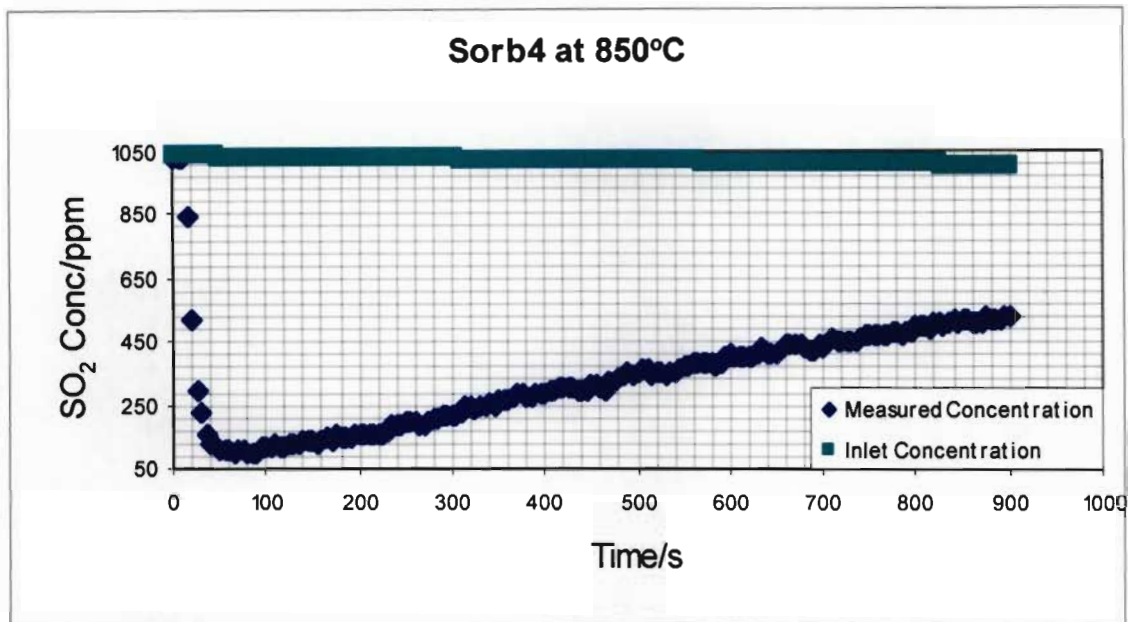
Figure G-4 Performance graph of sorbent Sorb4 of particle size 850-1000µm at 600°C
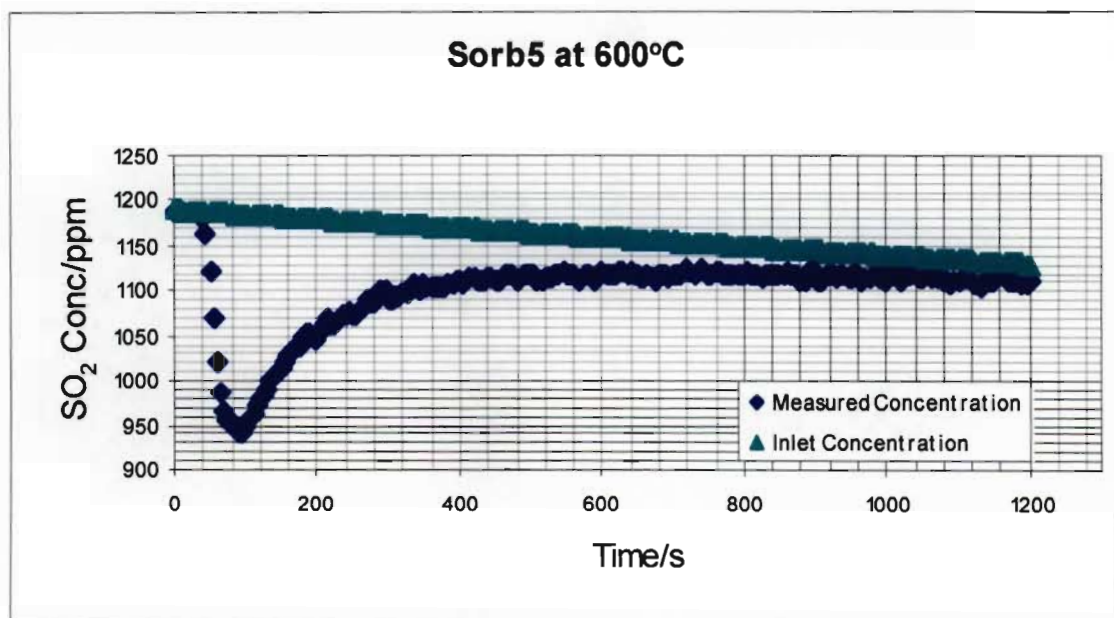
Figure G-5 Performance graph of sorbent Sorb5 of particle size 850-1000µm at 600°C
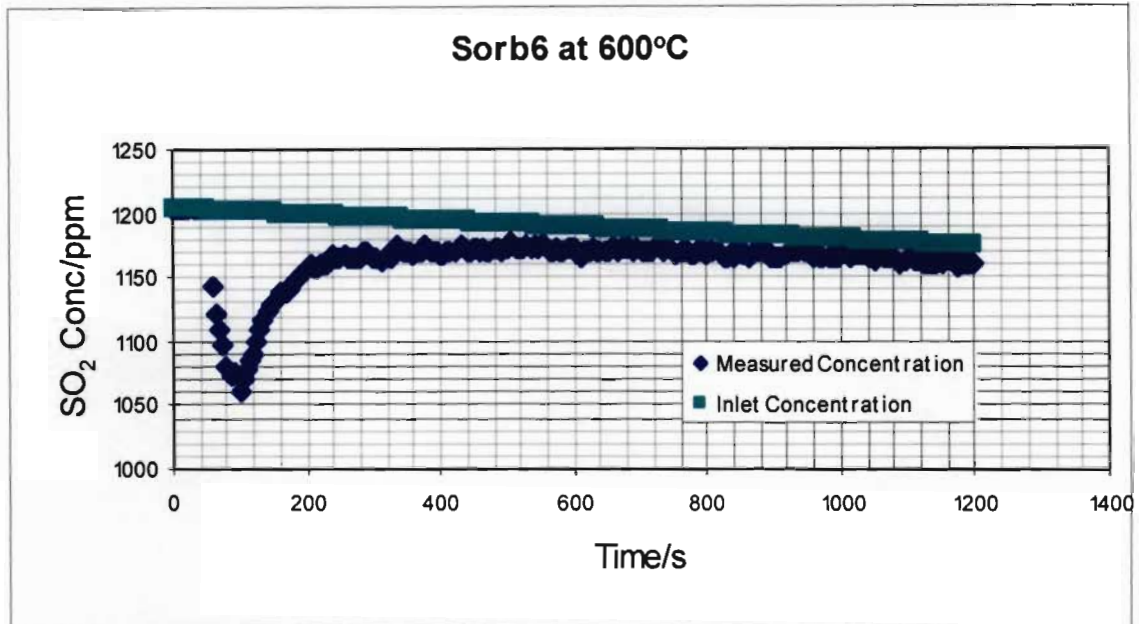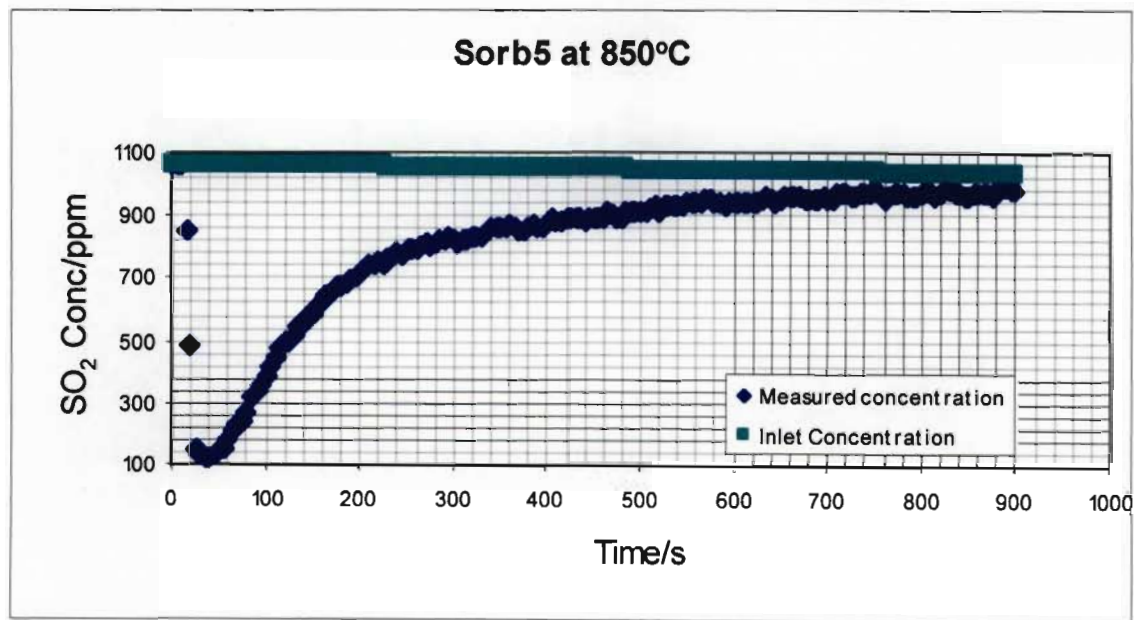
Figure G-6 Performance graph of sorbent Sorb6 of particle size 850-1000μm at 600°C
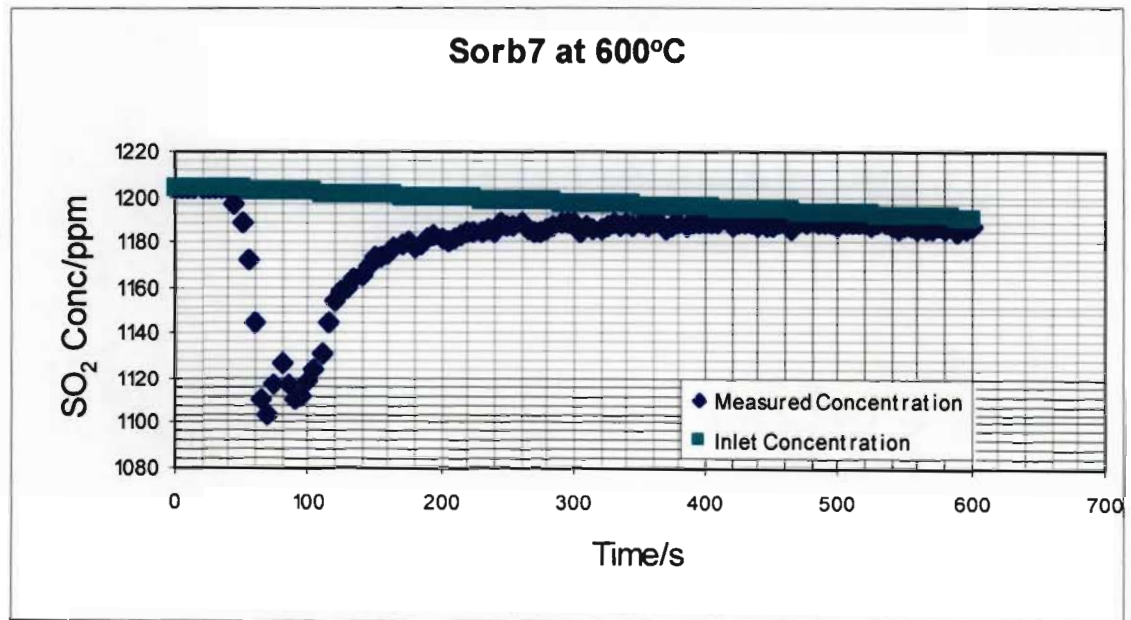
Figure G-7 Performance graph of sorbent Sorb7 of particle size 850-1000μm at 600°C
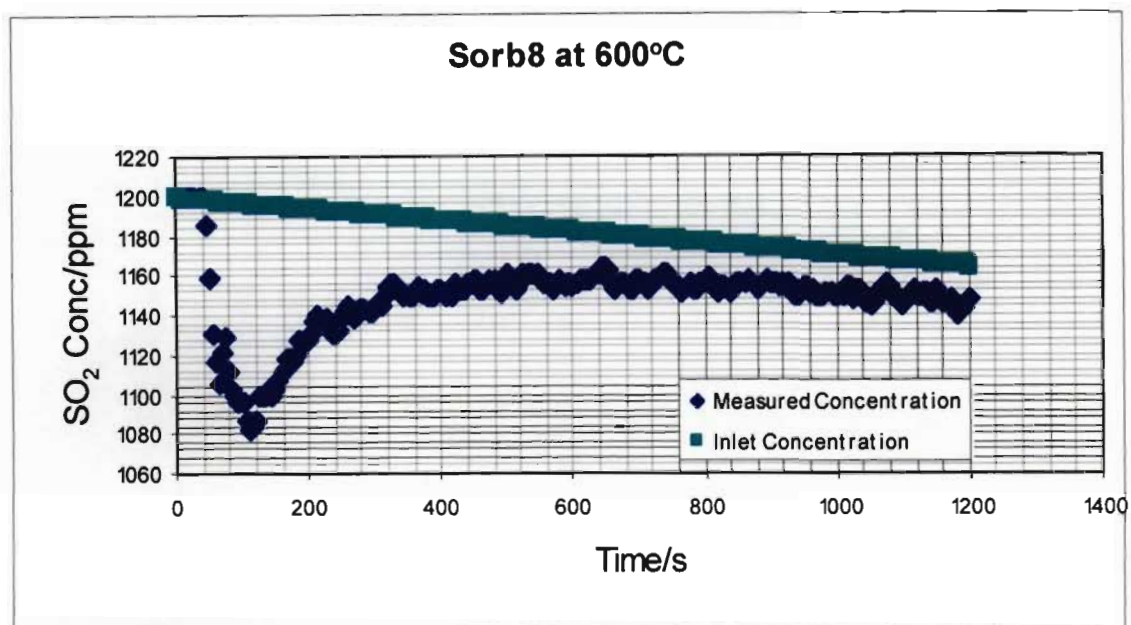
Figure G-8 Performance graph of sorbent Sorb8 of particle size 850-1000µm at 600°C

Temperature: 700°C
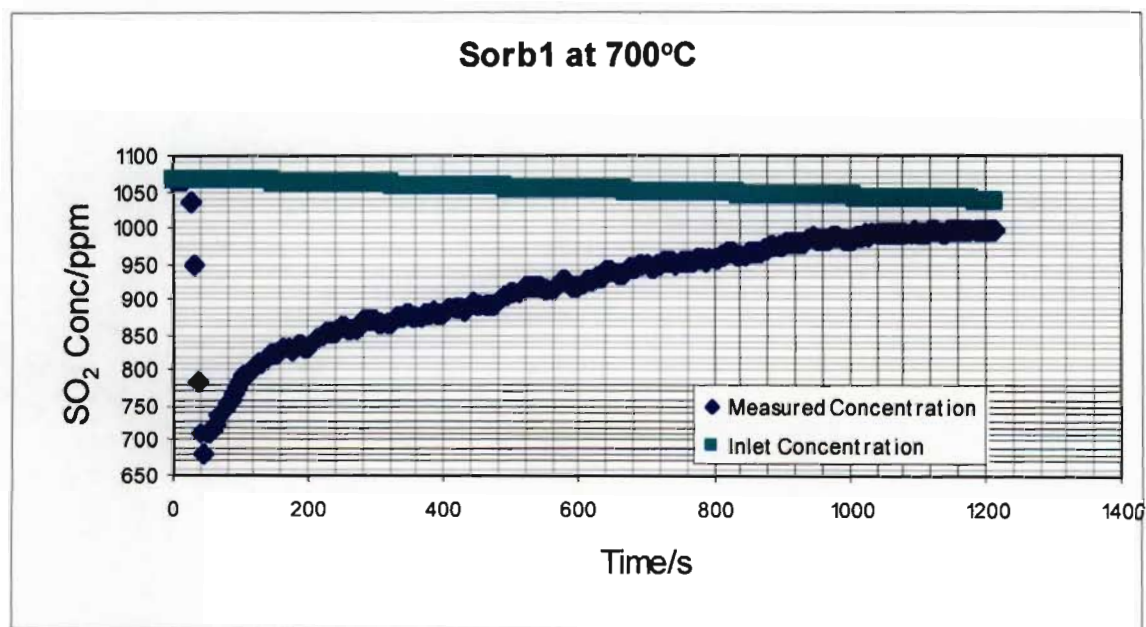
Figure G-9 Performance graph of sorbent Sorb1 of particle size 850-1000µm at 700°C
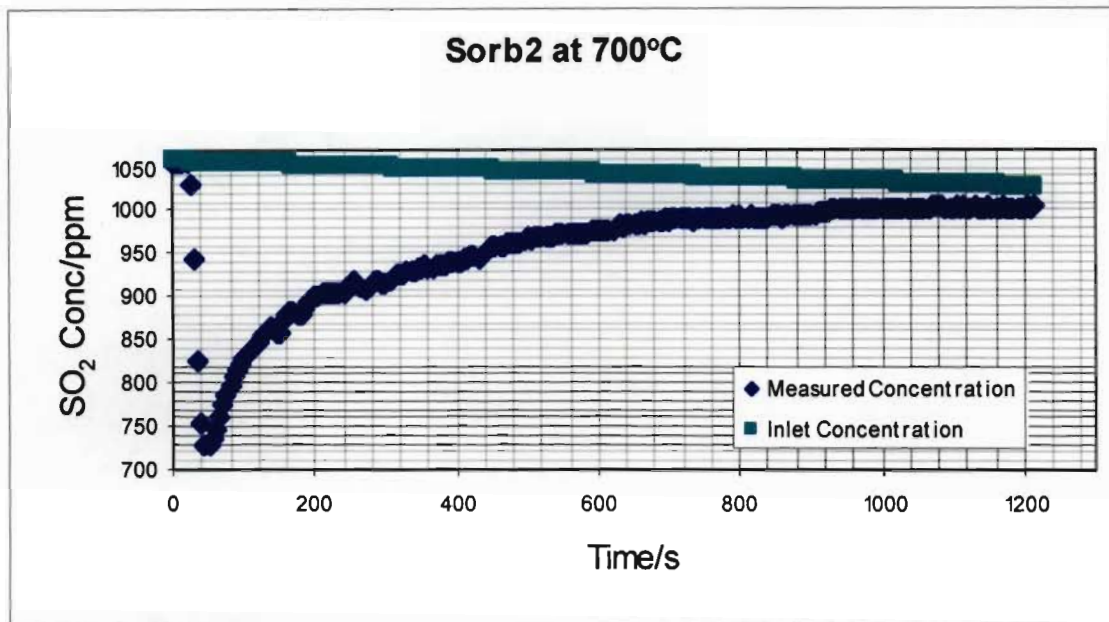
Figure G-10 Performance graph of sorbent Sorb2 of particle size 850-1000µm at 700°C
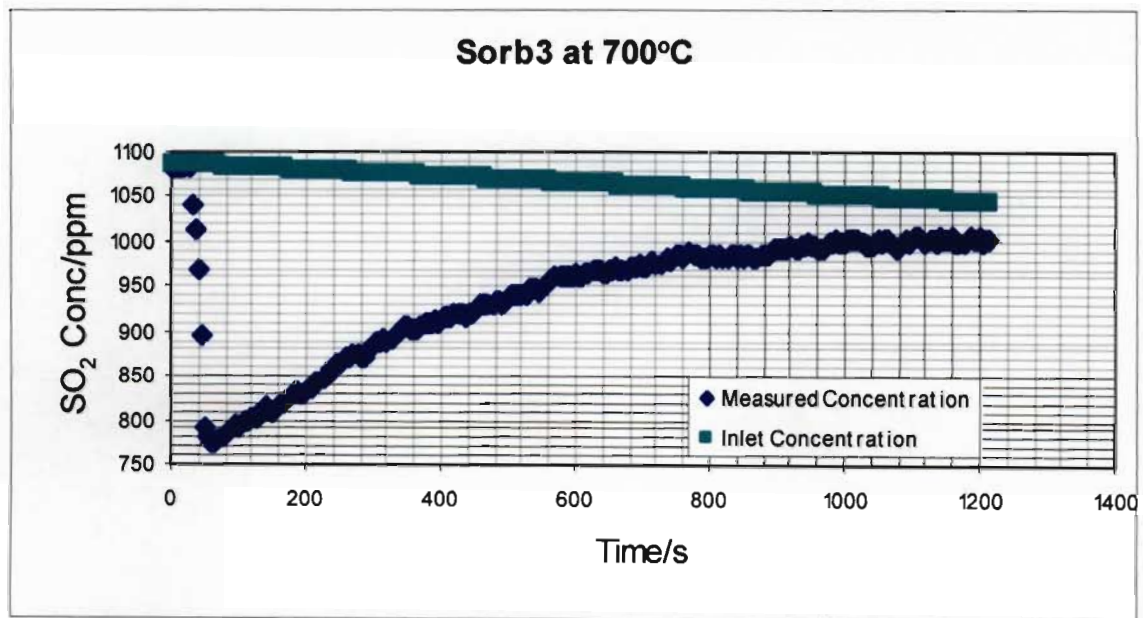
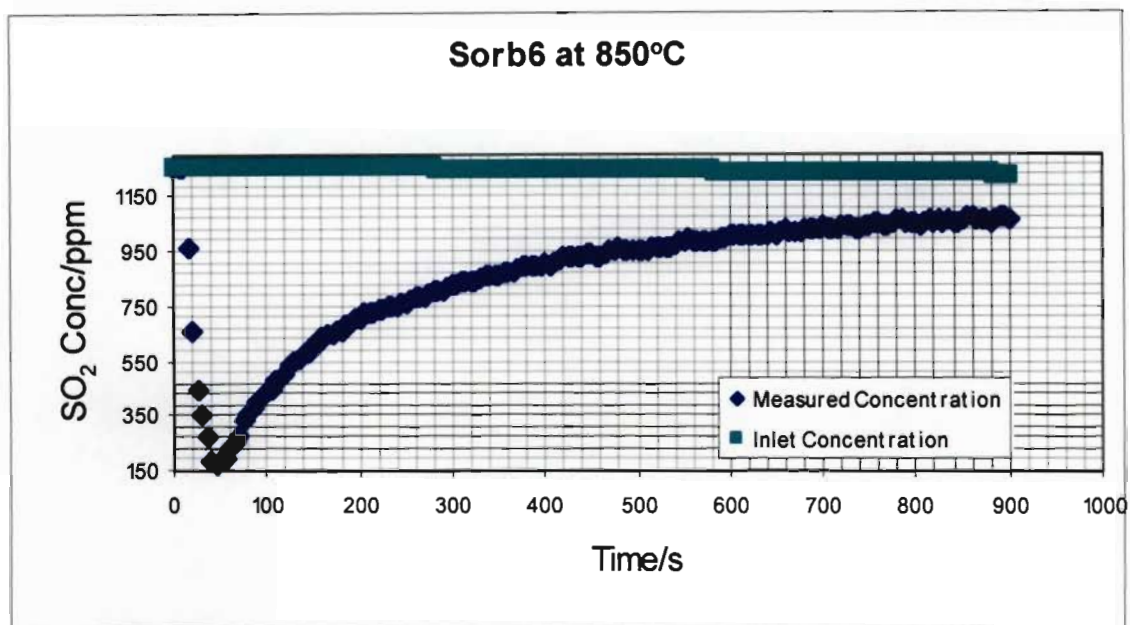Figure G-11 Performance graph of sorbent Sorb3 of particle size 850-1000µm at 700°C
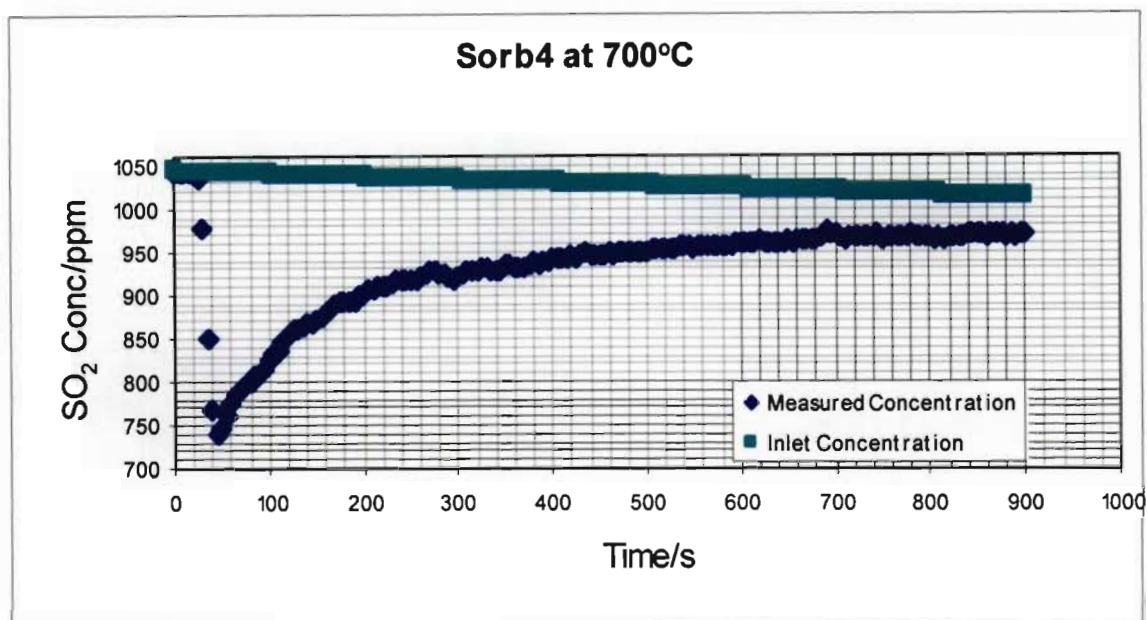
Figure G-12 Performance graph of sorbent Sorb4 of particle size 850-1000μm at 700°C
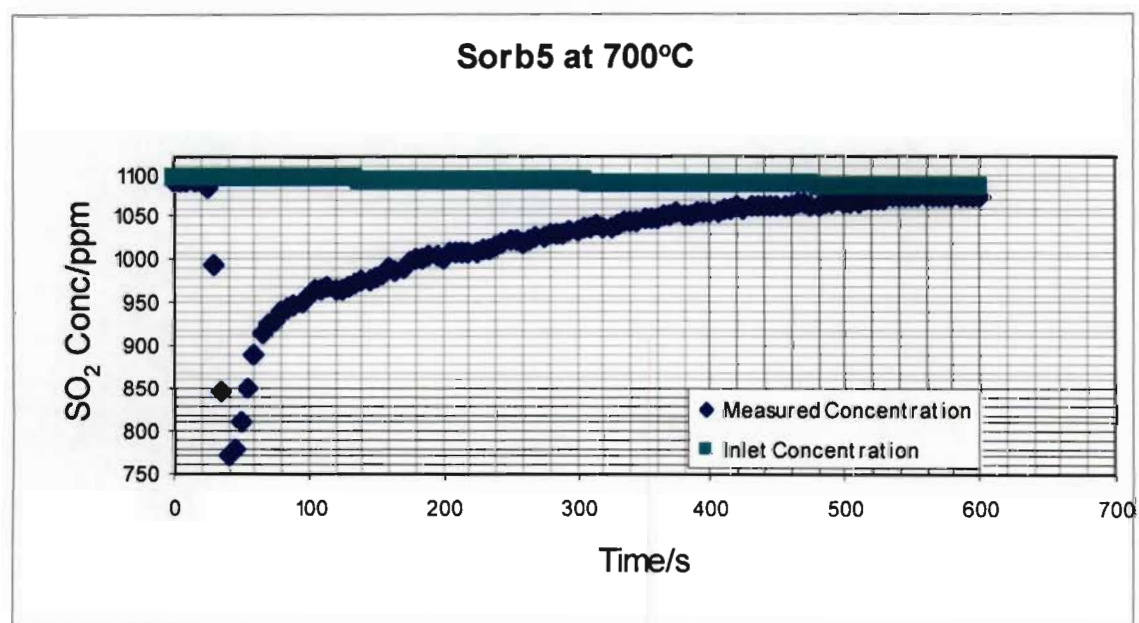
Figure G-13 Performance graph of sorbent Sorb5 of particle size 850-1000μm at 700°C
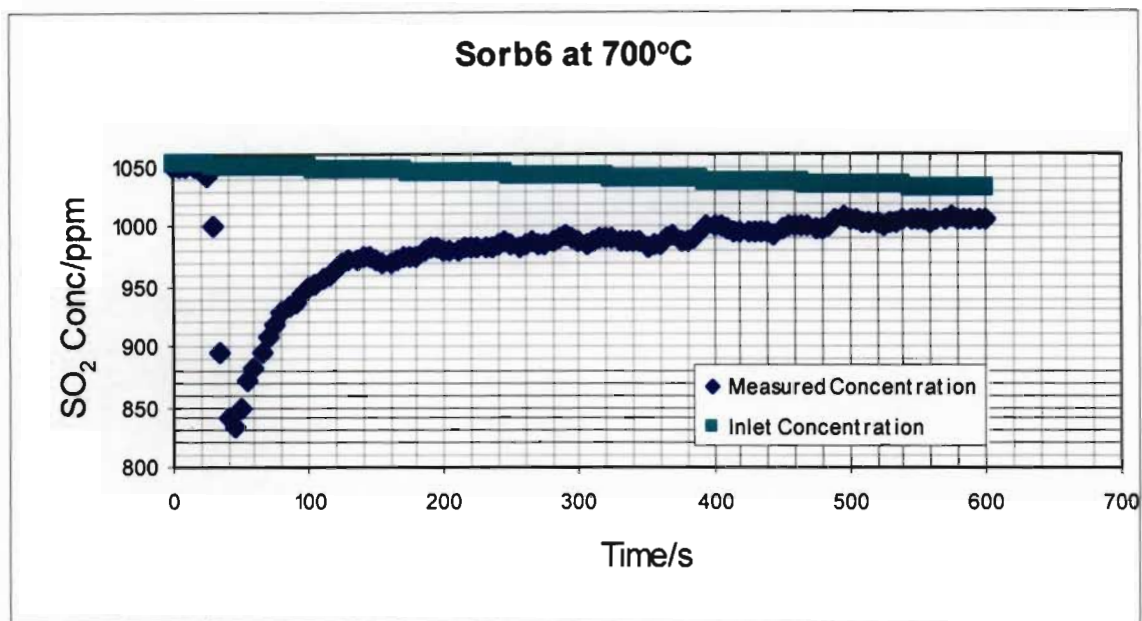
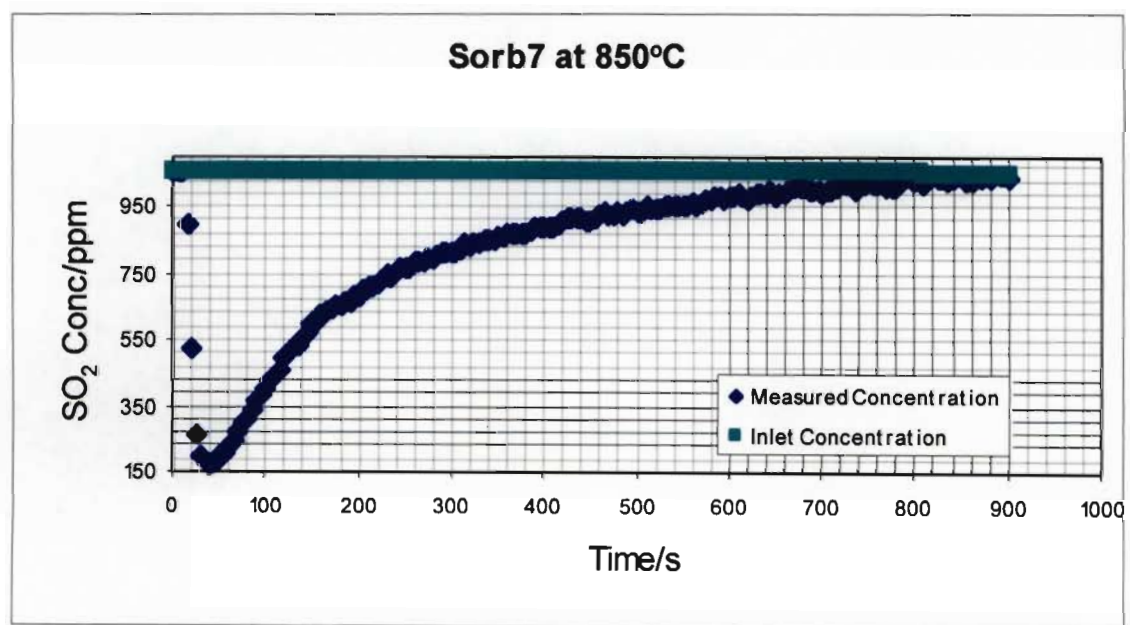Figure G-14 Performance graph of sorbent Sorb6 of particle size 850-1000μm at 700°C
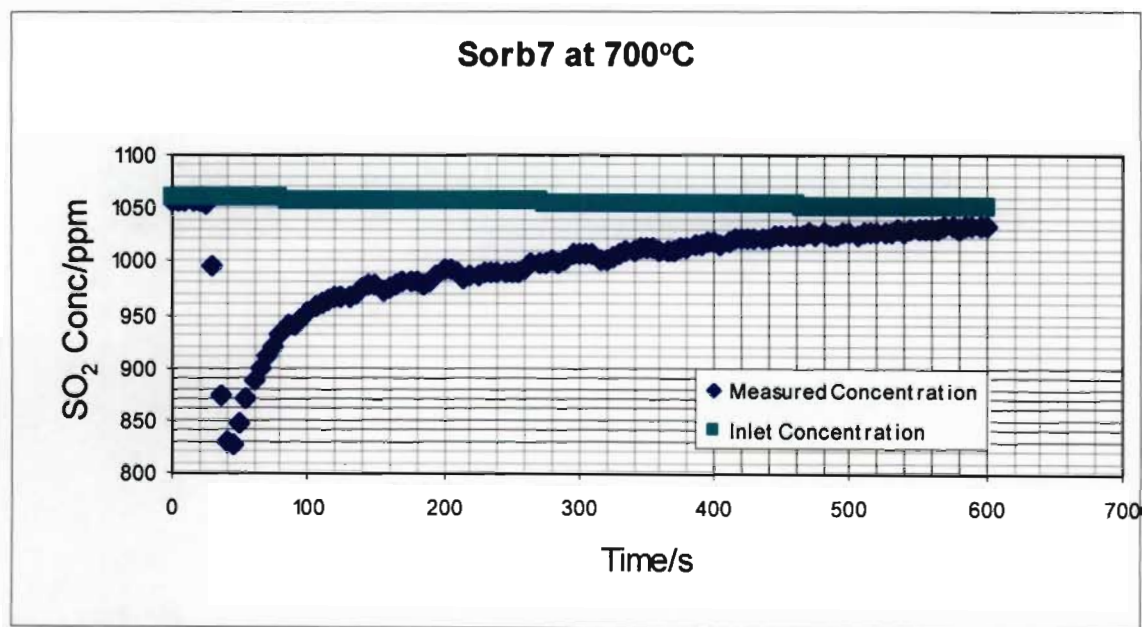
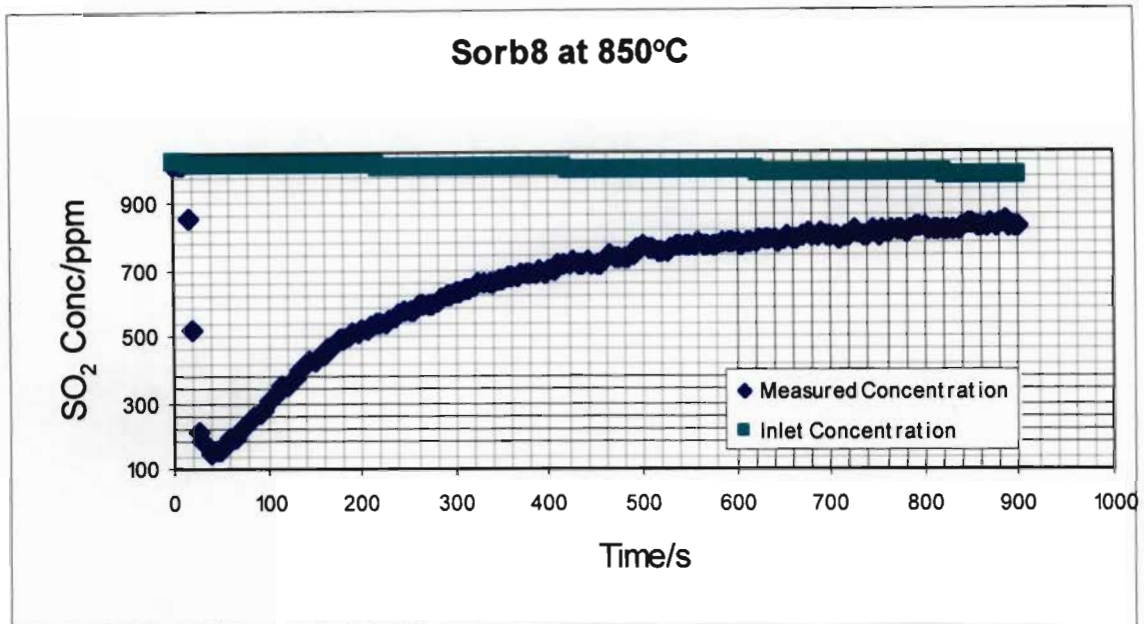Figure G-15 Performance graph of sorbent Sorb7 of particle size 850-1000μm at 700°C

G8
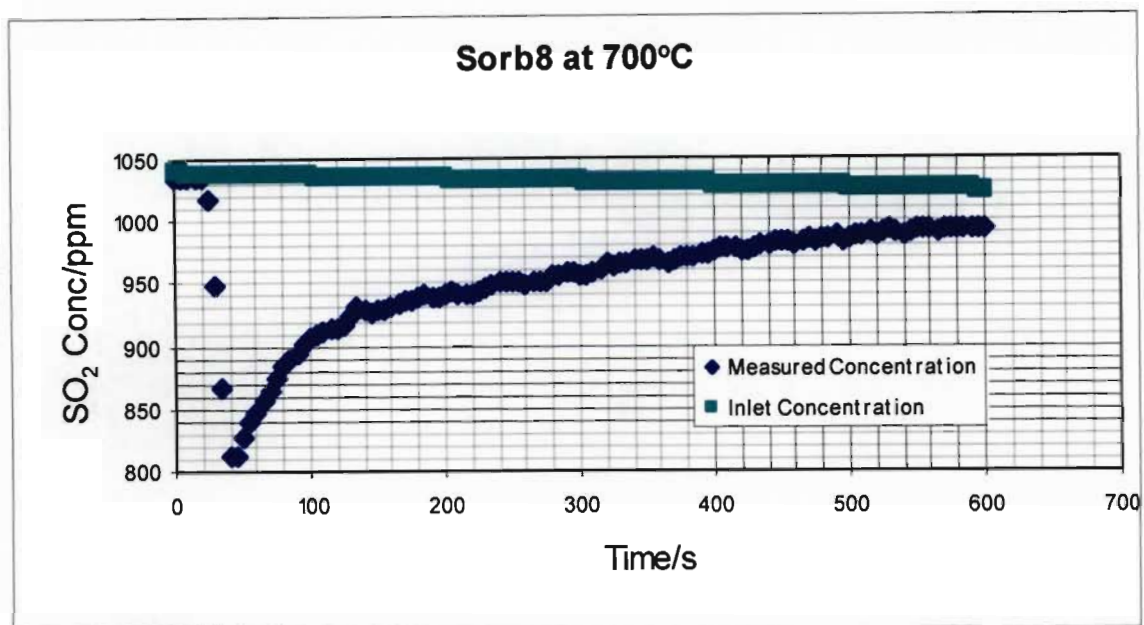
Figure G-16 Performance graph of sorbent Sorb8 of particle size 850-1000μm at 700°C

Temperature: 800°C
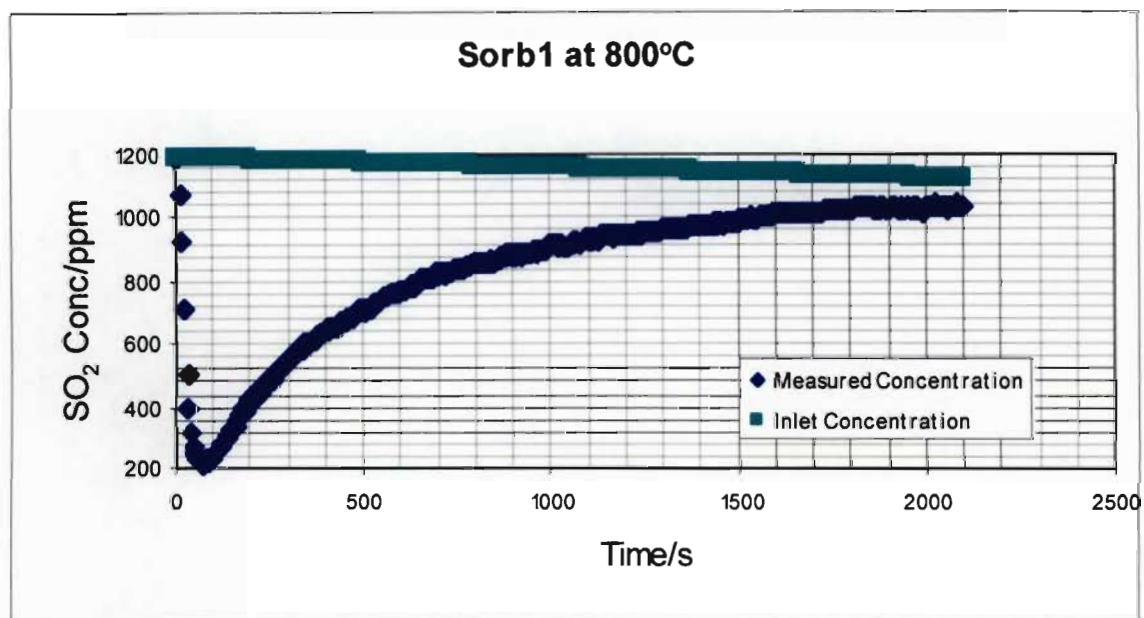
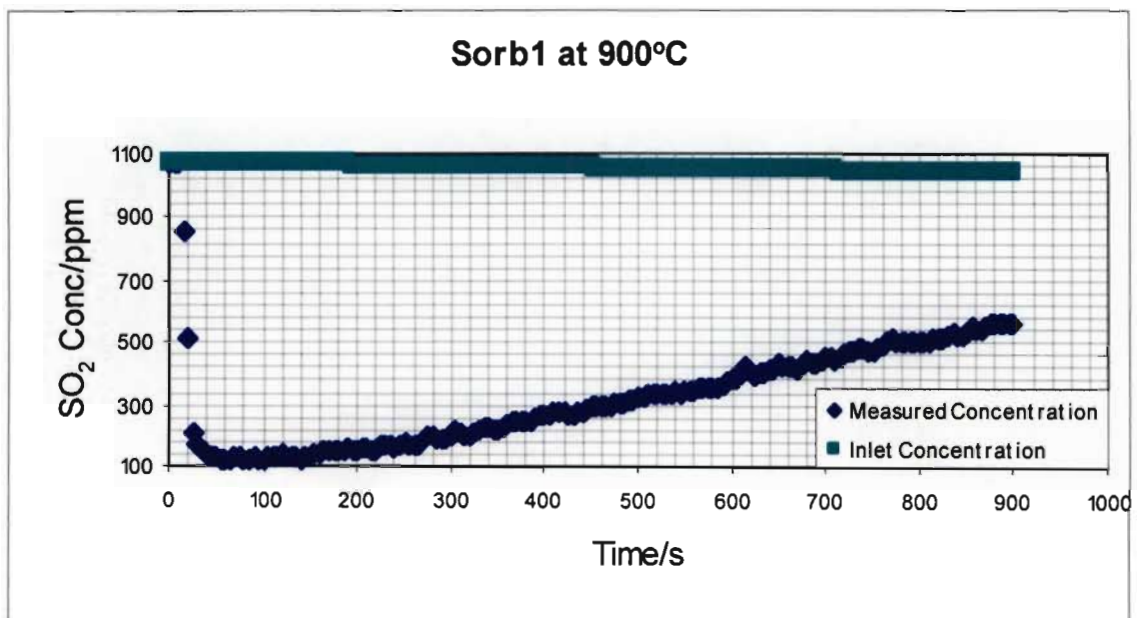Figure G-17 Performance graph of sorbent Sorb1 of particle size 850-1000μm at 800°C
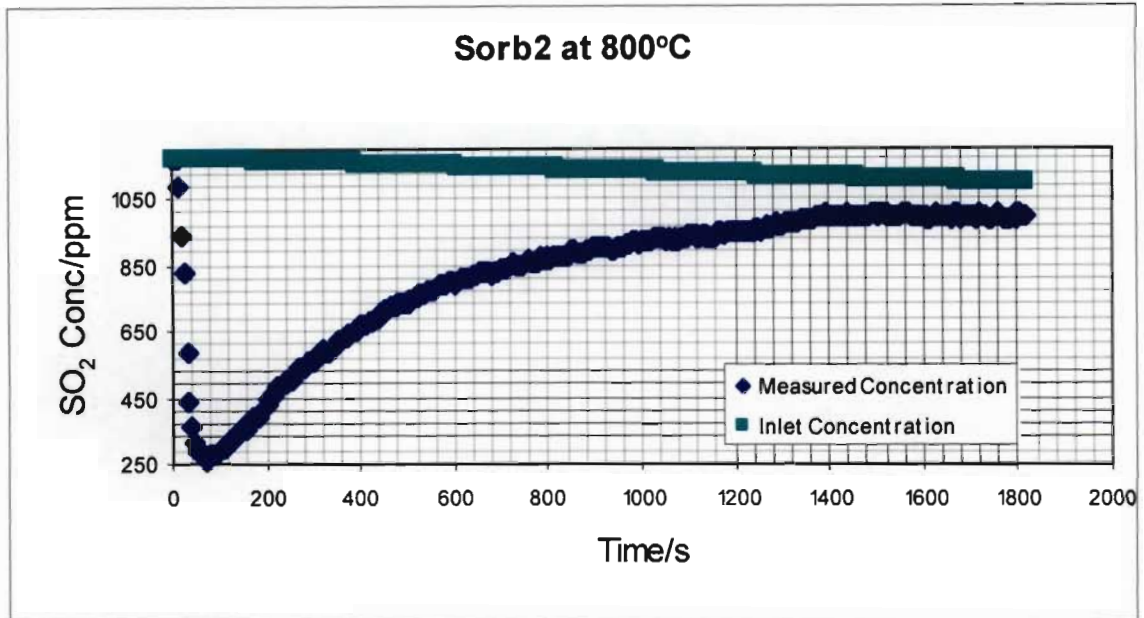
Figure G-18 Performance graph of sorbent Sorb2 of particle size 850-1000μm at 800°C
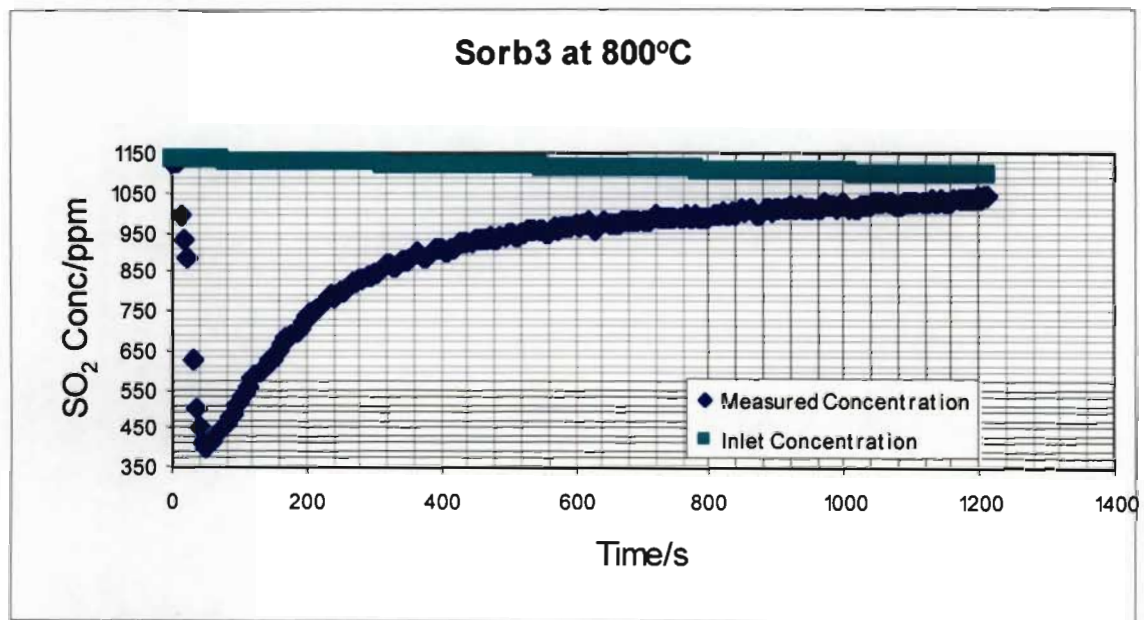
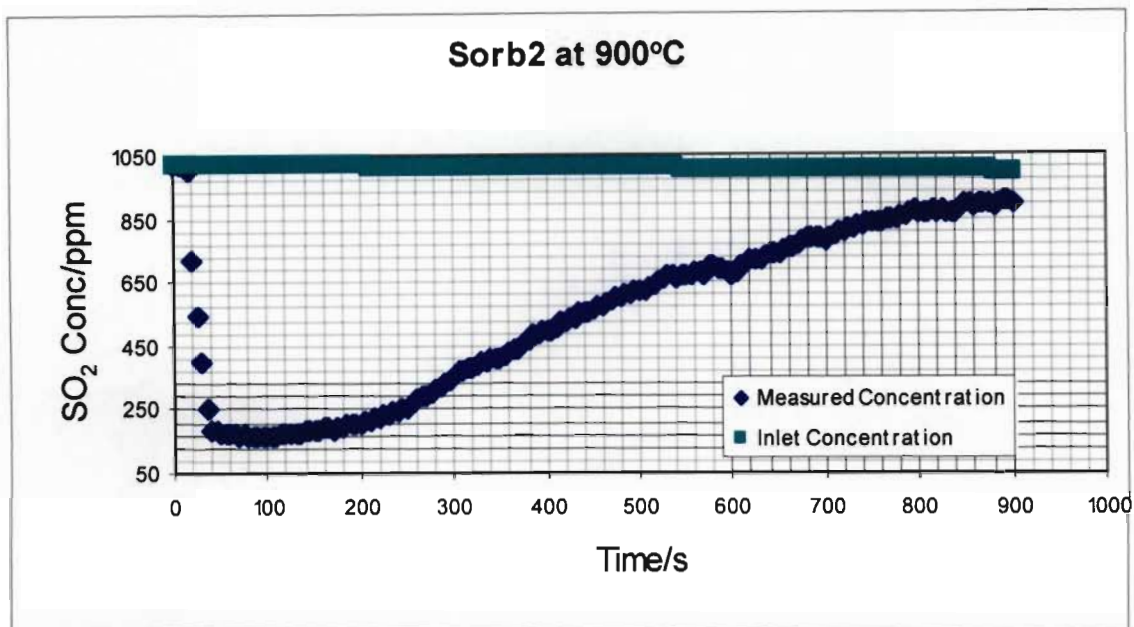Figure G-19 Performance graph of sorbent Sorb3 of particle size 850-1000μm at 800°C
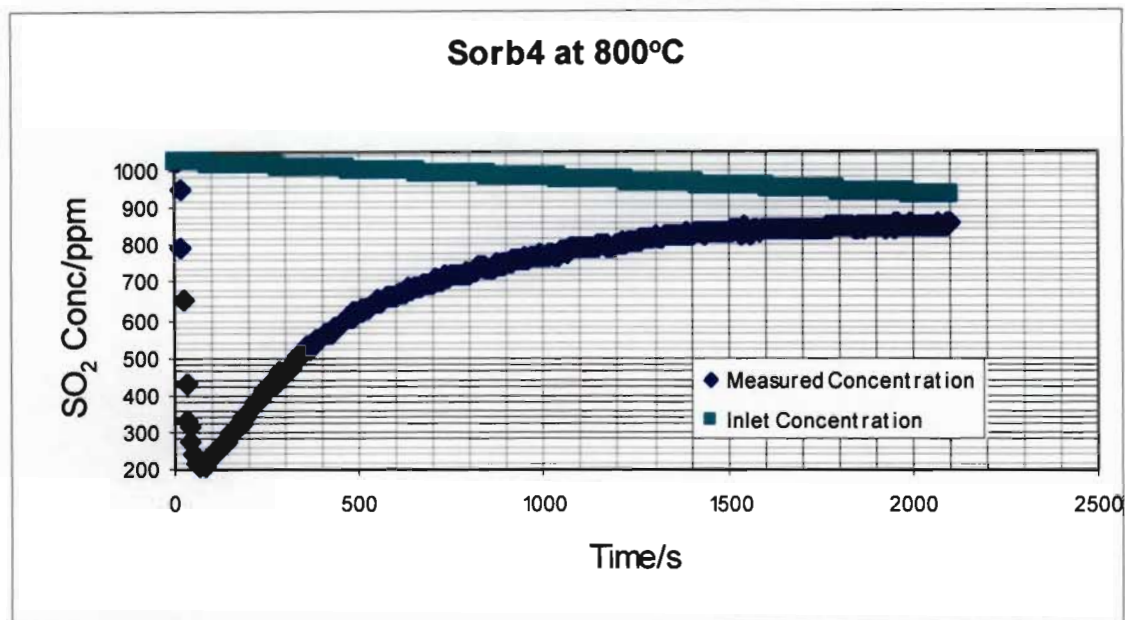
Figure G-20 Performance graph of sorbent Sorb4 of particle size 850-1000μm at 800°C
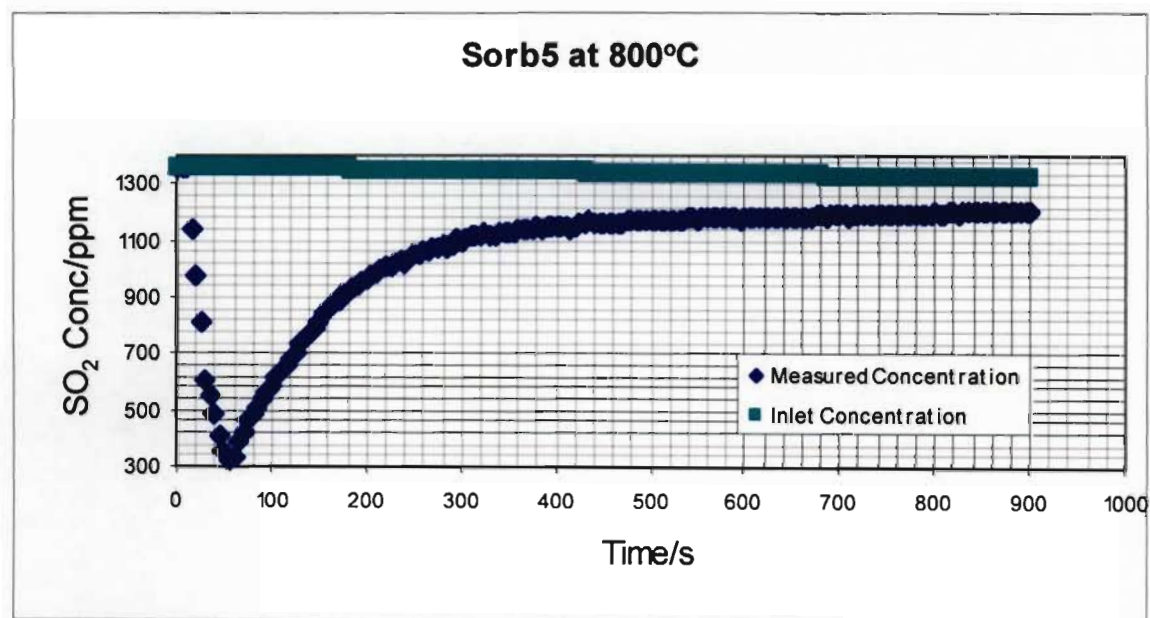
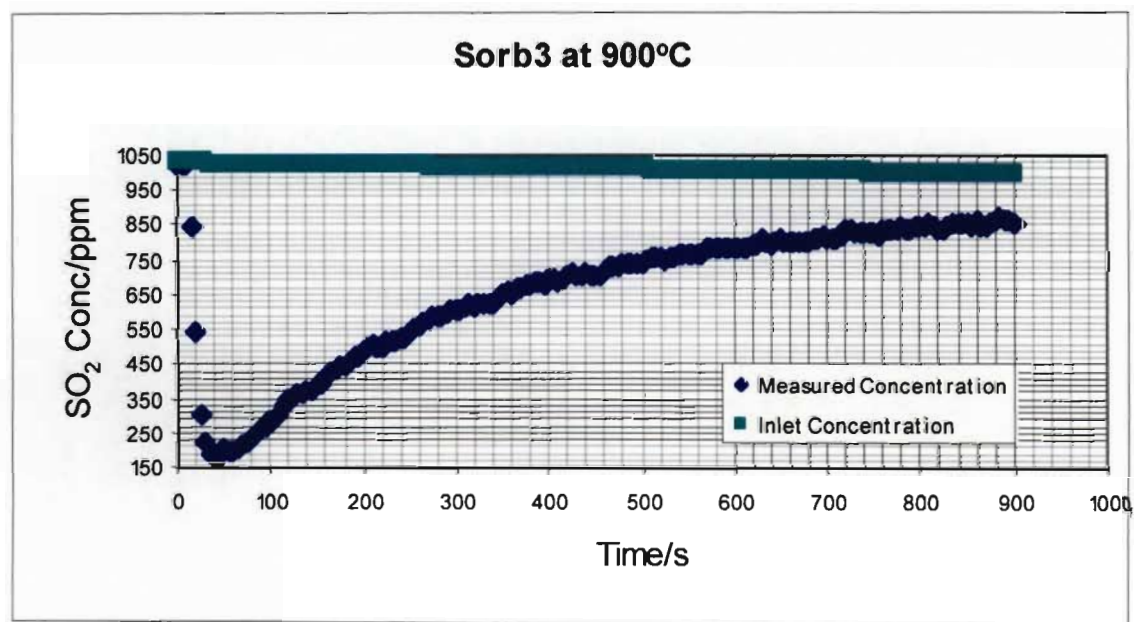Figure G-21 Performance graph of sorbent Sorb5 of particle size 850-1000μm at 800°C
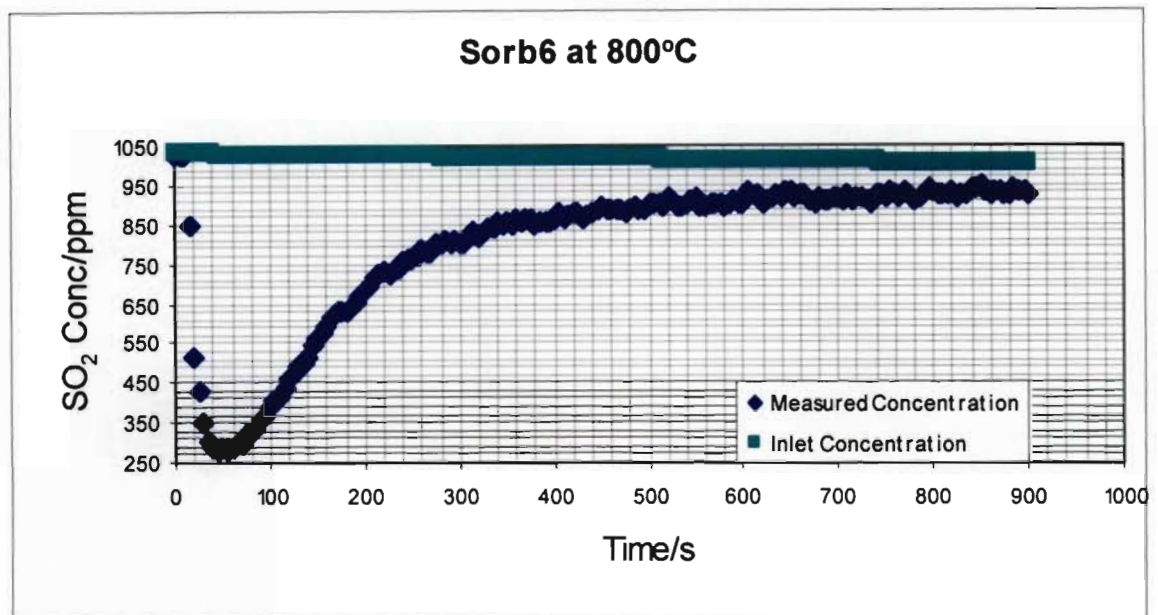
Figure G-22 Performance graph of sorbent Sorb6 of particle size 850-1000μm at 800°C
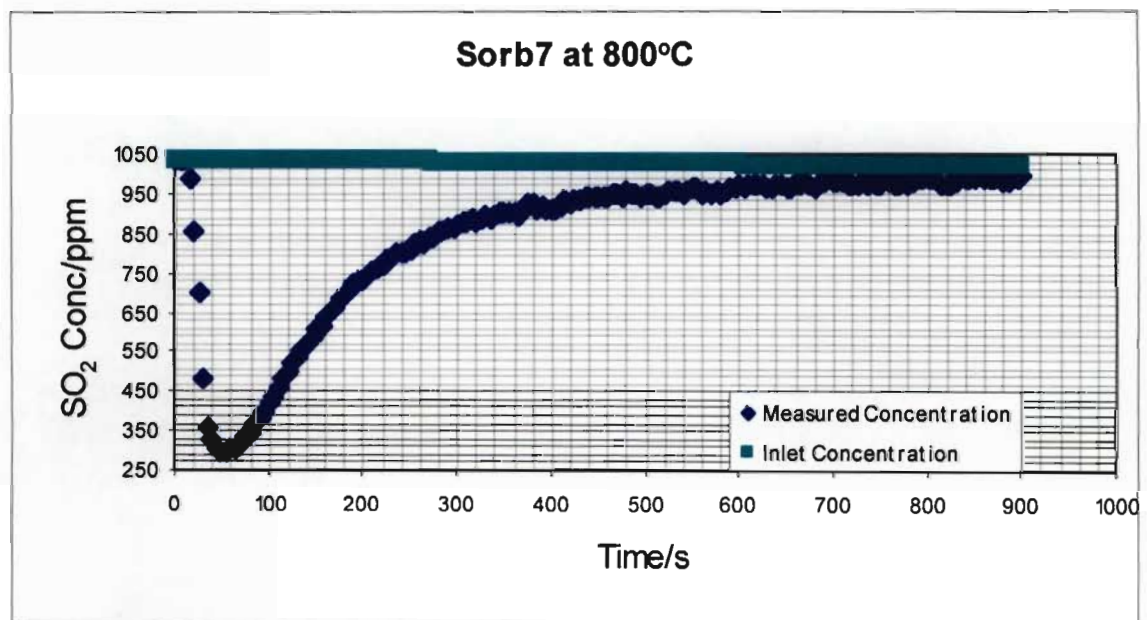
Figure G-23 Performance graph of sorbent Sorb7 of particle size 850-1000μm at 800°C
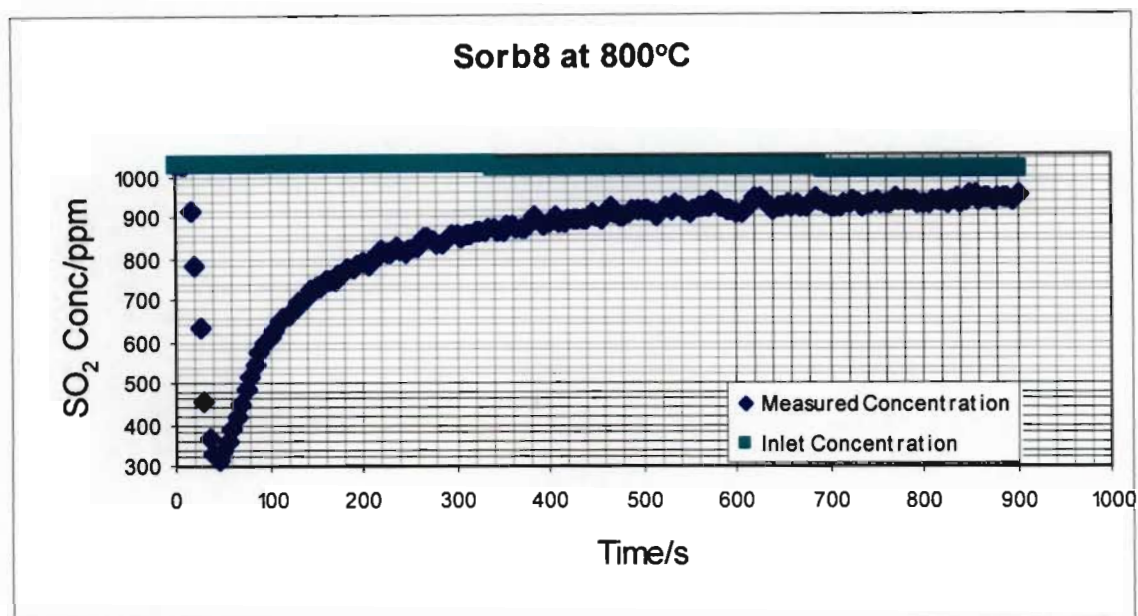
Figure G-24 Performance graph of sorbent Sorb8 of particle size 850-1000μm at 800°C
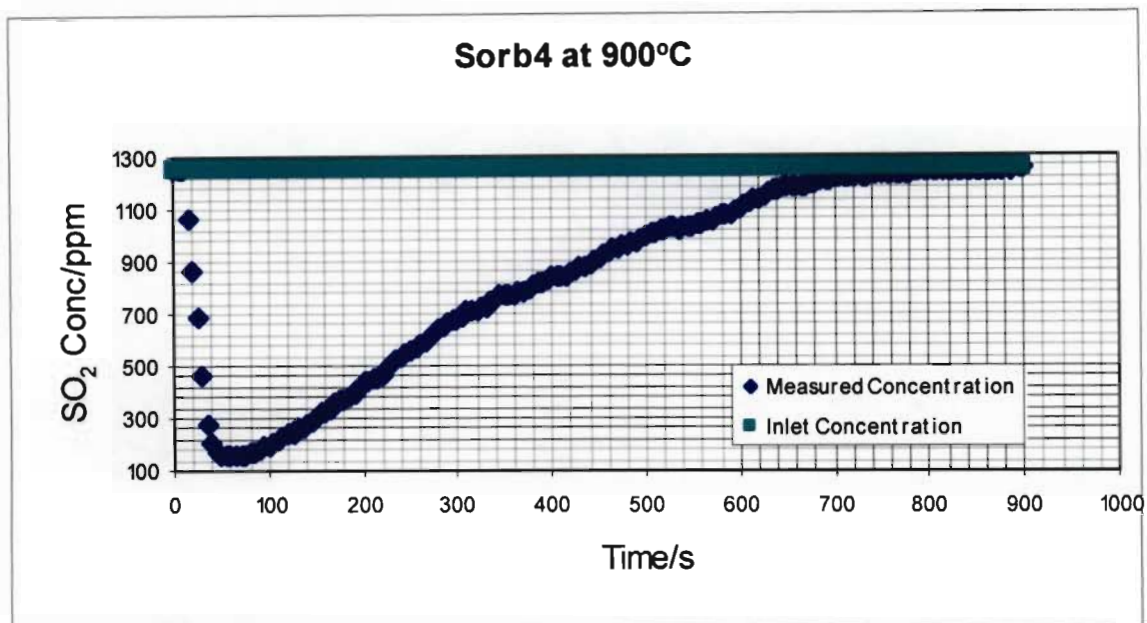
Temperature: 850°C
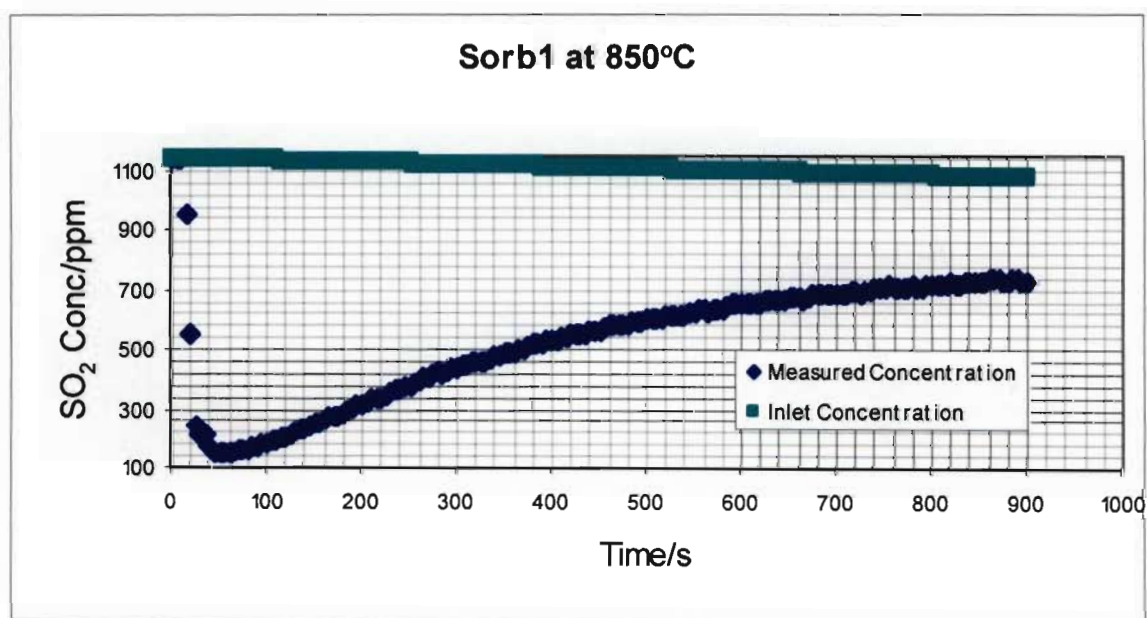
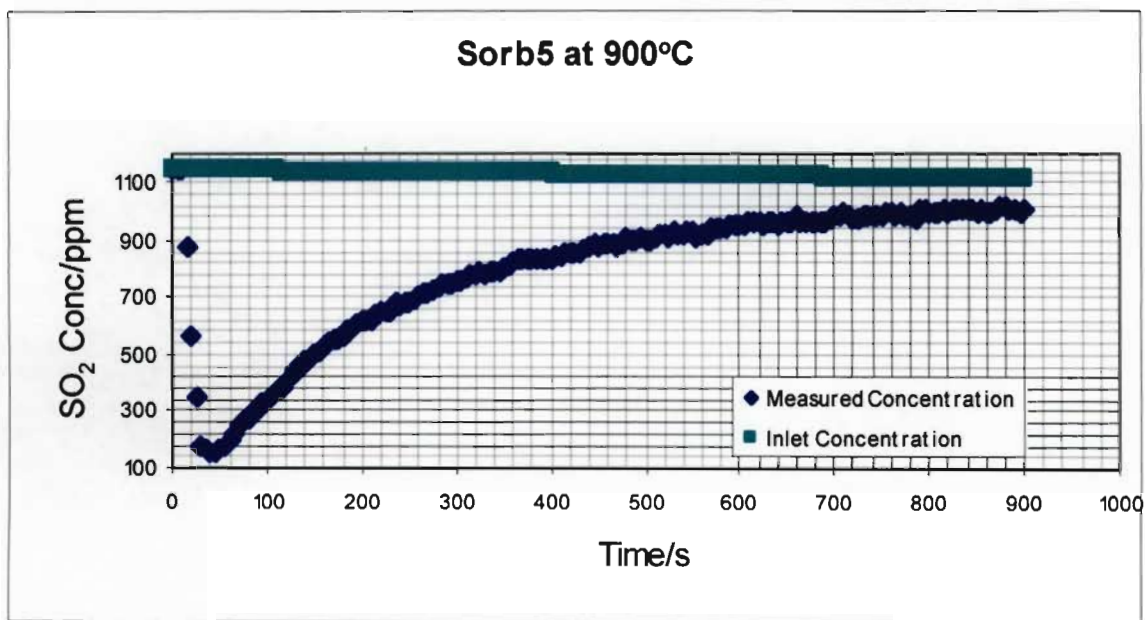Figure G-25 Performance graph of sorbent Sorb1 of particle size 850-1000μm at 850°C
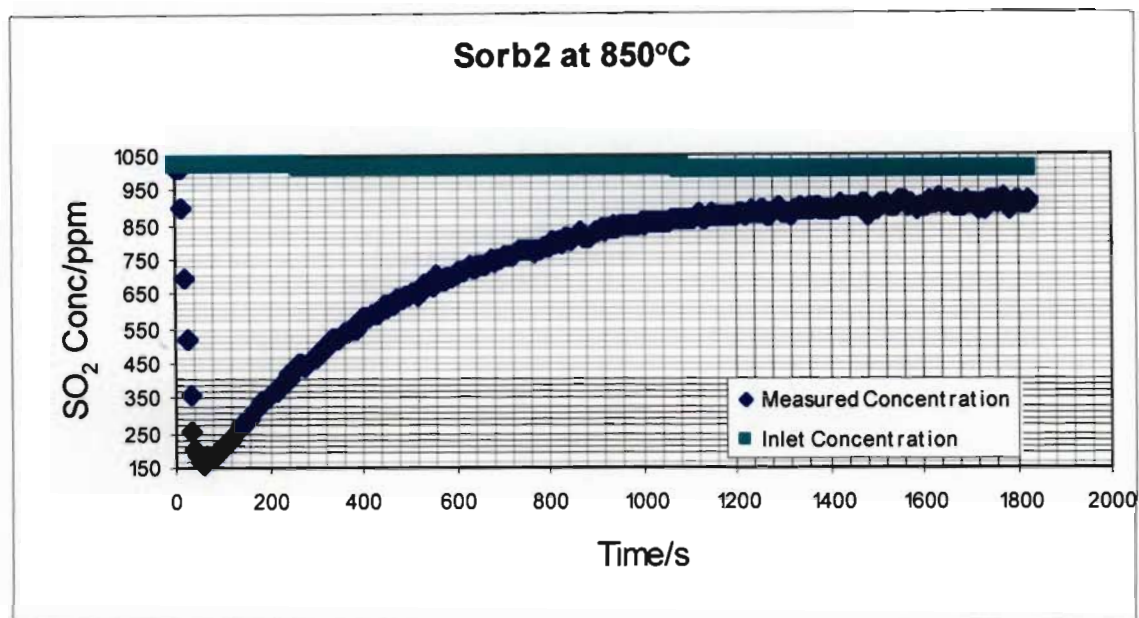
Figure G-26 Performance graph of sorbent Sorb2 of particle size 850-1000μm at 850°C
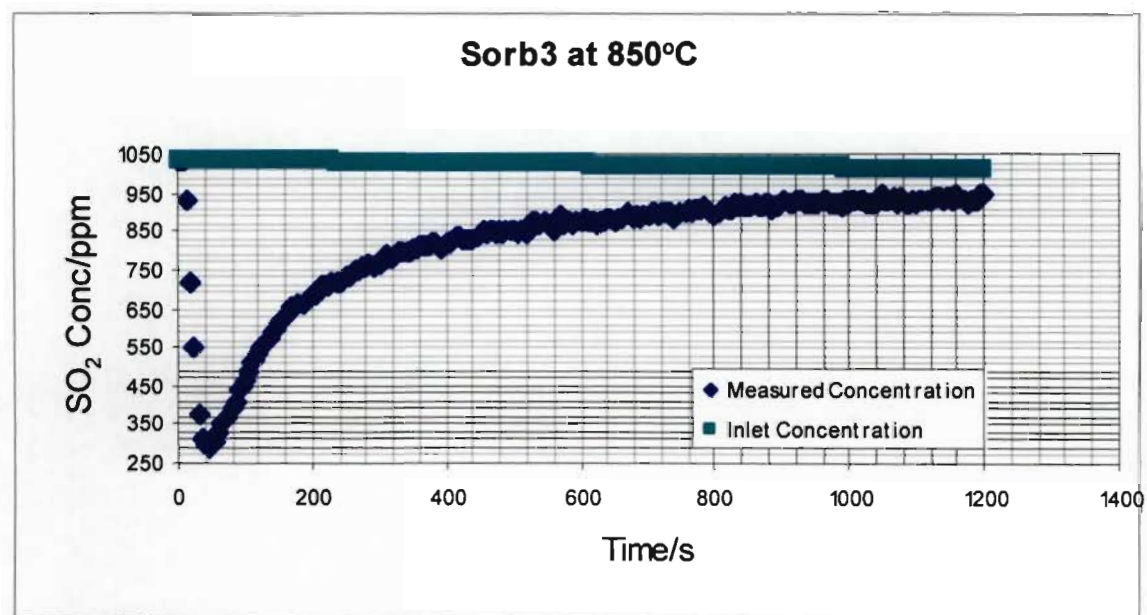
Figure G-27 Performance graph of sorbent Sorb3 of particle size 850-1000μm at 850°C
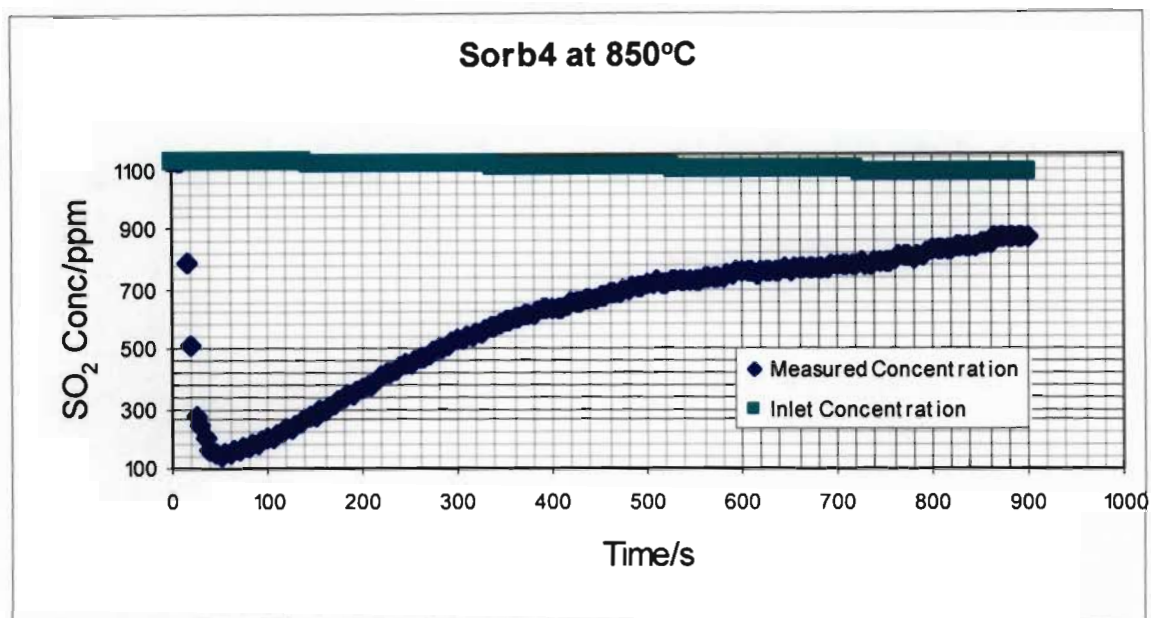
Figure G-28 Performance graph of sorbent Sorb4 of particle size 850-1000μm at 850°C
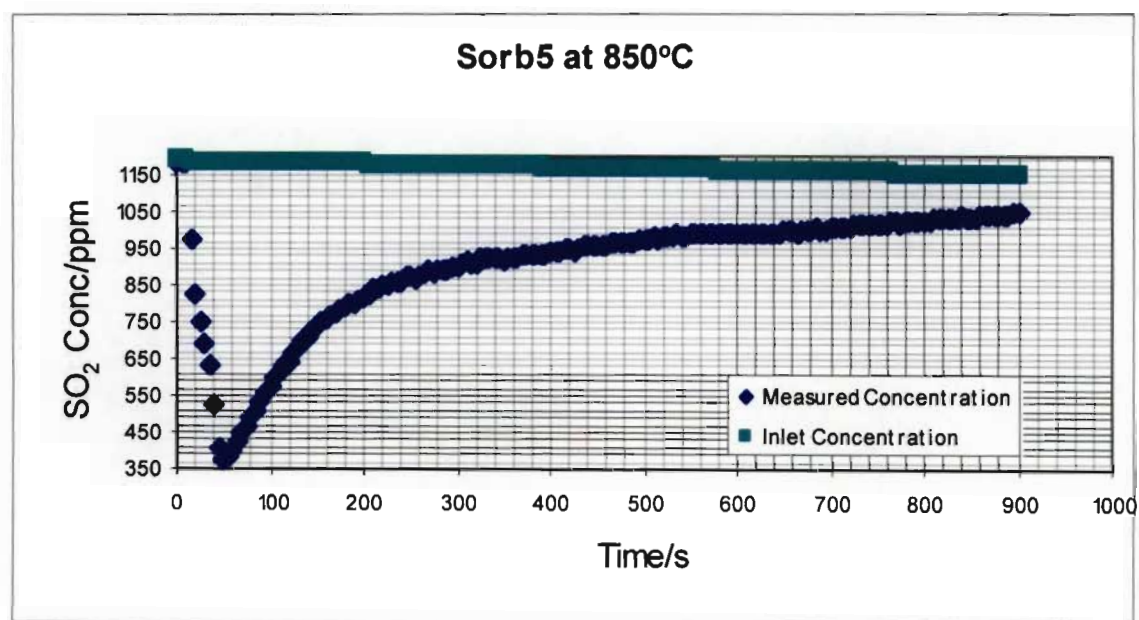
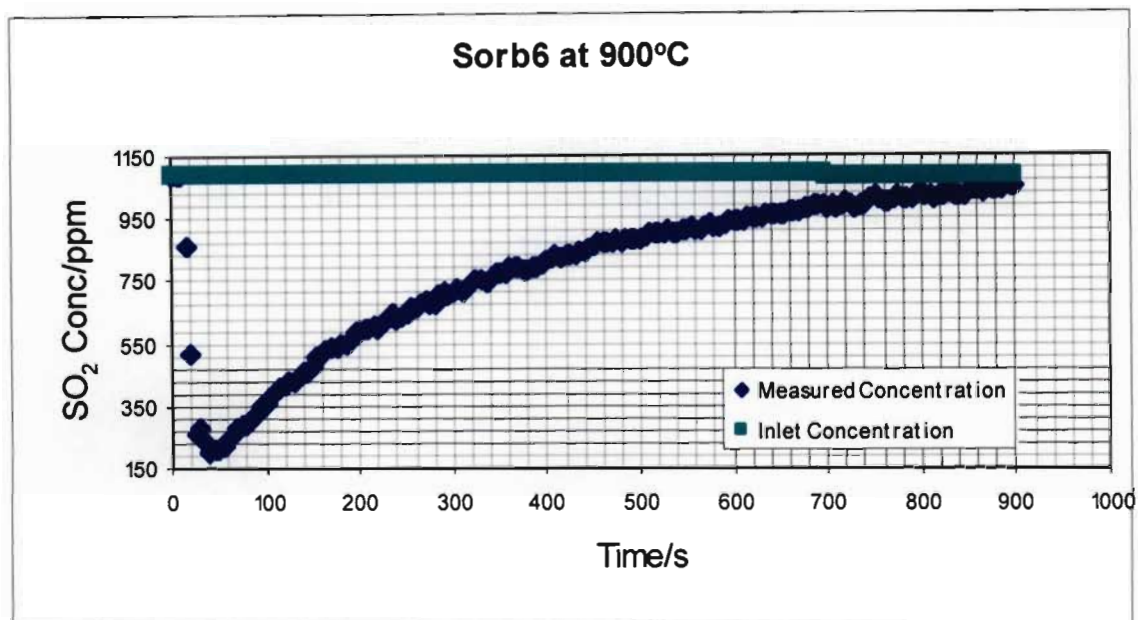Figure G-29 Performance graph of sorbent Sorb5 of particle size 850-1000μm at 850°C
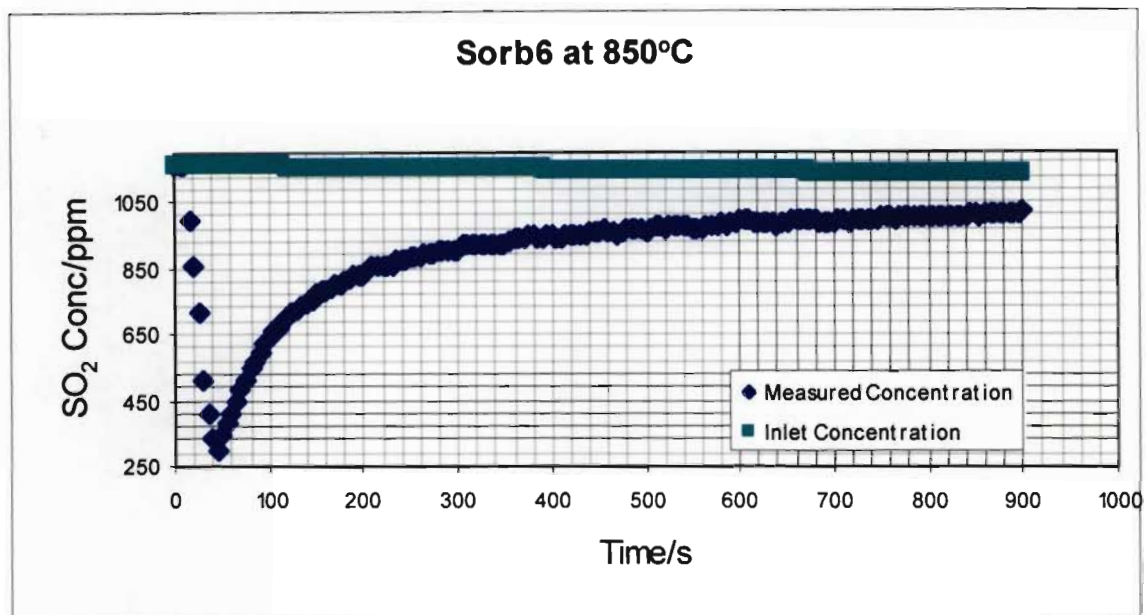
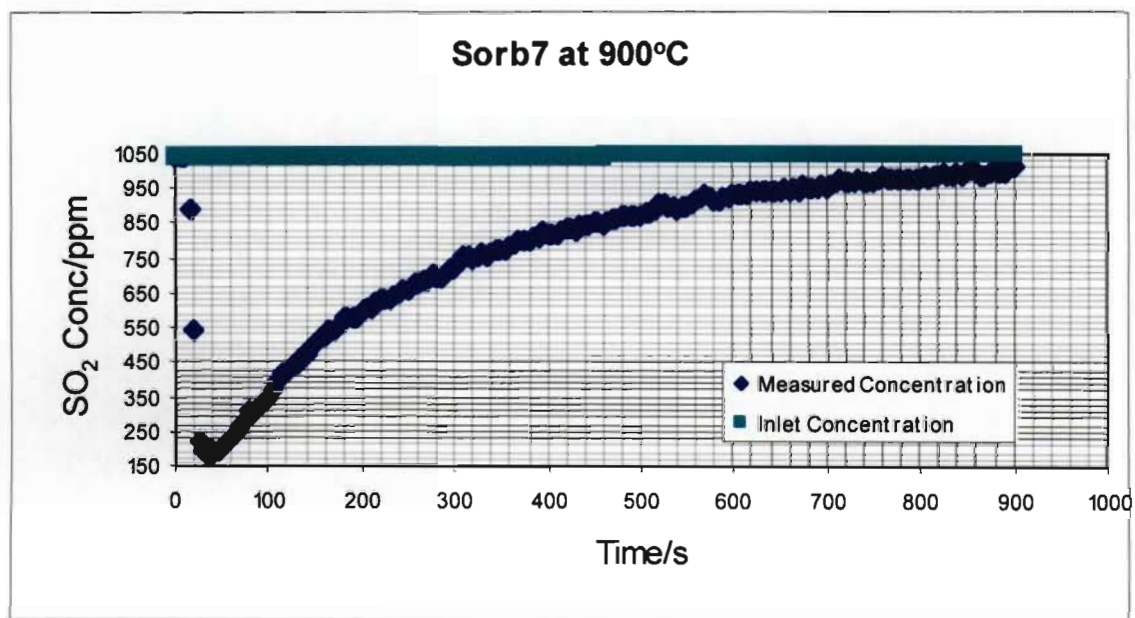Figure G-30 Performance graph of sorbent Sorb6 of particle size 850-1000μm at 850°C
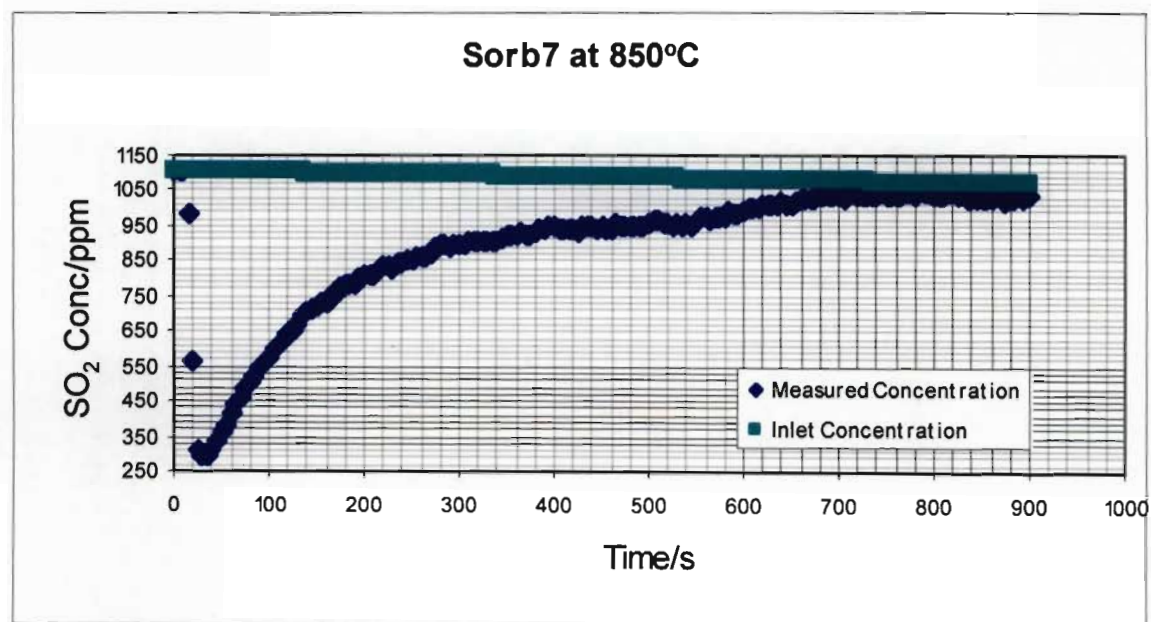
Figure G-31 Performance graph of sorbent Sorb7 of particle size 850-1000μm at 850°C
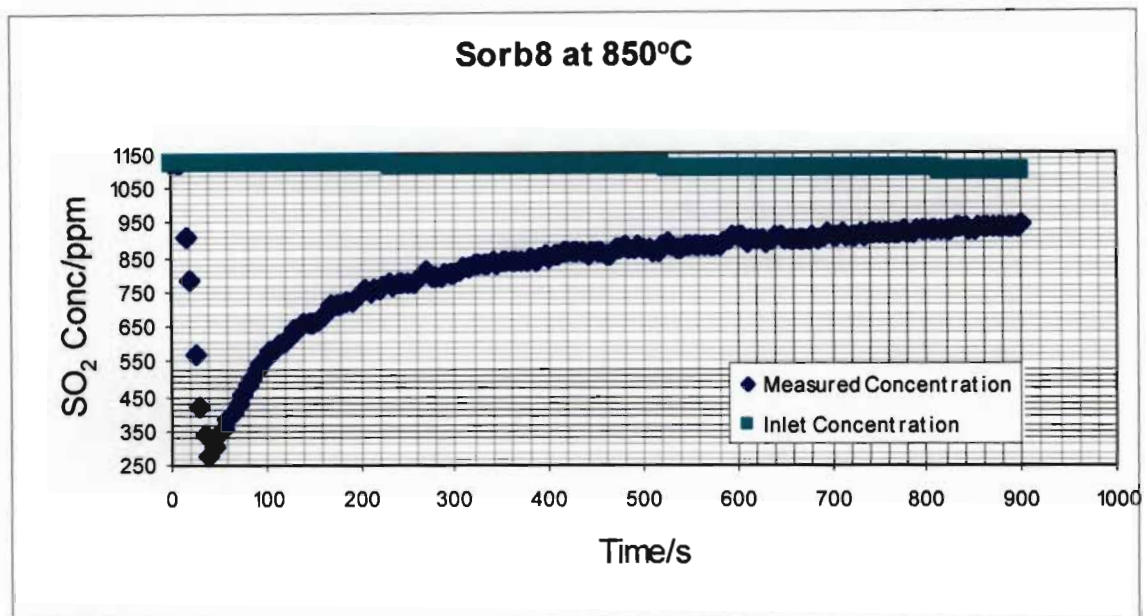
Figure G-32 Performance graph of sorbent Sorb8 of particle size 850-1000µm at 850°C

Temperature: 900°C
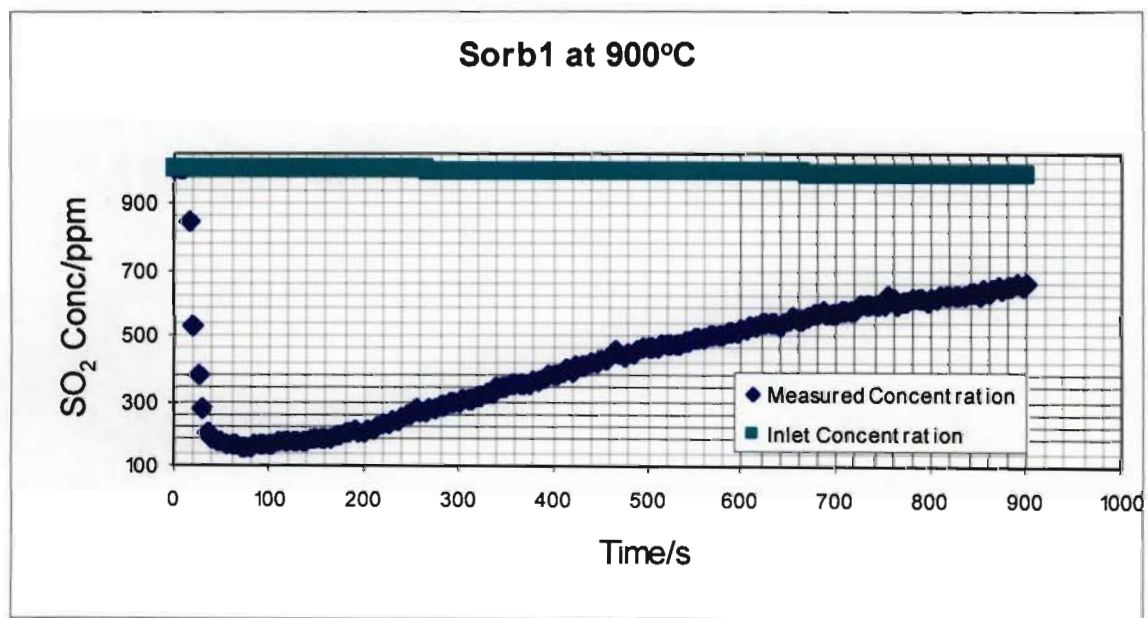
Figure G-33 Performance graph of sorbent Sorb1 of particle size 850-1000µm at 900°C
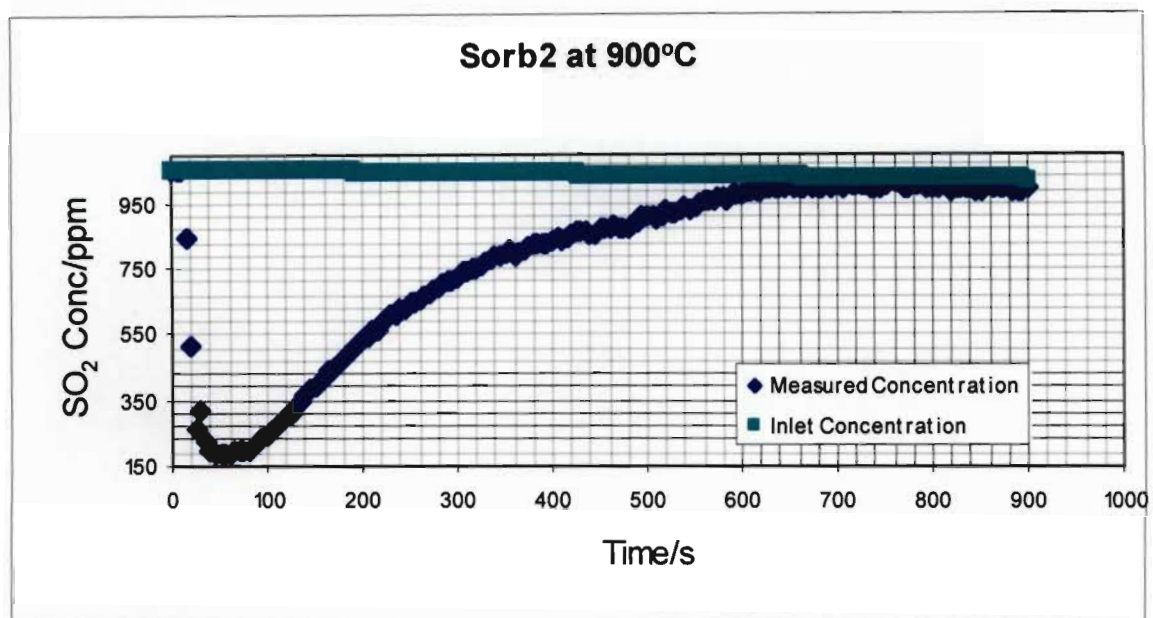
Figure G-34 Performance graph of sorbent Sorb2 of particle size 850-1000μm at 900°C
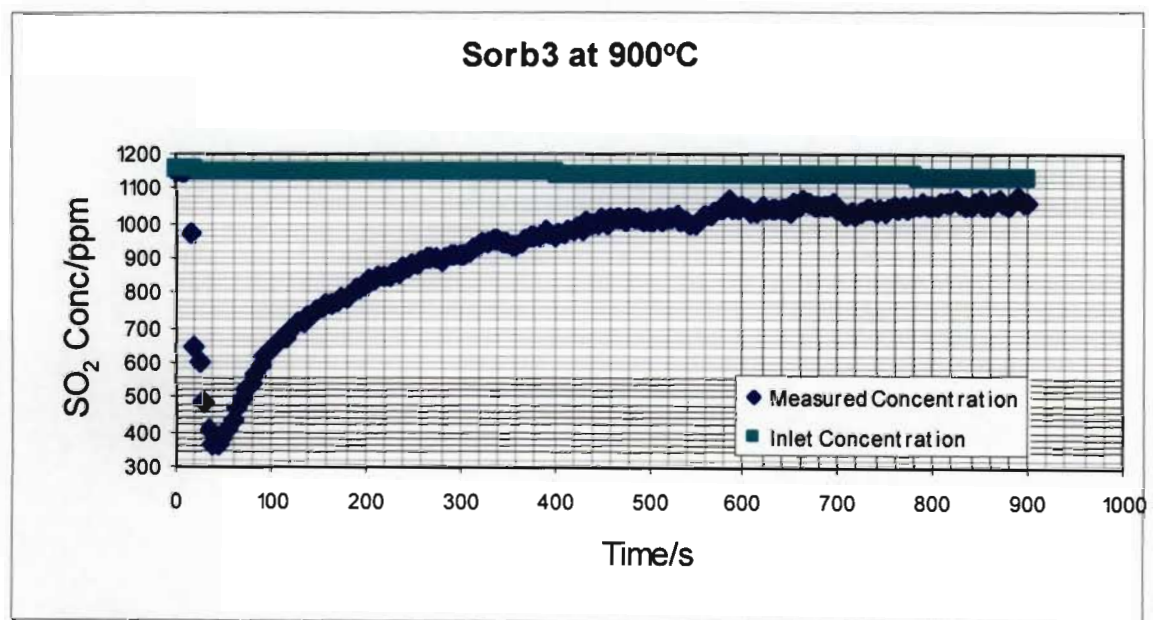
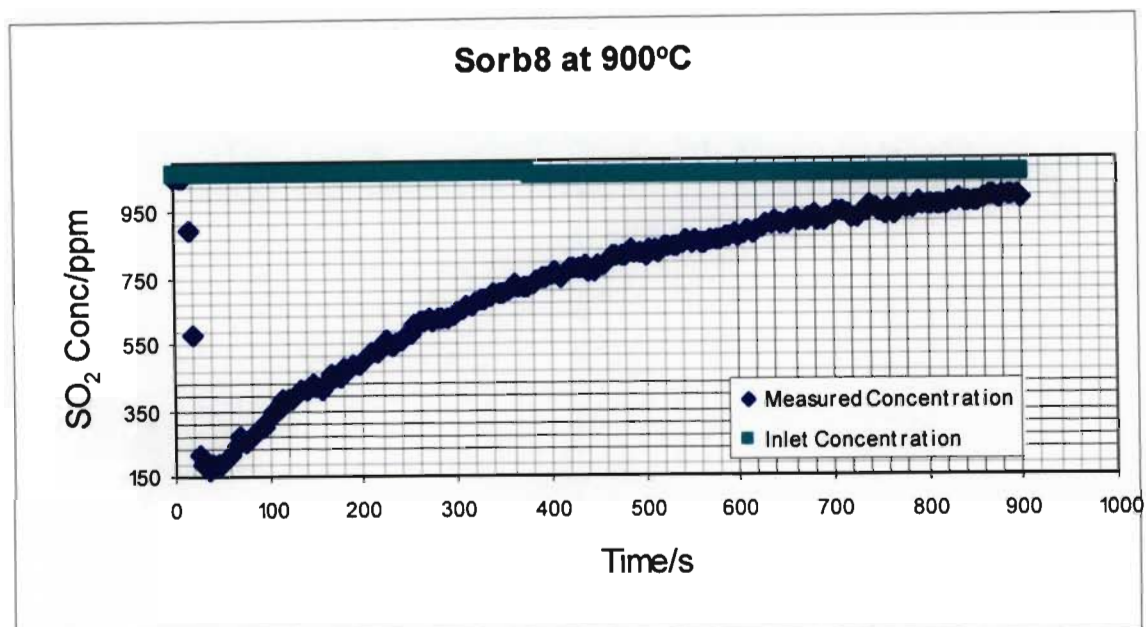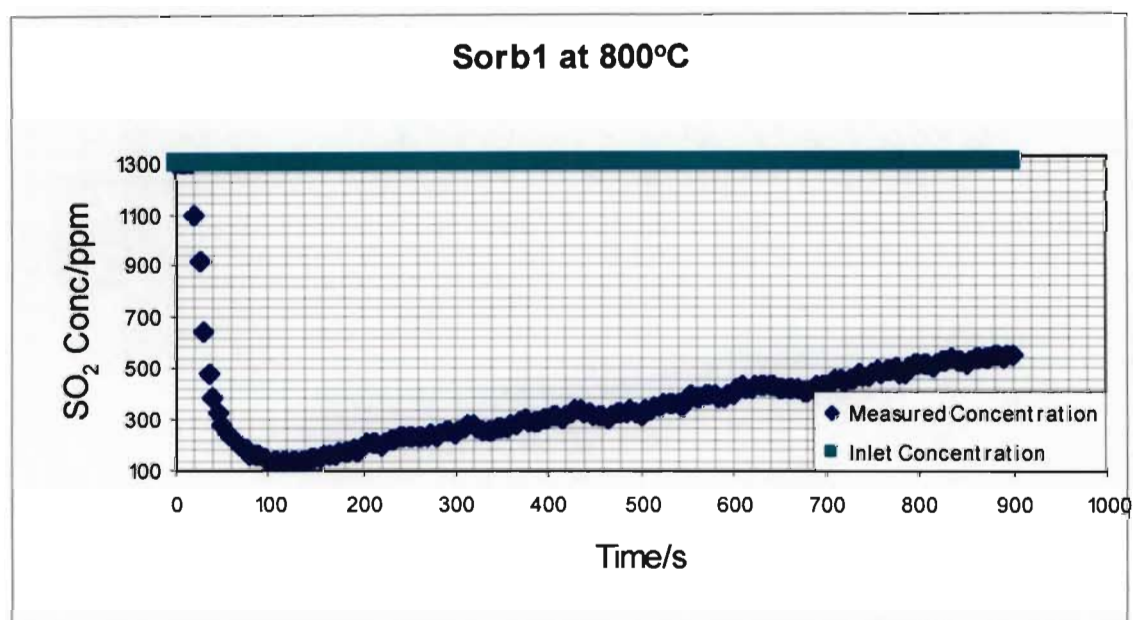Figure G-35 Performance graph of sorbent Sorb3 of particle size 850-1000μm at 900°C
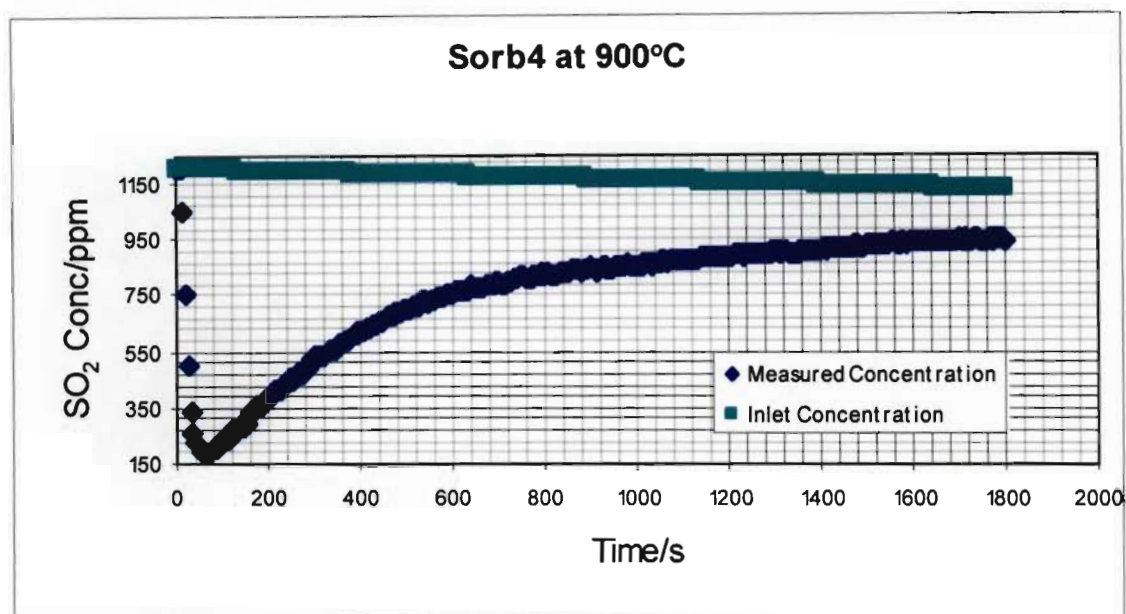
Figure G-36 Performance graph of sorbent Sorb4 of particle size 850-1000µm at 900°C
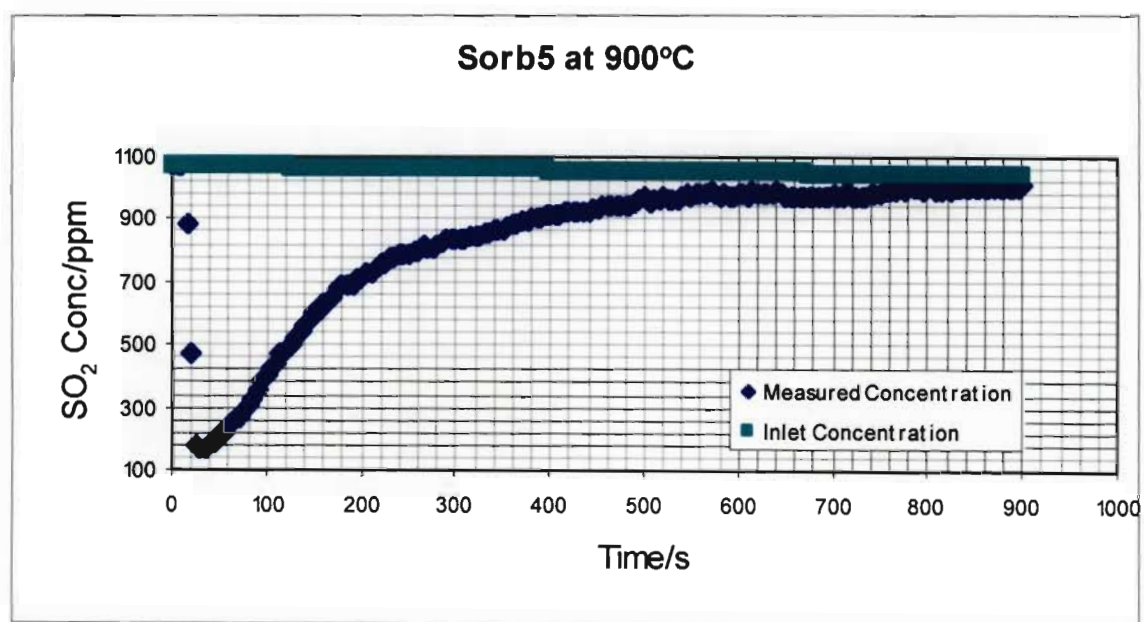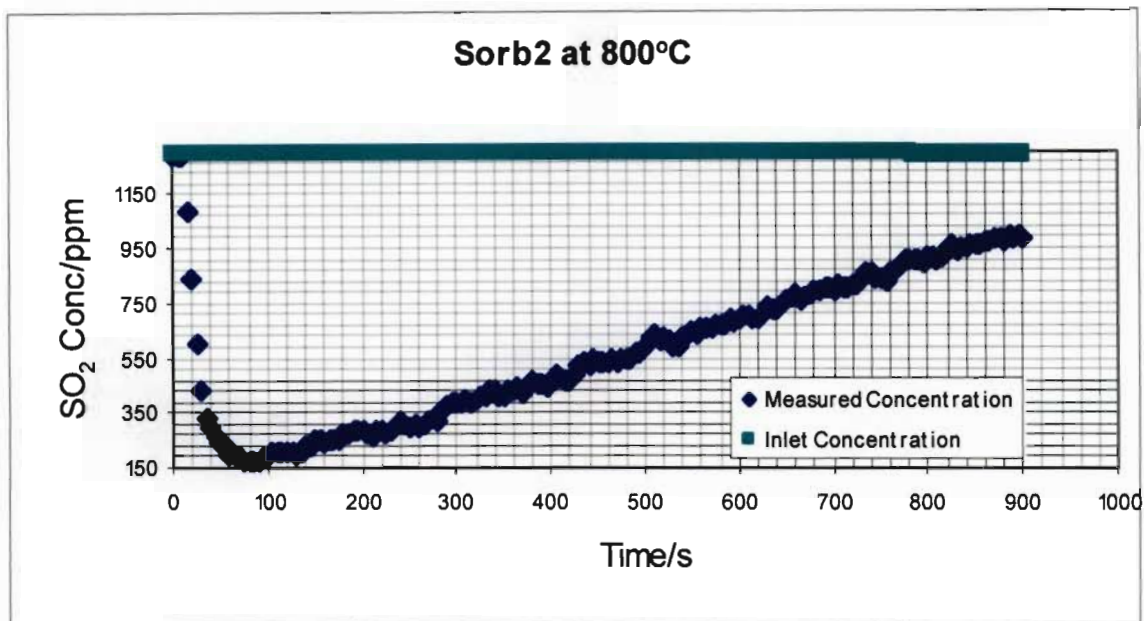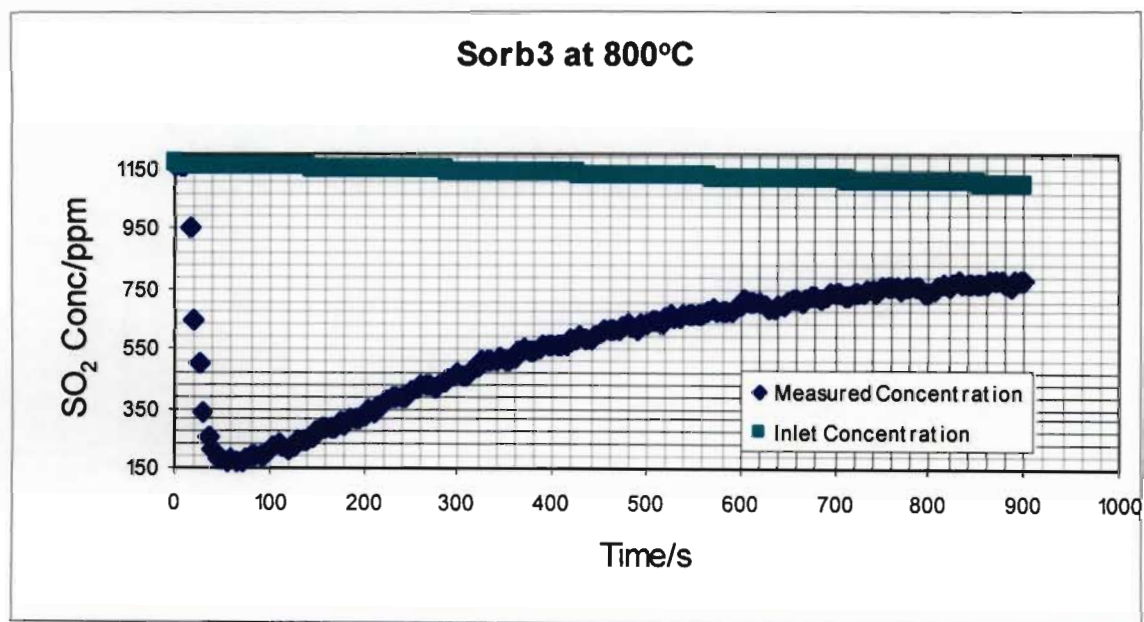

Figure G-37 Performance graph of sorbent Sorb5 of particle size 850-1000µm at 900°C
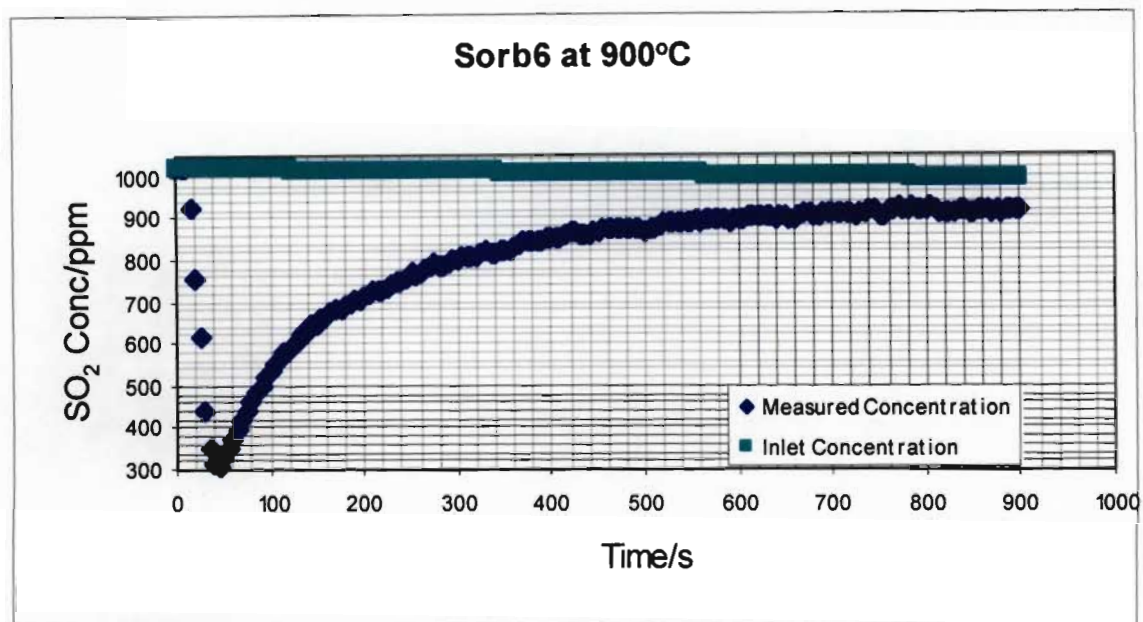
Figure G-38 Performance graph of sorbent Sorb6 of particle size 850-1000μm at 900°C
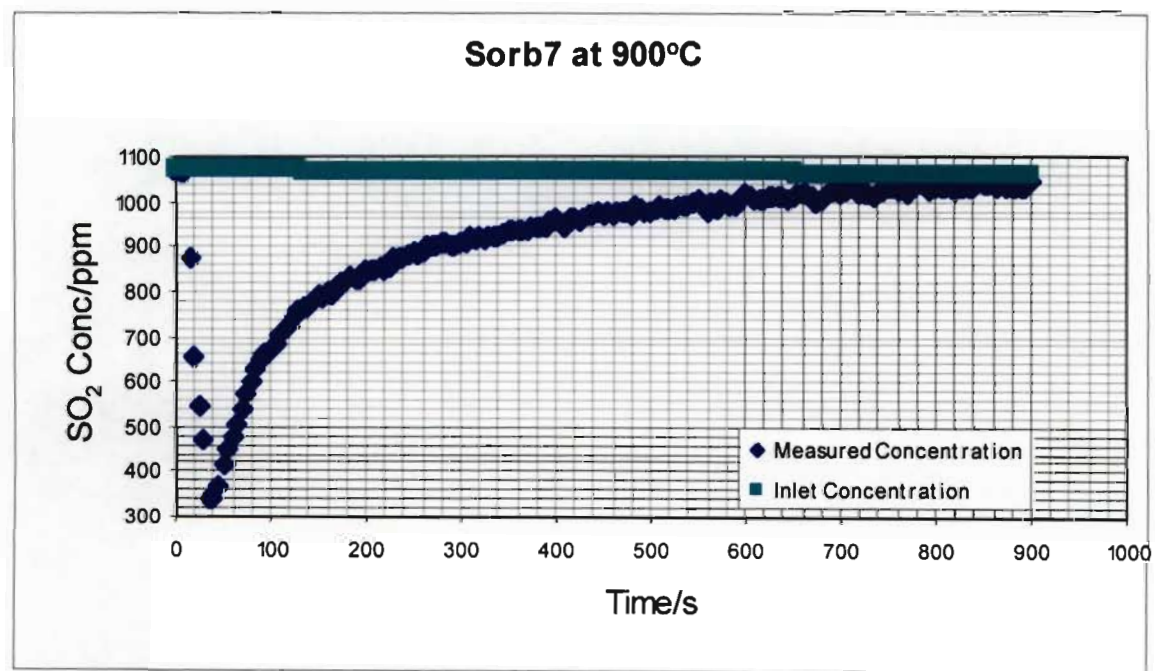
Figure G-39 Performance graph of sorbent Sorb7 of particle size 850-1000μm at 900°C
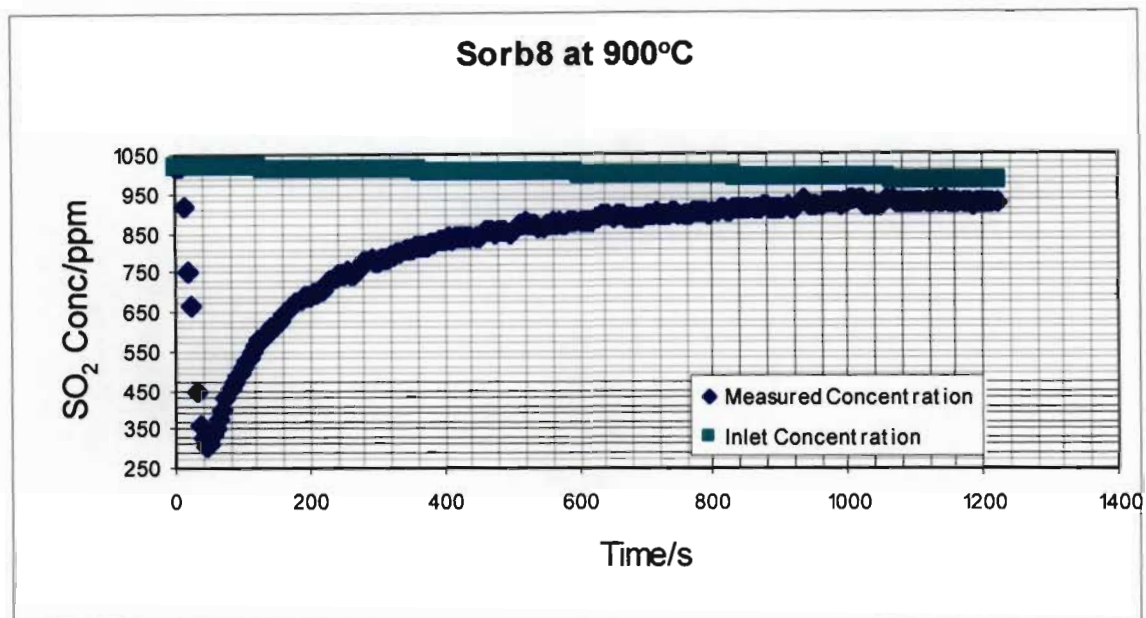
Figure G-40 Performance graph of sorbent Sorb8 of particle size 850-1000μm at 900°C

Temperature: 950°C
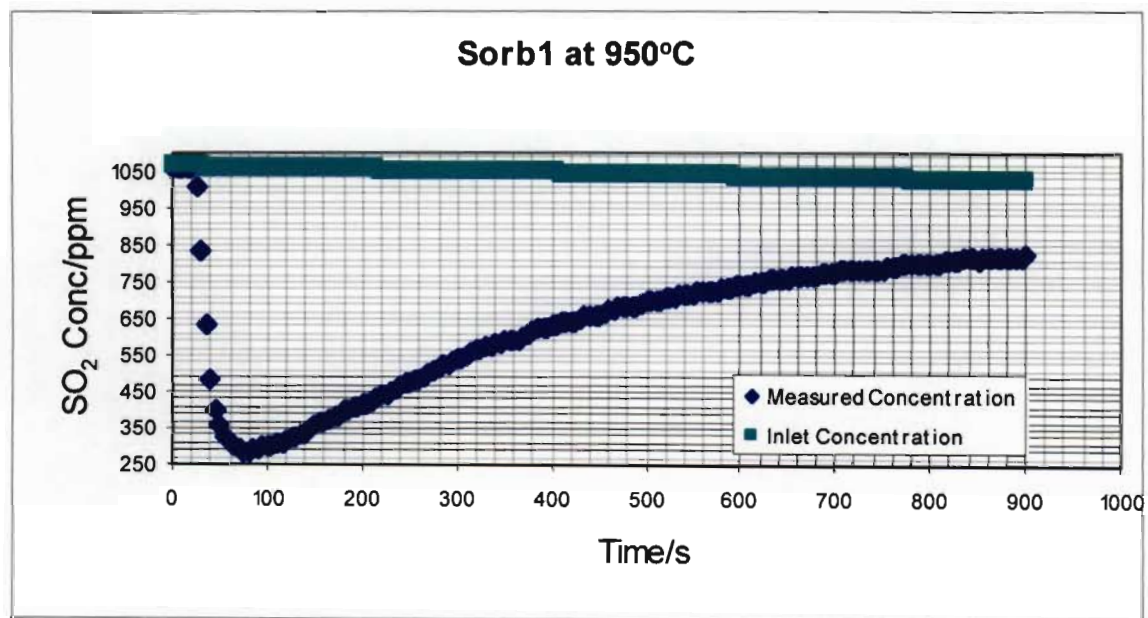
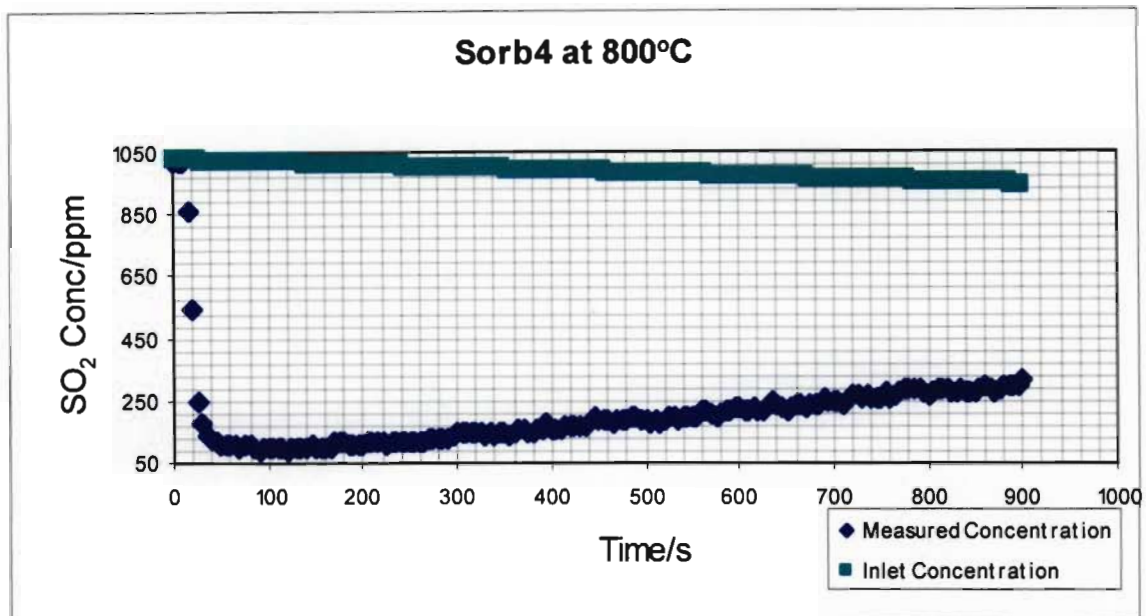Figure G-41 Performance graph of sorbent Sorb1 of particle size 850-1000μm at 950°C
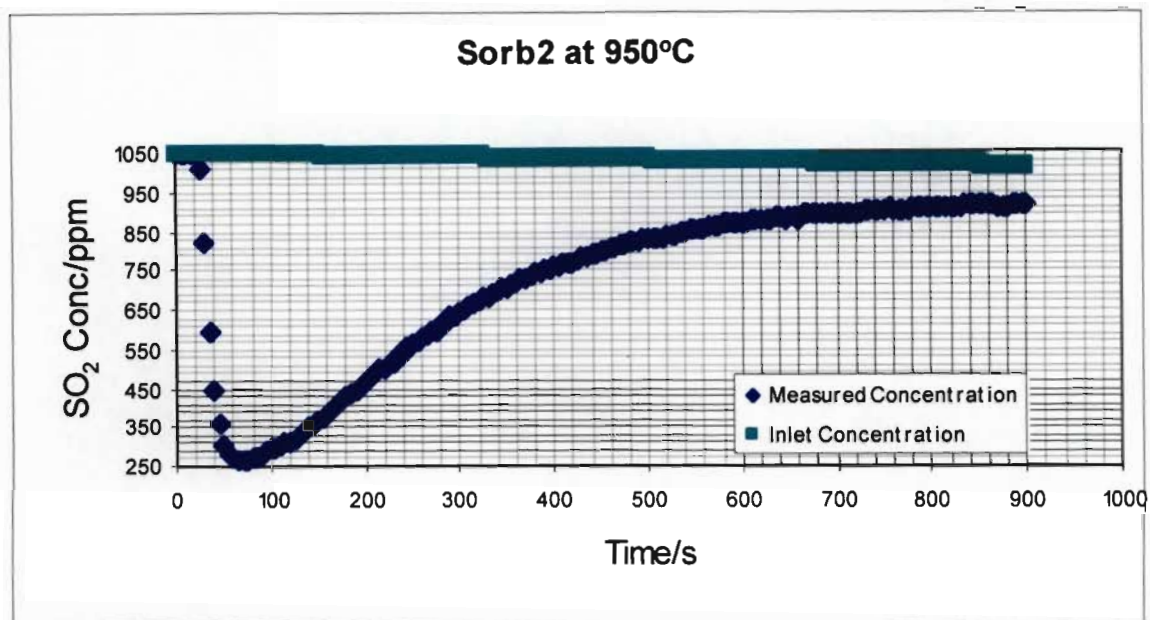
Figure G-42 Performance graph of sorbent Sorb2 of particle size 850-1000μm at 950°C
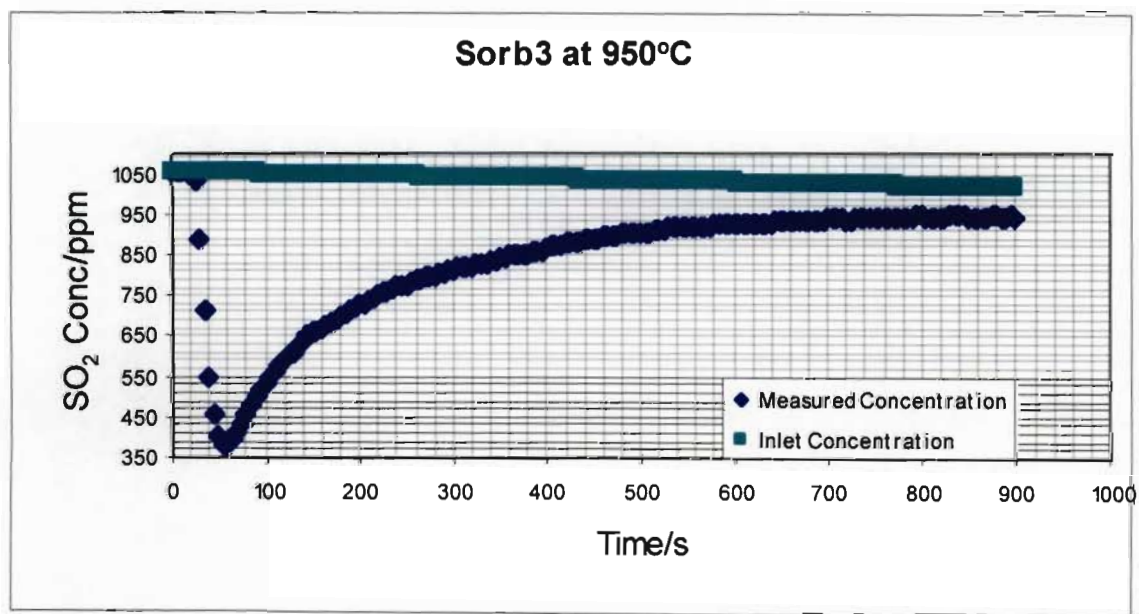
Figure G-43 Performance graph of sorbent Sorb3 of particle size 850-1000μm at 950°C
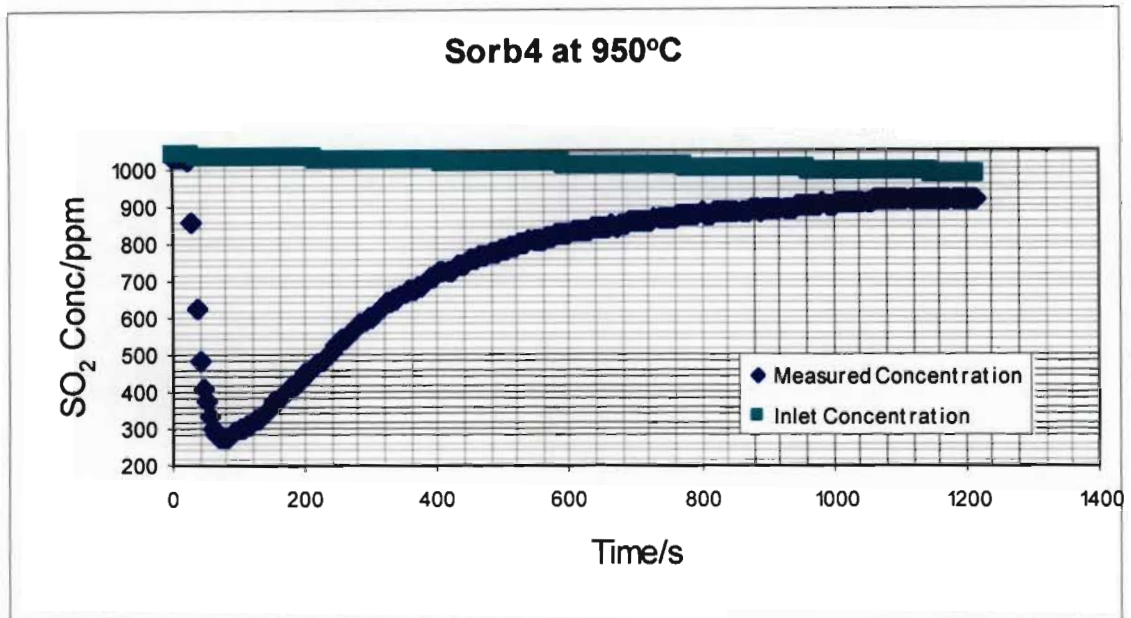
Figure G-44 Performance graph of sorbent Sorb4 of particle size 850-1000µm at 950°C
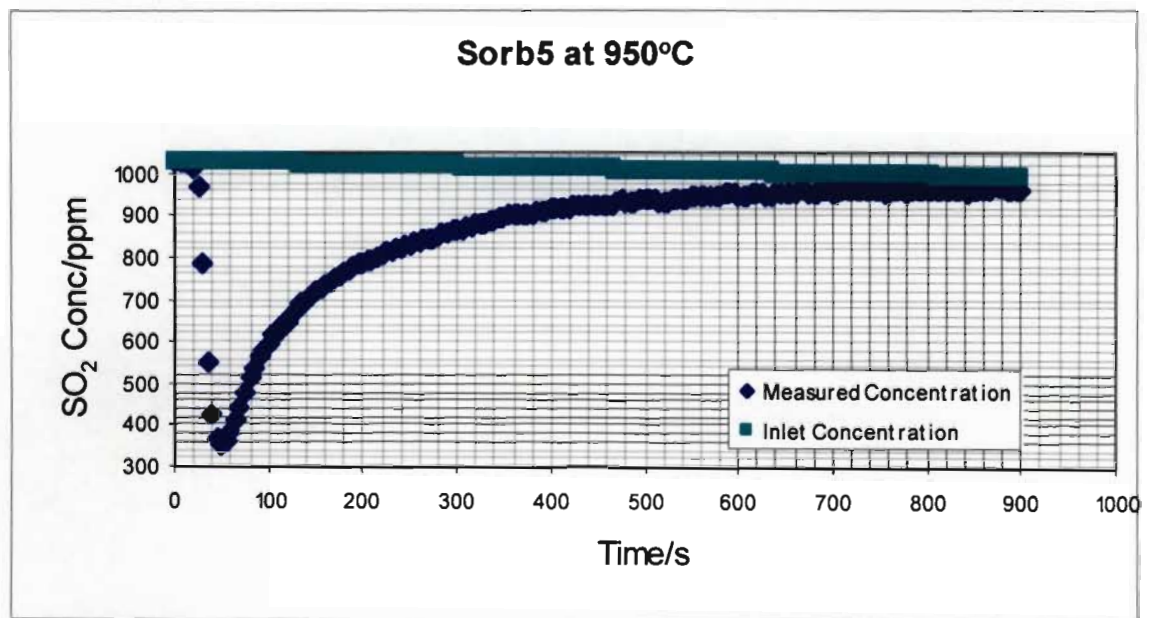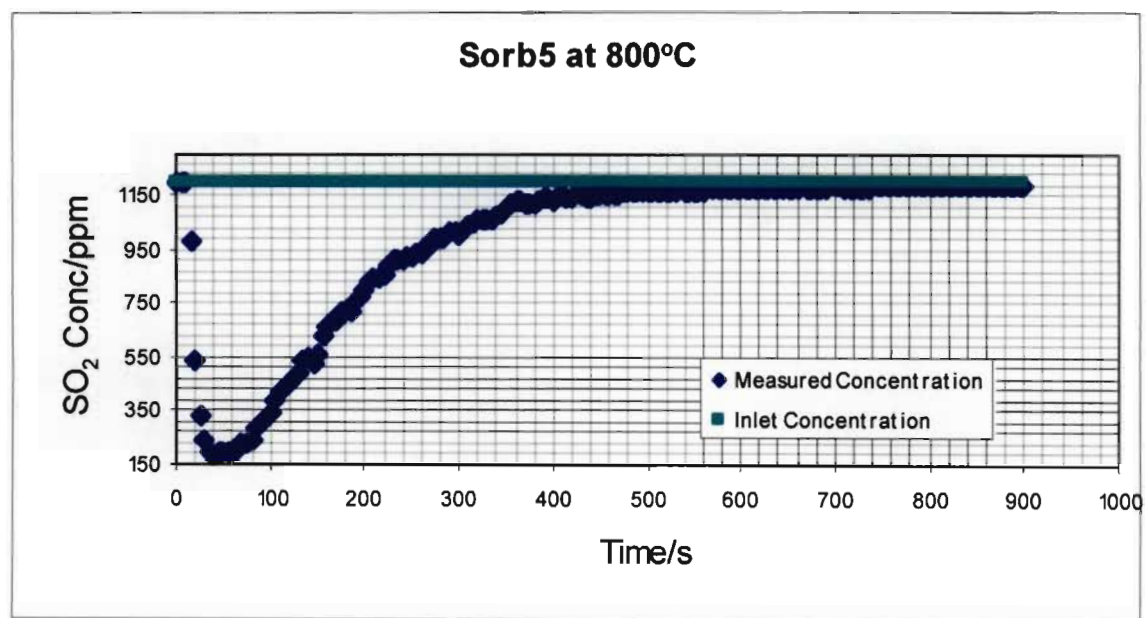

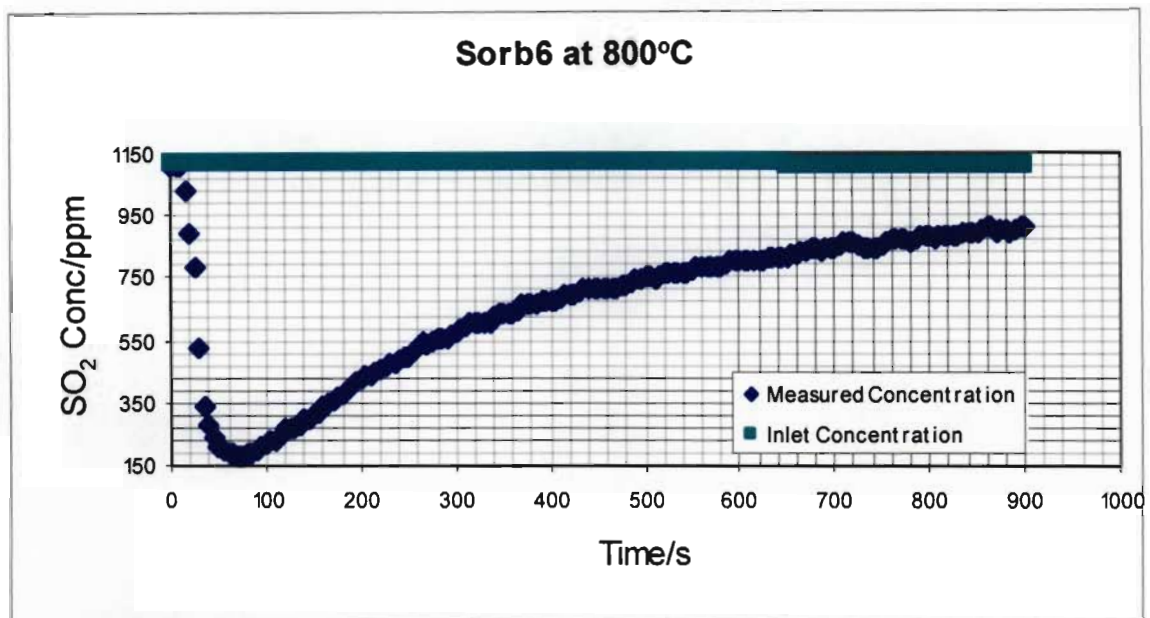Figure G-45 Performance graph of sorbent Sorb5 of particle size 850-1000µm at 950°C
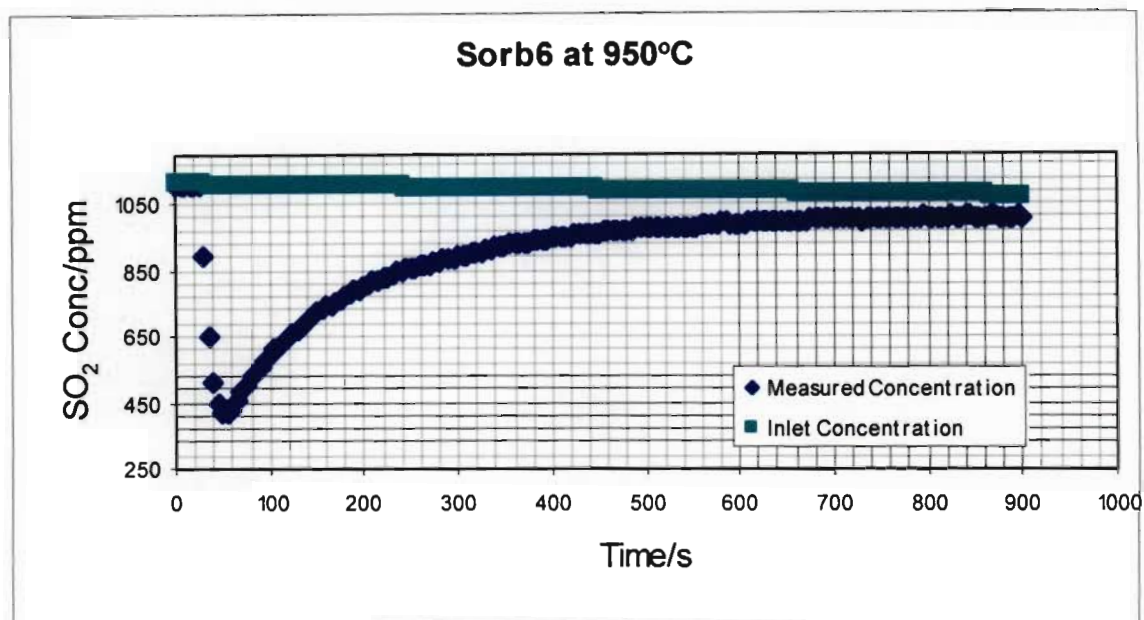
Figure G-46 Performance graph of sorbent Sorb6 of particle size 850-1000μm at 950°C
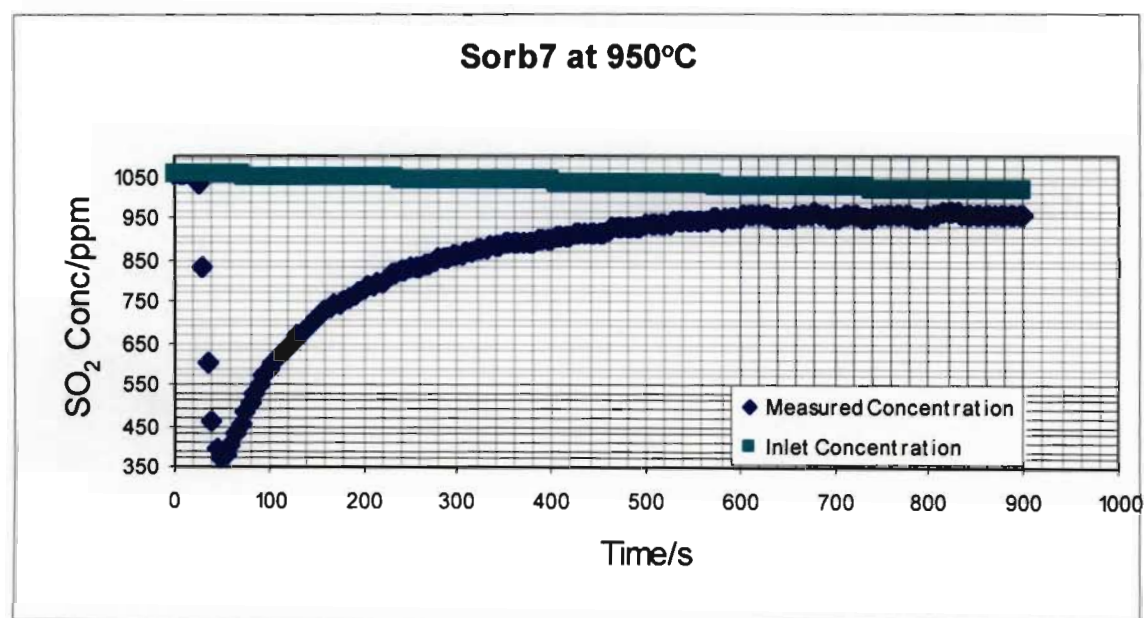
Figure G-47 Performance graph of sorbent Sorb7 of particle size 850-1000μm at 950°C

G24
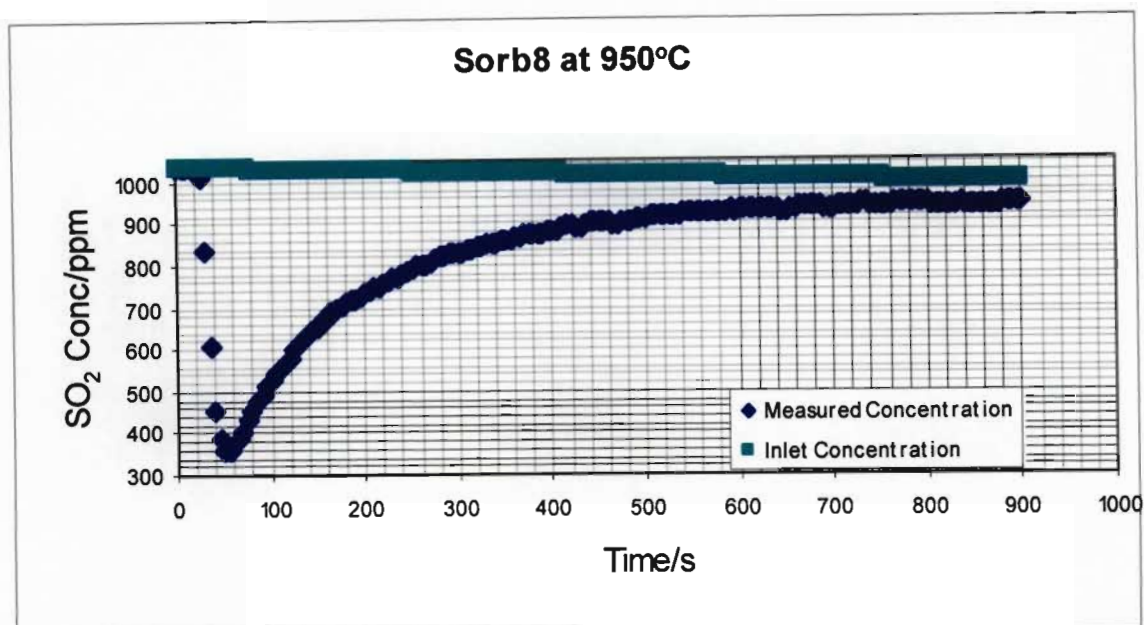
Figure G-48 Performance graph of sorbent Sorb8 of particle size 850-1000μm at 950°C

Particle Size: 600-710μm

Temperature: 800°C
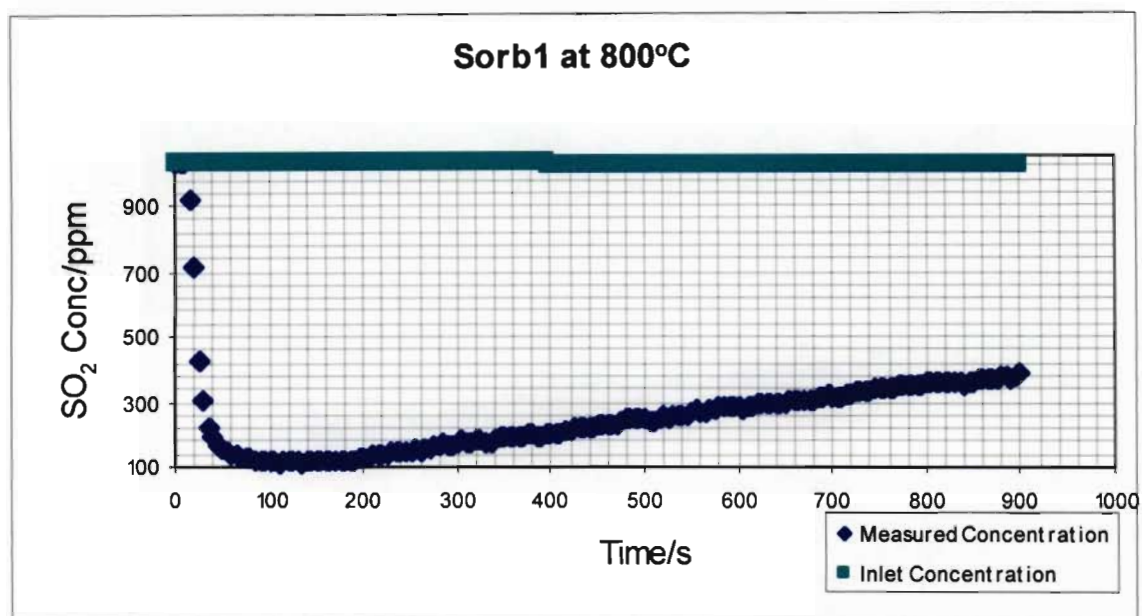
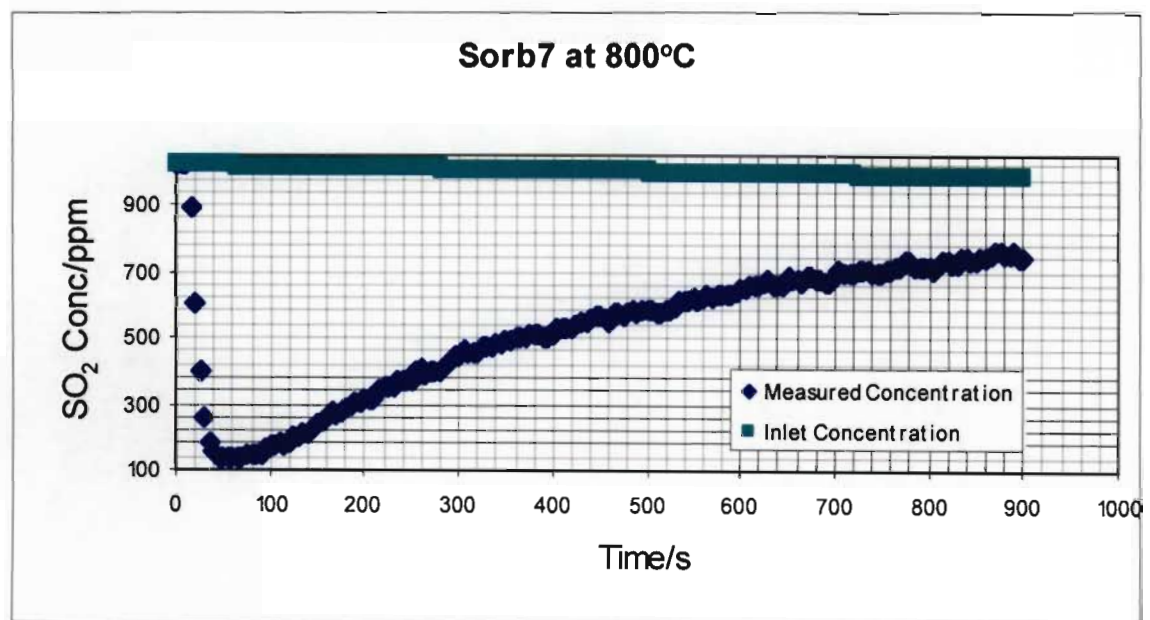Figure G-49 Performance graph of sorbent Sorb1 of particle size 600-710μm at 800°C
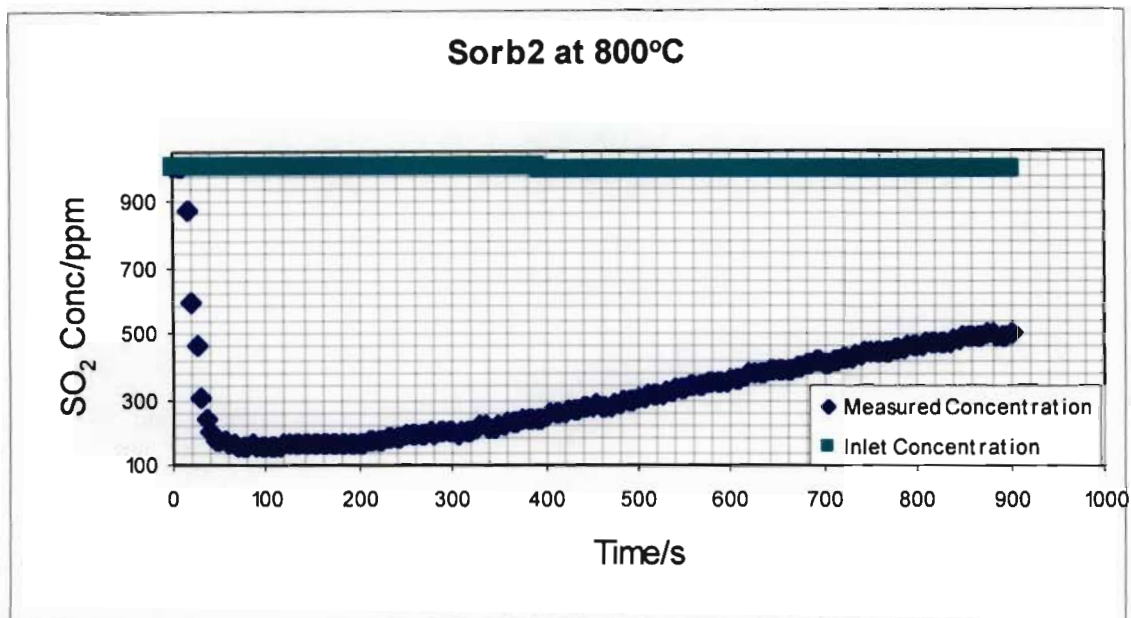
Figure G-50 Performance graph of sorbent Sorb2 of particle size 600-710μm at 800°C
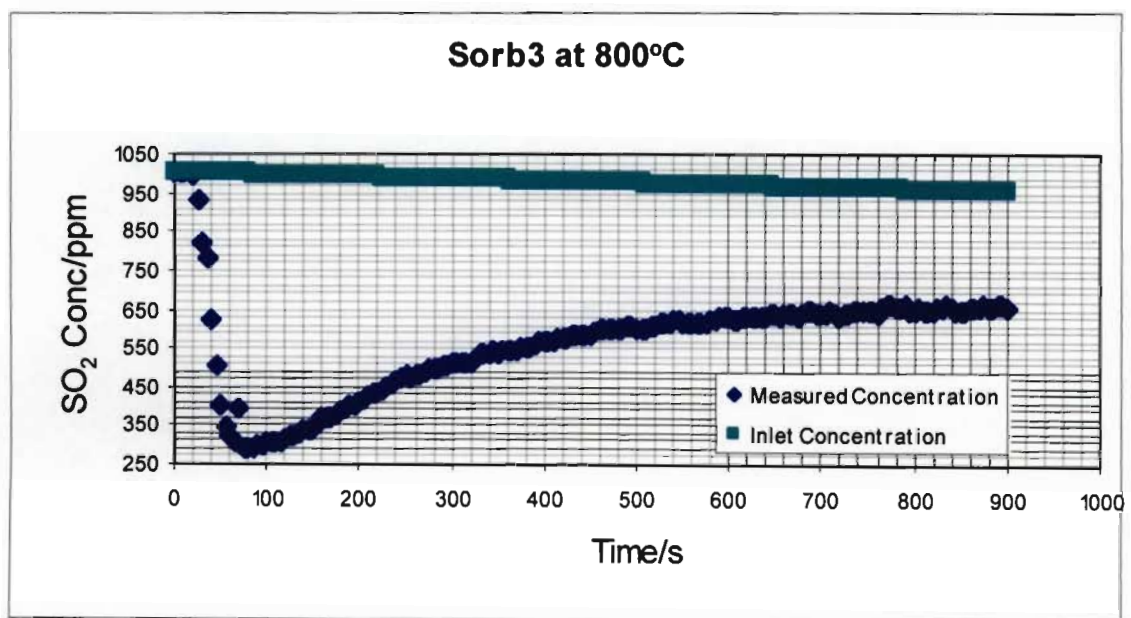
Figure G-51 Performance graph of sorbent Sorb3 of particle size 600-710μm at 800°C
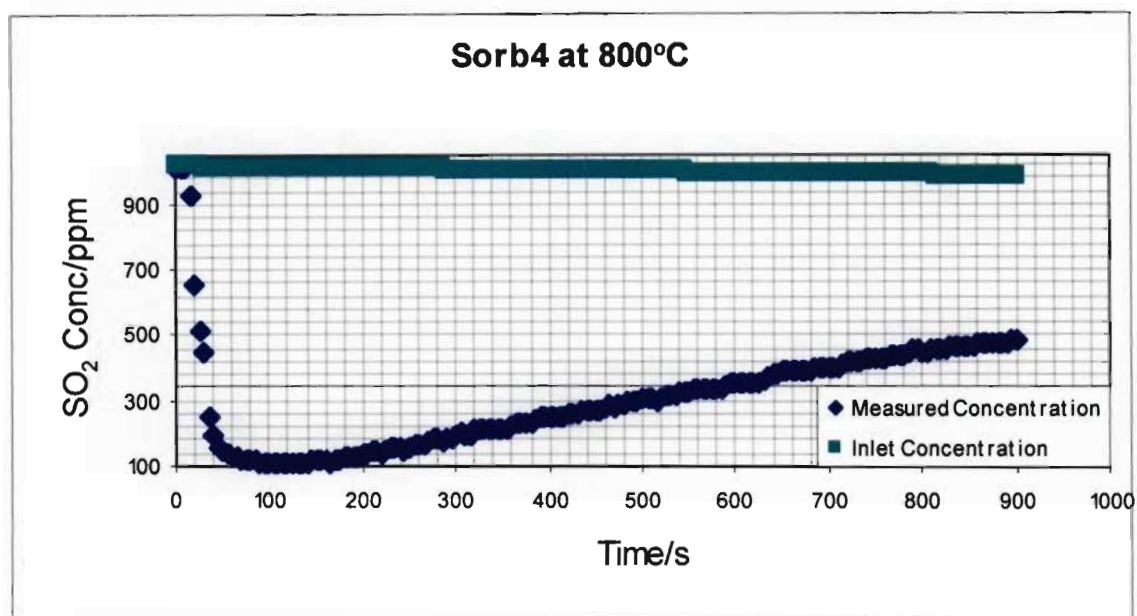
Figure G-52 Performance graph of sorbent Sorb4 of particle size 600-710μm at 800°C
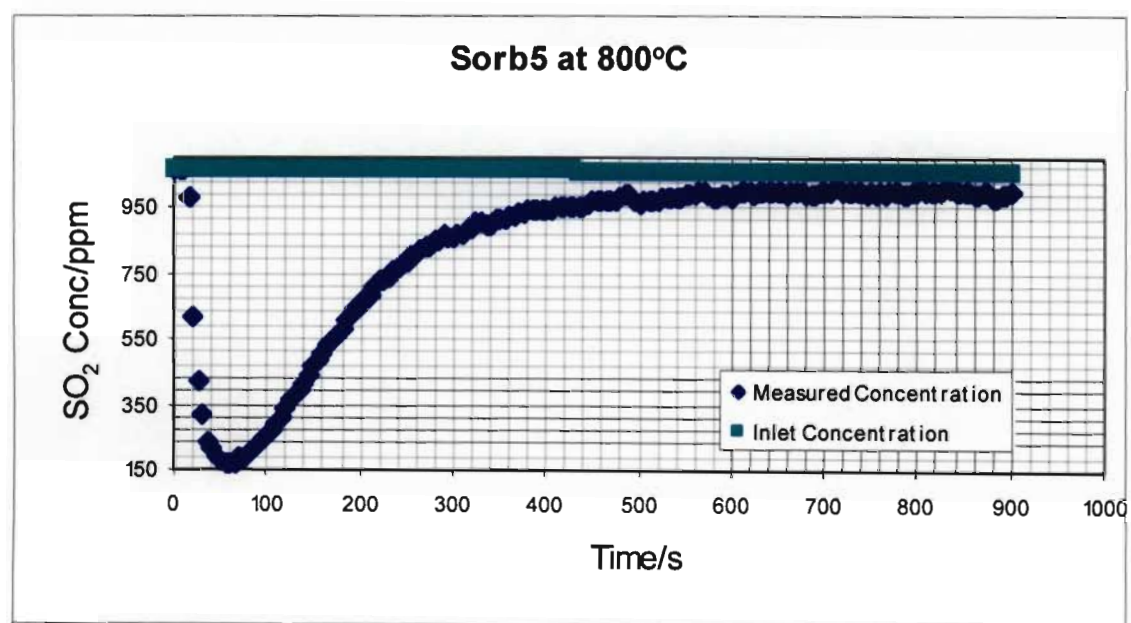
Figure G-53 Performance graph of sorbent Sorb5 of particle size 600-710μm at 800°C
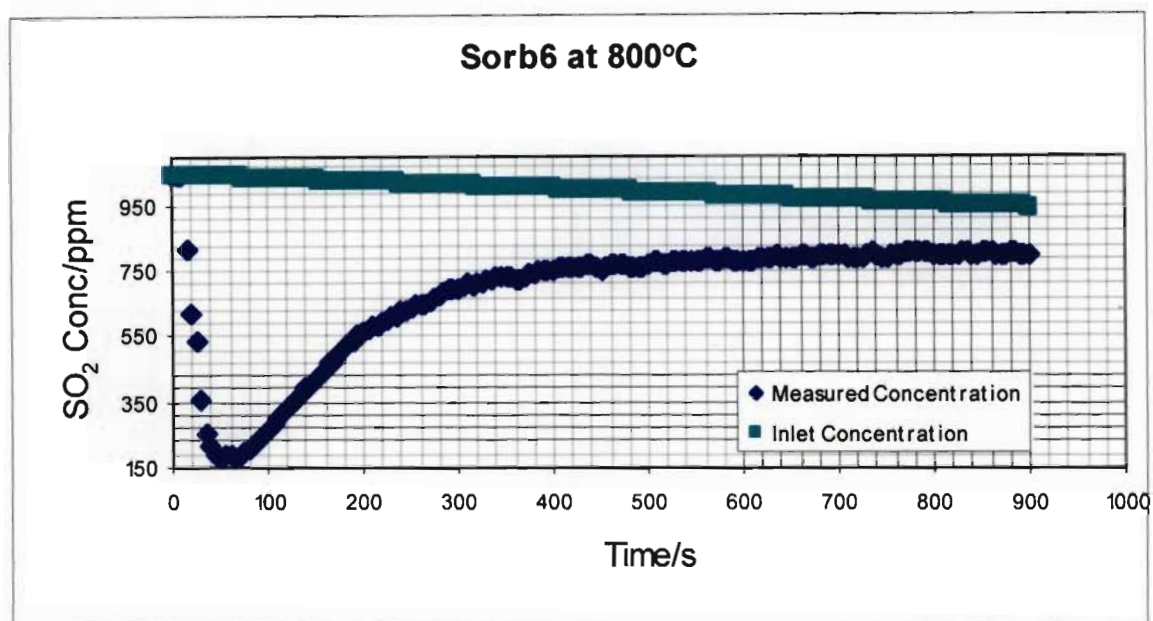
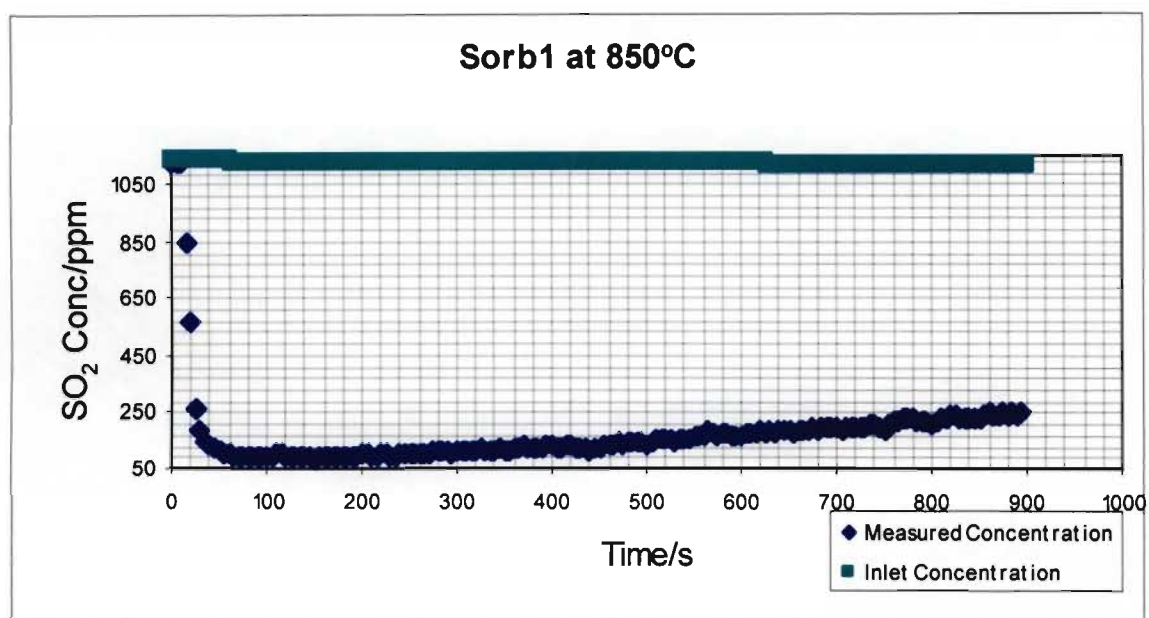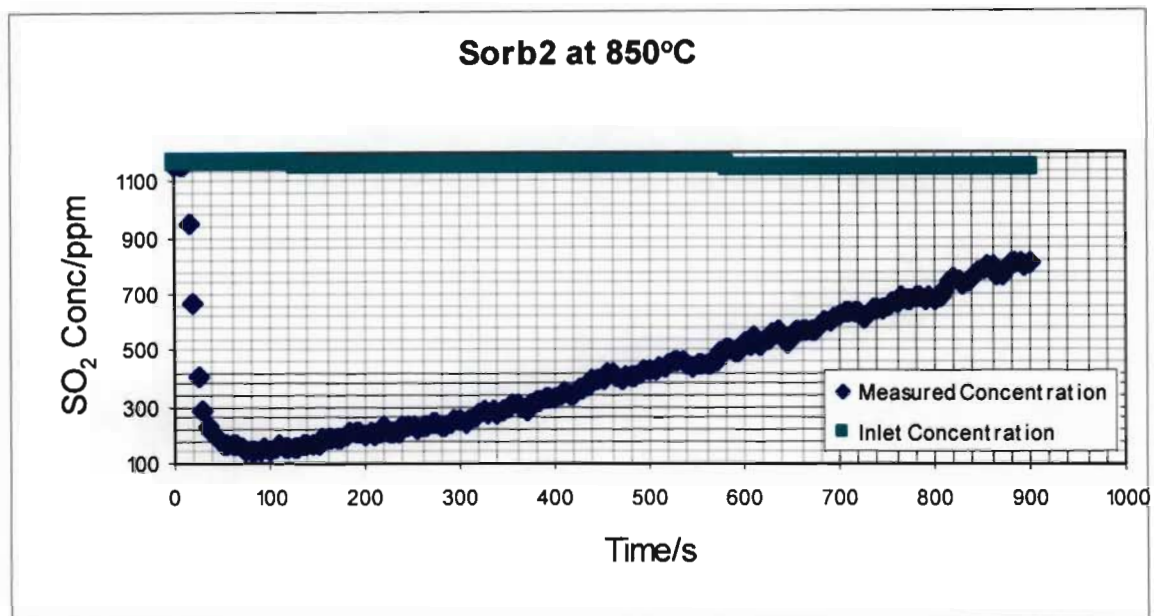Figure G-54 Performance graph of sorbent Sorb6 of particle size 600-710μm at 800°C
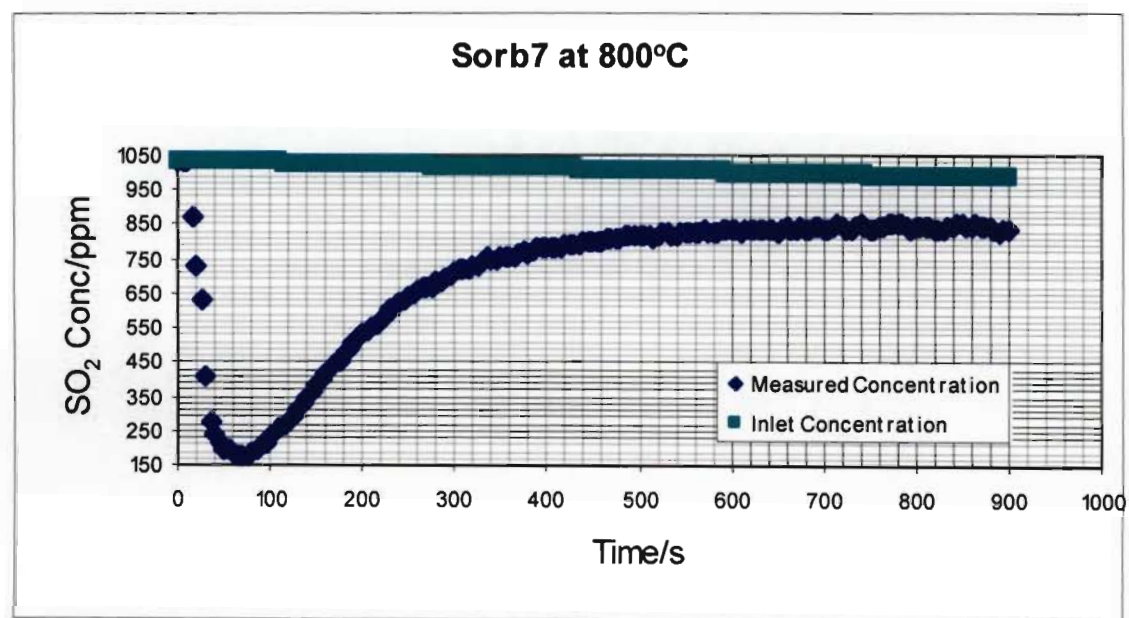
Figure G-55 Performance graph of sorbent Sorb7 of particle size 600-710μm at 800°C
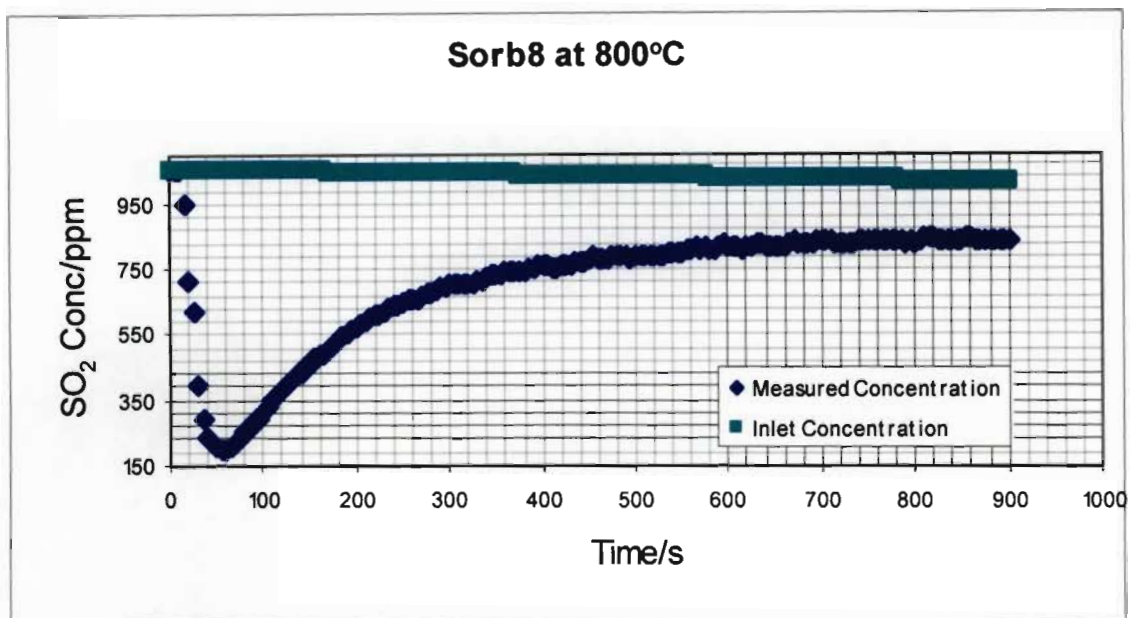
Figure G-56 Performance graph of sorbent Sorb8 of particle size 600-710μm at 800°C

Temperature: 850°C

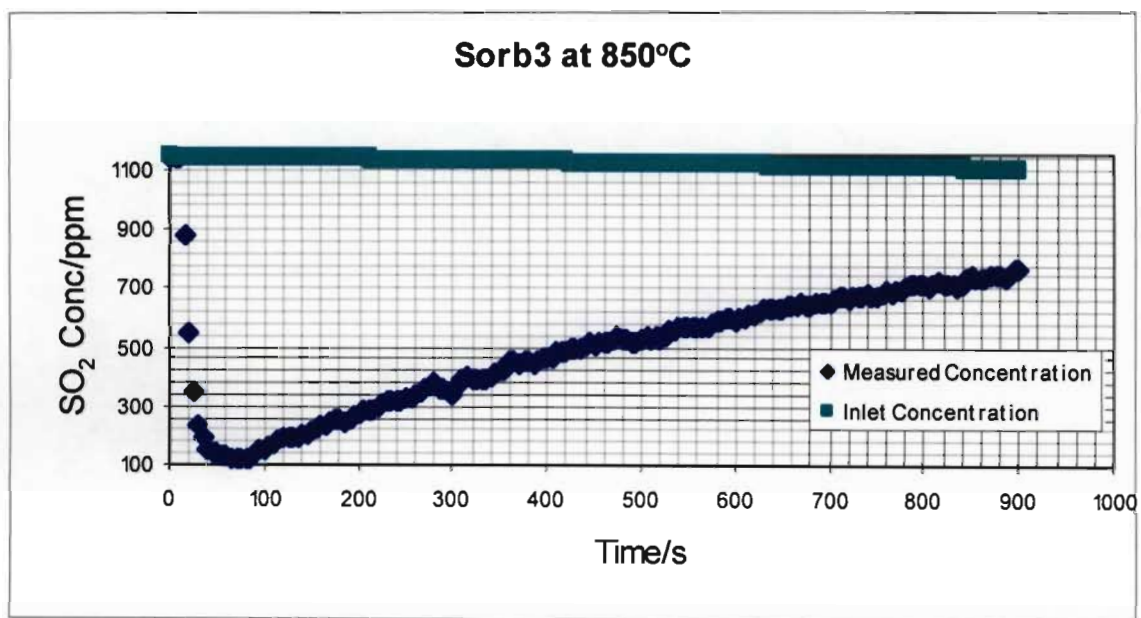Figure G-57 Performance graph of sorbent Sorb1 of particle size 600-710μm at 850°C

Figure G-58 Performance graph of sorbent Sorb2 of particle size 600-710μm at 850°C

Figure G-59 Performance graph of sorbent Sorb3 of particle size 600-710μm at 850°C

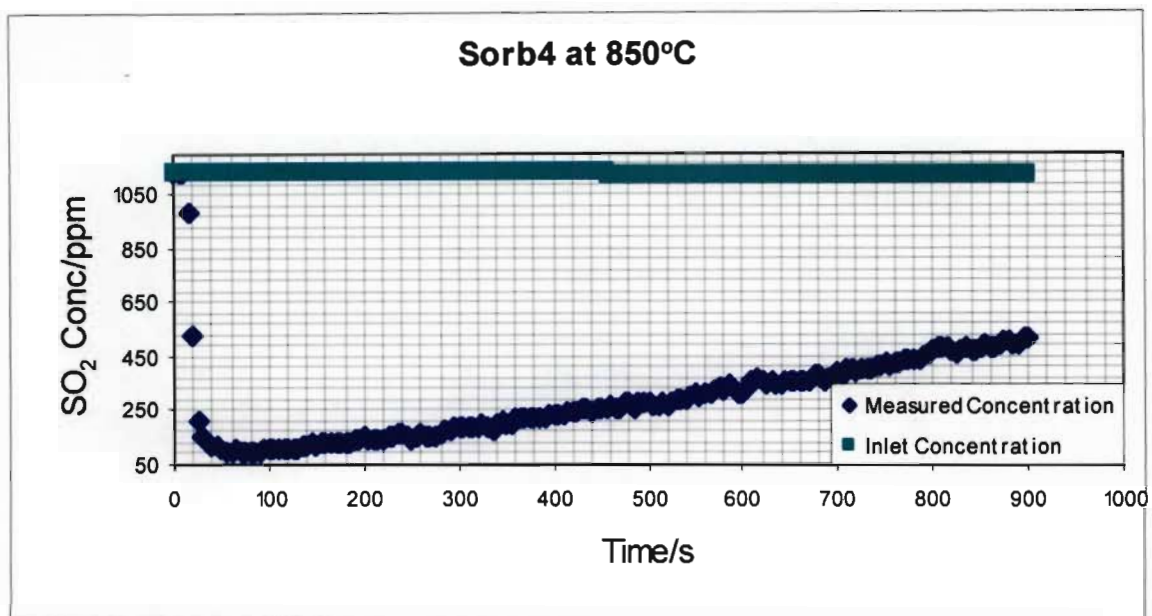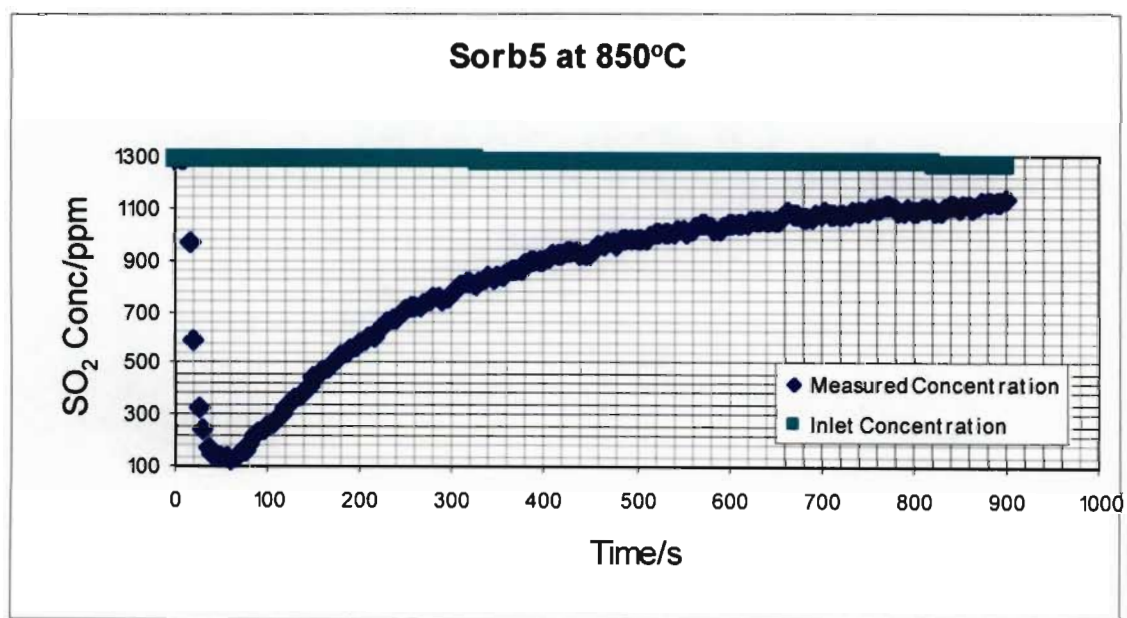Figure G-60 Performance graph of sorbent Sorb4 of particle size 600-710μm at 850°C

Figure G-61 Performance graph of sorbent Sorb5 of particle size 600-710μm at 850°C
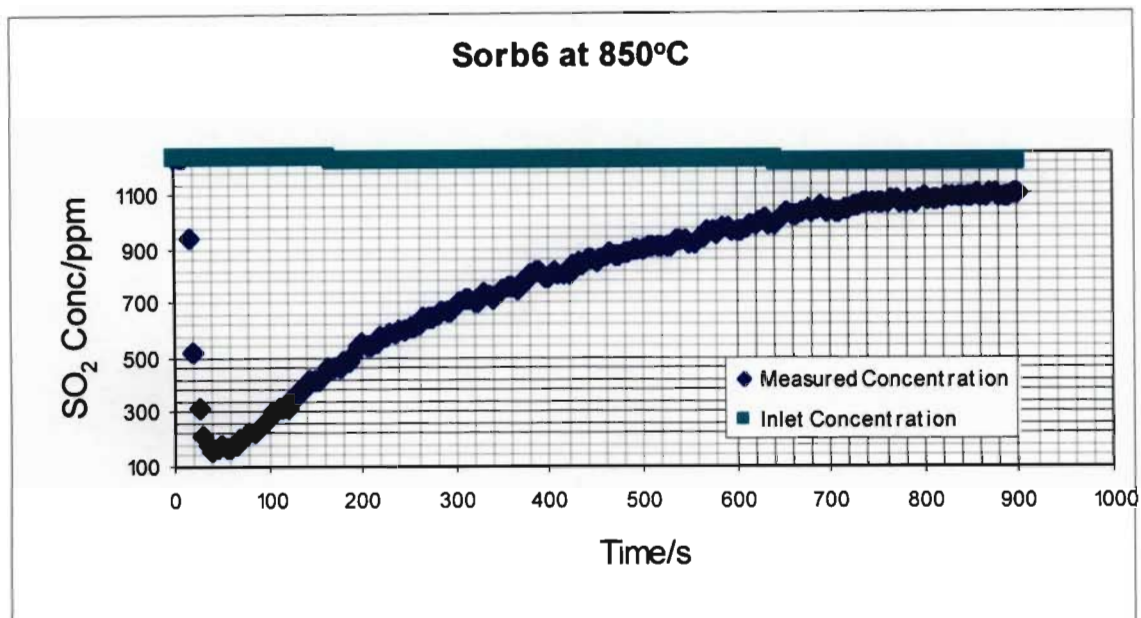
Figure G-62 Performance graph of sorbent Sorb6 of particle size 600-710µm at 850°C

Figure G-63 Performance graph of sorbent Sorb7 of particle size 600-710µm at 850°C

Figure G-64 Performance graph of sorbent Sorb8 of particle size 600-710μm at 850°C

Temperature: 900°C

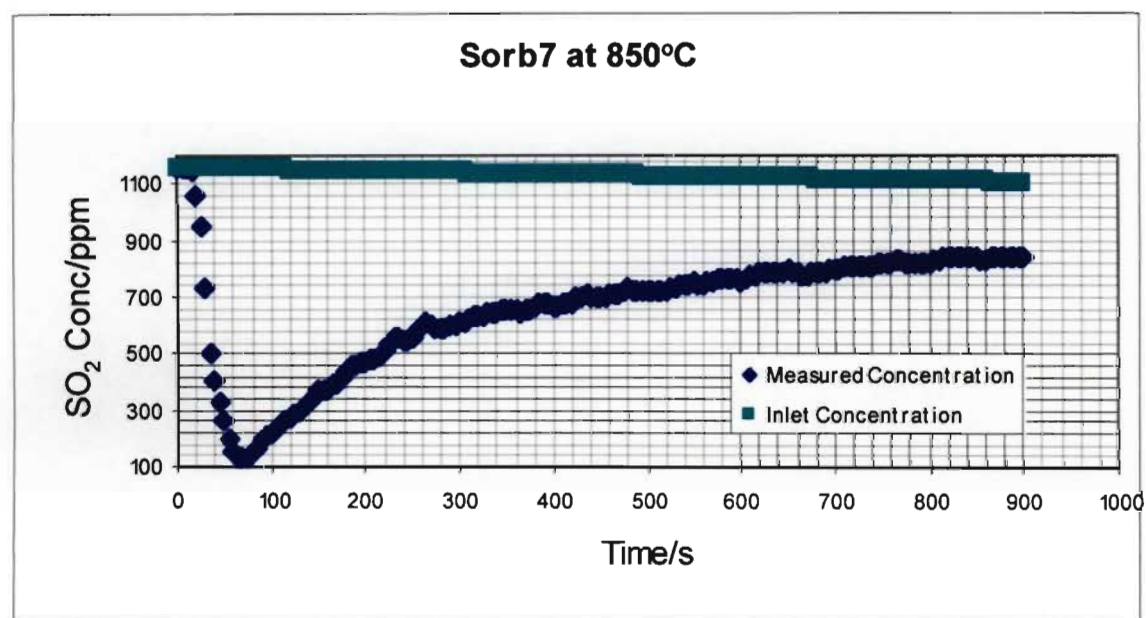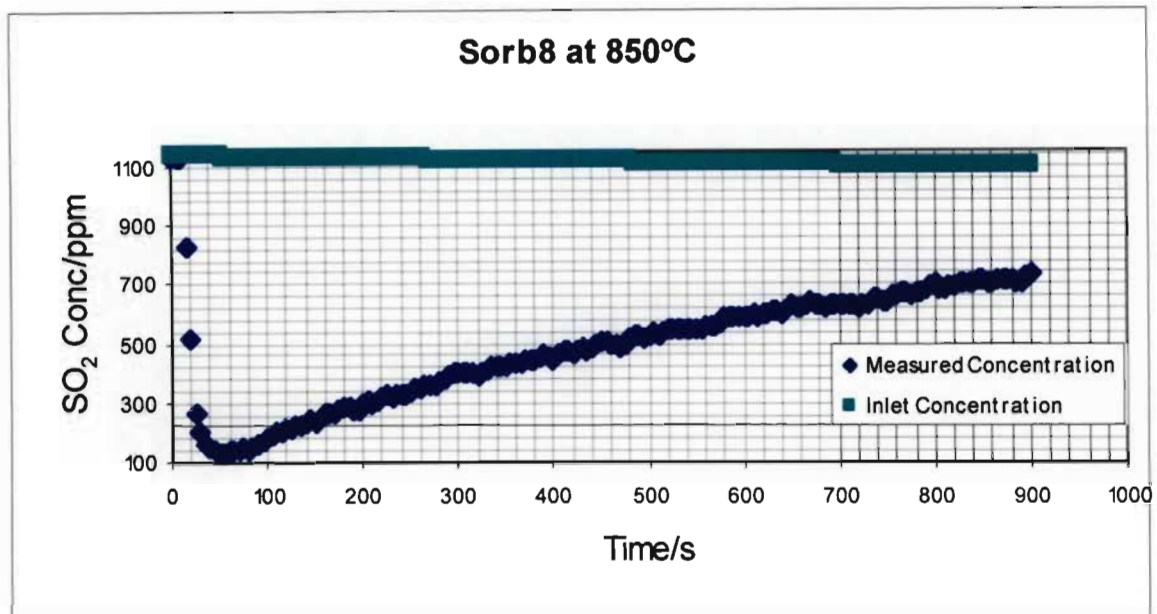Figure G-65 Performance graph of sorbent Sorb1 of particle size 600-710μm at 900°C

Figure G-66 Performance graph of sorbent Sorb2 of particle size 600-710μm at 900°C

Figure G-67 Performance graph of sorbent Sorb3 of particle size 600-710°C at 900°C

Figure G-68 Performance graph of sorbent Sorb4 of particle size 600-710μm at 900°C

Figure G-69 Performance graph of sorbent Sorb5 of particle size 600-710μm at 900°C
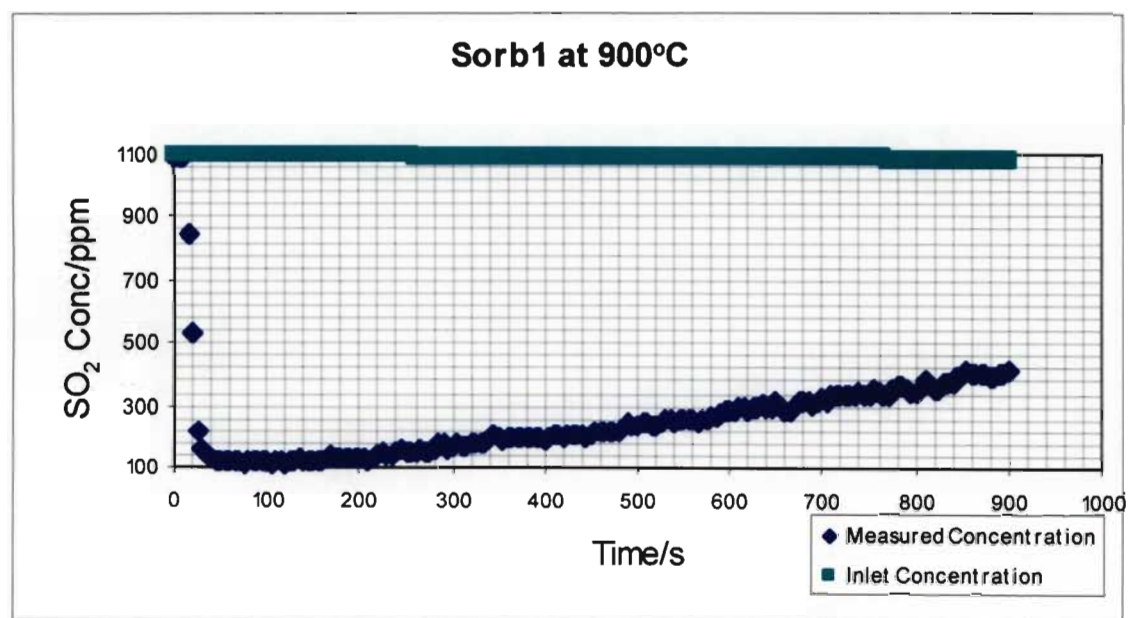
Figure G-70 Performance graph of sorbent Sorb6 of particle size 600-710μm at 900°C

Figure G-71 Performance graph of sorbent Sorb7 of particle size 600-710μm at 900°C

Figure G-72 Performance graph of sorbent Sorb8 of particle size 600-710μm at 900°C

Particle Size: 425-500μm

Temperature: 800°C

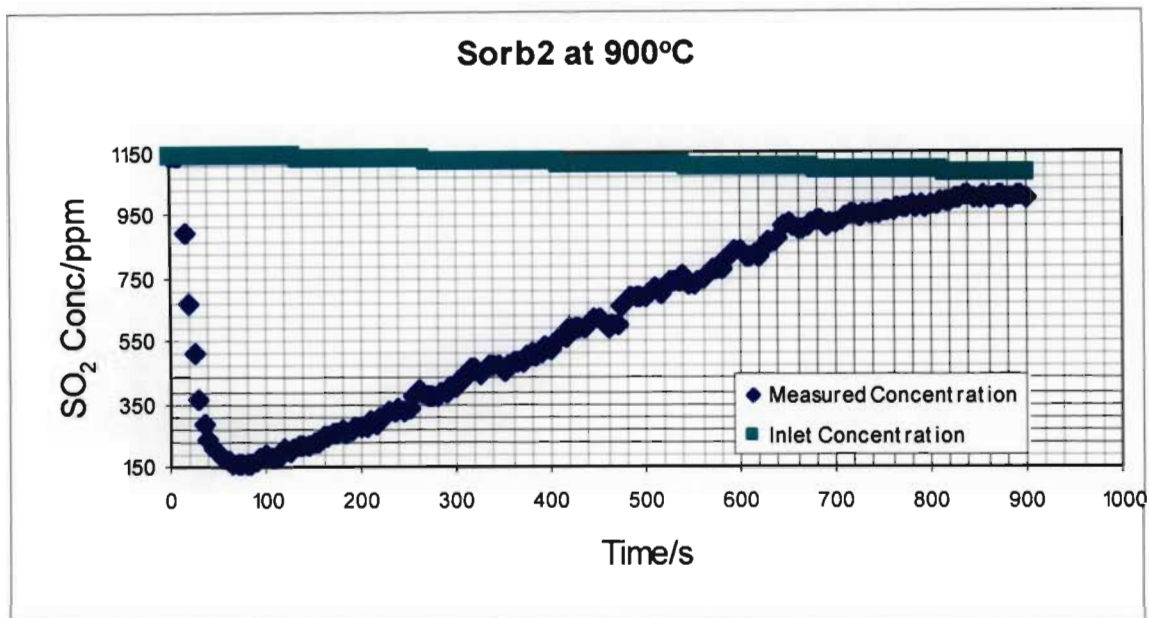Figure G-73 Performance graph of sorbent Sorb1 of particle size 425-500μm at 800°C

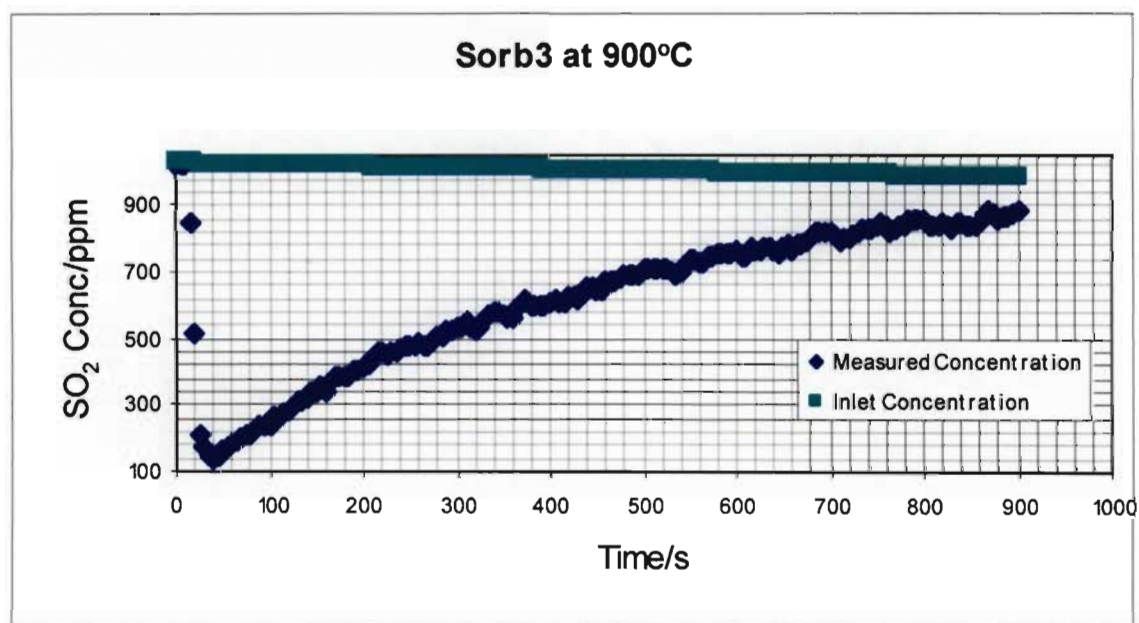Figure G-74 Performance graph of sorbent Sorb2 of particle size 425-500μm at 800°C

Figure G-75 Performance graph of sorbent Sorb3 of particle size 425-500μm at 800°C

Figure G-76 Performance graph of sorbent Sorb4 of particle size 425-500μm at 800°C

Figure G-77 Performance graph of sorbent Sorb5 of particle size 425-500μm at 800°C

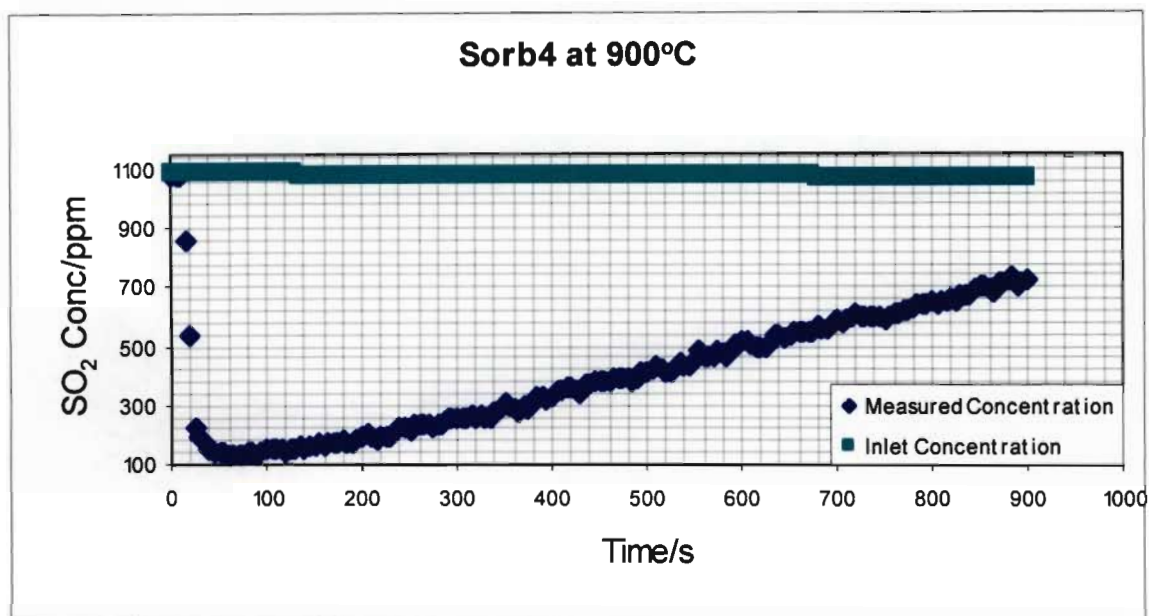Figure G-78 Performance graph of sorbent Sorb6 of particle size 425-500μm at 800°C
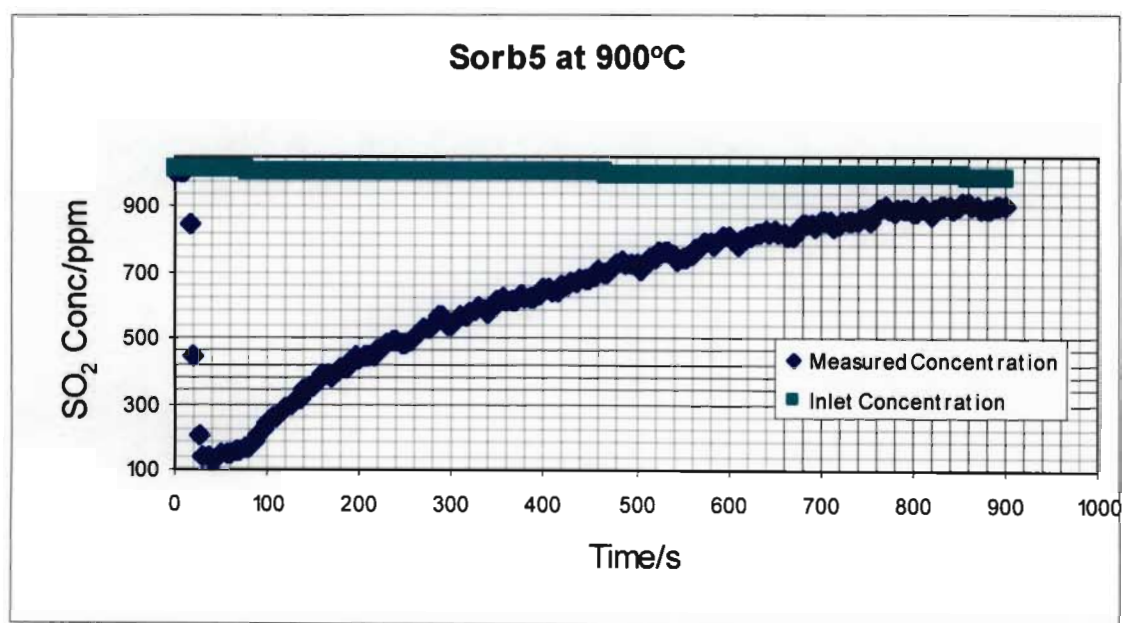

Figure G-79 Performance graph of sorbent Sorb7 of particle size 425-500μm at 800°C

G40
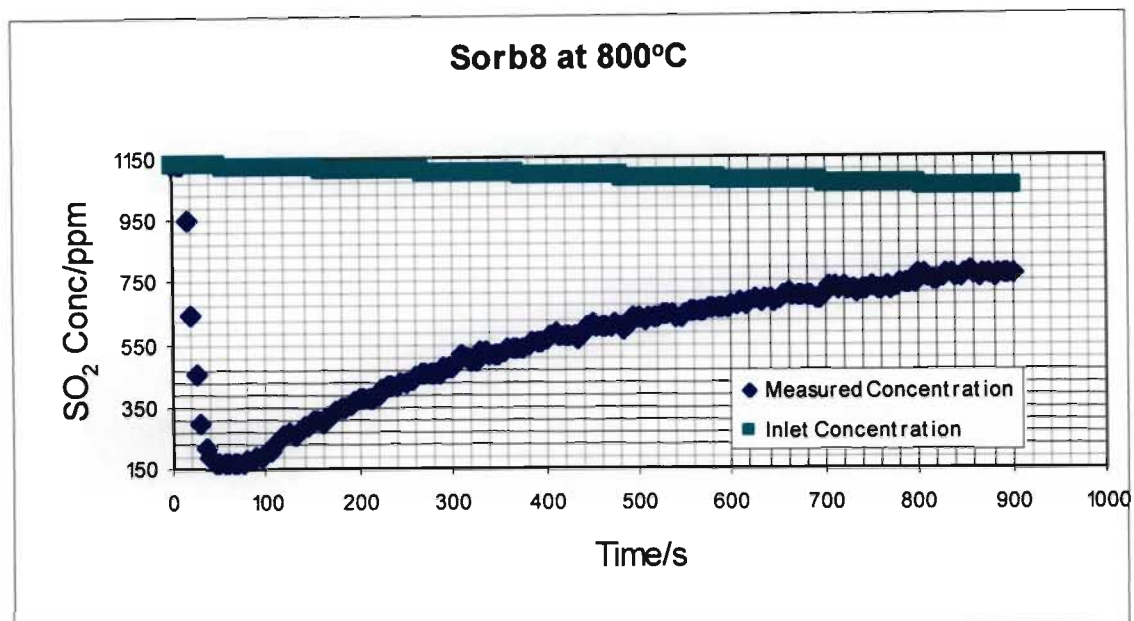
Figure G-80 Performance graph of sorbent Sorb8 of particle size 425-500μm at 800°C

Temperature: 850°C

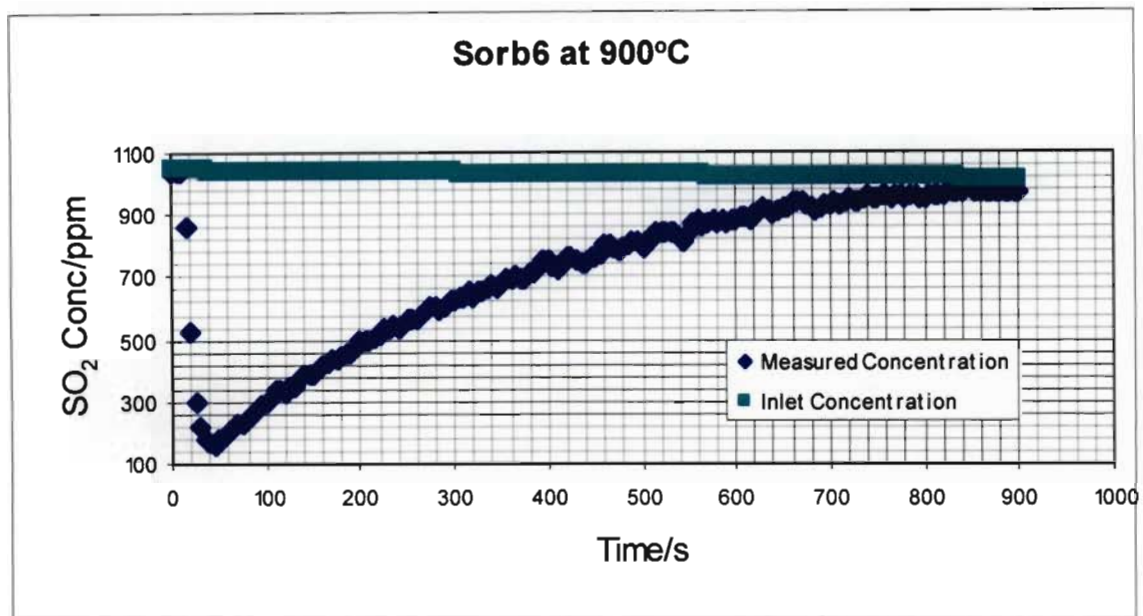Figure G-81 Performance graph of sorbent Sorb1 of particle size 425-500μm at 850°C

Figure G-82 Performance graph of sorbent Sorb2 of particle size 425-500µm at 850°C

Figure G-83 Performance graph of sorbent Sorb3 of particle size 425-500µm at 850°C

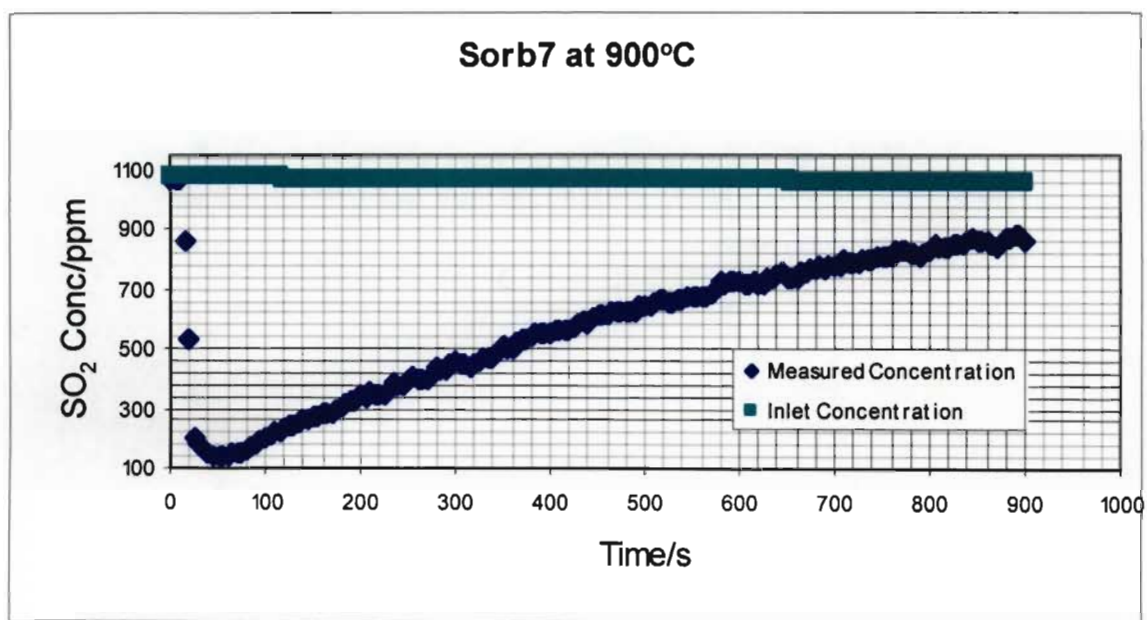Figure G-84 Performance graph of sorbent Sorb4 of particle size 425-500μm at 850°C

Figure G-85 Performance graph of sorbent Sorb5 of particle size 425-500μm at 850°C

Figure G-86 Performance graph of sorbent Sorb6 of particle size 425-500µm at 850°C

Figure G-87 Performance graph of sorbent Sorb7 of particle size 425-500µm at 850°C

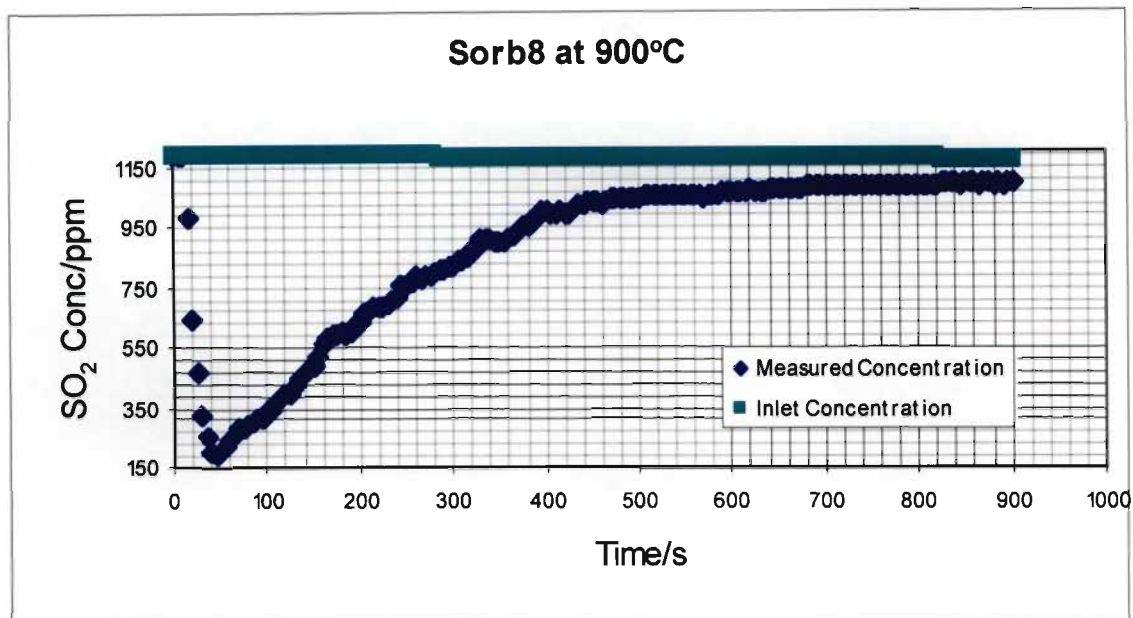Figure G-88 Performance graph of sorbent Sorb8 of particle size 425-500μm at 850°C

Temperature: 900°C

Figure G-89 Performance graph of sorbent Sorb1 of particle size 425-500μm at 900°C

Figure G-90 Performance graph of sorbent Sorb2 of particle size 425-500μm at 900°C

Figure G-91 Performance graph of sorbent Sorb3 of particle size 425-500μm at 900°C

Figure G-92 Performance graph of sorbent Sorb4 of particle size 425-500µm at 900°C

Figure G-93 Performance graph of sorbent Sorb5 of particle size 425-500µm at 900°C

Figure G-94 Performance graph of sorbent Sorb6 of particle size 425-500μm at 900°C

Figure G-95 Performance graph of sorbent Sorb7 of particle size 425-500μm at 900°C

Figure G-96 Performance graph of sorbent Sorb8 of particle size 425-500μm at 900°C
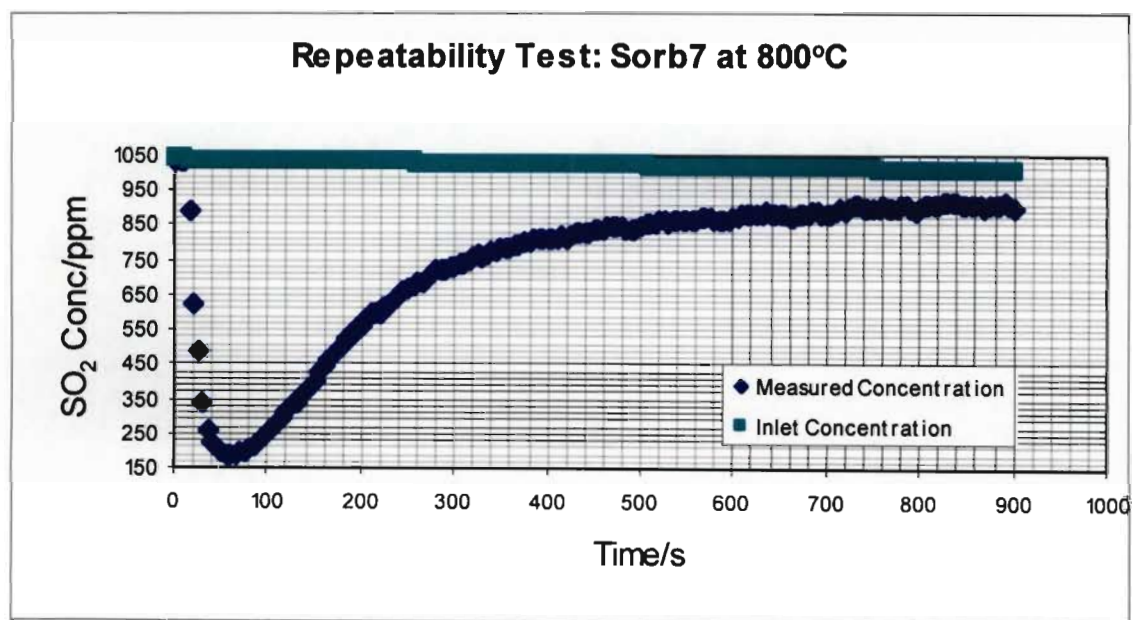
Repeatability Tests
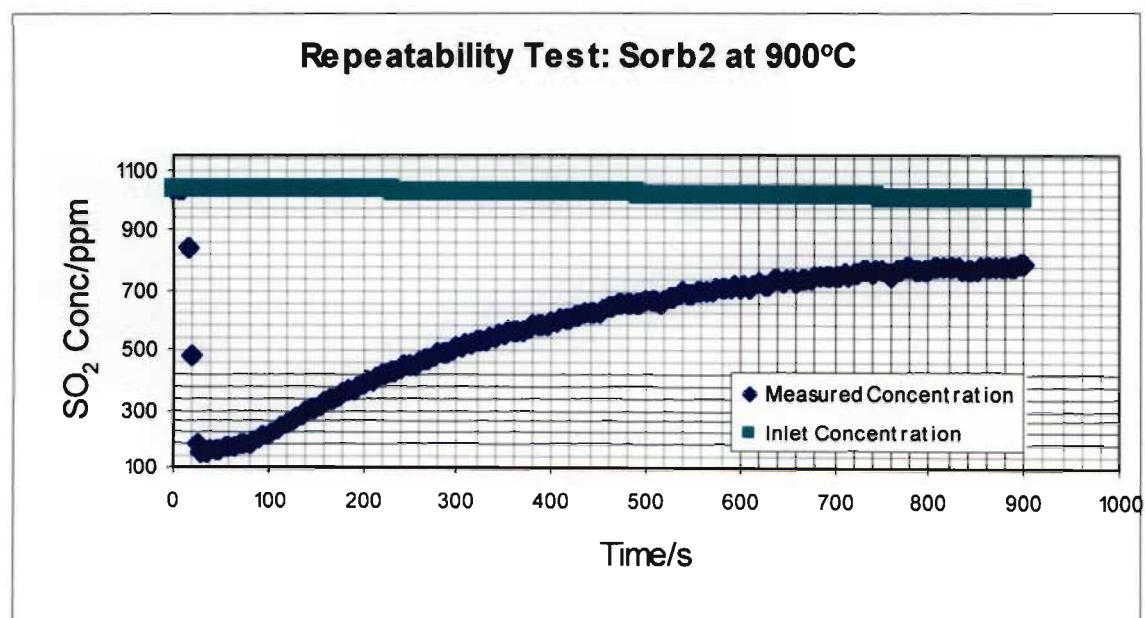
Figure G-97 Repeatability Test Graph on the performance of sorbent Sorb2 of particle size 850-1000μm at 900°C
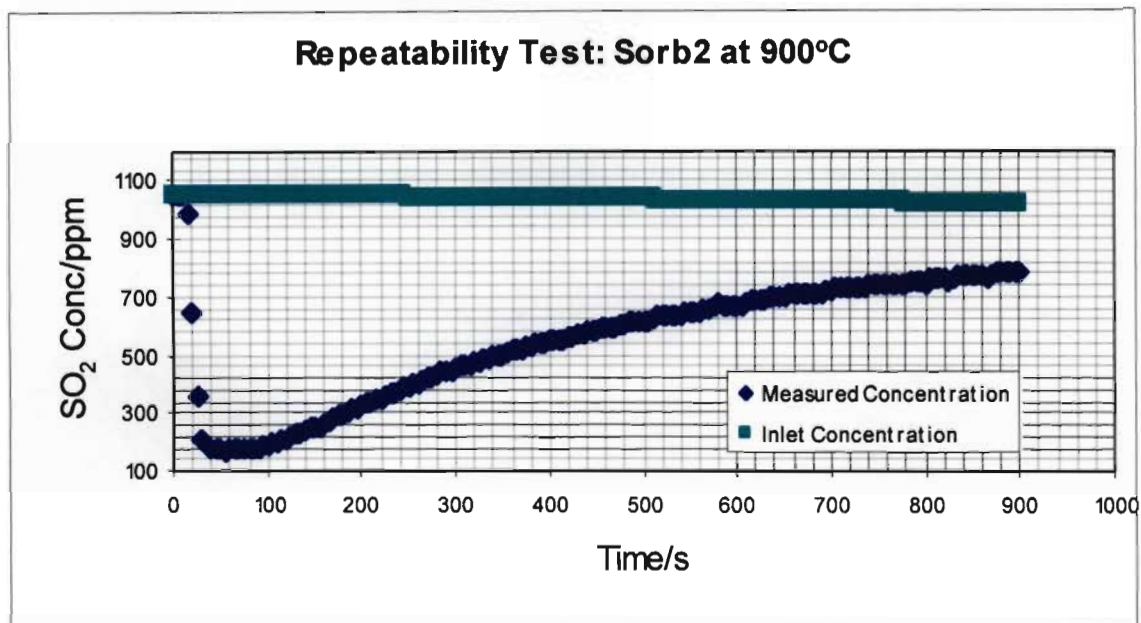
Figure G-98 Repeatability Test Graph on the performance of sorbent Sorb2 of particle size 850-1000µm at 900°C

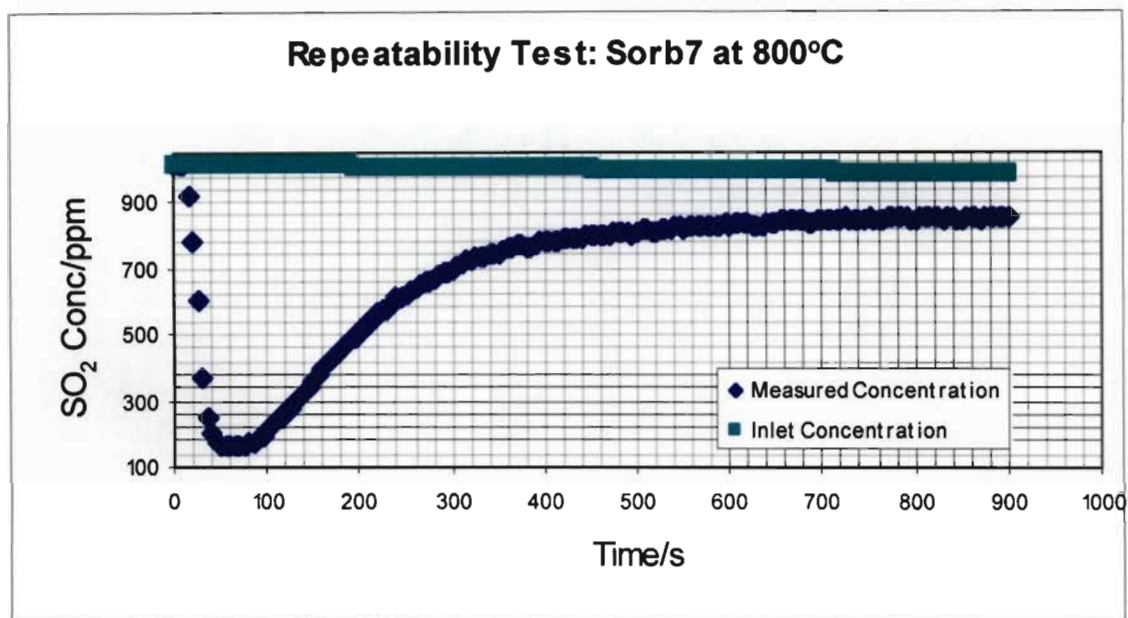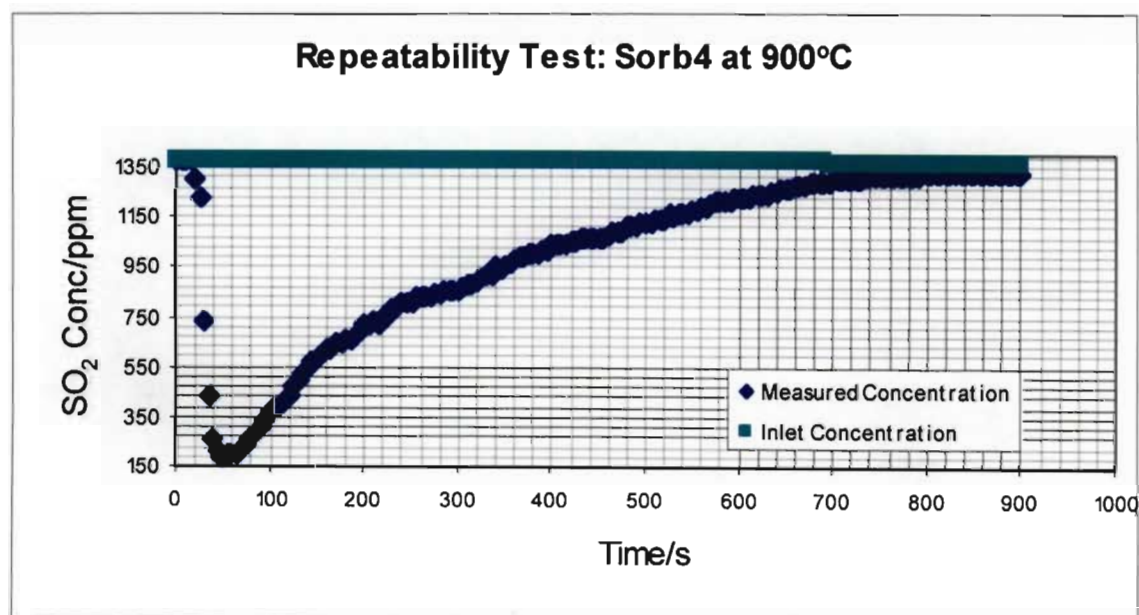Figure G-99 Repeatability Test Graph on the performance of sorbent Sorb7 of particle size 600-710µm at 800°C

Figure G-100 Repeatability Test Graph on the performance of sorbent Sorb7 of particle size 600-710μm at 800°C

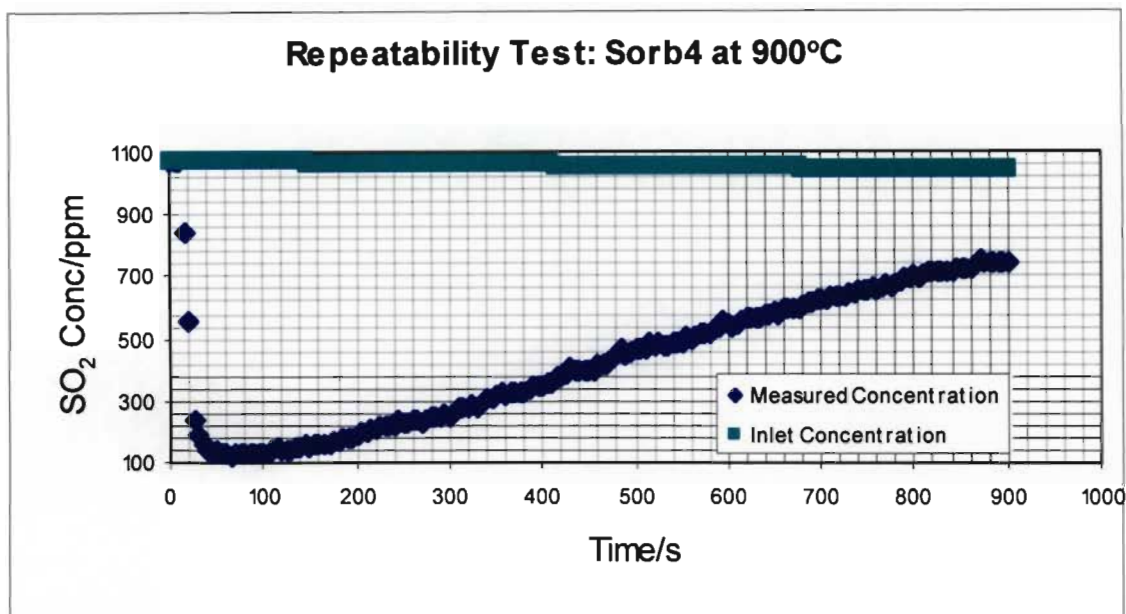Figure G-101 Repeatability Test Graph on the performance of sorbent Sorb4 of particle size 600-710μm at 900°C

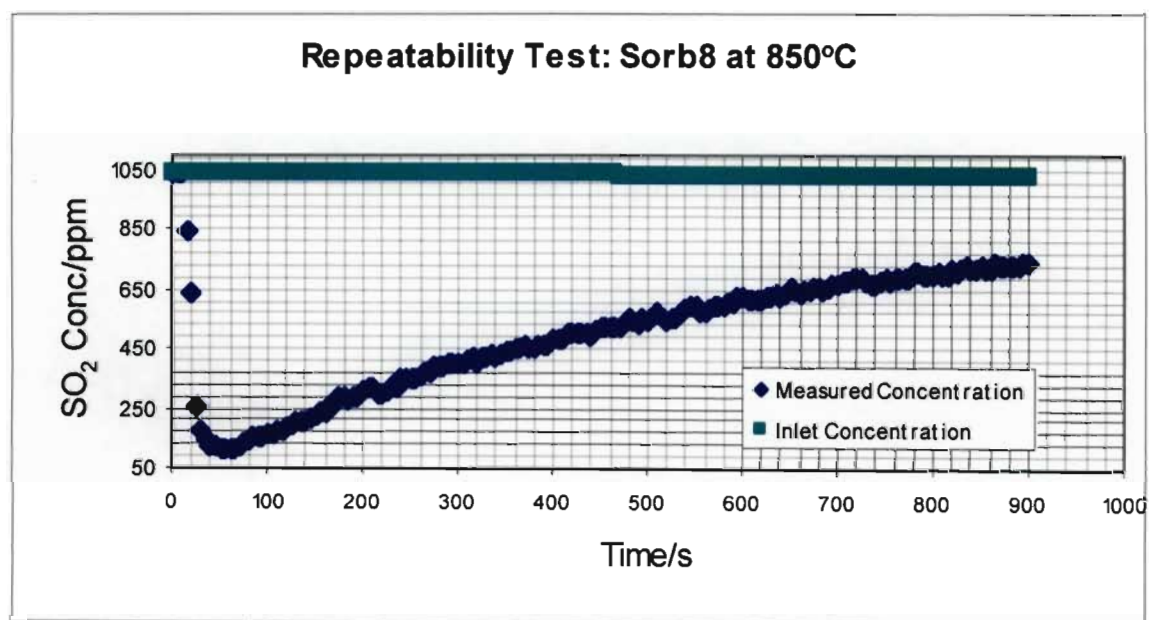Figure G-102 Repeatability Test Graph on the performance of sorbent Sorb4 of particle size 600-710µm at 900°C

Figure G-103 Repeatability Test Graph on the performance of sorbent Sorb8 of particle size 425-500µm at 850°C

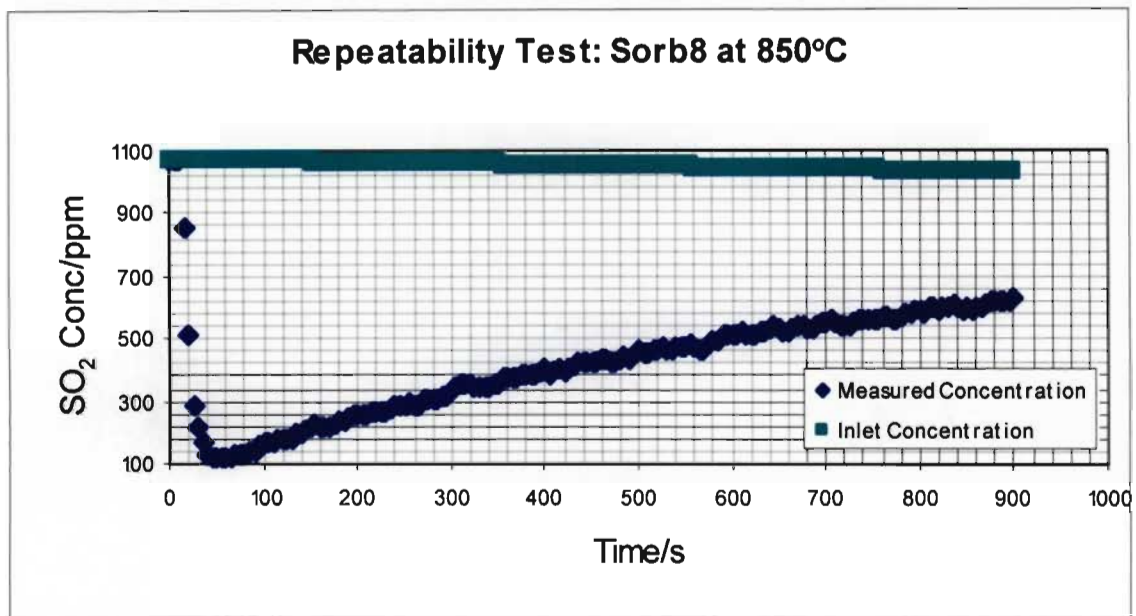**Repeatability Test: Sorb8 at 850°C**

Figure G-104 Repeatability Test Graph on the performance of sorbent Sorb8 of particle size 425-500µm at 850°C

Quantity of Sorbents Tests

Quantity of Sorbents Test: Sorb4 at 850°C
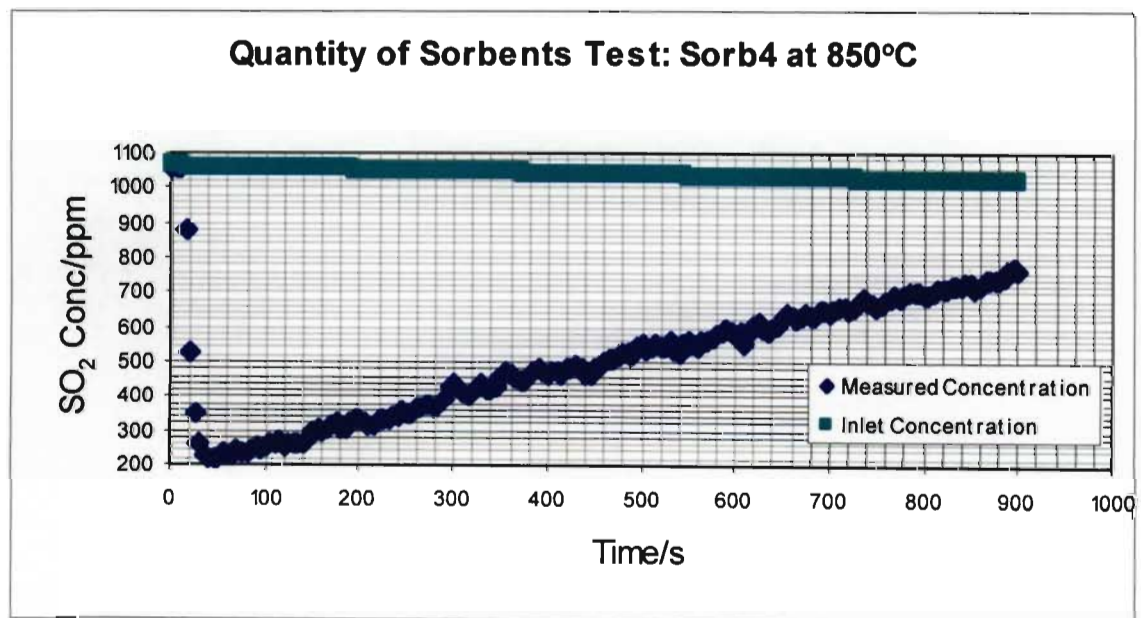
Figure G-105 Quantity of Sorbents Test Graph on the performance of 10 grams of sorbent Sorb8 of particle size 425-500µm at 850°C
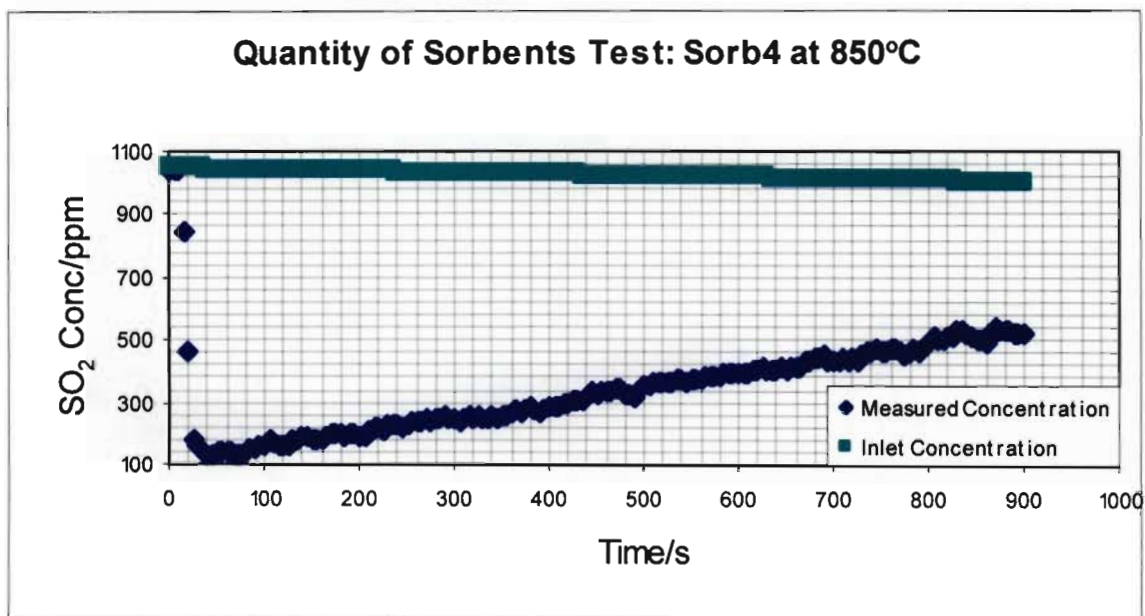
Figure G-106 Quantity of Sorbents Test Graph on the performance of 15 grams of sorbent Sorb8 of particle size 425-500μm at 850°C
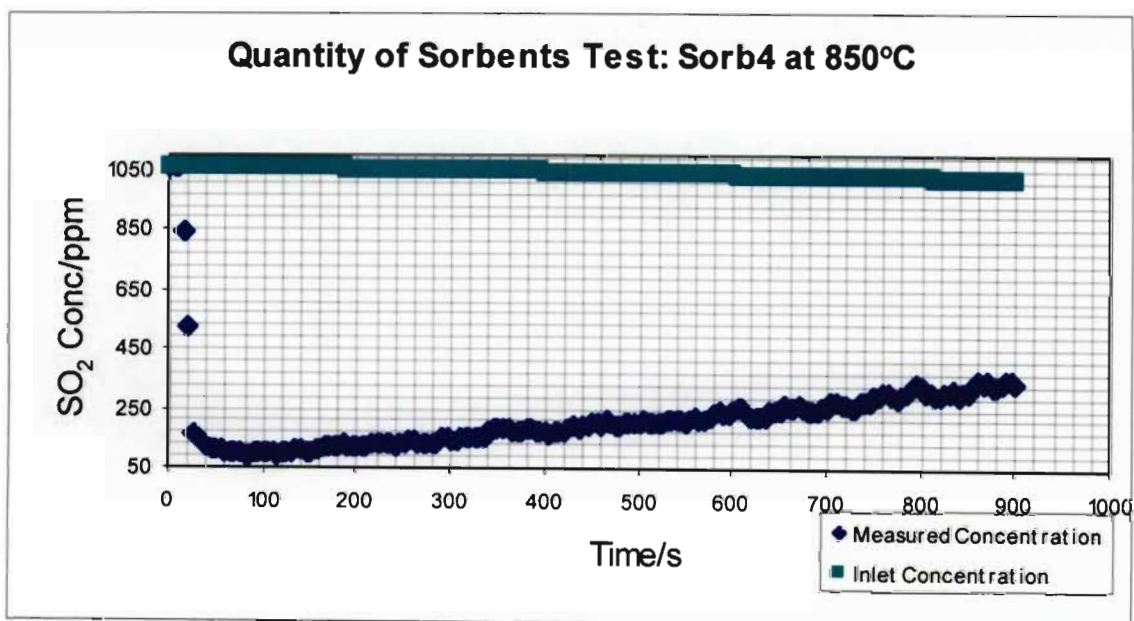

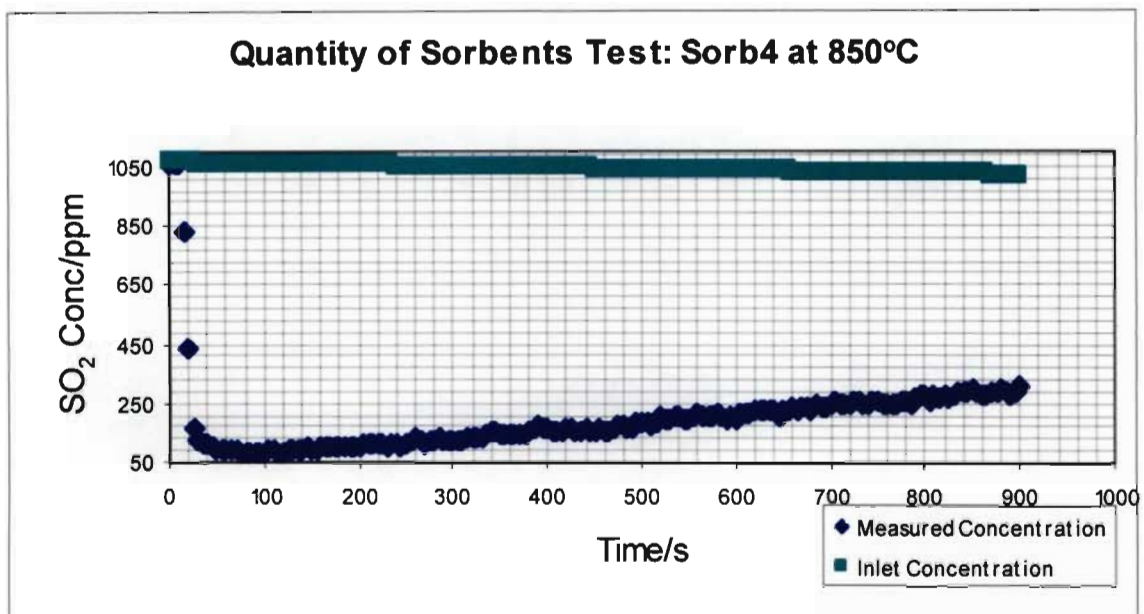Figure G-107 Quantity of Sorbents Test Graph on the performance of 20 grams of sorbent Sorb8 of particle size 425-500μm at 850°C

Figure G-108 Quantity of Sorbents Test Graph on the performance of 25 grams of sorbent Sorb8 of particle size 425-500μm at 850°C
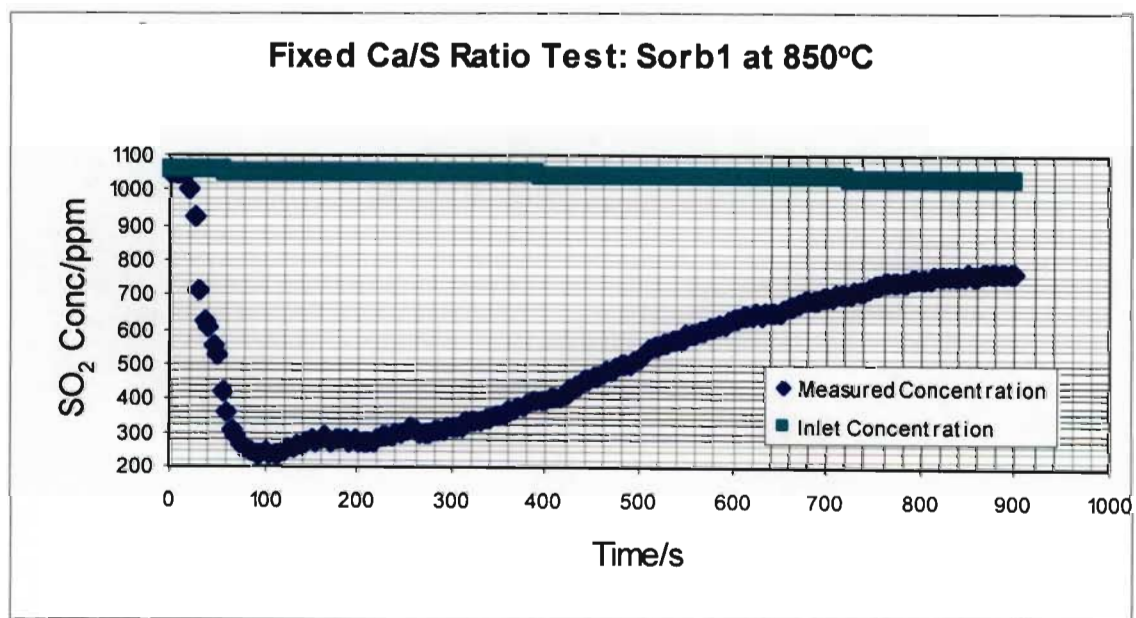
Fixed Ca/S Ratio Tests

Figure G-109 Fixed Ca/S Ratio of 2 Test Graph on the performance of sorbent Sorb1 of particle size 425-500μm at 850°C
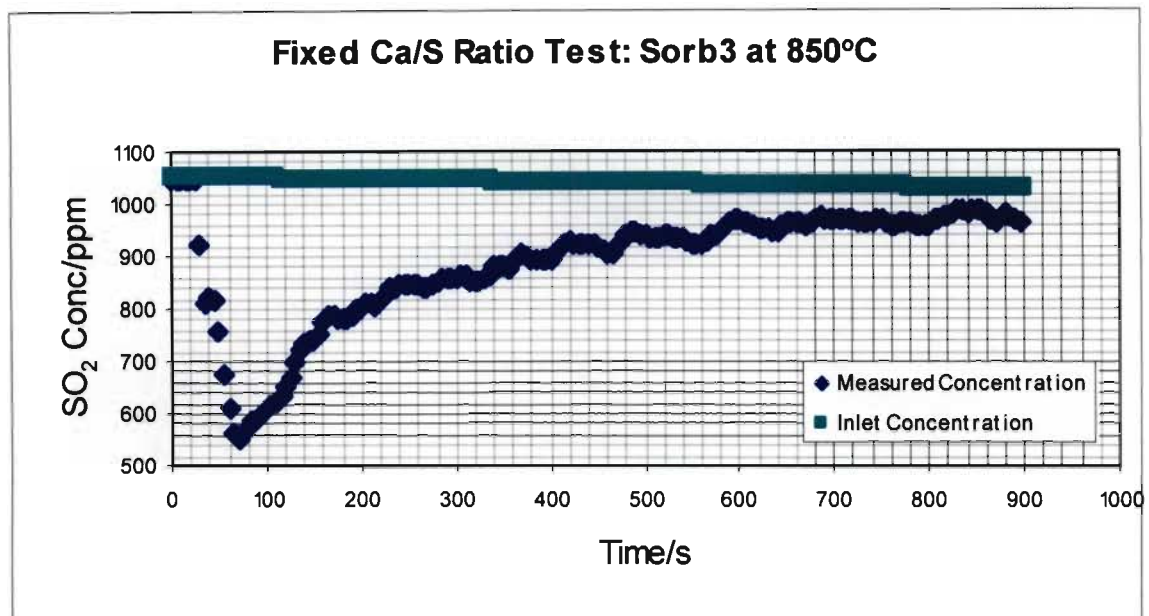
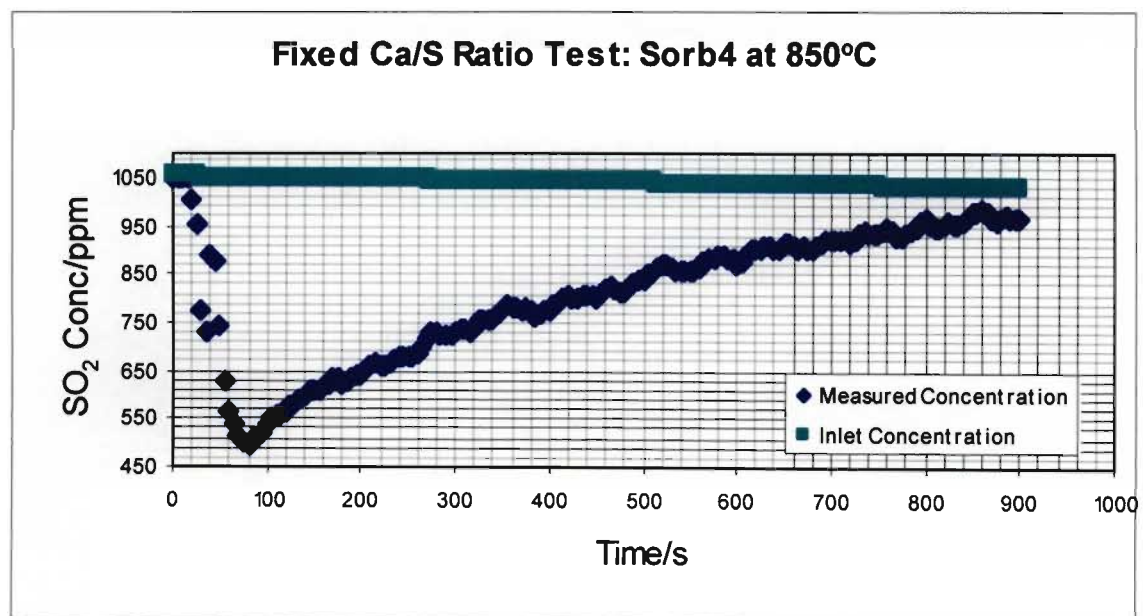Figure G-110 Fixed Ca/S Ratio of 2 Test Graph on the performance of sorbent Sorb3 of particle size 425-500μm at 850°C

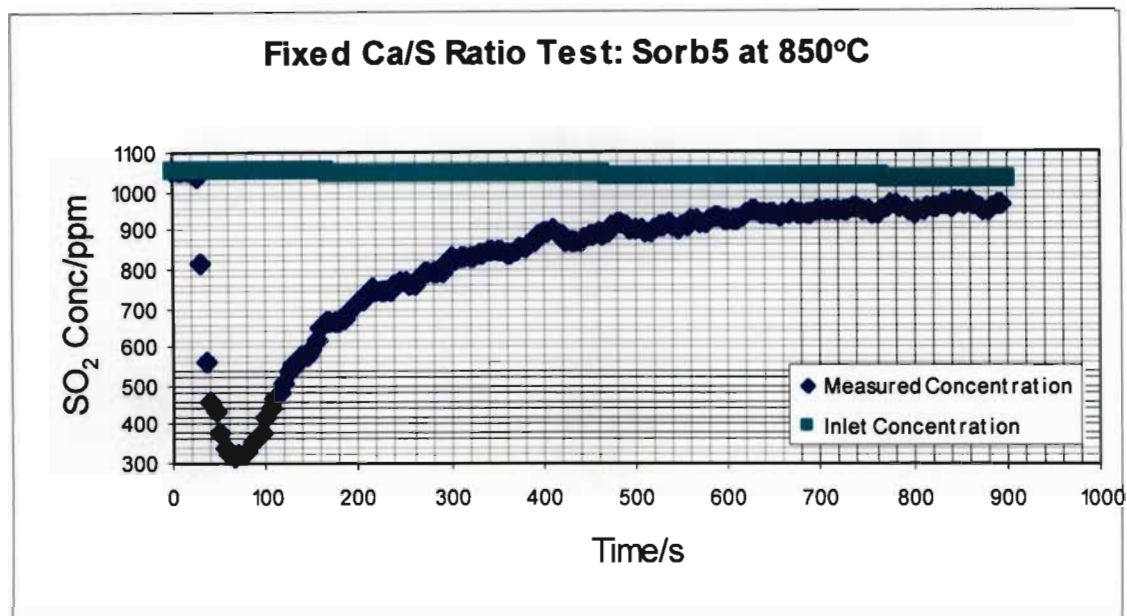Figure G-111 Fixed Ca/S Ratio of 2 Test Graph on the performance of sorbent Sorb4 of particle size 425-500μm at 850°C

Figure G-112 Fixed Ca/S Ratio of 2 Test Graph on the performance of sorbent Sorb5 of particle size 425-500μm at 850°C

Table G-1 Results of the Removal Efficiency calculations under the performance graphs of the various Sorbents

425-500µm			
Sorbent	800°C	850°C	900°C
Sorb1	71.83	84.54	76.92
Sorb2	55.81	62.53	43.46
Sorb3	50.22	56.30	38.46
Sorb4	79.24	74.23	62.36
Sorb5	17.53	34.52	35.59
Sorb6	40.64	35.48	30.21
Sorb7	47.60	41.68	45.97
Sorb8	48.20	56.48	25.32

600-710µm			
Sorbent	800°C	850°C	900°C
Sorb1	75.09	68.76	69.32
Sorb2	68.30	52.05	45.45
Sorb3	42.42	37.19	35.10
Sorb4	69.78	67.69	32.29
Sorb5	21.60	22.54	29.75
Sorb6	31.79	30.98	27.66
Sorb7	30.53	20.75	25.66
Sorb8	32.03	33.78	31.15

600-710µm					
Sorbent	600°C	700°C	800°C	850°C	900°C	950°C
Sorb1	5.81	15.24	45.27	52.25	57.45	39.00
Sorb2	3.34	10.15	42.05	43.06	25.13	29.81
Sorb3	2.95	13.98	22.99	23.78	18.94	19.13
Sorb4	3.28	9.33	44.40	44.95	47.82	31.65
Sorb5	6.15	11.59	20.84	22.55	20.75	14.10
Sorb6	2.51	8.99	21.81	21.48	19.91	17.39
Sorb7	2.65	9.43	17.26	18.01	14.17	16.26
Sorb8	3.24	11.68	17.31	26.71	21.40	17.32

Desulphurisation of Various Quantities	
Sorb4 (425-500µm, 850°C)	
Quantity	Area
10	51.28
15	66.75
20	79.00
25	81.31

Desulphurisation on a Fixed Ca/S Ratio of 2		
425-500µm, 850°C		
Sorbent	Quantity	Area
Sorb3	11.42	14.69
Sorb4	8.73	22.38
Sorb5	17.55	20.53